Heat Transfer and Hydrodynamics
in
a Three-Phase Slurry Bubble Column

by

Hanning Li

Faculty of Engineering Science
Department of Chemical and Biochemical Engineering

A thesis submitted in partial fulfilment of
the requirements for the degree of
Doctor of Philosophy

Faculty of Graduate Studies
The University of Western Ontario
London, Ontario
July 1998

© Hanning Li 1998

National Library of Canada
Acquisitions and Bibliographic Services
395 Wellington Street
Ottawa ON K1A 0N4
Canada

Bibliothèque nationale du Canada
Acquisitions et services bibliographiques
395, rue Wellington
Ottawa ON K1A 0N4
Canada

Your file Votre référence

Our file Notre référence

The author has granted a non-exclusive licence allowing the National Library of Canada to reproduce, loan, distribute or sell copies of this thesis in microform, paper or electronic formats.

The author retains ownership of the copyright in this thesis. Neither the thesis nor substantial extracts from it may be printed or otherwise reproduced without the author's permission.

L'auteur a accordé une licence non exclusive permettant à la Bibliothèque nationale du Canada de reproduire, prêter, distribuer ou vendre des copies de cette thèse sous la forme de microfiche/film, de reproduction sur papier ou sur format électronique.

L'auteur conserve la propriété du droit d'auteur qui protège cette thèse. Ni la thèse ni des extraits substantiels de celle-ci ne doivent être imprimés ou autrement reproduits sans son autorisation.

0-612-31161-9

Canada

Abstract

Heat Transfer and hydrodynamics in a slurry bubble column have been investigated up to a slurry concentration of 40 vol.% and gas velocities up to 0.30 m/s. The two important hydrodynamic parameters investigated are gas holdup and axial solid dispersion. Particle hindered settling velocities and solid dispersion coefficients are studied based on the sedimentation-dispersion model. Also investigated are variations of small and larger bubble size population and their rise velocities with slurry concentration.

Local average heat transfer coefficients at different radial and axial locations have been investigated. The heat transfer coefficients in the bulk region are higher than in the distributor region. In the bulk region, the heat transfer coefficients at the center are higher than at the wall. The effects of the orientation of the heat transfer probe on heat transfer are analyzed. Generally, heat transfer coefficients decreases with slurry concentrations.

The fast response heat transfer probe used in this study provided instantaneous information on the heat transfer coefficients. The enhancement of heat transfer due to the turbulent bubble wake region has been studied to understand bubble wake dynamics over the range of operating conditions studied.

Literature correlations for predicting heat transfer coefficients in slurry bubble columns have been tested and their limitations are pointed out. Modifications to well known literature correlations have been proposed.

ACKNOWLEDGMENTS

The completion of this work represents a productive and effective contribution of others, whose efforts and talents are reflected in the final result. I would like to express my gratitude and appreciation to my chief supervisor, Dr. Anand Prakash. His constructive suggestions, criticisms, guidance and advice made this challenging work manageable. I have learned a great deal from him and I wish to thank him for his efforts. I am thankful to Dr. T. Base for his helpful suggestions, criticisms and contributions to this thesis. I thank you for all the time you spent with me.

I extend a sincere word of thanks to the mechanical shop staff for their technical assistance in the construction and maintenance of the equipment. Special thanks are also due to Mr. Souheil Afara for his valuable help in various aspects of the experiments. Thanks are also due to Tim Hunt and staff of the electronic shop for various helps in the maintenance of the electronic and computer equipment.

I wish to express my gratitude to the professors, staff and fellow students for making the Department of Chemical and Biochemical Engineering a conducive environment for learning. The staff of the Computer Laboratory and Library personnel are also thanked for their assistance.

I also wish to thank my mother and father. Their efforts and advice which have contributed significantly to my academic achievement, will remain to be my guidance forever. This work is delicated to them.

Lastly, I wish to thank my wife for her patience during my endeavor to complete this work.

Table of Contents

List of Tables

List of Figures

Nomenclature

a gas-liquid specific interfacial area (m^{-1})

a_s surface area per unit volume of particle (m^{-1})

A_1-A_4 coefficients in Equation (2.2.15)

A_c cross-sectional area of column (m^2)

A_p coefficient in Equation (4.2.12)

b_1,b_2 constant in Equation (4.1.11)

c coefficient in Equation (2.2.6)

c_1-c_4 coefficients in Equation (4.2.18a) and (4.2.18b)

c_b constant defined in Equation (4.2.16)

C_s solid concentration (kg/m^3)

C_{so} solid concentration at column bottom (kg/m^3)

C_1 coefficient in Equation (2.2.8)

C_2 coefficient in Equation (2.2.9)

C_3 coefficient in Equation (2.2.16)

C_4 coefficient in Equation (2.2.18)

C_5,C_6 coefficient in Equation (2.2.19)

C_7 coefficient in Equation (2.2.26)

C_8 coefficient in Equation (2.2.28)

C_9 coefficient in Equation (2.2.29)

C_{10},C_{11} coefficient in Equation (2.2.30)

C_p specific heat ($kJ/kg\ ^oC$)

d_b diameter of bubble (m)

d_{eq} equivalent hydraulic diameter of particle (m)

d_p particle diameter (m)

D column diameter (m)

D_e molecular diffusuvuty (m^2/s)

$E_{pot.p}$ potential energy of the particles in suspension (J)

E_s axial solids dispersion coefficient (m^2/s)

E_{wk} bubble wake enhancement factor (-)

F objective function

Fr_g gas Froude numner ($= \frac{V_g}{\sqrt{gD}}$)

Fr_g' gas Froude Numner defined in Equation (2.5.4)

g acceleration due to gravity (m/s^2)

Δh_m height difference measured from water manometer (m)

h heat transfer coefficient ($kW/m^2\,^oC$)

h_2 heat transfer coefficient in liquid-solid fluidized bed ($kW/m^2\,^oC$)

h_3 heat transfer coefficient in three phase fluidized bed ($kW/m^2\,^oC$)

h_{ave} average heat transfer coefficient ($kW/m^2\,^oC$)

h_i instantaneous heat transfer coefficient ($kW/m^2\,^oC$)

h_o heat transfer coefficient in column center ($kW/m^2\,^oC$)

h_w heat transfer coefficient in column wall ($kW/m^2\,^oC$)

H distance (m)

H_c column height (m)

H_d expanded bed height (with gas present) (m)

H_s static bed height (without gas) (m)

k relative wake holdup(ratio of wake volume to bubble volume) (-)

k_o relative wake holdup in solid free system (-)

k_l liquid thermal conductivity (kW/m^oC)

k_s solid particle thermal conductivity (kW/m^oC)

k_{sl} slurry thermal conductivity (kW/m^oC)

k_w wall-to-bed heat transfer coefficient (kW/m^oC)

K_w wall-to-bed mass transfer coefficient (m/s)

K_l mass transfer coefficient based on liquid side (m/s)

l mean distance between bubbles (m)

l_b bubble chord length (m)

L particle length (m)

L_p probe length (m)

n coefficient in Equation (2.2.6)

n_1-n_3 exponents in Equation (2.2.18)

n_d flux of solids particles due to dispersion (kg/m^2s)

N number of collected data (-)

Nu Nusset number ($\frac{hD}{k_l}$)

Nu_b Nusset number based on bubble diameter ($=\frac{hd_b}{k_l}$)

Nu_w Nusset number ($\frac{h_w D}{k_l}$)

Nu' Nusset number defined in equation (2.5.4)

P pressure (Pa)

Pe Peclet number ($=\frac{V_g D}{E_s}$)

Pr Prandtl number ($=\frac{C_{pl}\mu_l}{k_l}$)

$P_{in,g}$ incoming power with the gas phase (W)

P_o pressure at atmospheric conditions (Pa)

P_v energy dissipation rate (m^2/s^3)

q heat transfer rate (kW/m^2)

q_{ave} average heat transfer rate (kW/m^2)

Q heat flux (kW/m^2)

$Q_{o,g}$ volumetric flowrate of gas at atmospheric conditions (m^3/s)

r radial distance from column center (m)

R radii of the column (m)

R_p radii of cylindrical probe (m)

Re Reynolds number ($=\frac{V_g d_p}{\nu_l}$)

Re' Reynolds number defined in equation (2.5.4)

Re_g gas Reynolds number ($=\frac{V_g D\rho_l}{\mu_l}$)

Re_b Renolds number based on bubble diameter ($=\frac{P_v d_b^4}{\nu_l^3}$)

Re_c Renolds number based on probe radii ($=\frac{U_{b,o}R_p}{\nu_l}$)

Re_p particle Renolds number ($=\frac{U_t d_p}{\nu_l}$)

Sc Schmidt number ($=\frac{\nu_l}{D_e}$)

Sh_b Sherwood number based on bubble diameter ($=\frac{K_l a d_b^2}{6\varepsilon_g D_e}$)

Sh_w Sherwood number based on column diameter ($=\frac{K_w D}{D_e}$)

St Stanton number ($\frac{h}{\rho C_{pl} V_g}$)

t time (s)

t_c contacting time (s)

T temperature (^oC)

T_b bed temperature (^oC)

T_{si} probe surface temperature (^oC)

T_w wall temperature (^oC)

$U_{b,ave}$ average bubble rise velocity (m/s)

$U_{b,o}$ average bubble rise velocity in column center (m/s)

$U_{b,L}$ larger bubble rise velocity (m/s)

$U_{b,s}$ small bubble rise velocity (m/s)

U_{lmf} minimum fluidization velocity (m/s)

U_p particle hindered settling velocity (m/s)

U_{st} generalized solids settling velocity (m/s)

U_t single particle terminal velocity (m/s)

U_{trans} velocity at which transition occurs from dispersed flow to churn flow regime(m/s)

U_∞ terminal bubble rise velocity (m/s)

V_a, V_r axial and radial components of liquid velocities (m/s)

V_c liquid circulation (m/s)

$V_{b,L}$ larger bubble superficial gas velocity (m/s)

$V_{b,s}$ small bubble superficial gas velocity (m/s)

$V_{b,\infty}$ characteristic terminal bubble rise velocity (m/s)

V_g superficial gas velocity (m/s)

V_l superficial liquid velocity (m/s)

V_o drift velocity (m/s)

V_p solids convective velocity (m/s)

V_r reactor volume (m^3)

V_{sl} superficial slurry velocity (m/s)

W_s the mass of solids in the column (kg)

x ratio of solids concentration in bubble wake to liquid-solid region (-)

$\overline{X}$ average peak height of heat transfer coefficient (kW/ m^2 °C)

y distance (m)

z axial distance along the column (m)

Greek symbols

α thermal diffusivity (m^2/s)

β constant in Equation (2.5.23)

ε phase holdup (-)

ε_0 bed voidage for zero gas flow (-)

ε_2 gas holdup in two phase (-)

ε_3 gas holdup in three phase (-)

$\varepsilon_{b,L}$ larger bubbles gas holdup (-)

$\varepsilon_{b,s}$ small bubbles gas holdup (-)

ε_{L2} liquid holdup in liquid-solid fluidized bed (-)

ε_{L3} liquid holdup in three phase fluidized bed (-)

ε_{sf} solids holdup in the liquid-solid fluidized region (-)

ε_{sw} solids holdup in bubble wake (-)

ε_{w} wake volume fraction (-)

ρ density (kg/m^3)

μ viscosity (kg/m s)

ν kinematic viscosity (m^2/s)

ν_l kinematic liquid viscosity (m^2/s)

ν_{sl} effective kinematic slurry viscosity (m^2/s)

$\nu_{eff,rad}$ radial momentum transfer coefficient (m^2/s)

δ thickness of thermal boundary layer (m)

δ_o thickness of laminar viscous boundary layer (m)

θ_c contacting time (s)

η_l length scale (m)

υ velocity scale (m/s)

ρ density (kg/m^3)

σ_l liquid surface tension (kg/s^2)

σ variance of peak height distribution

ϕ liquid or solid fraction in slurry phase (-)

ϕ_i area fraction of peak height i (-)

ϕ_p particles shape factor

$\bar{\varphi}_l$ average fraction of liquid in slurry phase (-)

Θ normalized heat transfer coefficient (-)

Δ difference

Subscripts

g	gas
l	liquid
p	particle
s	solid
sl	slurry
w	water

1.0 Introduction

Slurry bubble columns belong to the general class of multiphase reactors. A multiphase reactor is a system in which gas and liquid phase are contacted with a solid phase (usually a catalyst). The multiphase reactors can be classified into three main categories: the trickle bed reactor (fixed or packed bed), the gas-liquid-solid fluidized bed reactor and the bubble (slurry) column reactor. These reactors have diverse applications in chemical, biochemical, petrochemical, and waste water treatment industries. In most applications, the reaction occurs between a dissolved gas and a liquid-phase reactant in presence of a solid catalyst.

Figure 1.1 shows a schematic diagram of a typical slurry bubble column reactor. Gas enters the bottom of the reactor through a gas distributor rising in the form of bubbles through a continuous slurry phase. Liquid/slurry enters at the bottom of the reactor and exits from the side. A heat exchanger may also be necessary to control temperature. The column can be operated in a batch or continuous mode with cocurrent or countercurrent flow.

The applications of bubble columns and slurry bubble columns have been listed in literature (Shah et al., 1982; Fan, 1989; Dudukovic and Devanathan, 1992). These reactors have found application in such diverse processes as hydrotreating and conversion of heavy oil, liquid fuels production by Fischer-Tropsch synthesis, methanol synthesis, dimethyl ether production, polymerization (production of polyolefines), fermentation (production of ethanol and mammalian), biological waste water treatment and flue gas desulphurization. Biomedical engineering is another area of application of bubble column. One blood oxygenator is a typical bubble column. For example during the operation of the human heart (in some cases) or malfunction of the human lung, oxygen is supplied to human blood through a blood oxygenator which is a typical bubble column.

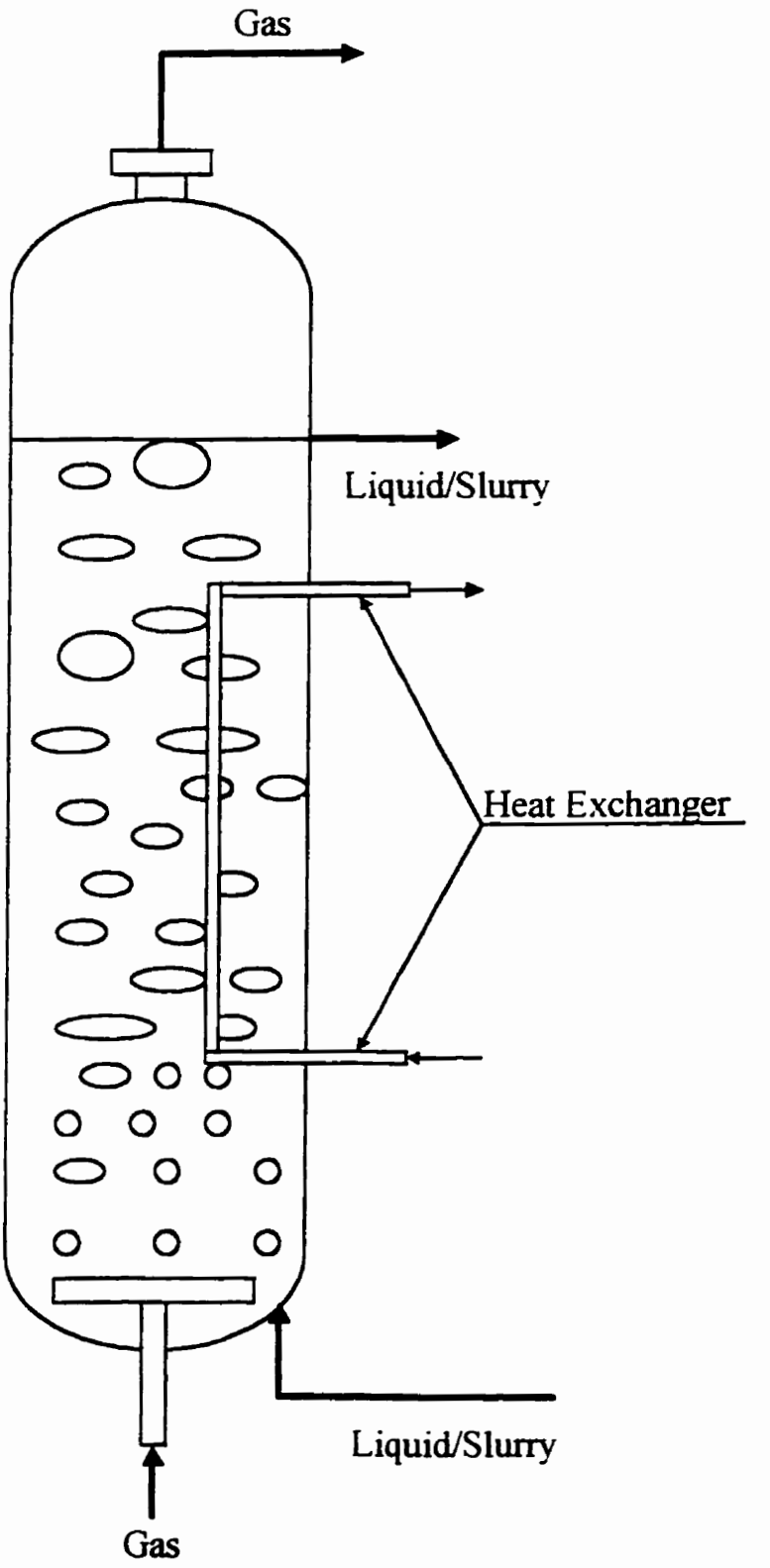

Figure 1.1 Slurry Bubble Column Reactor

One important area of current interest in slurry bubble columns is the production of environmentally benign liquid fuels via Fischer-Tropsch synthesis. As reported by Zhou et al. (1992), the development of slurry bubble column technology for these processes is an area of high priority research at the US Department of Energy Pittsburgh Energy Research Center (DOE-PETC). The slurry process presents substantial potential advantages over conventional fixed-bed and entrained bed processes (Bukur and Daly, 1987; Bukur et al., 1987). Deckwer and Schumpe (1993) summarized the advantages of bubble columns over other types of multiphase reactors:

- High liquid (slurry) phase content for the reaction to take place;
- Reasonable interphase mass transfer rates at low energy input;
- High selectivity and conversion per mass;
- Excellent heat transfer properties and easy temperature control;
- Online catalyst addition and withdrawal;
- Washing effect of the liquid on the catalyst;
- Solid can be handled without serious erosion or plugging problems;
- Little maintenance is required due to simple construction and no problem with sealing due to absence of any moving parts;
- Bubble column reactors are relatively cheap to construct and operate.

The disadvantages of these reactors include:

- Considerable backmixing in both the liquid (slurry) phase and the dispersed gas phase;
- Low volumetric catalyst loading;
- Bubble coalescence;
- Difficult to scale up.

In addition industry has identified some problems of practical importance. For example, the catalyst deactivation rate can increase with increasing slurry concentrations. Separation of fine catalyst particles from liquid products can also be difficult. Foaming can also become a problem in certain applications. For continuous systems, the solids can produce erosion in the impeller and pump housings. Abrasion in the slurry reactor also interfaces with the flow of product.

1.1 Objectives of the Study

Although of relatively simple construction, slurry columns are difficult to scale up due to lack of information on hydrodynamics and transport processes over a wide range of operating conditions of practical interest. For example, productivity of a catalytic slurry reactor could be enhanced by increasing catalyst loadings and high gas flow rates would be required to increase reactor throughputs. It is, therefore, important to identify practical operational limits at high slurry concentrations. For example, gas distributor design and configurations and column start up procedure could be influenced by high slurry concentration.

This study investigates hydrodynamics and heat transfer (both instantaneous and average) in a slurry bubble column over a wide range of operating conditions. The slurry concentration is varied up to 40 vol.% and gas velocities up to 0.30 m/s. The two important hydrodynamic parameters investigated are gas holdup and solids dispersion. Also variations of small and large bubble size population and their rise velocities with slurry concentrations are analyzed.

A good understanding of heat transfer rate is required for a proper design of heat transfer surface in slurry bubble columns. This is especially important for exothermic reactions like Fischer-Tropsch synthesis. Reported heat transfer studies in slurry bubble column have been limited to low slurry concentrations and low gas velocities (Deckwer et al., 1980; Saxena et al., 1990a, 1990b). Moreover, little attempt has been made to study

radial and axial variations of heat transfer coefficients. This study investigates heat transfer coefficients at different radial and axial locations at slurry concentrations up to 40 vol.% and gas velocities up to 0.30 m/s. The differences in heat transfer rates in distributor and bulk region are analyzed as a function of operating conditions. The new fast response heat transfer probe provided quasi-instantaneous measurements of heat transfer coefficients. The enhancement of heat transfer coefficient due to turbulent bubble wake region has been analyzed to understand bubble wake dynamics over the range of operating conditions investigated in different regions of column.

Literature correlations for prediction of heat transfer coefficients in slurry bubble columns have been tested and their limitations have been pointed out. Necessary modifications to well known literature correlations have been proposed wherever needed.

2.0 Literature Review

2.1 Classification and Flow Regime

The classification of three phase systems can be extended from that of gas-liquid, gas-solid or liquid-solids systems. It is convenient to classify them according to the state of particle motion. Particle motion can be subdivided into three basic operating regimes: the fixed bed regime, the expanded (fluidized) bed regime and the transport regime. Figure 2.1 shows an operating regime map for the air-water-solid system with cocurrent upward flow of gas and liquid (Fan et al., 1987a). The fixed bed regime exists when the drag force on the particles induced by the flow of a gas-liquid mixture is smaller than the effective weight of the particles in the system. With an increase in gas and/or liquid velocity, the drag force counterbalances the effect of particle weight in the system. This point is known as the minimum fluidization velocity (U_{lmf}) as the bed is in a state of minimum fluidization. This mode of operation is known as the expanded bed regime as the gas and/or liquid velocity is further increased beyond the minimum fluidization velocity. The expanded bed regime continues until the gas and/or liquid velocity reaches the terminal velocity of the particle (U_t) beyond which the transport regime begins.

Typical operating ranges for three phase fluidized beds and slurry bubble columns are shown in Figure 2.2 (Fan et al., 1987a). Three phase fluidized beds operate in the expanded bed regime covering U_t from 3 to 50 cm/s. Slurry bubble columns may operate in both the expanded and transport regimes covering U_t from 0.03 to 7 cm/s.

Bubble columns normally operate with a height to diameter ratio of greater than five and with superficial gas velocities from 1 to 30 cm/s and liquid velocities from 0 to 2 cm/s.

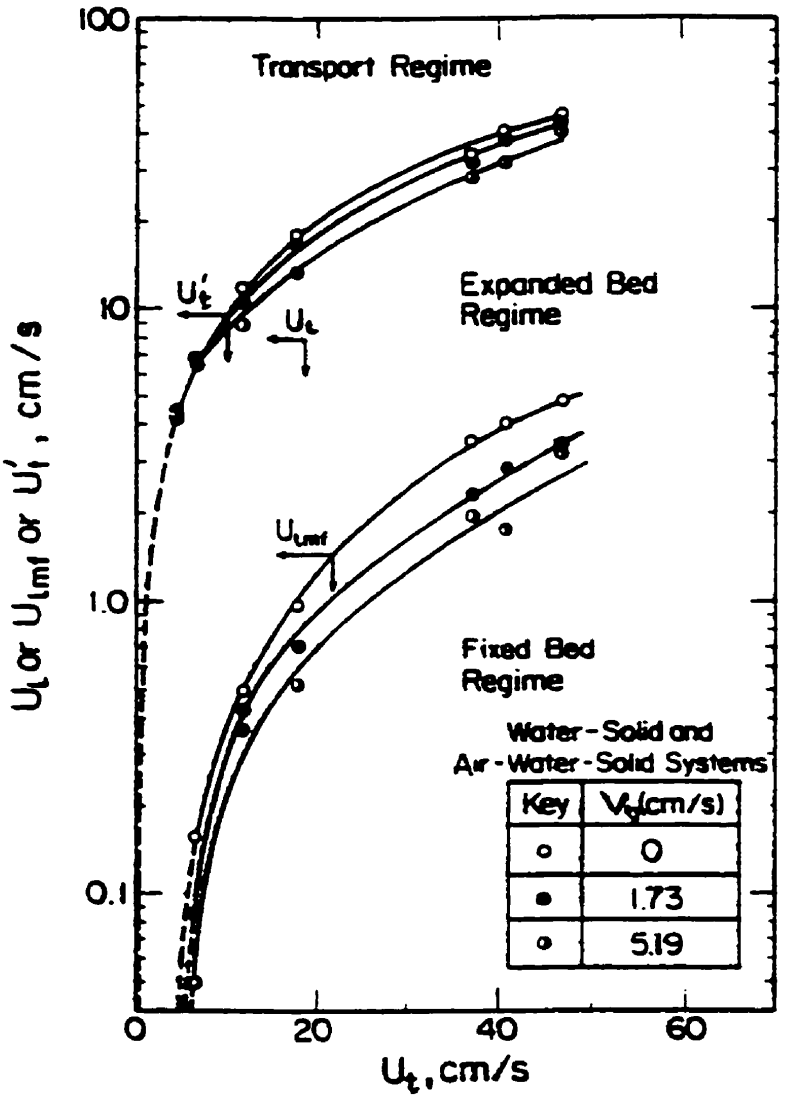

Figure 2.1 Operating regimes for cocurrent upward gas-liquid-solid systems with liquid as the continuous phase (from Fan et al., 1978a)

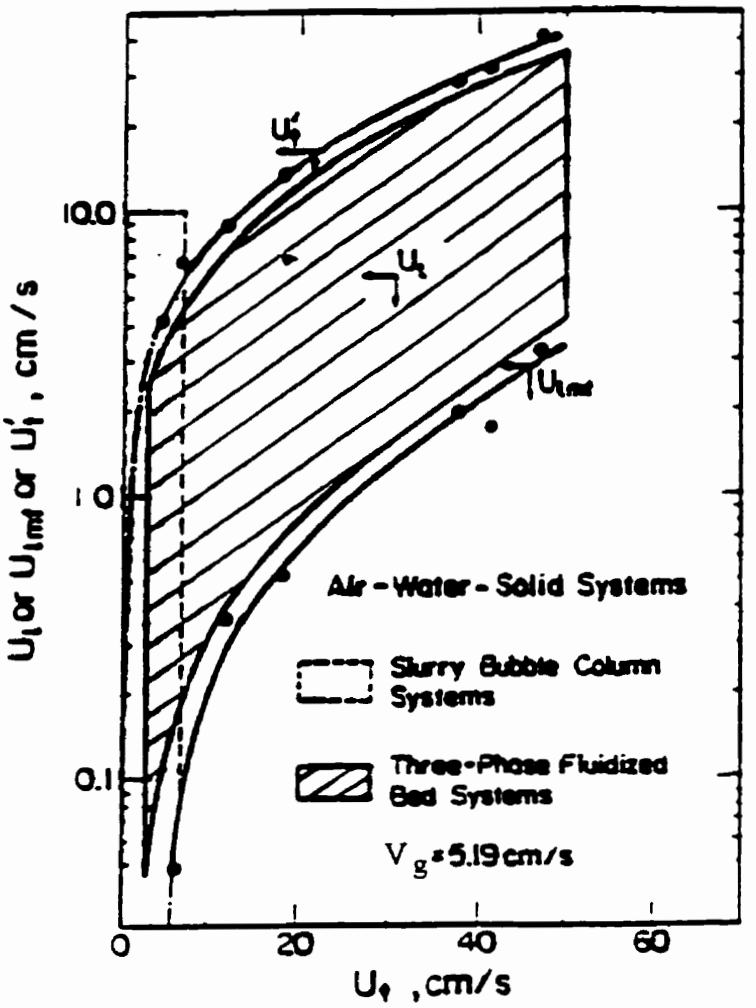

Figure 2.2 Common operating ranges for three-phase fluidized bed and slurry bubble column systems (from Fan et al., 1987a)

2.1.1 Flow Regimes in Bubble Column

The hydrodynamics and heat transfer characteristics in bubble columns depend on the nature of the flow pattern in the three phase fluidized bed and slurry bubble columns. Various flow patterns have been described with the help of flow regime maps (Figure 2.3). Researchers have outlined different criteria to differentiate the flow regimes (Darton and Harrision, 1975; Hills, 1976; Kawagoe et al., 1976; Matsuura and Fan, 1984). The flow regimes and their boundaries have often been determined based on visual observations. Three types of flow regimes have been observed in slurry bubble columns. They include dispersed bubble regime, the coalesced bubble regime and slug flow regime. For bubble columns, the terminology used for the corresponding regimes is slightly different. The dispersed bubble regime is referred to as the homogeneous or bubble flow regime and the coalesced bubble regime as the heterogeneous or churn turbulent regime.

2.1.1.1 Bubble Flow Regime

This flow regime is characterized by bubbles of relatively uniform size which are distributed over the entire cross sectional area of the column. This regime has been reported to exist at superficial gas velocities less than 0.05 m/s in batch columns (Hills, 1974; Fan, 1989). In the bubble flow regime, the gas holdup rapidly increases with an increase of superficial gas velocity. Kawagoe et al. (1976) found that the gas holdup in the bubble flow regime was increasing linearly with superficial gas velocity.

2.1.1.2 Churn Turbulent Regime

At higher gas velocities, the pseudo homogeneous dispersion of gas in liquid can no longer be maintained and an unsteady flow pattern with turbulent motion caused by the formation of larger bubbles is obtained. This heterogeneous flow regime is characterized

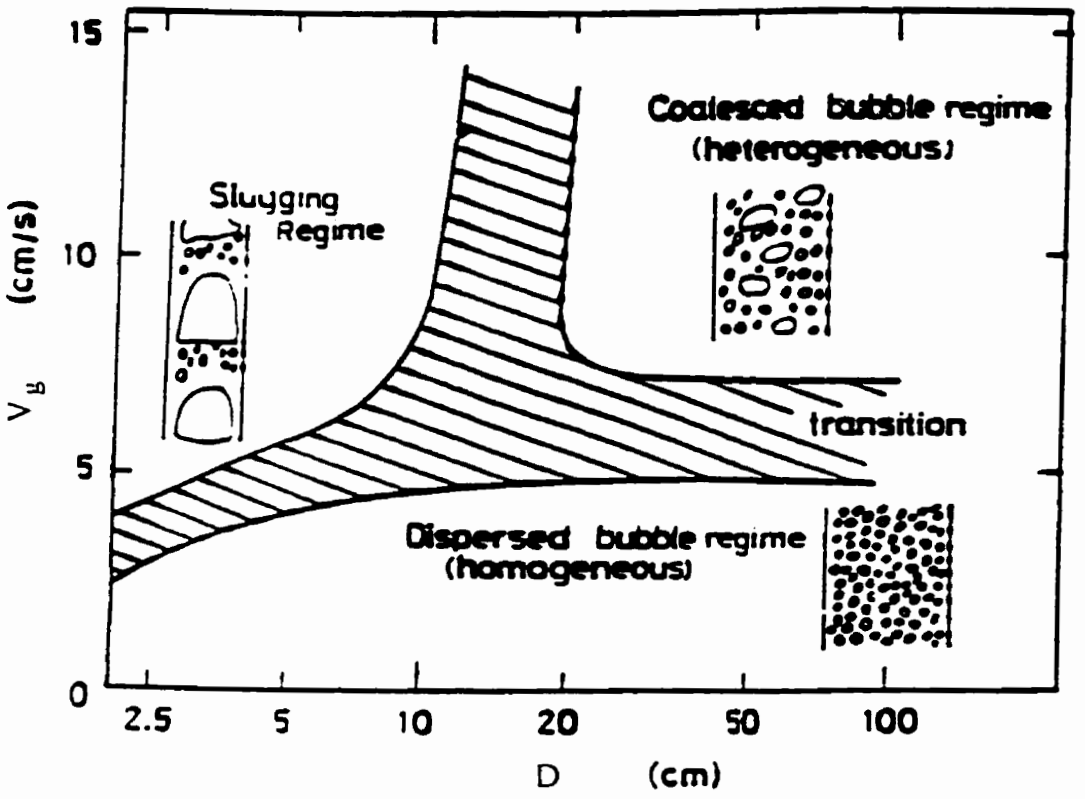

Figure 2.3 Flow regime map for a liquid-batch bubble column or a slurry-batch bubble column containing a low viscosity liquid phase
(from Deckwer et al., 1980)

by bubble coalescence and break up, resulting in a wide bubble size distribution. This flow regime has been found to exist at superficial gas velocities higher than 0.05 m/s in a batch bubble column (Hills, 1976). Matsuura and Fan (1984) reported that the coalesced bubble regime consisted of a mixture of larger and small bubbles with diameters ranging from a few millimeters to a few centimeters.

2.1.1.3 Slug Flow Regime

This regime has been observed in small diameter columns, at high gas flow rates when larger bubbles are stabilized by the column wall leading to the formation of bubble slugs. Bubble slugs have been observed in the column diameter up to 0.15 m (Hills, 1976; Miller, 1980).

2.1.2 Flow Regime Charts

Several flow regime charts have been presented in literature to identify the boundaries of various flow regimes (Shah et al., 1982; Fan et al., 1985; Muroyama and Fan, 1985). The transition from one regime to another is usually identified by visual observations which make a difficult determination of the boundaries. Deckwer et al. (1980) proposed the typical flow regime map shown in Figure 2.3 for both bubble and slurry bubble columns with a batch liquid phase.

The operating conditions for the transitions between the three regimes depend on particle size and density, gas and liquid flowrate, column diameter and liquid properties. Bukur and Daly (1987) observed the coalesced bubble regime for gas superficial velocities between 2 and 5 cm/s. Krishna et al. (1991) noted that the influence of increased pressure was to "delay" the transition to churn-turbulent regime. Wilkinson et al. (1992) reported that higher liquid viscosity promoted bubble coalescence which favored transition to the coalesced bubble regime at lower gas velocities. Higher gas density or higher pressure extended the dispersed bubble regime to higher gas velocity due to the

promotion of bubble breakup (Clark, 1990; Wilkinson and Dierendonck, 1990; Krishna et al., 1991). Kara et al. (1982) observed that an increase in solids concentration, particle size and slurry velocity resulted in early transition to coalesced bubble regime from the dispersed regime.

2.2 Phase Holdups

The phase holdup in a multiphase system is defined as the volume fraction occupied by the considered phase in the system. In a slurry bubble column, the solids holdup is almost uniformly distributed along the column height. Thus, the following expression represents phase holdups relationship:

$$\varepsilon_g + \varepsilon_l + \varepsilon_s = 1 \qquad (2.2.1)$$

The average solids holdup can be calculated using:

$$\varepsilon_s = W_s / (\rho_s A_c H_d) \qquad (2.2.2)$$

where, A_c is the cross-sectional area of the column; H_d is the height of dispersion; W_s is the mass of solids in the column.

The static pressure gradient, neglecting frictional pressure drop, is expressed by:

$$\Delta P / \Delta z = g(\varepsilon_g \rho_g + \varepsilon_l \rho_l + \varepsilon_s \rho_s) \qquad (2.2.3)$$

Equation (2.2.1) through (2.2.3) can be used to calculate individual holdups.

2.2.1 Phase Holdup Measurement Technique

Gas holdup is one of the important parameters characterizing the hydrodynamics of bubble columns (Shah et al., 1982). The following section reviews the various techniques that have been used in measuring the phase holdup. They will be grouped into two sections: overall (average) and local phase holdup.

2.2.1.1 Overall Phase Holdups

Various techniques have been used to measure average gas holdup in bubble columns and slurry bubble columns. They include

2.2.1.1.1 Phase holdup from pressure profile

2.2.1.1.2 Simultaneous Closure of Gas and Liquid Flows

2.2.1.1.3 Gas Disengagement technique

2.2.1.1.4 Gamma ray attenuation

2.2.1.1.5 Shutter plate technique

2.2.1.1.1 Phase Holdup Based on Pressure Profile

The most widely used technique in measuring phase holdups is the pressure profile method (Hikita et al., 1980; Miller, 1980; Fan et al., 1985; Reilly et al., 1986; Wachi et al., 1987; Prakash, 1991; Del Pozo, 1992; Gandhi, 1997). Pressure profile along the column height can be obtained by measuring the static pressure at two or more points along the column. This can be accomplished by using manometers or pressure transducers.

The measurement based on manometers has been proven to be very accurate at low gas velocities. The fluctuations in the manometer levels are small and accurate readings of static pressure can be obtained. However, as the gas velocity increases, larger liquid

level fluctuations in the manometers reduce the accuracy. Prakash (1991) and Gandhi (1997) inserted capillaries in the manometer lines to dampen the liquid level fluctuations. In slurry system, fine particles present another problem. The fine particles present in the system can enter the manometer lines and introduce measurement errors due to plugging.

2.2.1.1.2 Simultaneous Closure of Gas and Liquid Flows

The average gas holdup can be determined over the column height by simultaneously stopping the gas and liquid flow and measuring bed height before and after gas escape. This technique is based on the knowledge of the gas-liquid dispersion height (H_d) and static height (H_s). The volume of the gas present is equal to the difference between the dispersion height and the static bed height:

$$H_d A_c \varepsilon_g = (H_d - H_s) A_c \qquad (2.2.4)$$

and

$$\varepsilon_g = \frac{H_d - H_s}{H_d} \qquad (2.2.5)$$

In continueous bubble columns, the dispersion height is usually assumed to correspond to the column height (H_c), while in batch bubble columns, the dispersion height varies with the initial bed height. A number of researchers have used this technique to measure phase holdups in two and three phase systems (Akita and Yashida, 1973; Kato et al., 1973; Grover et al., 1986; Hatate et al., 1986; Morooka et al., 1986; Ozturk et al., 1987).

This technique is relatively simple, and able to provide a wide range of information about bubble column hydrodynamics. However, there are several errors which can reduce the accuracy of the results.

1)In batch systems, it is difficult to determine an accurate gas-liquid dispersion height when there are large fluctuations at the interface. In continuous bubble columns, it is

also inaccurate to assume a dispersion height equal to the column height because of weir effects (Prakash, 1991).

2)The design of gas and liquid sparger plays a vital role in limiting the magnitude of the errors. Some gas is capable of flowing into the column after the gas has been turned off due to higher pressure found inside the distributor before the gas is turned off. The gas velocity gradually reduces to zero as pressure equilibrates. Also, liquid may drain into the gas sparger and into the gas line (Schumpe and Grund, 1986). In continuous bubble columns, shutting off the gas promotes surface waves due to the escaping gas bubbles, resulting in some liquid entrainment out of the column.

2.2.1.1.3 Gas Disengagement Technique

The dynamic gas disengagement technique can be used to estimate the holdup structure and bubble rising velocities. The bubble size distribution affects the gas holdup, the interfacial area, and residence time distribution.

The technique was first used by Sriram and Mann (1977). It required an accurate measurement of the rate at which the level of gas-liquid dispersion dropped once the gas flow was closed. The change in gas-liquid dispersion height was originally determined by fast filming the drop after turning off the gas. The measured disengagement profile was used to estimate the holdup structure. This technique also provided information on the bubble size distribution and bubble rise velocities (Schumpe and Grund, 1986). It requires that the holdup structure remain undisturbed by bubble interactions (i.e. coalescence and breakup) after shutting off the gas (Schumpe and Grund, 1986). The resulting disengagement profile can be used to separate the contributions of smaller and larger bubbles to the gas holdup (Schumpe and Grund, 1986). However, the fluctuations in the larger bubble disengagemnet become significant, thus the averaging of repeat runs is essential.

Lee et al. (1985) applied a novel digital sensor to measure the level of dispersion height. This technique provided a more accurate measurement. A level measuring procedure was automated, which was readily interfaced with a computer to record the real time dynamic gas disengagement profile. The sensor consisted of a buoy and a light emitter-detector pair. At higher gas velocities (> 3 cm/s), the fluctuations in the buoy become significant, thus a heavier buoy and averaging of repeat runs were essential.

Daly et al. (1992) used a presure transducer to measure the rate of the liquid level drop as gas flow was closed. A pressure transducer permits the use of the gas disengagement technique in opaque systems, and they reduce the uncertainty involved in estimating the rate at which the liquid level dropped during larger bubble disengagment (Daly et al., 1992).

2.2.1.1.4 γ -ray Attenuation

The γ -ray attenuation method is a non-intrusive technique based on the attenuation of the radiation in a mixture. Lockett and Kirkpatrick (1975) applied the γ -ray attenuation technique to obtain the mean gas holdup in gas-liquid dispersion, which were in good agreement with the results by shutting off the gas and liquid flow. Vasalos et al. (1982) used the γ -ray attenuation technique to estimate the bed height, and liquid and gas holdups. Disadvantages with this technique are the requirements for elaborate handling arrangement and precautions with respect to radiation.

2.2.1.1.5 Shutter Plate Technique

Kato et al. (1985) used a shutter plate technique to obtain the phase holdups in slurry systems. The holdups of each phase was obtained by measuring the volume of trapped gas and solid particles between two shutter plates. The accuracy of this technique is greatly limited by the requirement of simutaneous and quick closure of the shutter plates.

2.2.1.2 Local Phase Holdups

Various techniques have been used to measure local gas holdup in bubble columns and in slurry bubble columns. They include

2.2.1.2.1 Electroconductivity Technique

2.2.1.2.2 Impedance Probe Technique

2.2.1.2.3 Optical Probes

2.2.1.2.4 Ultrasonic Technique

2.2.1.2.5 Laser Holography

2.2.1.2.6 Particle Image Velocimetry

2.2.1.2.1 Electroconductivity Technique

This technique, based on the electrical conductivity measurement, depends on the concentration of each phase. Some methods are based on the difference in the conductivity between the liquid phase (conductive) and the gas phase (relatively non-conductive). Different conductivity responses are given by the liquid and gas phases. This holdup measurement technique can be used to measure the cross-sectional average and local gas holdups.

The reliability of the probe for the measurement of the gas holdup can, however, be affected by the interference of the electroconductivity probe with the local hydrodynamics, especially with bubble motion. Another major limitation of this technique is that it fails to detect very small bubbles and very large bubbles that avoid the probe (Hudson, 1996).

This technique has been used in bubble coiumns, liquid-solids bed and three-phase beds (Rigby, 1970a; Turner, 1976; Sigrist et al., 1979; Hills, 1974; Ueyama et al, 1980; Marrchese et al., 1992).

Conductivity probes must be made of highly conductive material, and electrochemically stable to withstand the surrounding, conductive solution. One general disavantage of this technique is that solution has to be electroconductive. An electroconductive solution can create a harsh enviroment leading to the corrosion. The presence of salts in aqueous phase are also capable of changing the liquid coalescing properties.

2.2.1.2.2 Impedance Probe Technique

The determination of the gas holdup from electrical impedance measurements has been widely used by several researchers (Hardy and Hylton, 1984; Wolff et al., 1990). This technique, based on the electrical impedance, depends on the fraction and distribution of the phases. The impedance method provides a very rapid response but the accuracy of this technique is somewhat doubtful due to uncertainties in the data interpretation (Prakash, 1991). The main disavantage is its potential sensitivity to flow patterns. Gas bubbles may tend to swerve to avoid the probe and, depending on the flow configuration, a wide range of impedance values might be expected for a given void fraction (Prakash, 1991). Problems with noise may become predominant when cables are long.

2.2.1.2.3 Optical Probes

Optical probes detect the change in the index of reflection in the medium to provide local values of phase holdup. Several researchers have used this technique to measure phase holdup in three phase fluidized beds. Ishida and Tanaka (1980) used an optical probe in three phase beds. The probe consisted of a single optical fiber with two others connected. The single fiber was capable of projecting light and receiving its reflection. Nottenkamper et al. (1983) used a U-shape fibre optic probe to measure local gas holdup in bubble column. De Lasa et al. (1984) and Lee et al. (1984, 1987) used a silica optical fiber probe with a U-shaped tip sensor to measure the time average gas holdup and bubble characteristics. The gas holdup was determined from the summation of all gas

bubbles in contact with the probe. Yu and Kim (1988) used a U-shaped optical fiber probe to measure the gas holdup, bubble velocity, and bubble chord length.

The main advantages of this technique are useful in a non-conductive solution and fast response (less than 1 μs for a single fiber probe). The limitation of the probes are high equipment costs, poor small gas bubble detection, and their sensitivity to deposits.

2.2.1.2.4 Ultrasonic Technique

The ultrasonic technique is a relatively new technique that can be used to simultaneously measure phase holdups in three phase systems (Maezawa et al., 1993). This technique requires a transmitter to emit an ultrasonic wave that travels through a three phase system and an ultrasonic receiver located at the other end which will receive the transmitted signal. The technique uses the change in acoustic velocity and attenuation of sound wave to determine phase holdups. The acoustic velocity of the wave is generally higher in solids than in liquids which in turn is higher than in gases, therefore from the change in acoustic velocity, one can determine the makeup of the mixture. Since only a part of the wave is transmitted through the medium (the rest is reflected back or scattered by particles and bubbles), the amplitude of the wave will also be reduced. The change in amplitude (or attenuation) and acoustic velocity of a mixture depend on density, particle size and applied frequency. Warsito et al. (1995) applied the ultrasonic technique to gas-liquid and liquid-solid systems. Soong et al. (1995) and Stolojanu and Prakash (1997) applied the ultrasonic technique to three phase slurry systems to measure solids concentration.

2.2.1.2.5 Laser Holography

The laser holography technique is capable of providing the diameter, shape, and position of every gas bubble at a given time (Peterson, 1984). This technique can provide the information without interfering with the bubble motion. This technique does have some

drawbacks in that it is expensive, hard to set up, and difficult to use at higher gas velocities.

2.2.1.2.6 Particle Image Velocimetry

Particle Image Velocimetry system is capable of providing instantaneous, quantitative results on a flow plane including instantaneous velocity distributions of different phase, gas and solid holdups, bubble sizes and their distribution (Chen et al., 1994). The system can be used to measure local flow properties in 2-dimentional and 3-dimentional bubble columns and fluidized beds (Chen and Fan, 1992; Chen et al., 1994; Lin et al., 1996). The PIV system consists of schemes which identify the particle image and compute the displacement between the particle images from successive frame. The main advantage of this technique over the probe type system is its ability to operate without affecting the flow characteristics in the column. This system is not suitable for slurry systems because of the opacity of the system.

2.2.2 Effects of Operating Parameters on Phase Holdups

Studies on slurry bubble columns have shown that the gas holdup can be affected by parameters such as gas and liquid velocities, liquid physical properties, gas density and pressure, column dimeter, gas distributor, and solids concentration, size, and density.

2.2.2.1 Effects of Gas Velocity

Gas holdup in bubble columns depends mainly on superficial gas velocity (Shah et al., 1982). For bubble columns and slurry bubble columns, gas holdup has been found to increase with increasing superficial gas velocity (Kim et al., 1972; Koide et al., 1984; Fan et al. 1987; Saxena et al., 1989, 1990a). In the dispersed bubble flow regime, this increase has been found to be proportional to surperfical gas velocity (Bach and Pilhofer, 1978; Lockett and Kirkpatrick, 1975; Kara et al., 1982). For coalesced bubble regime,

the effect of superficial gas velocity on gas holdup is less pronounced (Kara et al., 1982; Koid et al., 1984). Ying et al. (1980) found that at lower gas velocities (Vg < 0.03 m/s), the existence of solids did not change the gas holdup. However, Sauer and Hempel (1987) observed that the presence of small light particles (dendity < 1300 kg/m3) at low gas velocity (Vg < 0.04 m/s) produced smaller bubbles and consequently higher gas holdup. Wolff et al. (1990) also reported higher gas holdup at low gas velocity and low solids concentration. Some researchers (Sauer and Hempel, 1987; Wolff et al., 1990) reported that high superficial gas velocity, higher solids concentrations and particle densities resulted in larger bubbles and consequently lower gas holdup.

The relation between the gas holdup and gas velocity is generally of the form:

$$\varepsilon_g = c V_g^{\,n} \qquad (2.2.6)$$

where, c and n are empirical constants, obtained from experimental data. The value of n depends on the flow regime (Shah et al., 1982). For the dispersed flow regime, n varies from 0.7 to 1.2 (Bach and Pilhofer, 1978; Deckwer et al., 1980; Ozturk et al., 1987). In the churn turbulent regime, the exponent n takes values from 0.4 to 0.7.

The shapes of radial gas holdup profiles are also influenced by gas flowrate. At low gas velocities, the gas holdup is almost independent of the radius, with only a slight decrease near the wall (Nottenkaemper et al., 1983). Hills (1974) observed that the radial profile of gas holdup was relatively flat gas velocities below 0.03 m/s. With increasing gas velocity, the profile of local gas holdups showed a parabolic shape and a sharp maximum at the center. Wachi et al. (1987) observed the gas holdup to be 10% to 20% lower at the column wall than at the center. Lin et al. (1996) also reported the same conclusions using the particle image velocimetry technique.

2.2.2.2 Effects of Liquid Velocity

Bukur et al. (1989, 1990) studied the effect of the operating mode on the gas holdup. They used two types of solids (iron oxide and silica) in two size ranges(0 to 5 μm and 20 to 44 μm), with solids concentrations of 0 to 30 wt%. Nitrogen was used as gas phase and superficial gas velocity was varied from 0.02 to 0.12 m/s. Hydrotreated reactor wax (FT-300 paraffin) and SASOL wax were used as the liquid phase. They observed that even a small upward liquid flow (0.005 m/s) lowers gas holdup significantly; however, a further increase of liquid flow had a marginal effect on the gas holdup. It appears that the difference between the batch and continuous modes of operation are due to changes in the foaming characteristics of the medium. For the batch case , the foam accumulates at the top of the dispersion and increases the gas holdup, whereas in the continuous mode the foam is removed by the recirculating slurry. These results were confirmed by Pino et al. (1990a, 1990b) who found that the operating mode strongly affects the gas holdup of foaming systems. They also found that an increase in liquid velocity (0 to 3.21 cm/s) in foaming systems resulted in a decrease in gas holdup and then, as liquid velocity increased, gas holdup went through a minimum and then increased again. They did not observe any influence of liquid velocity on the gas holdup for non-foaming systems.

Results obtained in the continuous mode of operation by other researchsers indicated that liquid velocity either has no effect on the average gas holdup (Shah et al., 1982; Kelkar et al., 1984; Ying et al., 1980) or decreases the gas holdup slightly (Kara et al., 1982; Kelkar et al., 1984). This was also confirmed by Wilkinson et al. (1992). According to Kellar et al. (1984), the effect of slurry velocity on the gas holdup was more pronounced at lower gas velocity where bubbling flow regime prevailed. However, it should be noted that most previous studies were conducted with a liquid without a tendency to foam. In the case of foaming systems, the method used to measure the gas holdup is important.

2.2.2.3 Effect of Liquid Physical Properties

The effect of liquid properties on the gas holdup is related to the bubble formation and/or coalescing tendencies. An increase in liquid viscosity results in larger bubbles and thus higher bubble rising velocities and lower gas holdup.

Adding a small amount of a surface acting material (surfacant) to water, such as a short chain alcohol, produced significantly higher gas holdup (Kelkar et al., 1983). The presence of electrolyte or impurities also leads to a higher gas holdup (Hikita et al., 1980; Kelkar et al., 1984; Morooka et al., 1986; Sada et al., 1986a). Sada et al. (1986a) also noted that the presence of suspended solids particles has a much smaller influence on gas holdup in electrolyte solutions than in non-electrolyte solutions. The gas holdup increased with increasing liquid density according to Akita and Yoshitda (1973), Hikita et al. (1980) and Bach and Pilhofer (1978).

2.2.2.4 Effects of Gas Density and Pressure

Studies have shown that gas holdup in bubble volumes generally increases with increasing operating pressure or gas density (Idogawa et al., 1987; Clark, 1990; Krishna et al., 1991, 1994). In solid-free bubble columns, several equations have been developed based on high pressure operation (Idogawa et al., 1986, 1987) or experiments using various gases (Reilly et al., 1986). The effect of pressure due to bed height on gas holdup is negligibly small, compared with that from external pressure.

2.2.2.5 Effect of Column Diameter

Saxena et al. (1990a) showed that the gas holdup is not highly dependent on column diameter when the column diameter is larger than 0.10 m. Pino et al. (1992) also studied the effect of column diameters (0.1m and 0.29 m) on gas holdup in slurry bubble

columns using a foaming liquid (kerosene). They found that both column height and diameter do not affect the gas holdup in three phase systems at high gas velocities when foaming occurs.

2.2.2.6 Effect of Gas Distributor Design

Gas holdup has been found to be strongly affected by type of gas distributor, especially for gas velocities below 0.06 m/s (Yamashita and Inoue, 1975; Oels et al., 1978). Yamashita and Inoue (1975) found a maximum in gas holdup as a function of hole size. They found that two distinct types of regimes could be observed when hole sizes were less than 1 mm. At low gas velocity(<0.06 m/s), gas holdup increased linearly with gas velocity, corresponding to the dispersed flow regime. At higher gas velocity, there was significant deviation from linearity. They also found that the gas holdup depended on the number, pitch and diameter of orifice holes. For orifice diameters greater than 1.0 mm, the effect of orifice diameter became insignificant (Yamashita and Inoue, 1975).

2.2.2.7 Effect of Particle Size

A number of researchers have investigated the effects of particle size and concentration on gas holdup (Kato et al., 1973; Kara et al., 1982; Sada et al., 1986a; Morooka et al., 1986). The influence of particle size has benn found to depend on a number of factors including flow regime, gas velocity, liquid properties and slurry concentration. Khare and Joshi (1990) found gas holdup to increase with particle size up to 67 μm at low solids loading (< 10 vol.%). The increase in gas holdup was more significant for spargers generating fine bubbles at low gas velocities. For larger particles (> 70μm), Khare and Joshi (1990) observed gas holdup to decrease with particle size. The results of Khare and Joshi (1990) can be compared with those of Sada et al. (1986a) who also observed an increase in gas holdup with 3 μm alumina particles using low solids loadings (0.1 wt%) and a porous plate distributor. However, no increase of gas holdup was observed when a perforated plate was used for gas distribution. In dilute suspension (< 1 vol.%), Pandit

and Joshi (1984) observed a slight increase in gas holdup for very fine particles (< 50 μm), followed by a decrease for medium size particles (50-350 μm) followed by another increase for larger size particles (> 350 μm). Their results were not representive of higher slurry concentrations. Saxena et al. (1992b) also concluded that the effect of particle size is more pronounced for low concentration slurry systems.

Kara et al. (1982) did not observe significant differences of gas holdup between gas-liquid and gas-liquid-solid system when 10 μm size particles were used at the slurry concentration of 9-18 vol.%. They observed, however, that an increase in solid size (up to 70 μm) for slurry concentrations of about 10 vol.% decreased the gas holdup. Kato et al. (1973) also observed this using higher solids concentrations and particle size from 60-175 μm, as did Morooka et al. (1986).

Kelkar et al. (1984) tested solids wettability and found that wettability played an important role in enhanceing the bubble coalescence tendencies in the liquid phase, thereby reducing gas holdup.

2.2.2.8 Effect of Slurry Concentration

Most literature studies have been conducted in the slurry concentration ranges below 20 vol.% solids. Several researchers concluded that an increase in solids concentration generally reduced the gas holdup (Kato et al., 1973; Deckwer et al., 1980; Kara et al., 1982; Koid et al., 1984; Pandit and Joshi, 1984; Sada et al., 1986; Yasunishi et al., 1986; Nigam and Schumpe, 1987; Sauer and Hempel, 1987; Ying et al., 1980; Clark, 1990). For low solids loading (< 5 vol.%), the behavior of the slurry bubble column is close to that of solid-free bubble column (Sada et al., 1986; Sauer and Hempel, 1987; Wolff et al., 1990). Kato et al. (1973) found that this effect becomes significant at high gas velocities (> 0.10 - 0.20 m/s). Kara et al. (1982) found the strong dependence of gas holdup on solids concentration at low solids concentrations.

Krishna et al. (1997) observed gas holdups of small and larger bubbles. They concluded that the holdup of small bubbles in the heterogeneous regime of operation was reduced with increasing slurry concentrations and the gas holdup of large bubbles was virtually independent of slurry concentrations. The total gas holdup was decreased with slurry concentrations.

2.2.2.9 Conclusion and Recommendation

Generally, the gas holdup increases with increasing gas velocity and operating pressure (or gas density). Gas holdup decreases with increasing liquid viscosity and solids concentration.

Variation of the gas holdup with liquid velocity depends on operation modes. Liquid velocity has no effect on gas holdup in continuous mode. In operating mode switching from batch mode to continuous mode, the gas holdup decreases with increasing liquid velocity due to reduced foam layers.

At low gas velocity, gas holdup depends on the number, pitch and diameter of orifice holes. For orifice diameters larger than 1.0 mm, the effect of orifice diameter become insignificant.

Systematic studies are required to further investigate the effect of column diameters on gas holdups in three phase systems.

2.2.3 Correlations for Gas Holdup

2.2.3.1 Bubble Columns

Hughmark (1967) used a wide range of operating parameters to develop the following correlation for average gas holdup in a bubble column:

$$\varepsilon_g = \frac{V_g}{2V_g + 0.35(\sigma_l \rho_l / 72)^{1/3}} \qquad (2.2.7)$$

This correlation was valid in column diameter from 0.025 m to 1.1 m; gas velocities from 0.004 m/s to 0.45 m/s; and liquid density from 780 kg/m^3 to 1700 kg/m^3. Although this correlation does account for liquid physical properties, the effects of gas physical properties and column diameter have been neglected.

Akita and Yoshida (1973) also used a wide range of conditions to propose following empirical equation:

$$\frac{\varepsilon_g}{(1-\varepsilon_g)^4} = a\left(\frac{gD^2\rho_l}{\sigma_l}\right)^{1/8}\left(\frac{gD_c^3}{\nu_l}\right)^{1/12}\left(\frac{V_g}{\sqrt{gD}}\right) \qquad (2.2.8)$$

where. the value of a was 0.2 for pure liquid and non-electrolyte solutions and 0.25 for electrolyte solutions. This correlation was applied for column diameter from 0.152 m to 0.6 m; gas velocities from 0.006 m/s to 0.42 m/s; and liquid density from 790 kg/m^3 to 1590 kg/m^3.

Hikita et al. (1980) recorded gas holdup measurements in a 0.10 m diameter column using various gases and liquids. They proposed following correlation:

$$\varepsilon_g = 0.672 f_l \left(\frac{V_g \mu_l}{\sigma_l}\right)^{0.578} \left(\frac{\mu_l^4 g}{\rho_l \sigma_l^2}\right)^{-0.131} \left(\frac{\rho_g}{\rho_l}\right)^{0.062} \left(\frac{\mu_g}{\mu_l}\right)^{0.107} \qquad (2.2.9)$$

where, f_l was a function of the ionic strength and has a value of 1 for non-electrolyte solutions and salt solutions. This correlation is valid for gas velocities from 0.004 m/s to 0.38 m/s and liquid density from 790 to 1170 kg/m^3.

Krishna et al. (1991) proposed a gas holdup model based on two bubble classes. They proposed that the gas holdup consisted of small bubbles and larger bubbles. This correlation was further developed by Wilkinson et al. (1992) and generalized to incorporate the effects of both gas and liquid phisical properties. Nitrogen was used as the gas phase along with different liquids. The correlation was expressed as:

$$\varepsilon_g = \frac{U_{trans}}{U_{s.b.}} + \frac{V_g - U_{trans}}{U_{l.b.}} \qquad (2.2.10)$$

where $U_{s.b.}$ and $U_{l.b.}$ were bubble rising velocities of smaller and larger bubbles. U_{trans} was the velocity at which the transition from dispersion flow regime to churn turbulent regime takes place. $U_{s.b.}$, $U_{l.b.}$ and U_{trans} can be obtained as follows:

$$\frac{U_{s.b.}\mu_l}{\sigma_l} = 2.25 \left(\frac{\sigma_l^3 \rho_l}{g \mu_l^4}\right)^{-0.273} \left(\frac{\rho_l}{\rho_g}\right)^{0.03} \qquad (2.2.11)$$

$$\frac{U_{l.b.}\mu_l}{\sigma_l} = \frac{U_{s.b.}\mu_l}{\sigma_l} + 2.4 \left(\frac{\mu_l (V_g - U_{trans})}{\sigma_l}\right)^{0.757} \left(\frac{\sigma_l^3 \rho_l}{g \mu_l^4}\right)^{-0.077} \left(\frac{\rho_l}{\rho_g}\right)^{0.077} \qquad (2.2.12)$$

$$\frac{U_{trans}}{U_{s.b.}} = 0.5 \exp\left(-193 \rho_g^{-0.61} \mu_l^{0.5} \sigma_l^{0.11}\right) \qquad (2.2.13)$$

Correlations of Akita and Yoshida (1973) and Hikita et al. (1980) have been obtained over a wide range of operating conditions. These correlations should give reasonable

estimates of gas holdups in bubble columns operting at low pressure. For high pressure operations the correlation by Krishna et al. (1991) is recommended.

2.2.3.2 Slurry Bubble Column

For systems with low solids concentration (< 10 vol.%), Smith et al. (1984) proposed the following correlation:

$$\varepsilon_g = \frac{V_g}{2.25 V_g + 0.339(\sigma_l \rho_{sl} / 72)^{0.31} \mu_{sl}^{0.016}} \qquad (2.2.14)$$

where,

$$\mu_{sl} = \mu_l \exp\{(5/3)\phi_s / (1-\phi_s)\}$$

The correlation was based on experimental results in a 0.108 m diameter with varying gas velocities from 0.03 m/s to 0.20 m/s and liquid densities from 820 kg/m^3 to 1100 kg/m^3. This correlation dose not take account for larger column diameter.

Kara et al. (1982) proposed the following correlation based on cocurrent up flow of gas and slurry phase:

$$\varepsilon_g = \frac{Re_g}{A_1 + B_1 Re_g + C_1 Re_{sl} + D_1(\varepsilon_s / (\varepsilon_s + \varepsilon_l))} \qquad (2.2.15)$$

where, parameters A_1, B_1, C_1, D_1 depended on particle size from 0 to 70 μm (Kara et al. 1982). This correlation was applied for gas velocities from 0.03 m/s to 0.30 m/s, slurry flowrate from 0 to 0.10 m/s, slurry concentration from 0 to 40 wt%, solid density of around 1.3 kg/m^3.

Koide et al. (1984) worked with air, various aqueous solution, and glass and bronze spheres to develop the following correlation:

$$\frac{\varepsilon_g}{\left(1-\varepsilon_g\right)^4}=\frac{k_1\left(V_g\mu_l/\sigma_l\right)^{0.918}\left(g\mu_l^4/\left(\rho_l\sigma_l^3\right)\right)^{-0.252}}{1+4.35\phi_s^{0.748}\left[\left(\rho_s-\rho_l\right)/\rho_l\right]^{0.88}\left(DV_g/\rho_l\right)^{-0.168}} \quad (2.2.16)$$

where, k_1 is 0.227 for water and aqueous solutions of glycerol and glycol and 0.364 for inorganic electrolyte solutions. Particle concentrations between 0 and 12 vol.% were used with particle sizes from 48 μm to 200 μm. Gas velocities were from 0.01 m/s to 0.18 m/s.

Sada et al. (1986) proposed following correlation for fine solids suspension:

$$\frac{\varepsilon_g}{\left(1-\varepsilon_g\right)^3}=0.019\,U_t^{1/16}\phi_s^{-0.125U_t^{-0.16}}V_g \quad (2.2.17)$$

where, U_t was particle terminal velocity. The experiments were carried out in small column of 0.078 m diameter. Gas velocity was from 0.02 m/s to 0.20 m/s. Solids concentration from 0 to 10 vol.%.

Sauer and Hempel (1987) proposed following correlation:

$$\frac{\varepsilon_g}{1-\varepsilon_g}=c_1\left(\frac{V_g}{\left(\nu_{sl}gV_g\right)^{0.25}}\right)^{c_2}\left(\frac{\nu_{sl}}{\nu_{eff,rad}}\right)^{c_3}\left(\frac{C_s}{C_{so}}\right)^{c_4} \quad (2.2.18)$$

where, c_1-c_4 were constants depended on distributor type; ν_{sl} was the effective kinematic slurry viscosity; $\nu_{eff,rad}$ was effective radial momentum transfer coefficient. ν_{sl} and $\nu_{eff,rad}$ can be calculated as follows:

$$\nu_{sl}=\frac{\mu_l\left(1+2.5\phi_s+10.05\phi_s^2+0.00273\exp(16.6\phi_s)\right)}{\phi_s\rho_s+(1-\phi_s)\rho_l}$$

$$\nu_{eff,rad}=0.011D_c\sqrt{gD}\left(V_g^3/\nu_l g\right)^{0.125}$$

This correlation was valid for particle diameter from 110 um to 2900 um, particle density from 1020 to 2780 kg/m^3, solid concentration from 0 to 20 vol.%.

2.2.3.3 Gas Holdup based on Drift Flux

The drift flux is generally defined as the volumetric flux of gas relative to a surface moving with the average velocity of the dispersion (Nicklin, 1962; Darton and Harrison, 1975; Fan, 1989; Saxena and Chen, 1994). According to this concept, for a general three phase system, the gas holdup can be expressed (Pandit and Joshi, 1984; Smith et al., 1984; O'Dowd et al., 1987; Saxena et al., 1992; Saxena and Chen, 1994):

$$\varepsilon_g = \frac{V_g}{c_1 + c_2 V_g} \tag{2.2.19}$$

where c_1 and c_2 were constant. Smith et al. (1984) and O'Dowd et al. (1987) estimated c_2 to be 2.0. Pandit and Joshi (1984) found c_2 to be 2.0 to 2.8. Saxena and Chen (1994) calculated c_2 to be 2.5. Other researchers (Nicklin, 1962; Hill, 1976) observed c_2 to be close to 1. Generally, c_1 has been identified as the characteristic terminal rise velocity ($V_{b\infty}$). Pandit and Joshi (1984) found $U_{b\infty}$ to vary from 0.22 to 0.55 m/s. O'Dowd et al. (1987) found $U_{b\infty}$ to range between 0.36 and 0.50 m/s. Saxena and Chen (1994) analyzed previous studies to develop the following correlation for $V_{b\infty}$:

$$V_{b\infty} = 1.80 C(P_v)(\sigma_l \rho_{sl} / 72)^{0.333} \mu_{sl}^{0.289} \tag{2.2.20}$$

here, $C(P_v)$ is the pressure corresponding to the midpoint of the dispersion in the column.

2.3 Bubbles and Bubble Wake Properties

2.3.1 Bubble Size Measurement

It is important to characterize bubble properties since mass and heat transfer behavior and mixing are dependent on the bubble size and velocity distributions. The commonly used techniques for determining bubble properties are:

1) Photographic Method;
2) Dynamic Gas Disengagement;
3) Two Electrode Conductivity Probe;
4) Optical Probe.

2.3.1.1 Photographic Method

The photographic method has been widely used by a number of researchers (Stewart and Davidson, 1964; Rigby and Capes, 1970; Akita and Yoshida, 1974; Tsuchiya and Fan, 1986; Tzeng et al., 1993; Chen et al., 1994). It can be used in either two-dimensional or three dimensional columns. In two dimensional column, liquid-solid phase was accommodated between two transparent plates. Movie photographs were taken with high speed camera to film bubble and its wake passage. In three dimensional column, curvature effect can be reduced by arranging a rectangular box around test section which is filled with column liquid. The advantage of this technique is that the bubble properties and structure of bubble wake can be directly observed. This technique, however, is very time consuming and is limited to the measurement near the column wall.

2.3.1.2 Dynamic Gas Disengagement Technique

This technique requires an accurate measurement of the rate at which the level of gas-liquid dispersion dropped once the gas has been shut-off. The rate at which the height

drops would depend on the concentration and velocity of the gas bubbles in the dispersion. This technique has been used to obtain the holdups and rise velocities of larger and smaller bubbles (Schump et al., 1985; Idogawa et al., 1986, 1987; Daly et al., 1990).

2.3.1.3 Electroconductivity Technique

This method uses the difference in conductivity between the liquid and the gas phases. The resistance of water is much lower than that of air bubbles. The probe, consisting of two electrodes and separated by a small distance, can detect the presence of a gas bubble from the resulting high electrical resistance when the gas bubble meets with the probe and spans the distance between the electrodes. The time during which the resistance reains high is representative of the bubble size. The bubble size can be estimated if the bubble velocity is known, which can be obtained by using two probes. This technique was further developed and improved to measure the bubble diameter, velocity and frequency (Hill, 1974; Yamashita et al., 1979; Ueyama et al., 1980; Buchholz et al., 1981). This technique was also applied for gas holdup measurement (see 2.2.1.2.1).

The use of a probe may interfere with the bubble flow due to a poor probe design and the orientation of the probe in the column. Also due to limitations in the probe design, some probes cannot detect small bubbles of diameters less than 1mm (Hudson, 1996). Wachi et al. (1987) found that the probe technique failed to detect 30 % of the gas holdup.

Main problems in determining bubble velocity are that any error in bubble velocity will affect the calculated bubble diameter and bubbles will be slowed down by their collision with the probe (Hudson, 1996).

2.3.1.4 Optical Probes

In this technique, a light source sends a beam of light through the dispersion, and the transmitted, reflected, or scattered light is analyzed by a photocell, camera or some other electronic detector. This technique was developed to measure the bubble rise velocity (Weiland et al., 1980; Saxena et al., 1988; Genenger and Lohrengel, 1992). This technique was also applied to measure gas holdup (see 2.2.1.2.3).

2.3.2 Bubble Size and Bubble Rising Velocity

The average bubble size in a bubble column has been found to be affected by gas velocity, liquid properties, gas distribution, operating pressure and column diameter.

Some researchers have reported a decrease in bubble size with increasing gas flowrates (Akita and Yoshida, 1974). Ueyama et al. (1980) and Fukuma et al. (1986) observed that the average bubble size gradually increased with gas velocity. Both used dual-electroresistivity probe and multi-nozzle as the distributor. They explained that Akita and Yoshida (1974) obtained results photographically near the wall and by using single orifice as the gas distributor. Idogawa et al. (1986, 1987) obtained cross-sectional average bubble size in perforated plate and found that the average bubble size was almost independent of gas velocity. The different tendency of the average bubble size from different researchers could be explained by differences in distributor design, column diameter and range of gas velocity studied.

The average bubble size has been observed to derease with decreasing surface tension of liquid (Akita and Yoshida, 1974; Idogawa, 1987). and increase with increasing liquid viscosity (Bhavaraju et al., 1978).

At low operating pressures, average bubble size was observed to depend on the distributor type (Idogawa et al., 1986). Lower average bubble size was obtained with a porous distributor as compared to a single nozzle sparger. The difference disappeared with increasing operating pressure.

Koide et al. (1979) and Ueyama et al. (1980) measured average bubble size in column diameters of 5.5 and 0.6 m. Their results indicated that a higher average bubble size was obtained in the column of larger diameter.

Yu and Kim (1988) observed that bubble chord length in the column center was higher than that near the wall.

The rise velocities of a single gas bubble depends on its size. For small bubbles, the rise velosity is affected by liquid properties such as surface tension and viscosity. For larger bubbles, the rise velocity is insensitive to liquid properties, and can be predicted by Davies-Taylor relationship for spherical-cap bubbles in inviscid liquids. Peel and Garber (1953) found that for very large bubbles with a spherical cap shape, both viscosity and surface tension did not affect bubble rise velocity for various liquids. Henriken and Ostergaard (1974) and Wallis (1974) found that for large single bubbles in two-dimensional column, the bubble rise velocity could be successfully correlated by a Davies-Taylor type relationship. Wallis (1974) and Jamialahmadi et al. (1994) have proposed correlations for predicting terminal rise velocities of small bubbles and large bubbles at different bubble sizes.

In multi-bubble systems, the bubble rise velocity follows a log-normal distribution (Fan, 1989). Several investigators have related the bubble rise velocity in multi-bubble system to the bubble size. Fan (1989) has tabulated and reviewed various correlations for bubble rise velocities in multi-bubble systems.

2.3.3 Bubble Wake Structure

The bubble wake has been recognized as a key factor in explaining various phenomena occuring in three-phase fluidized beds such as solids mixing, particle entrainment and heat transfer (Fan, 1989; Kumar et al., 1992). The bubble wake structure has been directly observed by photographic techniques (Stewart and Davidson, 1964; Rigby and Capes, 1970; Tsuchiya and Fan, 1986).

In gas-liquid systems, the wake geometry has been grouped into closed laminar/toroidal wake and open or closed turbulent wakes (Coppus et al., 1977). Bubble wakes in three phase fluidized beds may be different from those in gas-liquid system. However, in beds of fine particles a resemblance should exist in the wake structure with gas-liquid systems.

Laminar wakes have been observed behind large spherical-cap bubbles rising in viscous liquid or behind the corresponding circular-cap bubbles in narrow two-dimensional bed. The closed laminar wake is hydrodynamically stable, consists of a well-defined boundary and a toroidal vortex ring inside, and exchanges no liquid with the external flow (Coppus et al., 1977; Bhaga and Weber, 1981). The stability of the closed laminar wake is due to viscous and/or wall effects. Increasing Reynolds number by decreasing liquid viscosity at a constant bubble volume made wake flow less stable and it started shedding vortices (Bhaga and Weber, 1981). The smaller the gap between two plates of two dimensional system, the more stablized the wake flow (Crabtree and Bridgwater, 1967).

Turbulent wakes have been visualized behind large bubbles rising in low viscosity liquids. There is considerable disagreement among researchers(Maxworthy, 1967; Coppus et al., 1977; Slaughter and Wraith, 1968). While some of them observed an open turbulent wake (Maxworthy, 1967; Slaughter and Wraith, 1968), others observed a closed turbulent wake structure (Davies and Taylor, 1950; Coppus et al., 1977).

An open geometry of turbulent wakes seems to be a more accurate description of the phenomenon. As discussed in literature (Maxworthy, 1967), a turbulent wake cannot be confined to a completely closed region due to the momentum defect in the liquid following the passage of the bubble.

Using photography, Tsuchiya and Fan (1988) studied the wake flow of a bubble rising in a liquid (water)-solid (774 μ m glass beads) fluidized bed. The internal structure of bubble wake was characterized by the dynamic behavior of vortices, (Figure 2.4). As shown in Figure 2.4, the region included two growing vortices. One was represented by a well-established circulation (right side) and the other was being formed (left side). This region, denoted as primary wake, had nearly the same rise velocity as the bubble, and was suggested to play a primary role in hydrodynamic/ transport phenomena. The region beneath the primary wake, denoted as secondary wake, included shed vortices. It was also observed that solids concentration was lower immediately beneath the bubble base and around a vortex center, and higher solids concentration occurred around the vortices, especially in the regions where the two vortices interacted. The solids concentration in a vortex center would be reduced due to the centrifugal force generated by circulating flow.

2.3.4 The Ratio of Wake Volume to Bubble Volume

The ratio of wake volume to bubble volume is usually given by a dimensionless parameter, k:

$$k = \varepsilon_w / \varepsilon_g \qquad (2.3.1)$$

when solid particles are considered not to be present in the bubble wake, the parameter k_0 is used in place of of k. Some correlations for parameters k and k_0 are listed in Table 2.3.1. These empirical correlations were generally in agreement: k_0 increased with V_l to

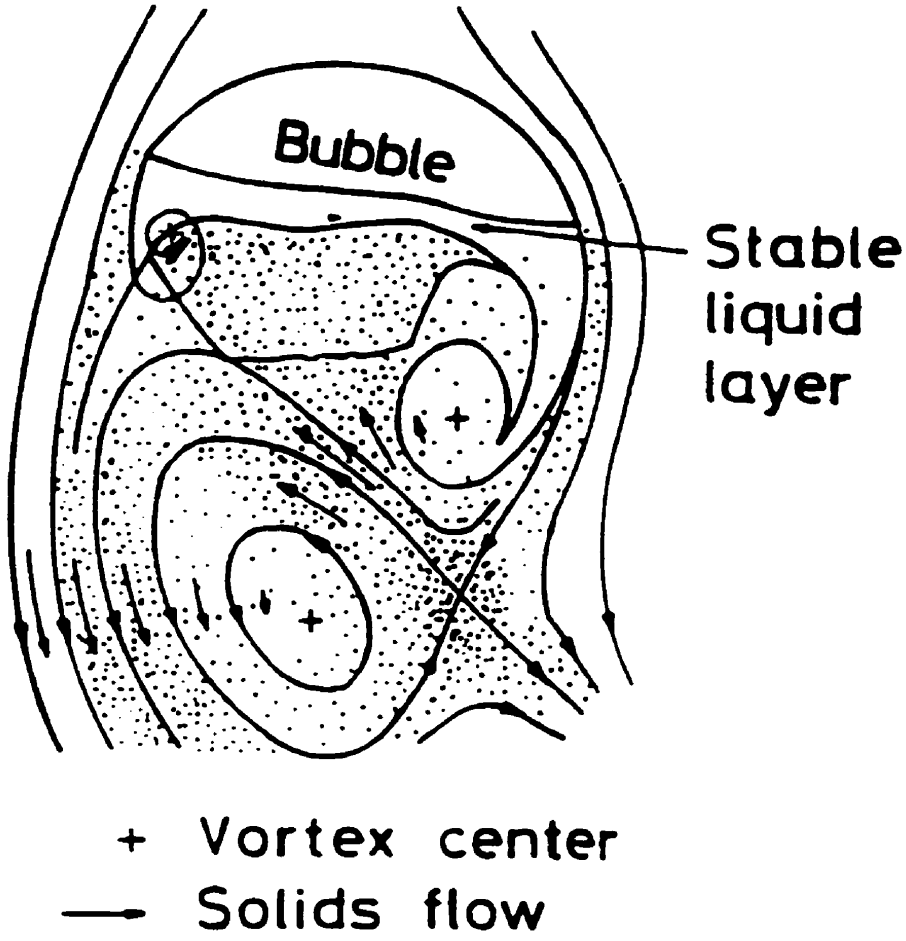

Figure 2.4 Schematic interpretation of the wake flow for bubble rising in a water-glass bead (774 μm) fluidized bed (from Tsuchiya and Fan, 1988)

the power of 0.2 - 1.0 and decreased with V_g to the power of 0.6 - 0.7. The correlations proposed by Bhatia and Epstein (1974) and Baker et al. (1977) are commonly recommended.

Table 2.3.1 Correlations of phase holdups based on the wake models

Investigators	Correlations	Assumed x
Efremov & Vakhrushev (1970)	$k=5.1\,\varepsilon_0^{4.85}\left[1-\tanh\left(\frac{40V_g\varepsilon_0^{10}}{V_l}-3.32\varepsilon_0^{5.45}\right)\right]$	x=0
Bhatia & Epstein (1974)	$k=\left(0.61+\frac{0.037}{\varepsilon_g+0.013}\right)(1-\varepsilon_s)^3$	0<x<1
Darton & Harrison (1975)	$k=1.4\left(V_l/V_g\right)^{0.33}-1$	x=0
Baker et al. (1977)	$k=1.617\left(V_l/V_g\right)^{0.610}\sigma^{-0.654}$	x=0

The solids holdup in bubble wakes is characterized by dimensionless parameter, x. This parameter is defined as the ratio of average solid holdup in the wake region (ε_{sw}) to that in liquid-solid fluidized region (ε_{sf}):

$$x=\varepsilon_{sw}/\varepsilon_{sf} \qquad (2.3.2)$$

In most cases, x is restricted to values between 0 and 1. El-Temtamy and Epstein (1978) presented an empirical correlation for x (see Table 2.3.1).

Kitano and Fan (1988) computed the average solids holdup within the primary wake region based on the experimental observation. They found that ε_{sw} was constant around 0.42 regardless of bubble size, particle properties, and liquid velocity. Their founding indicates that the solids holdup inside the primary wake is determined by the fluid mechanic properties. Kitano and Fan (1988) proposed a simple correlation for x:

$$x=0.42/\varepsilon_{sf}, \qquad 0.25<\varepsilon_{sf}<0.52 \qquad (2.3.3)$$

2.4 Liquid Backmixing and Solids Distribution

2.4.1 Liquid Backmixing

Liquid backmixing in three phase fluidized beds has been measured by the following techniques:

-imperfect tracer pulse method (Ostergaard and Michelsen, 1969)

-continuous injection of colored tracer (Kim et al., 1972)

-pulse of saline tracer (Kim and Kim, 1983; Morooka et al., 1986)

-continuous injection of saline tracer (El-Temtamy et al., 1979)

The axial dispersion coefficient is obtained from the residence time distribution data as measured with these techniques.

Liquid backmixing was generally found to increase with an increase in gas velocity (Ostergaard and Michelsen, 1969; Kim et al., 1972; Kim and Kim, 1983; Morooka, 1986).

The effect of liquid velocity on liquid dispersion has been found to vary with the bed particle size. Tha axial dispersion coefficient was generally found to increase with increasing liquid velocity in the beds of particles ranging from about 1.0 mm to 6.0 mm in diameter(El-Temtamy et al., 1979; Kim and Kim, 1983). For the beds of 0.45 mm particles, El-Temtamy et al. (1979) found that the axial dispersion coefficient decreased with increasing liquid velocity.

Ostergaard and Michelsen (1969) found that the beds of 0.25 and 1.0 mm particles were characterized by a high degree of backmixing while beds of 6 mm glass beads were characterized by very low degree of backmixing.

The liquid axial dispersion has been found to increase with column diameter (Kim and Kim, 1983).

The effect of liquid viscosity on liquid mixing was studied by Kim and Kim (1983). In a bed of 6 mm particles, axial mixing generally increased with increasing liquid viscosity. In beds of 1.7 and 3.0 mm particles, axial mixing increases with liquid viscosity at low gas velocity (< 0.01 m/s) and decreased at higher gas velocity.

2.4.2 Solid Distribution Profile

The solids mixing behavior in a batch slurry bubble column resembles that in the freeboard region of gas-liquid-solid fluidized bed containing particles (Fan, 1989). The solids concentration shows a decreasing tendency with axial distance. The flow regime also has an effect on the axial solids concentration profile. Fan (1989) noted that within the same flow regime (dispersed or coalesced bubble regime), the effect of gas velocity on axial solids concentration profile is not significant. Tang and Fan (1989) studied local solids holdup in the dispersed bubble regime and found that gas velocity had a slight effect on the holdup distribution. Smith and Ruether (1985), Smith et al. (1986), O'Dowd et al. (1987) and Murray and Fan (1989) found no appreciable differences in axial slurry concentration in the coalesced bubble regime.

The sedimentation-dispersion model has been used extensively to determine the axial solids concentration profiles in batch slurry column. The model was originally proposed by Cova (1966) and developed and simplified by Kato et al. (1972) and Smith and Ruether (1985). The following assumptions have been made in formulating the sedimentation-dispersion model;

1. no radial gradients in solid particles concentration;
2. all solids particles have identical terminal velocity.
3. gas holdup, solids dispersion coefficient and settling velocity of solids are all constant along the column axis;

4. gas and liquid velocities are such that all solids particles are completely suspended in liquid

The simplified model for axial solids distribution in batch slurry systems may be expressed as:

$$\frac{C}{C_0} = \exp\left(-\frac{V_p z}{E_s}\right) \qquad (2.4.1)$$

where, E_s is solid dispersion coefficient; V_p is the average solids convective velocity in the particulate fluidization phase and can be directly related to the particle hindered settling velocity U_p.

Various empirical correlations have been proposed in literature to account for U_p and E_s, which are summerized in Table 2.4.1. The dispersion coefficient is expressed as Peclet Number which in turn is related to the gas Froude Number ($Fr_g = V_g / \sqrt{gD}$).

Generally, solids dispersion coefficient increases with increasing gas velocity and column diameter. Hindered settling velocity increases with increasing particle terminal velocity and decreasing solids concentration. However, reported studies have not measured solids dispersion coefficient and hindered settling velocity at high slurry concentration (> 20 vol.%).

Table 2.4.1 Correlations for solids axial dispersion coefficient and particle hindered settling velocity in slurry bubble column

Investigators	Correlation for E_s and U_p	System	Range of Variables
Kato etal. (1972)	$Pe=\frac{V_g D}{E_s}=13\,Fr_g\,\frac{1+0.009\,Re_p\,Fr_g^{-0.8}}{1+8Fr_g^{0.85}}$ $U_p=1.33U_t\left(\frac{V_g}{U_t}\right)^{0.25}\varphi_l^{2.5}$	Gas : air Liquid: water solids: glass beds $(75.5<d_p<163\ \mu m)$ $\rho_s=2520\ kg/m^3$ (perforated plate distributor)	$0.0066<D<0.214$ m $2.01<H_d<4.05$ m $0.02<V_g<0.30$ m/s $0.02<V_{sl}<0.022$ m/s $48<C_s<202$ kg/m3 (2 vol.% to 8 vol.%)
Smith and Ruether(1985)	$Pe=\frac{V_g D}{E_s}=9.6\left(\frac{Fr_g^6}{Re_g}\right)^{0.1114}+0.019\,Re_p^{1.1}$ $U_p=1.91\,V_g^{0.26}U_t^{0.8}\,\varphi_l^{3.5}$	Gas : nitrogen Liquid: water, ethanol solids: glass beds $(48.5<d_p<164\ \mu m)$ $\rho_s=2420, 3990\ kg/m^3$ (single bubble cap distributor)	$D=0.108$ m $H_d=1.94$ m $0.03<V_g<0.20$ m/s $0.0071<V_{sl}<0.02$ m/s $0<C_s<150$ kg/m3 (0 vol.% to 7 vol.%)
O'Dowd et al. (1987)	$Pe=\frac{V_g D}{E_s}=7.7\left(\frac{Fr_g^6}{Re_g}\right)^{0.098}+0.019\,Re_p^{1.1}$ $U_p=1.69\,V_g^{0.23}U_t^{0.8}\,\varphi_l^{1.28}$	Gas : nitrogen Liquid: water solids: glass beds $(88<d_p<105\ \mu m)$ $\rho_s=2420\ kg/m^3$ (perforated plate distributor)	$D=0.108$ m $H_d=1.94$ m $0.031<V_g<0.24$ m/s $V_{sl}=0.0077$ m/s $0<C_s<291$ kg/m3 (0 vol.% to 12 vol.%)

2.5 Heat Transfer

A number of literature studies have reported heat transfer measurements in two and three-phase fluidized bed systems. These measurements of heat transfer coefficients can be divided into: 1) bed-to-wall heat transfer coefficients; and 2) immersed object-to-bed heat transfer coefficients.

Bed-to-wall heat transfer have been investigated by Kato et al. (1980, 1981, 1984), Muroyama et al. (1984, 1986) and Chiu and Ziegler (1983, 1985). The investigations of immersed object-to-bed heat transfer have been reported by a number of researchers, including Baker et al. (1978), Deckwer et al. (1980), Kang et al. (1985), Kim et al. (1988), Magliotou et al. (1988) and Saxena et al. (1989, 1990). These studies can be further divided into those conducted in three-phase fluidized beds ($d_p \geq 500$ μm ; Baker et al., 1978; Kang et al., 1985; Chiu and Ziegler, 1985; Kim et al., 1988) and others conducted in slurry beds of fine particles ($d_p \leq 500$ μm ; Deckwer et al., 1980; Saxena et al., 1989, 1990).

These measurements of heat transfer coefficients normally require a heat source and measurements of surface and bed temperatures. In bed-to-wall heat transfer measurements, the heat source is mounted on the wall of the column with its inside diameter same as the column diameter. Heat is usually supplied by electric power or steam. The surface temperature is measured by thermocouples mounted on the inside surface of the heat source equipment. In immersed object-to-bed heat transfer measurements, the heat transfer probe is localized inside the column, normally at column center. An electrical heater is inserted into the probe as heat source. The surface temperature is measured by thermocouples mounted on the outside of the probe. In both measurements, the bulk temperature of the bed is measured by using thermocouples immersed in the bed at different axial locations.

While most literature studies have investigated average heat transfer coefficients, Kumar et al. (1992) studied local instantaneous heat transfer coefficient in bubble and three phase column. The local heat transfer rate (heat flux) was measured by a heat flow sensor/heater assembly. The fast response heat flux sensor recorded change in heat transfer rate due to passage of bubble over probe surface. Measurements of instantaneous heat transfer coefficients can provide more insights into bubble dynamics and mechanism of heat transfer in multiphase particulate system.

2.5.1 Effects of Operating Parameters on Heat Transfer Coefficient

In this section, the effects of various operation parameters on heat transfer in two and three phase fluidized beds are summarized based on literature studies. These parameters include gas and liquid velocity, liquid viscosity, particle size and density, slurry concentration, bed porosity, column diameter, the axial and radial location of the heat transfer section/probe.

2.5.1.1 Effect of Gas Velocity

The effects of gas velocity on heat transfer coefficients in two and three phase systems have been investigated by many researchers (Fair, 1962; Baker et al. 1978; Deckwer et al., 1980; Kang et al. 1985; Chiu and Ziegler, 1983; Saberian-Broudjenni et al., 1985; Saxena et al., 1989, 1990).

Generally, the introduction of gas into a liquid or liquid-solid bed augments the respective heat transfer coefficients for both bed-to-wall and object-to-bed heat transfer. Therefore heat transfer coefficients increase with an increase of gas velocity, irrespective of the liquid flow rate, particle properties (diameter, shape, and densities), liquid viscosity, slurry concentrations etc.. These results also showed that the rate of increase

of heat transfer coefficients with gas velocity was rapid at low gas velocity, then the rate decreased with further increase of gas velocity.

Baker et al. (1978) observed that the increase in the heat transfer coefficient with gas flowrate did not change the bed porosity significantly. However, a gas flow increased the bed turbulence and consequently, the heat transfer coefficient. Kang et al. (1985) also proposed that the introduction of a gas stream into a liquid-solid fluidized bed generates mixing of solid and liquid phase, which resulted in an increase of the heat transfer coefficient. Higher gas velocity increased overall liquid circulation but not micro scale eddies in the bed. Thus, the heat transfer coefficient did not increase appreciably at higher gas velocity.

2.5.1.2 Effect of Liquid Velocity

The effects of liquid velocities on heat transfer coefficients in two phase and three phase fluidized beds have been investigated by several researchers including Baker et al., 1978; Kato et al., 1981; Chiu and Ziegler, 1983; Kang et al. 1985, Kim et al. 1986, Magiliotou et al., 1988; Kumar et al., 1994.

Most of the results indicate that the heat transfer coefficient initially increases, passes through a maximum, and then decreases as a function of progressively increasing liquid velocity, or porosity.

The liquid velocity at which the heat transfer coefficient exhibits a maximum value is mainly dependent on the liquid and solid particles properties (Baker et al., 1978; Chiu and Ziegler, 1983; Kang et al., 1985). It increases with increasing particle size and density, but decreases as increasing liquid viscosity.

The initial increase of the heat transfer coefficient with liquid velocity has been attributed to an increase of turbulence and oscillatory motion of the particles resulting in

an erosion of the thermal boundary layer (Baker et al., 1978). At higher liquid velocities, the solid mixing is reduced due to the reduction in solid holdup. As a result of these two opposing effects, the heat transfer coefficient exhibits a maximum value as a function of liquid velocity or bed porosity, i.e. the sum of liquid and gas phase holdups in the bed. Maximum heat transfer coefficients have been reported to occur at a bed voidage of 0.55 to 0.8 (Baker et al., 1978; Chiu and Ziegler, 1983; Kang et al., 1985; Kim et al., 1986).

2.5.1.3 Effect of Particle Size

The influence of particle size on heat transfer coefficients in two and three phase fluidized beds has been investigated in both three phase fluidized beds (Baker et al. 1978; Chiu and Ziegler, 1983; Kang et al., 1985) and three phase slurry bubble columns (Saxena et al., 1990b).

In three-phase fluidized beds, the heat transfer coefficient increased with the particle size at low gas velocities (< 0.05 m/s). At higher gas velocities, it passed through a minimum value at a particle size of about 1.5 mm. In general, the effect of particle size on heat transfer coefficients was negligible at particle sizes larger than 3.0 mm, particularly at high gas velocities.

Chiu and Ziegler (1983) found that particle shape and type did not have much influence on heat transfer coefficients in three-phase fluidized beds.

In three phase slurry bubble column, Saxena et al. (1990a, 1990b, 1992) observed a weak dependence of small particle size (50 μ m-143 μ m) on heat transfer coefficients.

However, a systematic study to investigate effects of particle size, density and shape in different media is lacking.

2.5.1.4 Effect of Liquid Viscosity

The heat transfer coefficient has been found to decrease with increasing liquid viscosity in three phase fluidized systems (Deckwer et al., 1980; Kang et al., 1985; Kim et al., 1986; Kumar and Fan, 1994) regardless of particle size.

Kang et al. (1985) attributed the decrease in heat transfer coefficient to two factors. First in the region adjacent to the heater surface, the thickness of thermal boundary layer around the heating surface increases with increasing viscosity, thus increasing resistance to heat transfer. Second particle movement is retarded due to increasing viscosity diminishing their attack on the thermal boundary layer around the heating surface.

2.5.1.5 Effect of Slurry Concentration

The influence of slurry concentration on heat transfer coefficient has been investigated by Kolbel et al. (1958, 1960), Deckwer et al. (1980) and Saxena et al. (1989, 1990a, 1990b, 1992).

Heat transfer coefficients were found to increase with increasing slurry concentrations (Kolbel et al., 1958, 1960; Deckwer et al., 1980).

Deckwer et al. (1980) demonstrated that the increase in heat transfer coefficient with increasing slurry concentration could be accounted for by alternation of thermophysical properties of pseudo homogeneous slurry phase for small particles (d_p). This excluded the possibility of the heat transfer enhancement due to independent motion of particles leading to higher surface renewal rate of liquid at the heat transfer surface.

Recent reports showed that the variation of heat transfer coefficient with solids concentration slightly increase with the addition of high thermal conductivity magnetite

(Saxena et al., 1990b) and slightly decrease with the additionof low thermal conductivity sand in room temperature (Saxena et al., 1992).

2.5.1.6 Effect of Particle Densities

Nore et al. (1994) studied the effects of low density solid particles on wall-to-bed heat transfer coefficient. Five solid particles were selected for the investigation. The solid particles were all made of polypropylene with inclusions of fine fiberglass mica or talcum particles which modified their densities. Their results indicated that for a given gas and liquid velocities, the heat transfer coefficient decreased as an increase of the particle densities from 1070 to 1700 density (kg/m^3).

2.5.1.7 Effect of Axial Location of Heat Transfer Probe

Saxena et al. (1992a) compared the heat transfer coefficients at two different axial locations. The probes were at 2.9 m and at 0.52 m from the distributor. Their results indicate that the heat transfer coefficients at 2.9 m were systematically higher than that at the 0.52 m. This may be attributed to the influence of the distributor region. The influence of the distributor region usually extends up to 3 to 4 times the column diameter. The height of 0.52 m from bottom is less than two times the column diameter (0.302 m) which would be in the developing region for bubble growth and liquid phase flow pattern.

2.5.1.8 Influence of the Column Diameter

Kim and Laurent (1991) analyzed the published results to summarize the effect of column diameter on the heat transfer coefficient in three phase fluidized beds. The effect was found to be negligible for column diameters ranging from 0.052 m to 0.152 m.

Saxena et al. (1990a), however, observed that the heat transfer coefficients in a slurry bubble column of diameter 0.305 m were systematically higher than that in a column of diameter 0.108 m. Saxena et al. (1990) attributed the difference to higher mixing rate in a larger diameter column.

2.5.1.9 Effect of Internals

Saxena et al. (1990a) investigated the effects of the number of heat transfer tubes inside a column on heat transfer coefficients. They compared the experimental results obtained with single and 7-tube bundle immersed inside the column. It was found that the heat transfer coefficients with 7-tube bundle were systematically higher than that with single tube. The authors attributed the difference to improved liquid mixing in presence of the 7-tube bundle, compared to the single tube case.

Systematic studies are required to further investigate the effect of internals and their configurations on mixing and heat transfer coefficients.

2.5.1.10 Instantaneous Heat Transfer Coefficient

Recently, Kumar et al. (1992, 1994) applied a fast response heat flow sensor to measure instantaneous heat transfer coefficients. They used video camera to observe and record bubbles passing on the surface of the heat flow sensor in the air-water system. At the same time, the instantaneous heat transfer coefficients were obtained by the heat flow sensor. It was concluded that the maximum (or peak) instantaneous heat transfer coefficient occurred in the bubble wake region which induced rapid surface renewal of the liquid on the surface of the heat transfer probe. This technique was used to study single bubble and bubble chain rising in liquid and liquid-solid systems. Heat transfer coefficients enhanced with increase in bubble size (or wake) and with increasing bubbling frequency.

2.5.2.11 Conclusion and Recommendation

Generally, the heat transfer coefficient is an increasing function of gas and liquid velocities, and particle size, but a decreasing function of liquid viscosity and particle density.

The effect of slurry concentration on heat transfer coefficient depends on particle thermal conductivity. The addition of high thermal conductivity particles increases the heat transfer coefficient.

Axial profiles of heat transfer measurement indicate that the heat transfer coefficient in the developed region is higher than in the developing region.

Heat transfer coefficients with multiple-tube bundle immersed in the column are systematically higher than with single tube.

Systematic studies are required to further investigate the effect of internals (internal tubes and gas distributor) and their configurations on heat transfer.

2.5.2 Correlations and Models of Heat Transfer Coefficient in Two-Phase and Three-Phase Systems

2.5.2.1 Empirical Correlations for Heat Transfer Coefficient

This section summarizes various literature correlations and their ranges of application.

Correlations for heat transfer coefficients in two-phase (gas-liquid) system have been proposed by Fair et al. (1962) and Hikita et al. (1981).

Fair et al. (1962) were the first to obtain a correlation in air-water system and gas velocities used were up to 0.30 m/s:

$$h = 1200\, V_g^{0.22} \qquad (2.5.1)$$

Hikita et al. (1981) developed a generalized correlation for gas-liquid systems based on wall-to-bed heat transfer:

$$\frac{h}{\rho_l C_{pl} u_g}\left(\frac{C_{pl}\mu_l}{k_l}\right)^{2/3} = 0.411\left(\frac{V_g \mu_l}{\sigma_l}\right)^{-0.851}\left(\frac{\mu_l^4 g}{\rho_l \sigma_l^3}\right) \qquad (2.5.2)$$

This correlation is valid for following dimensionless numbers:

$$5.4 \times 10^{-4} < V_g \mu_l / \sigma_l < 7.6 \times 10^{-2}$$

$$4.9 < C_{pl}\mu_l / k_l < 93$$

$$7.7 \times 10^{-12} < \mu_l^4 g / \rho_l \sigma_l^3 < 1.6 \times 10^{-6}$$

The following correlations have been developed for three-phase (gas-liquid-solid) systems.

Baker et al. (1978) proposed a correlation based on the measurement of object-to-bed heat transfer in three phase beds:

$$h = 1977\, V_l^{0.070}\, V_g^{0.059}\, d_p^{0.106} \qquad (2.5.3)$$

This correlation is valid for gas velocities up to 0.25 m/s, liquid velocities up to 0.125 m/s, and particle diameters up to 5 mm.

Kato et al. (1981) proposed a dimensional correlation:

$$Nu' = 0.044\left(Re' Pr\right)^{0.78} + 2.0 Fr_g'^{0.17} \qquad (2.5.4)$$

with: $Nu' = h d_p \varepsilon_l / k_l (1 - \varepsilon_l)$

$$Pr = \mu_l C_{pl} / k_l$$

$$Re' = \rho_l d_p V_l \varepsilon_l / \mu_l (1 - \varepsilon_l)$$

$$Fr'_g = u_g^2 / g d_p$$

This correlation is based on data obtained in measurement of wall-to-bed heat transfer and is valid for air velocities up to 0.15 m/s, liquid velocities from 0.004 to 0.06 m/s, particle diameters from 0.42 mm to 2.2 mm, liquid viscosity from 0.001 Pa.s to 0.036 Pa.s, column diameters of 0.052 and 0.12 m.

Chiu and Ziegler (1985) noted that the relative increase of heat transfer coefficients in three phase fluidized beds was equal to the relative decrease of liquid holdup as follows:

$$h_3 / h_2 = \varepsilon_{L2} / \varepsilon_{L3} \qquad (2.5.5)$$

where h_3 and h_2 are heat transfer coefficients in liquid-solid and gas-liquid-solid fluidized beds respectively. Chiu and Ziegler (1985) proposed the following correlation to evaluate heat transfer coefficients in three-phase fluidized beds by combining their data with those of Richardson et al. (1976):

$$Nu = 0.762 \left(\frac{V_l \rho_l \varepsilon_3}{a_s (1-\varepsilon_3) \varepsilon_{L3} \mu_l}\right)^{0.646} \left(\frac{C_{pl} \mu_l}{k_l}\right)^{0.638} \left(\frac{U_{lmf}}{U_t}\right) u_R^{0.266} \phi_s^{-1} \frac{1-\varepsilon_{L2}}{\varepsilon_{L3}} \qquad (2.5.6)$$

here, a_s is surface area per unit volume of particle ($a_s = 6/d_p$ for spherical particles); ϕ_p is particles shape factor. This correlation accounts for the effect of the liquid phase properties and the particles properties on the heat transfer coefficient.

Muroyama et al. (1984) proposed the following correlation based on a wide range of operating conditions:

$$\frac{h_3}{h_2} = 1 + 0.0413 \left(\frac{V_g}{V_l}\right)^{0.30} \left[\frac{d_p}{D} \frac{\rho_s - \rho_l}{\rho_l}\right]^{0.61} \qquad (2.5.7)$$

The particle size were varied from 0.61 to 6.9 mm and density from 1330 to 3500 kg/m^3; air velocities ranged from 0.03 to 0.259 m/s and liquid velocities from 0.012 to 0.26 m/s.

The influence of liquid properties (i.e. viscosity, density) have been investigated (Kang et al., 1985; Saberian-Broudjennie et al., 1985; Kim et al., 1985) and suitable correlations have been proposed. Applications of these correlations are generally limited to the range of operating conditions used in the study. These correlations should be used with caution for conditions outside the range of operating variables applied. There is a need to obtain a unified correlation based on the accumulated data of heat transfer measurements in two and three-phase fluidized beds.

2.5.2.2 Models based on Surface Renewal Theory

Surface renewal theory has been applied to explain the heat transfer phenomena in two- and three-phase fluidization (Decker et al., 1980; Suh and Deckwer, 1989, Kumar et al., 1992). Wasan and Ahluwalia (1969) initially proposed a model based on surface renewal mechanism. In this model, a uniform film was viewed to lie adjacent to the wall and a mass of fluid was viewed to exchange heat by unsteady state conduction at the outer edge of this film. In addition the film was thinner than that predicted by film theory because of the fluid convection and the motion of particles near the surface. This is explained in Figure 2.5.

To apply this theory to predict heat transfer coefficient between three-phase bed and the heat transfer surface (i.e. heat transfer probe, column wall), the following assumption were suggested (Wasan and Ahluwalia, 1969):

1. The temperature of the interface between the film and the fluid element changed with time. The temperature of the mass of fresh fluid as it swept the outer surface of the film was assumed uniform and equal to the bulk fluid temperature.
2. For the instantaneous heat transfer rate to this fluid mass, no heat storage in

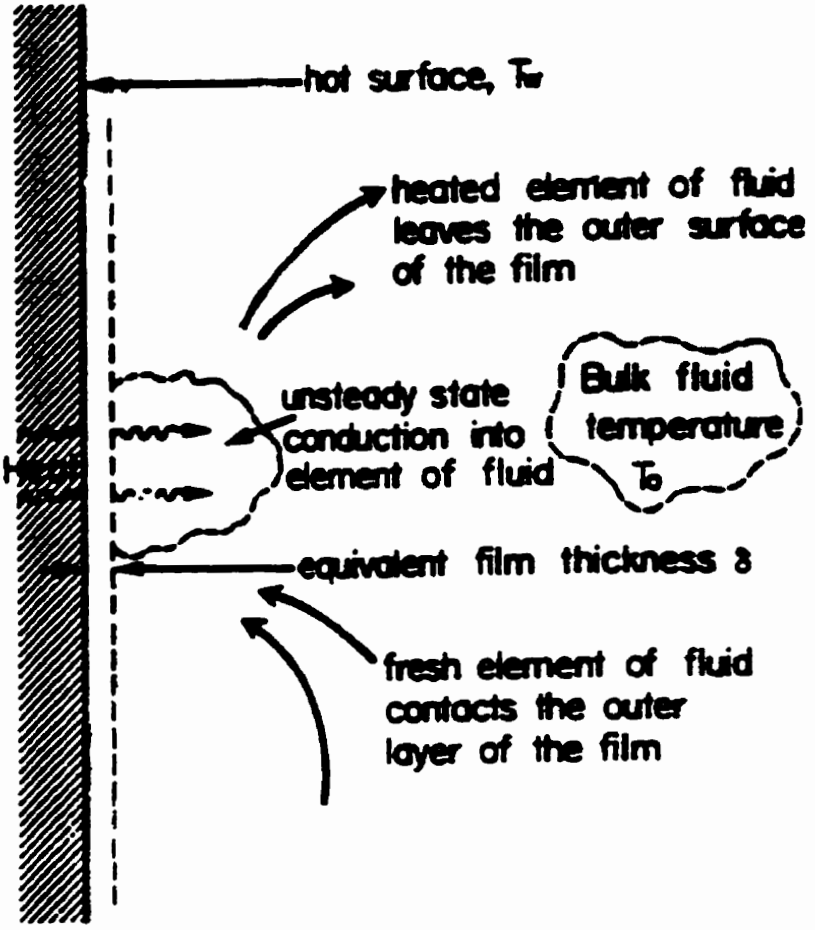

Figure 2.5 Main feature of proposed surface renewal model

the film.

3. The bulk temperature of the bed was constant.
4. Resistance to heat transfer was due to the film followed by penetration and unsteady state heating of an element resting at the outer edge of the film.

From assumption 2, heat flux on the surface of the heat transfer wall can be described as follow:

$$q = -k_l \left(\frac{dT}{dy}\right)_{y=0} = h(T_w - T_{y=0}) \qquad (2.5.8)$$

here, q is instantaneous heat flux. k is thermal conductivity; y is the distance measured from the edge of the film. T_w and $T_{y=0}$ are wall and bulk temperature; h is heat transfer coefficient, defined as:

$$h = \frac{k_l}{\delta} \qquad (2.5.9)$$

where, δ was the thickness of thermal boundary layer.

To describe instantaneous temperature profile, unsteady balance equation can be applied:

$$\frac{\partial T}{\partial t} = \alpha \frac{\partial^2 T}{\partial y^2} \qquad (2.5.10)$$

here α is thermal diffusivity. This equation represented the unsteady state heat conduction to the fluid mass. By integrating the above equation, Wasan and Ahluwalia (1969) obtained an expression of total heat transfer rate:

$$q_c = \int_0^{t_c} q\,dt$$

$$= \frac{2k_l t_c^{1/2}}{\sqrt{\pi\alpha}}(T_w - T_b) + \frac{k_l \delta}{\alpha}(T_w - T_b)\left[e^{\left(\frac{\alpha t_c}{\delta^2}\right)}(1 - \text{erf}\sqrt{\frac{\alpha t_c}{\delta^2}} - 1\right] \qquad (2.5.11)$$

The average heat transfer rate is defined as:

$$q_{ave} = \frac{1}{t_c}\int_0^{t_c} q\,dt = h_{ave}(h_w - h_b) \qquad (2.5.12)$$

combining equations (2.5.11) and (2.5.12), the average heat transfer coefficient can be obtained as:

$$h_{ave} = \frac{2k_l}{\sqrt{\pi\alpha t_c}} + \frac{k_l\,\delta}{\alpha\,t_c}\left[e^{\frac{\alpha t_c}{\delta^2}}\left(1 - \mathrm{erf}\frac{\sqrt{\alpha t_c}}{\delta}\right) - 1\right] \qquad (2.5.13)$$

here, t_c is contact time.

In the extreme when $\delta \to 0$, equation (2.5.13) can be simplified to:

$$h_{ave} = \frac{2k_l}{\sqrt{\pi\alpha t_c}} = 2\sqrt{\frac{\rho_l C_{pl} k_l}{\pi t_c}} \qquad (2.5.14)$$

here, ρ_l is the density of fluid; C_{pl} is specific heat capacity.

Deckwer (1980) developed a theoretical model to describe the heat transfer from wall or immersed tube to the bed. In this model, he applied Higbie's unsteady-state transfer theory to heat transfer and obtained a similar expression to equation (2.5.14):

$$h \propto (k_l \rho_l C_{pl} / t_c)^{0.5} \qquad (2.5.15)$$

here, contacting time t_c can be interpreted as the mean lifetime of microscale eddies which are generated by macroscale eddies resulting from the rising bubbles. It was assumed that contact time was connected with the length and velocity scale of the micro eddies. Thus,

$$t_c = \eta_l / \upsilon \qquad (2.5.16)$$

It was also assumed that the energy dissipation by the micro scale eddies was mainly governed by viscous forces. Thus, length scale η_l and velocity υ scale were formulated based on the correlation from Kolmogoroff's theory:

$$\eta_l = \left(\frac{\nu^3}{P_v}\right)^{1/4} \tag{2.5.17}$$

$$\upsilon = (\nu P_v)^{1/4} \tag{2.5.18}$$

here, ν is kinetic viscosity; P_v is dissipation rate per unit mass of liquid. Combining above equations, Deckwer (1980) obtained an expression as:

$$h \propto \left(\frac{k_l \rho_l C_{pl} P_v^{1/2}}{\nu^{1/2}}\right)^{0.5} \tag{2.5.19}$$

The energy dissipation rate per unit mass can be expressed as:

$$P_v = V_g\, g \tag{2.5.20}$$

Introducing equation (2.5.20) to equation (2.5.19), Deckwer (1980) proposed an expression of heat transfer coefficient:

$$h \propto k_l^{0.5} \rho_l^{0.75} C_{pl}^{0.5} \mu_l^{-0.25} g^{0.25} V_g^{0.25} \tag{2.5.21}$$

which was rearranged as:

$$\frac{h}{\rho_l C_{pl} V_g} \propto \left(\frac{V_g^3}{g\nu}\right)^{-.25} \left(\frac{\mu_l C_{pl}}{k_l}\right)^{-0.5} \tag{2.5.22}$$

or expressed by dimensionless number:

$$St = \beta (Re\, Fr\, Pr^2)^{-0.25} \tag{2.5.23}$$

here, β is an empirical constant. Based on experimental observation in gas-liquid system, Deckwer et al.(1980) proposed β=0.1. These authors also found this equation to be applicable for slurry (fine particles) systems.

Saxena et al. (1992a) modified the model proposed by Deckwer et al. (1980). They proposed the correlation based on experimental results in slurry bubble column with 0.305 m column diameter:

$$h = 3.5 \times 10^{-3} (k \rho C_p)_{sl}^{0.5} (\rho g / \mu)_{sl}^{0.47} V_g^{0.25} \qquad (2.5.24)$$

This correlation was valid for gas velocities up to 0.30 m/s and slurry concentrations below 10 vol.%.

Suh et al. (1985) extended the model proposed by Deckwer (1980) to three phase fluidized beds. In this model, it was assumed that the energy dissipation rate per unit mass of liquid phase was given by the energy input minus the energy recovery, since phase holdups in three phase was found to be uniform along the bed height (Kato et al., 1981; Kim et al., 1972; Bergovich and Watson, 1978). This lead to:

$$P_v = \frac{[(V_l + V_g)(\varepsilon_s \rho_s + \varepsilon_l \rho_l + \varepsilon_g \rho_g) - V_l \rho_l] g}{\varepsilon_l \rho_l} \qquad (2.5.25)$$

The heat transfer coefficients in three phase fluidized beds can then be expressed as:

$$h = C_7 [k_l \rho_l C_{pl} \{ \frac{[(V_l + V_g)(\varepsilon_s \rho_s + \varepsilon_l \rho_l + \varepsilon_g \rho_g) - V_l \rho_l] g}{\varepsilon_l \mu_l} \}^{1/2}]^{1/2} \qquad (2.5.26)$$

where, C_7 is a proportional constant which can be determined from the experimental data of heat transfer coefficients. Suh et al. (1985) proposed C_7=0.0647 based on experimental results from (Baker et al., 1978; Kato et al., 1981; Chiu and Ziegler, 1983; Kang et al., 1984).

Suh and Deckwer (1989) modified the model proposed by Suh et al. (1985) by replacing liquid viscosity μ_l by the bed effective viscosity. They compared experimental bed effective viscosity at slurry concentration up to 50 vol.% with a model proposed by Vand (1948):

$$\mu_{sl} = \mu_l \exp\left[\frac{2.5\phi_s}{1-0.609\phi_s}\right] \qquad (2.5.27)$$

where, ϕ_s is fraction of solids in slurry phase. The heat transfer coefficients in three phase fluidized beds can be expressed by the placement of bed effective viscosity in equation (2.5.26):

$$h = C_8 [k_l \rho_l C_{pl} \{\frac{[(V_l + V_g)(\varepsilon_s \rho_s + \varepsilon_l \rho_l + \varepsilon_g \rho_g) - V_l \rho_l] g}{\varepsilon_l \mu_{sl}}\}^{1/2}]^{1/2} \qquad (2.5.28)$$

This correlation is valid for predicting heat transfer coefficient in three phase fluidized bed (particle size > 1mm).

Kim et al. (1986) extended surface renewal model to correlate heat transfer coefficient in three phase slurry-fluidized bed:

$$h = C_9 [k_{sl} \rho_{sl} C_{psl} \{\frac{[(V_{sl} + V_g)(\varepsilon_s \rho_s + \varepsilon_{sl} \rho_{sl} + \varepsilon_g \rho_g) - V_{sl} \rho_{sl}] g}{\varepsilon_{sl} \mu_{sl}}\}^{1/2}]^{1/2} \qquad (2.5.29)$$

In their experiments, air was used as gas phase, 1.7 to 8.0 mm glass beads as the solid phase, water, kerosene and mineral oil as liquid phase. Pulverized bituminous coal (<100 mesh) in mineral oil or kerosene as slurry phase. Based on their experimental results and previous results (Baker et al., 1978; Kato et al., 1981; Kang et al., 1984), They found C_9=0.0772 in equation (2.5.29). This semi-theoretical correlation of heat transfer coefficient in two- and three-phase fluidized beds covered the range of variables 1.1 < V_{sl} < 12 cm/s; 0 < V_g < 14.0 cm/s; 0 < dp < 0.8 cm; 0.92 < Cp_{sl} < 4.18 J/gK; 0.14 < k_{sl} < 0.59 W/mK; and 1.0 < μ_{sl} < 38.9 mPa.s.

Magiliotou et al. (1988) analyzed the mechanism of heat transfer in three phase fluidized beds. They suggested that in a three phase fluidized bed, particle movement might play an important role for the surface renewal. To account for this independent renewal

contribution of particle movement, they extended the heat transfer coefficient into following equation:

$$h=C_{10}[k_l\rho_l C_{pl}(P_v/\nu)]^{0.5}+C_{11}\{k_l\rho_l C_{pl}[\varepsilon_s^{1/3}(V_l-U_{lmf})/(\phi_p d_{eq})]\}^{0.5} \tag{2.5.30}$$

where, d_{eq} was equivalent hydraulic diameter of particle. ϕ_p was particle sphericity. U_{lmf} was minimum fluidization velocity.

The main difference between equation (2.5.28) and equation (2.5.30) is that equation (2.5.30) had an additional second term, which indicated the contribution of particle movement to surface renewal. They stated that the particle renewal mechanism expressed in equation (5.2.30) might not be applicable to a very fine particles system, such as slurry bubble column. The suspended fine particles might not have enough inertia to induce major particle collision effects.

2.5.2.3 Models based on Recirculation Flow of Liquid Phase

Joshi and Sharma (1976, 1978, 1979) proposed the annular flow pattern in bubble columns. Based on their analysis, these authors obtained the average liquid circulation V_c, average axial and radial components of liquid velocities (V_a, V_r):

$$V_c=1.31\left\{gD\ (V_g-\varepsilon_g V_{b\infty})\right\}^{1/3} \tag{2.5.31}$$

$$V_a=1.18\left\{gD\ (V_g-\varepsilon_g V_{b\infty})\right\}^{1/3} \tag{2.5.32}$$

$$V_r=0.42\left\{gD\ (V_g-\varepsilon_g V_{b\infty})\right\}^{1/3} \tag{2.5.33}$$

Joshi et al. (1980) applied the above equations and obtained the correlation of heat transfer coefficients in bubble columns based on analogy with mechanically agitated contactor and liquid flow through the pipes:

analogy with mechanical agitated tank:

$$\frac{hD}{k_l}=0.48\left[\frac{D^{1.33}g^{0.33}(V_g-\varepsilon_g U_{b\infty})^{1/3}\rho_l}{\mu_l}\right]^{0.66}\left(\frac{C_{pl}\mu_l}{k_l}\right)^{1/3}\left(\frac{\mu_l}{\mu_w}\right)^{0.14} \tag{2.5.34}$$

analogy with liquid flow through a pipe:

$$\frac{hD}{k_l}=0.48\left[\frac{D^{1.33}g^{0.33}(V_g-\varepsilon_g U_{b\infty})^{1/3}\rho_l}{\mu_l}\right]^{0.66}\left(\frac{C_{pl}\mu_l}{k_l}\right)^{1/3}\left(\frac{\mu_l}{\mu_w}\right)^{0.14} \tag{2.5.35}$$

Zehner (1986a, 1986b) suggested a flow model with cylindrical eddies. Based on this flow model, he obtained the following expression for heat transfer coefficient:

$$h=0.18(1-\varepsilon_g)\left[\frac{k_l^2\rho_l C_{pl} V_c}{l\mu_l}\right]^{1/3} \tag{2.5.36}$$

where,

$$l=d_b(\pi/6\varepsilon_g)^{1/3} \tag{2.5.36a}$$

$$V_c=\left[\frac{1}{2.5}\left(\frac{\rho_l-\rho_g}{\rho_l}\right)gD\ V_g\right]^{1/3} \tag{2.5.36b}$$

Saxena et al. (1989) concluded that both models proposed by Joshi et al. (1980) and Zehner (1986a, 1986b) poorly reproduced the experimental results in air-water bubble column.

2.6 Mass Transfer and Analogy with Heat Transfer

2.6.1 Mass Transfer in Three Phase Fluidized Bed

Various techniques used for the measurement of volumetric mass transfer coefficient can be divided into two categories: 1) physical methods and 2) chemical methods. The volumetric mass transfer by physical methods can be measured by analyzing dissolved oxygen in the liquid samples (Akita and Yashida, 1981). The chemical method involves gas absorption accompanied by a chemical reaction which is sufficiently fast to maintain gas concentration below its equilibrium concentration with respect to the sparging gas stream (Prakash, 1991).

The parameters affecting the gas-liquid mass transfer rate in bubble column and three phase bed has been reviewed by Prakash (1991) and Kim and Kang (1997). The volumetric mass transfer coefficient has been found to increase with gas velocity (Akita and Yoshita, 1973; Godbole et al., 1984). The liquid velocity was generally not found to have any effect on the mass transfer coefficient (Deckwer et al., 1974; Schuegerl et al., 1977). The mass transfer coefficient has been found to decrease with increasing liquid viscosity (Kang et al, 1990, Lee et al., 1993). The mass transfer coefficient was found to decrease with an increase of solids concentration in slurry column (Kato, 1973; Koid, 1983; Schumpe et al., 1987). The mass transfer coefficient has been found to increase with an increase of the particle size (Kim and Kim, 1991; Lee et al., 1993). The effect of low particle densities (1000~1800 kg/m^3) on the mass transfer coefficient has been generally found to be not considerable in three phase beds of relatively larger particle size.

The following techniques have been used to measure the liquid-solid mass transfer coefficient in fluidized bed.

1) Dissolution of soluble solids. This technique is based on the measurement of the rate of dissolution of one or a few solid particles in a bed of inert solids (Prakash et al., 1984, 1987; Prakash, 1991) or the dissolution rate of a whole bed of soluble particles (Ballesteros et al., 1982; Arters and Fan, 1986). The mass transfer rate can be obtained by weighting loss of the soluble solid particles or analyzing the liquid exit concentration.
2) Electrochemical techniques. This technique utilizes the principle of limiting current when the mass transfer to the electrode surface is diffusion-controlled (Prakash, 1991).
The liquid-solid mass transfer coefficient in fluidized bed can be also measured by other methods, such as ion exchange method, photographic technique, etc.

The liquid-solid mass transfer coefficient in three phase fluidized beds has been found to be practically independent of liquid velocity and increase with gas velocity (Hassannien et al., 1984; Arters and Fan, 1986; Prakash et al., 1984; Fukuma et al., 1988). Hassanien et al. (1984) reported that the particle size has almost no influence on mass transfer coefficient in the particle diameters from 5 to 10 mm. Arters and Fan (1986) reported that the mass transfer coefficient was independent of the particle size at low gas velocity (< 0.066 m/s) while it was dependent on the particle size at high gas velocity. Nikov and Delmas (1987) studied the effect of particle density and found that the rate of increase of the mass transfer coefficient with the gas velocity was large for light particles near the minimum fluidization velocity, became smaller with increasing solids densities and liquid velocities.

2.6.2 Analogy between Heat and Mass Transfer

In the design and operation of three phase fluidized bed reactors, the effects of operating variables (gas and liquid velocities, particle and liquid properties) on the heat and mass transfer have a similar trend. In general, the heat transfer coefficient in three phase fluidized beds is an increasing function of gas and liquid velocities (Deckwer, 1980), the particle size (Baker et al, 1978), but a decreasing function of the dynamic viscosity of the liquid (Kang et al., 1985; Kim et al., 1986). The gas-liquid mass transfer coefficient

($k_l a$) increases with increasing gas and liquid velocities, and the particle size, but decreases with increasing liquid viscosity (Kang et al., 1990; Lee et al., 1993).

For the correlations of heat and mass transfer coefficients in three-phase fluidized beds, some correlations had similar expressions, and thus those correlations can be exchanged with each other.

Kim and Kang (1997) proposed similar correlations for heat and mass transfers:

for heat transfer: $$Nu = 0.436\,Pr^{0.333}\,Re_b^{0.196} \qquad (2.5.37)$$

for mass transfer: $$Sh = 2.694\,Pr^{0.333}\,Re_b^{0.196} \qquad (2.5.38)$$

where, $Re_b = \frac{V_g d_b}{\nu_l}$. The correlation for heat transfer was based on experimental ranges: V_g up to 0.25 m/s, V_l from 0.004 to 0.25 m/s, d_p from 1 to 8 mm, and μ_l from 0.001 to 0.0985 Pa.s. The correlation for mass transfer was based on experimental ranges: V_g from 0.005 to 0.19 m/s, V_l from 0.008 to 0.175 m/s, d_p from 1 to 8 mm, and μ_l from 0.001 to 0.0967 Pa.s.

From these equations, the following relation can be made (Kim and Kang, 1997):

$$Nu/Sh = 0.162\,(Pr/Sc)^{1/3} \qquad (2.5.39)$$

In wall-to-bed heat and mass transfer systems, the correlations of heat and mass transfer coefficients based on the energy dissipation rate per unit mass of liquid have been correlated according to Colburn j-factor (Yasunishi et al., 1988). The mass transfer coefficient in the wall-to-bed mass transfer coefficient can be correlated as:

$$Sh = 0.13\left(\frac{P_v^{1/3} D^{4/3}}{\nu_l}\right)^{0.75} Sc^{1/3} \qquad (2.5.40)$$

Based on the analogy between the heat and mass transfer, equation (2.5.40) can be converted into the corresponding dimensionless groups for heat transfer as:

$$Nu = 0.13\left(\frac{P_v^{1/3} D^{4/3}}{\nu_l}\right)^{0.75} Pr^{1/3} \qquad (2.5.41)$$

It has been reported that the wall-to-bed heat transfer coefficients in three-phase fluidized bed were well correlated by equation (2.5.41) (Yasunishi et al., 1988). Thus, it is apparent that an analogy between heat and mass transfers exists in the wall-to-bed system.

3.0 Experimental

This chapter describes the designs of equipment and probes and methodology of experimental investigations.

3.1 Experimental Setup

Experiments were conducted in a Plexiglas column of 0.28 m inside diameter and total height of 2.4 m. The column was designed with three sections for easy construction and flexibility, as shown in Figure 3.1a. The main support structure was constructed using 2" (0.0508 m) piping ensuring that the column was held firmly at times of high vibration (i.e. high gas velocities). The liquid or slurry phase heights before fluidization were maintained at 1.4 m. The liquid used was tap water and solid particles were 35 μm glass beads. The glass beads were supplied by Flex-o-lite Co. (St. Thomas, Canada). The density of the glass beads was 2450 kg/m^3. The slurry concentration ranged from 5 vol.% to 40 vol.%. The gas phase was oil-free compressed air. The superficial gas velocity was varied from 0.05 to 0.35 m/s. Gas flow rate was measured by a rotameter, supplied by OMEGA (FL-1660). The gas flow rate at rotameter pressure and temperature was corrected to obtain flow rate at reference pressure and temperature (see Appendix A). Gas sparger was located at the bottom of the column. Its details are given in the following section. A ball valve was installed at the bottom of the column to drain the slurry and clean the column.

Two pressure transducers, supplied by OMEGA (PX541, Montreal, Canada) were located on the wall of the column. One was placed at 0.07 m above the bottom of the column and other at 1.33 m above the bottom of the column (Figure 3.1b). Five pressure taps were spaced on the wall of the column, which were 0.07, 0.52, 0.73, 1.13 and 1.53 m above the bottom of the column (Figure 3.1a). Each pressure tap was connected to a

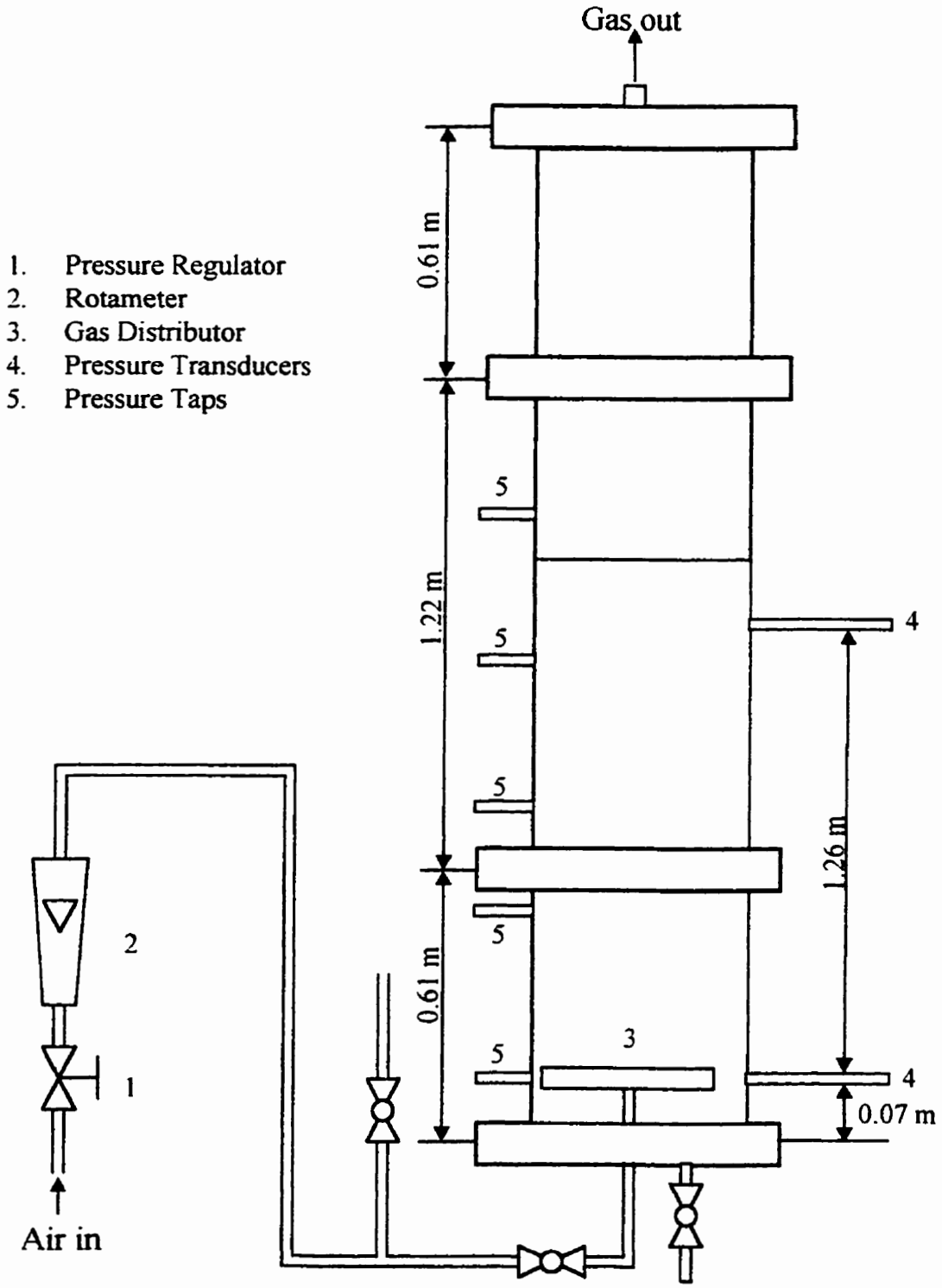

Figure 3.1a Schematic diagram of the experimental setup

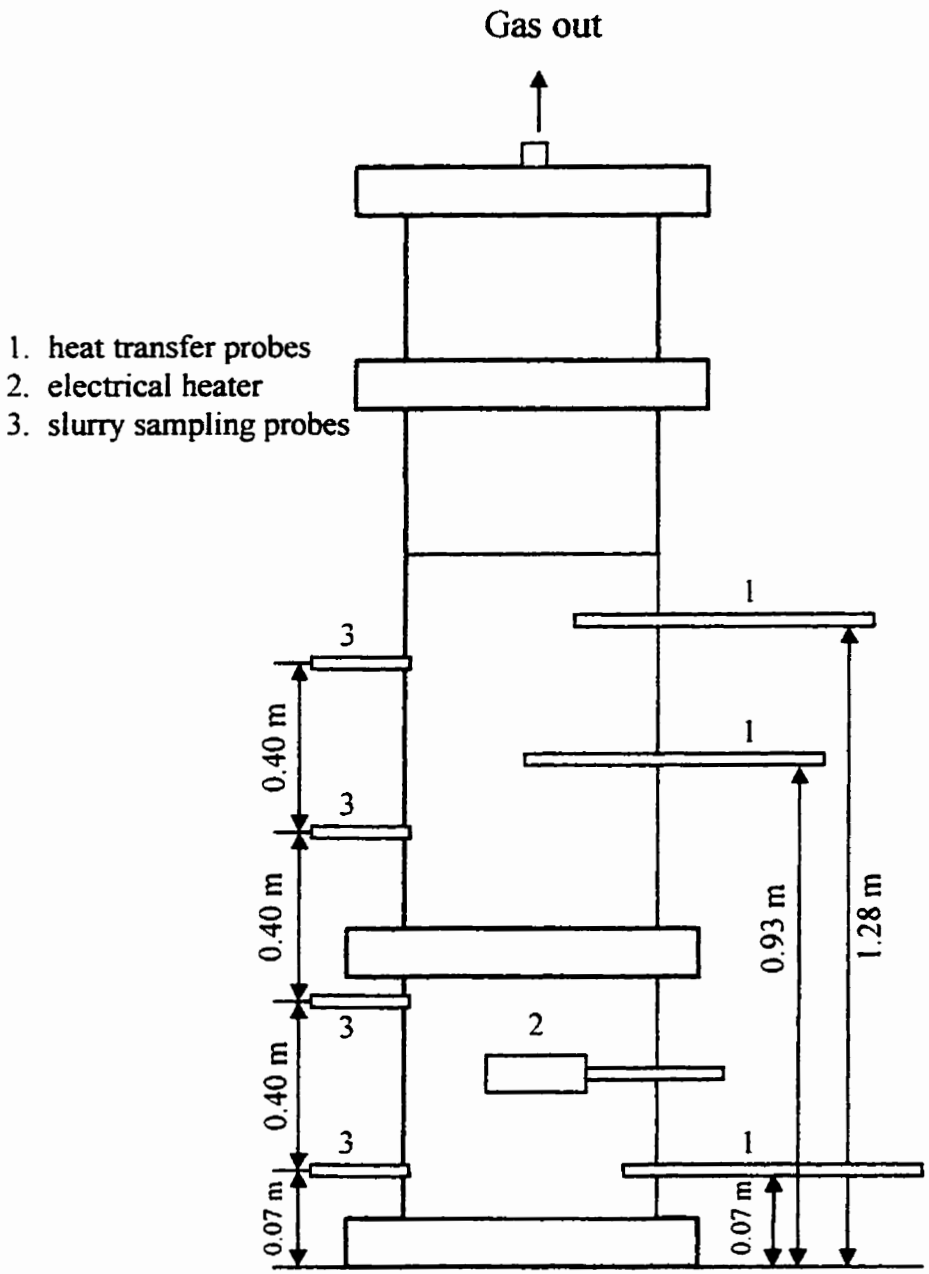

Figure 3.1b Locations of heat transfer probes and slurry sampling probes on the column

water manometer by flexible tubing. Pressure transducers provided instantaneous pressure signals which were used for gas holdup measurement and gas disengagement studies. Pressure taps were mainly used to verify the measurements by pressure transducers.

Two heat transfer probes were located at the same vertical location as the two pressure transducers on the wall of the column, but at a 90^{o} degrees angle in horizontal plane (Figure 3.1b). The heat transfer probes were movable along radial direction to measure radial variation of heat transfer. The heat transfer probe could also be rotated to study the effect of probe orientation on heat transfer. The heat transfer probe provided instantaneous heat transfer rate which could be averaged over time to obtain an average heat transfer coefficient.

Four solids sampling probes were located on the column. One was located just below the gas sparger, 0.07 m above the bottom of the column. Other three probes were arranged above the sparger, equally spaced at 0.4 m each (Figure 3.1b). The probes were used to measure axial solids concentration distribution during the operations.

Three thermocouple probes were used to monitor bed temperatures. An electrical heater was located near the bottom of the column to maintain a constant bed temperature. The input power for the electrical heater was controlled by variable autotransformer.

3.1.1 Gas Distributor

Gas distributor was located at the bottom of the column. As shown in Figure 3.2, the gas sparger consisted of six arms and connecting tube. Each arm was made of brass tube 0.112 m long and 6.3 mm in diameter. On each arm there were four downward facing orifices of 1.5 mm diameter for each. The orifices were located at 28 mm, 79 mm, 105 mm and 115 mm from the center of the column to ensure approximately even distribution of gas across column cross-section. The distance from the bottom of the

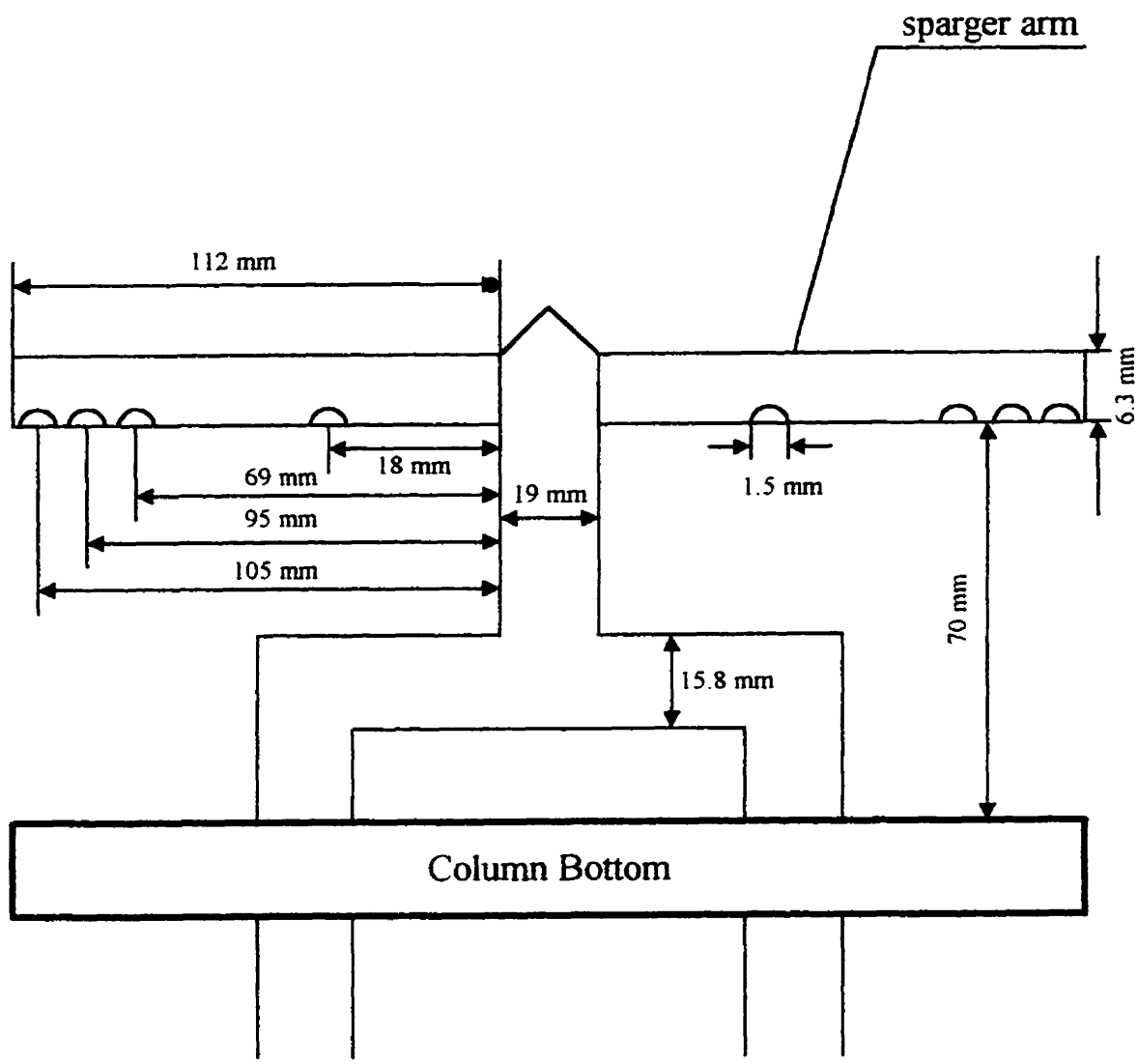

Figure 3.2 Details of gas distributor design

column to the arm of the sparger was 0.07 m. The ratio of pressure difference of grid to pressure difference of the bed is up to 16.5.

3.2 Probes and Transducers

A heat transfer probe was designed to measure local and instantaneous heat transfer coefficients in the column. A slurry sampling probe was designed to obtain a representative sample of slurry from the column. Fast response pressure transducers were selected to obtain instantaneous and average pressure profiles along column height.

3.2.1 Heat Transfer Probe

The estimation of the heat transfer coefficient between an immersed object and surrounding fluid requires measurements of the heat flux at the surface of the object, and the surface and bulk temperatures. The heat transfer probe was designed to measure instantaneous heat flux and surface temperature.

The details of the heat transfer probe are shown in Figure 3.3. It consisted of a micro-foil heat flux sensor mounted flush on the surface of a brass cylinder of 11 mm O.D. and 25.4 mm length. The heat flux sensor was provided by RDF corporation (Hudson, U.S.A.) with overall dimension of 11 mm x 14 mm x 0.08 mm (No. 20453-1). The micro-foil sensor consisted of two foil-type thermocouples bonded on both sides of a known thermal barrier, the difference in temperature across the known thermal barrier being proportional to heat flow through the sensor. The heat flux sensor was factory-calibrated to provide a relationship between voltage output from the sensor and heat flux. Appendix B provides calibration details of the heat flux sensor. The calibration of the built-in thermocouple for the probe surface temperature measurement is given in Appendix C.

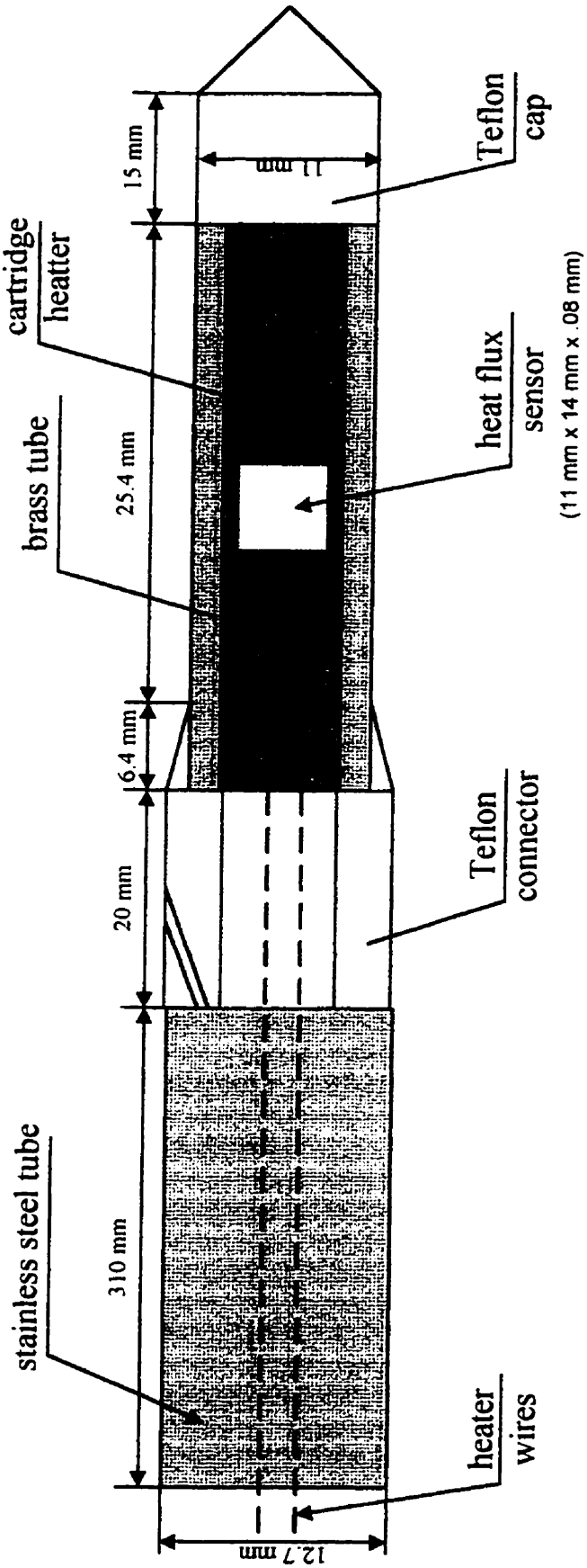

Figure 3.3 Heat transfer probe

A small electrical cartridge heater was installed inside the brass cylinder to provide a heat source. A steel tube was used to support the probe, and prevent its damage under high solids concentration and high gas velocity operations. A teflon tip was arranged on the end of the brass cylinder to reduce the heat loss from the end of the cylinder. On the other end of the brass cylinder, a teflon connector was used between the brass cylinder and the steel tube to reduce the heat loss from this side of the brass cylinder. On the surface of the teflon connector, a deep groove was made to accommodate the electrical wires of the heat flux sensor. At the middle of the teflon connector, a hole was drilled from the outside to carry the electrical wires of the heat flux sensor inside the steel tube. Epoxy was used to fill up the hole and fix electrical wires on the surface of the teflon connector. This prevented water or slurry from entering the inside of the teflon connector. A flexible connector was used between the steel tube and the wall of column. The steel tube could be moved along a radial direction to measure the heat transfer coefficient at various radial locations.

Two such heat transfer probes were mounted on the wall of the column, located at 0.07 m and 1.28 m from the bottom of the column.

The heat flux sensor provided a fast response time (0.02 s) and local measured heat flux and surface temperature. Thus the sensor could be used to measure local instantaneous heat flux and surface temperature. Signals for the measured heat flux and the surface temperature were collected at 60 Hz. The frequency of larger bubbles in a slurry bubble column is normally below 10 (1/s). The selection of sampling rate was therefore reasonable for measuring the frequency of larger bubbles.

The microvolt signals from the heat flux sensor were amplified to millivolts before data collection. The amplified signals from the heat flux sensor and the surface temperature probe were interfaced with a computer data acquisition system, provided by OMEGA (WB-21). The millivolt signals measured from the heat flux sensor were converted to the

corresponding heat transfer fluxes. The signals measured for surface temperature were converted to corresponding temperatures by using the software provided by OMEGA.

3.2.2 Pressure Transducers and Pressure Taps

Pressure transducers were used for measuring average and quasi-instantaneous pressures along column height. Compared with pressure taps, the advantage of pressure transducers are fast response (2 ms), and more accurate data. In addition, pressure transducers provided the quasi-instantaneous information to study dynamic variations of pressure and gas holdup during gas disengagement studies.

Two pressure transducers provided by OMEGA (PX1540) were used in the experiments. One transducer was located in the distribution section (0.07 m from the column bottom) and the other transducer was located in bulk region (1.33 m from the column bottom). Quasi-instantaneous pressures at two locations were measured at the same time.

These high accuracy pressure transducers provided the signal output of electrical current (4-20 mA). The data acquisition system supplied by OMEGA accepted the input signal as electrical voltage. Thus the signals collected from pressure transducers were converted from electrical current to electrical voltage by using resistors. The top and bottom transducers could measure pressures up to 3 .0 and 7.5 psi respectively.

The converted voltage signals were found to have a linear relationship with the height of water in the column in the range of desired experimental operation. The calibrations giving the relationship between the heights of water and the voltage output of both pressure transducers are given in Appendix C.

To measure axial gas holdup, five pressure taps were also placed on the wall of the column. One of taps was located below the gas sparger and other four were arranged above the distributor at heights of 0.07 m, 0.52 m, 0.64 m, 1.03 m, and 1.43 m from the

bottom of the column. The pressure taps were made of 6 mm stainless steel tubes and were connected by means of flexible plastic tubing to one side of a U-tube water manometer. The neighboring pressure tap was connected to the other side of the manometer. Five such manometers were used to measure local pressure drops and gas holdups between neighboring pressure taps.

The major problem in measuring the water levels in the manometers was the fluctuation of level in the glass tubes, particularly at higher gas velocities. To reduce the fluctuations and obtain a stable value, teflon capillary tubes (diameter less than 1 mm) were placed inside the plastic tubes connected to the manometers.

3.2.3 Slurry Sampling Probes

The slurry sampling probe was designed to measure solids concentration at various axial locations, along the column height. Figure 3.4 shows details of the slurry sampling probe. It consisted of a brass tube 12.7 mm in diameter and 0.35 m long. The sampling tube was inserted into the slurry column up to halfway between wall and center.

A teflon rod was inserted inside the tube. The rod could be moved radially with the help of a handle. The probe design therefore constituted a piston and cylinder arrangement. The movements of the rod were restricted by a screw and groove arrangement. The slurry sample was collected at the other end through an outlet placed at 30° angle to the tube. The inlet end was also tapered at 30° angle to minimize sampling errors due to sudden changes in flow direction. The inlet was oriented to be at 90° to the main bubble flow to avoid entrainment of bubbles into sampling line. The piston-cylinder arrangement also allowed self cleaning of the tube after sampling. Four such sampling probes were installed along the column height at 0.07 m, 0.47 m, 0.87 m, and 1.27 m from the bottom of the column.

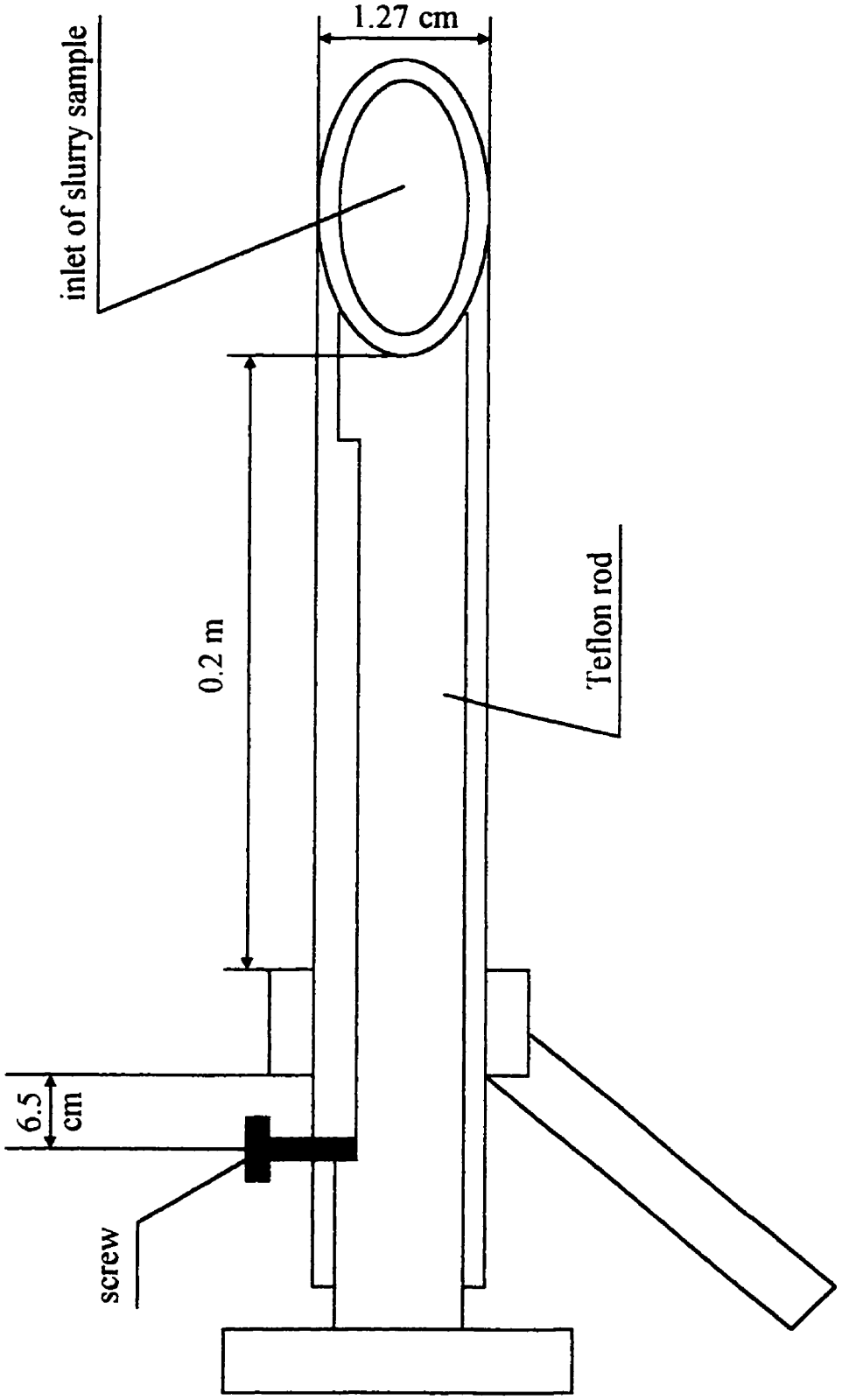

Figure 3.4 Sampling probe

The collected slurry sample volume was limited to 50-100 ml so as to minimize the effect on bulk solids concentration in the slurry bubble column. The samples were withdrawn after at least 40 min of startup to ensure that a steady operation had been reached. To maintain nearly constant amount of the solids in the slurry column, collected samples were returned to the column after measuring their solids and water contents.

3.2.4 Thermocouple Probes

A thermocouple probe was designed for measuring temperatures at various locations inside the slurry column.

As shown in Figure 3.5, the probe consisted of four copper-constantan thermocouples, which were placed inside a stainless steel tube with a diameter of 6.4 mm and a length of 0.15 mm. Four small holes were drilled on the tube. The tip of each thermocouple was placed in each hole and exposed to the inside of the slurry column. Silicone was filled inside the tube to fix the thermocouples in the tube.

Three such thermocouple probes were arranged along column height. The time and space averaged bed temperatures measured from thermocouple probes were monitored by a digital thermometer.

3.3 Experimental Procedures and Measurements

3.3.1 Heat Transfer Coefficient

As described in section 3.2, the heat transfer probe was used to measure heat flux and the surface temperature of the probe. The thermocouple probe was used to measure bed temperature. The fast response heat transfer probe provided instantaneous heat transfer

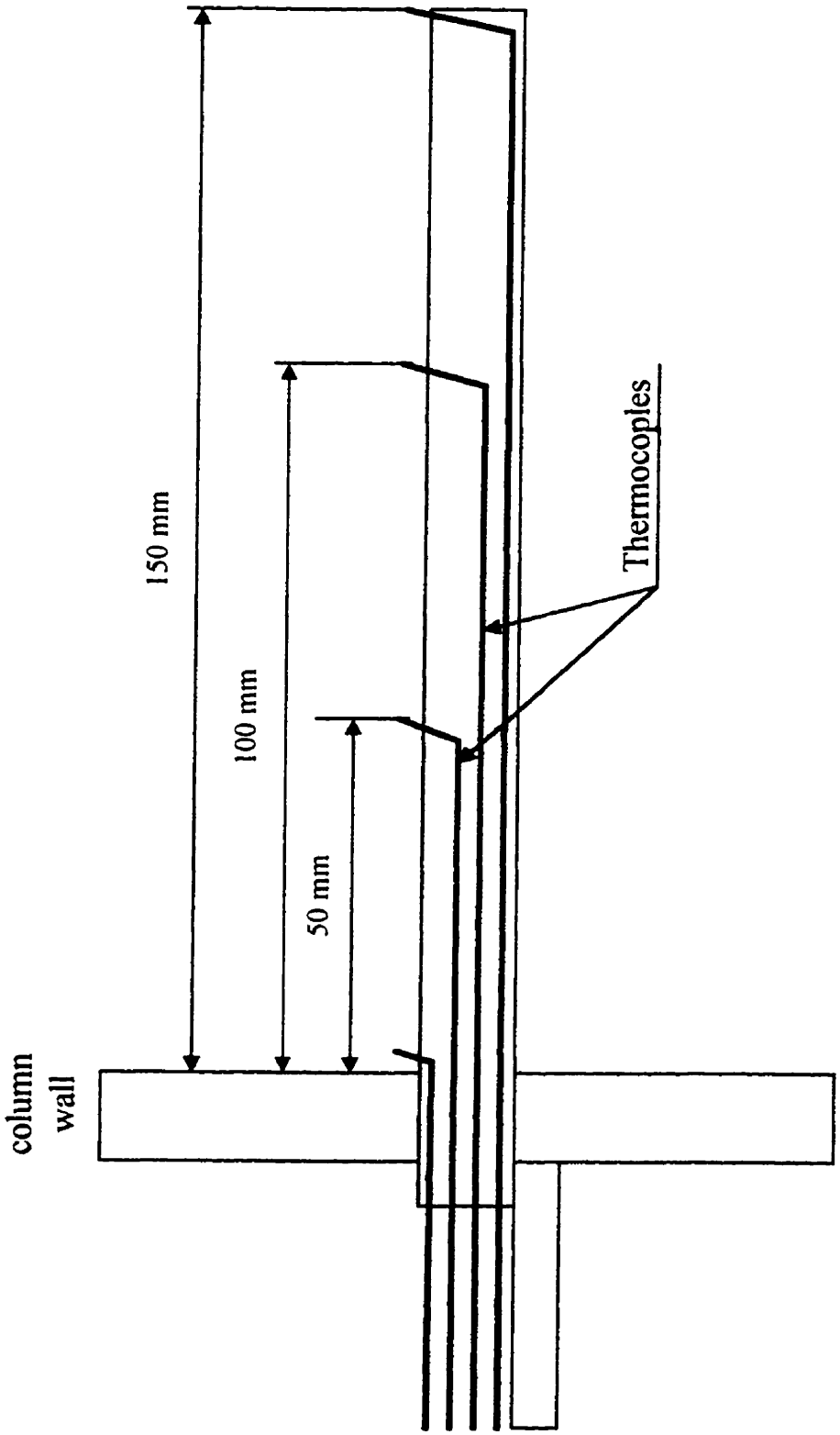

Figure 3.5 Probe design for thermocoples

coefficients based on measurements of heat flux, surface temperature and bed temperature:

$$h_i = \frac{q}{(T_{si} - T_b)} \qquad (3.1)$$

where, h_i is instantaneous heat transfer coefficient; q is heat flux; T_{si}, T_b are surface and bed temperatures respectively.

Experiments were initially conducted to study the probe response to single bubbles passing on probe surface. They were conducted in a small column with a diameter of 0.1 m and height of 0.39 m, as shown in Figure 3.6. Tap water was filled up to column overflow. A brass tube of a diameter of 12.7 mm with a single orifice of 1.5 mm was placed on the column bottom to generate single bubbles. The generated bubbles passed on the surface of the heat transfer probe. The bubble frequency was controlled at about 1 bubble per second by controlling gas input. To maintain a constant bed temperature, tap water at constant temperature flowed into the column at the bottom and overflowed at the top. The heat transfer probe was placed at the center near the top of column. The experimental results are shown in Figure 3.7. This figure indicates that the variation of heat transfer coefficient with time is cyclic with one peak per second (sampling frequency was 50 Hz), which corresponds the frequency of generated bubbles. This result showed that a sharp peak of instantaneous heat transfer coefficient was directly related to the bubble passage on the surface of the probe.
The generation of peaks can be attributed to enhancement of heat transfer by the turbulent wake region behind bubbles.

Kumar et al. (1992) collected photographical records as single bubbles passed on the surface of a fast response heat transfer probe. They found that the instantaneous heat transfer coefficient increased as a bubble approached the surface of the heat transfer probe. The instantaneous heat transfer coefficient continued to increase up to a maximum value which indicated a wake region behind the bubble. After the maximum

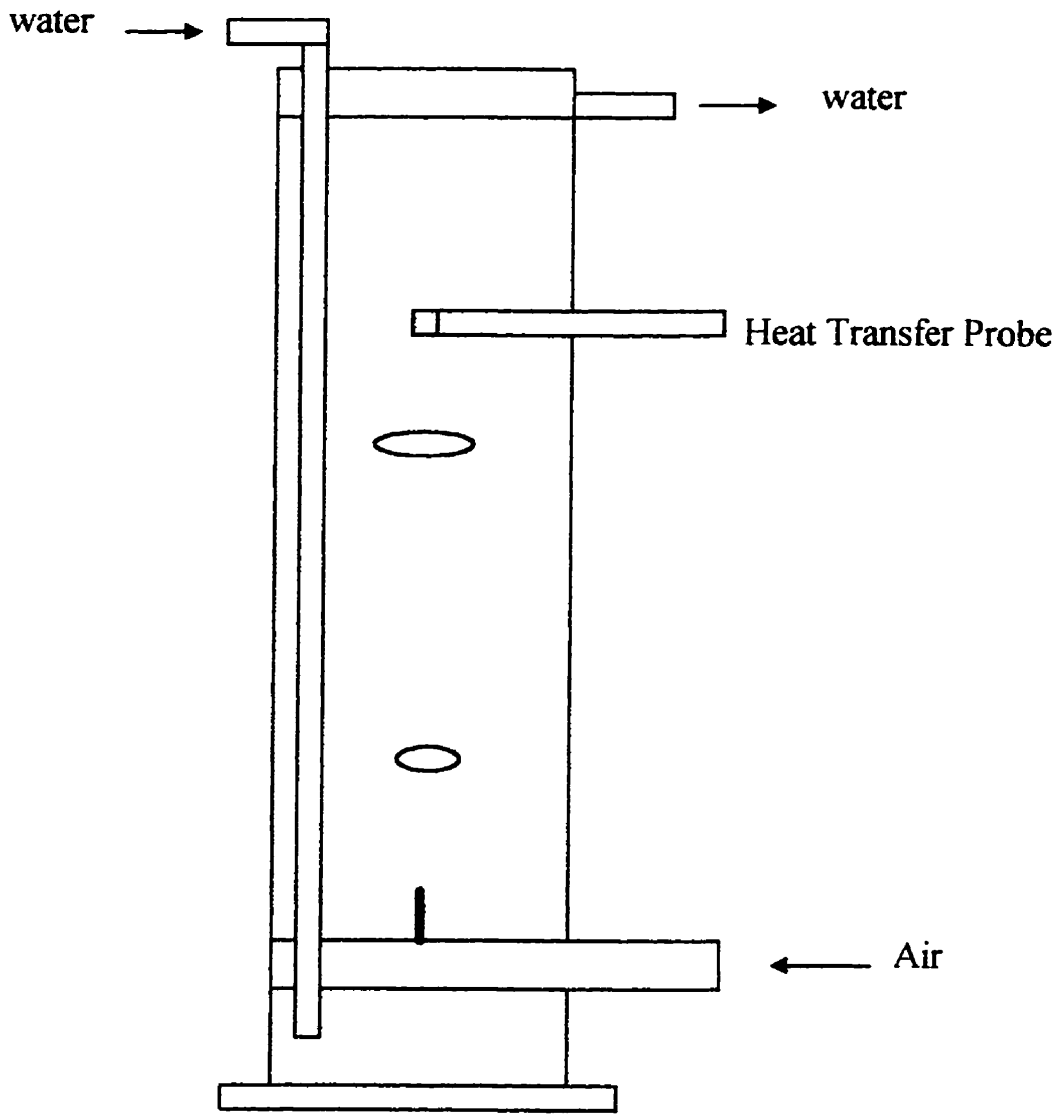

Figure 3.6 Diagram of single bubble experiment

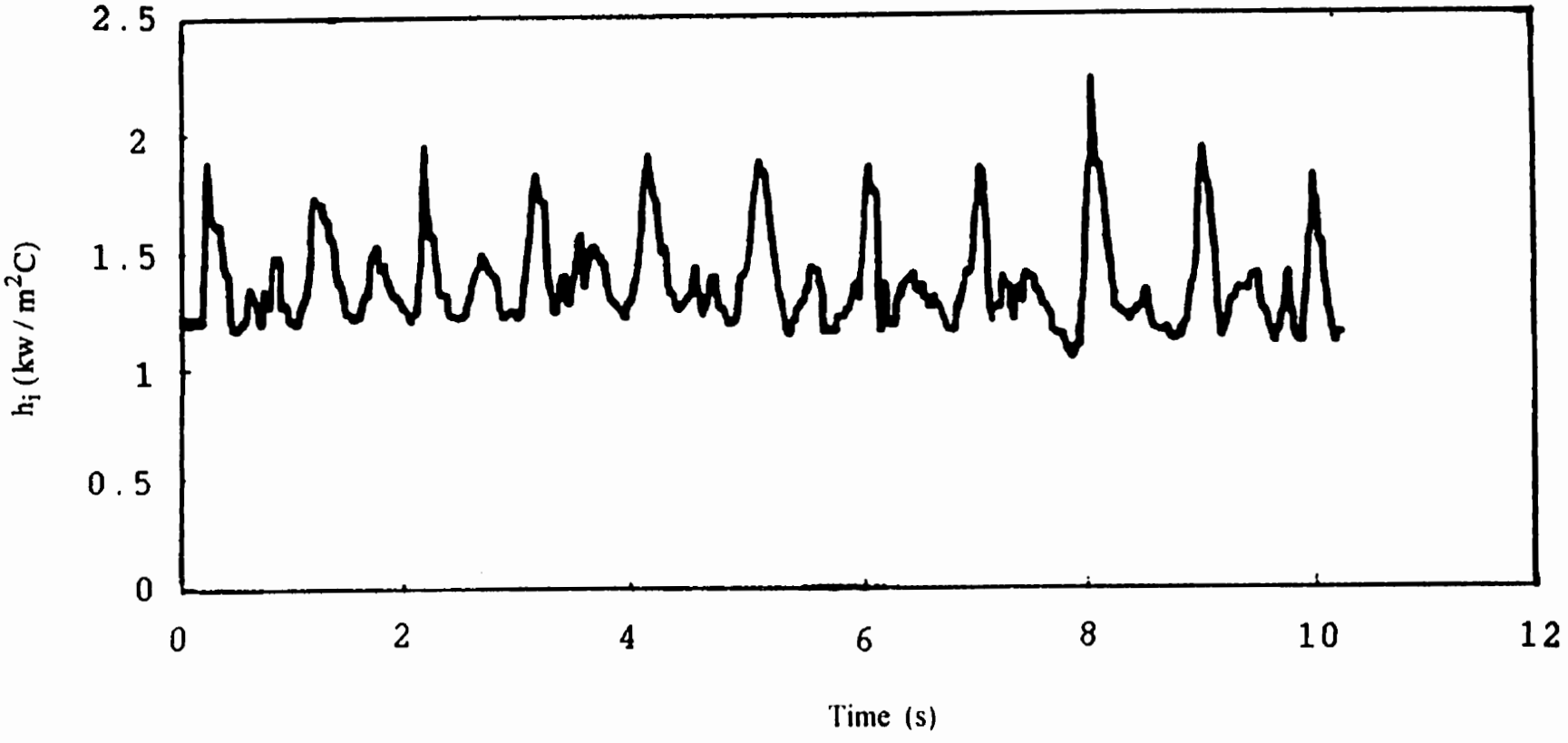

Figure 3.7 Instantaneous heat transfer coefficients with single bubbles rising in water

value, the heat transfer coefficient decreased. Their observation showed that the peak of instantaneous heat transfer coefficient was generated by bubble-wake-induced turbulence. It was also observed that the heat transfer coefficient increased with increasing bubble volume in different systems. A larger bubble would have a larger wake and stronger vortices associated with it. This would induce a stronger turbulence and enhance heat transfer rate. Kumar and Fan (1994) also observed higher instantaneous heat transfer coefficient with chain bubbling compared to single bubble injection, which was attributed to frequent bubble-wake effects and rapid bubble acceleration.

Figure 3.8 shows a typical time series observation of instantaneous heat transfer coefficients obtained in this study in the central region of air-water system. The higher and sharper increase of instantaneous heat transfer coefficient can be attributed to the wake region behind a bubble passing on probe surface.

The time averaged heat transfer coefficient is an important parameter for designing heat transfer surfaces for a slurry bubble column. This parameter can be obtained by averaging instantaneous heat transfer coefficients as follows:

$$h_{ave} = \frac{1}{N} \sum_{i=1}^{N} h_i \qquad (3.2)$$

here, h_{ave} is time averaged heat transfer coefficient; N is the total number of collected data. The value of N was selected to be 2100 to ensure a stable value of heat transfer coefficients.

Experiment conducted at different times were compared to verify the reproducibility of the probe response. Figure 3.9 compares the experimental results obtained over a six months period. The data points are plotted with 95 % confidence intervals. It can be seen that the results obtained are very close , verifying the reproducibility and stability of probe response.

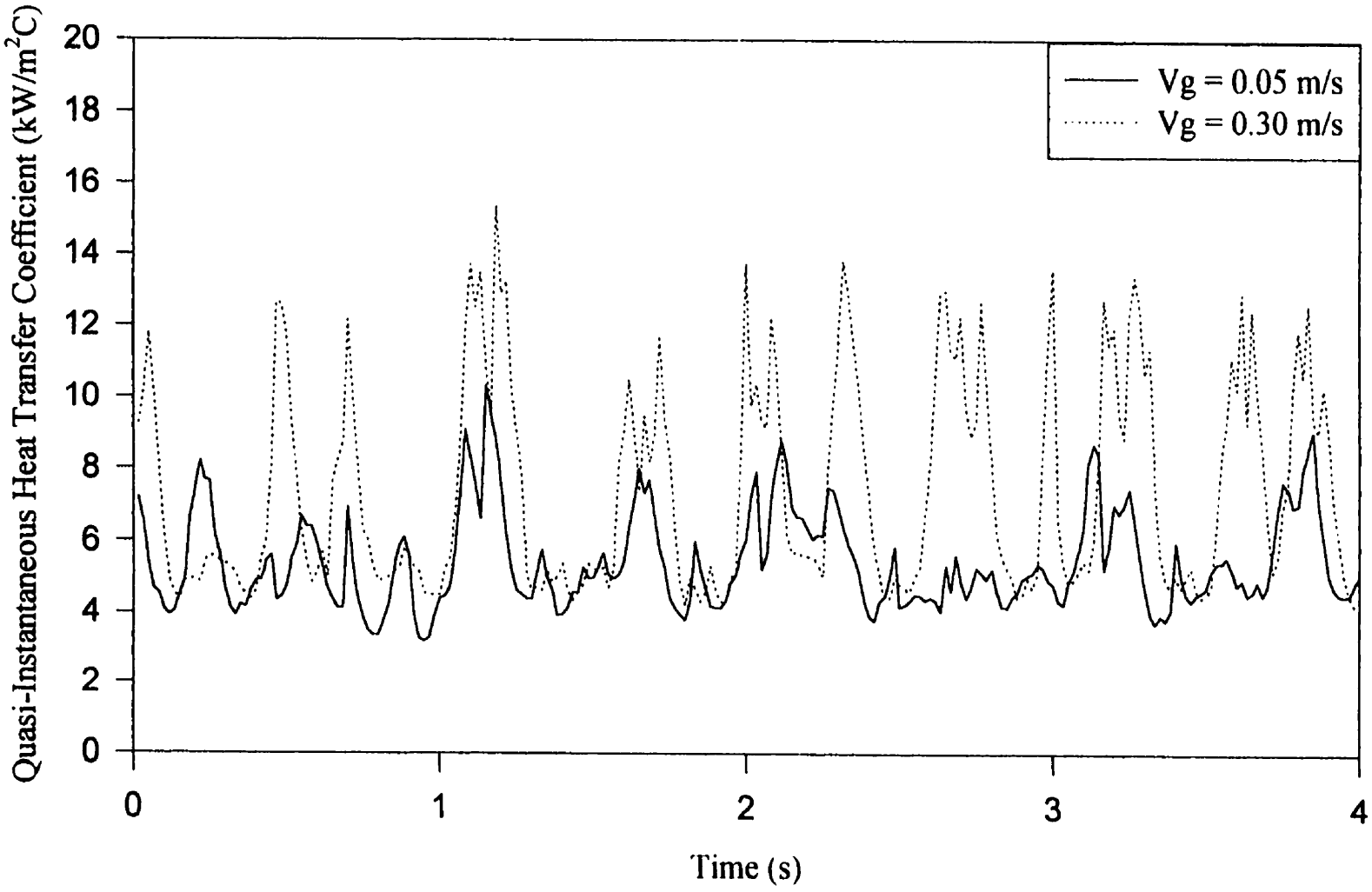

Figure 3.8 Instantaneous heat transfer coefficients measured in air-water at column center

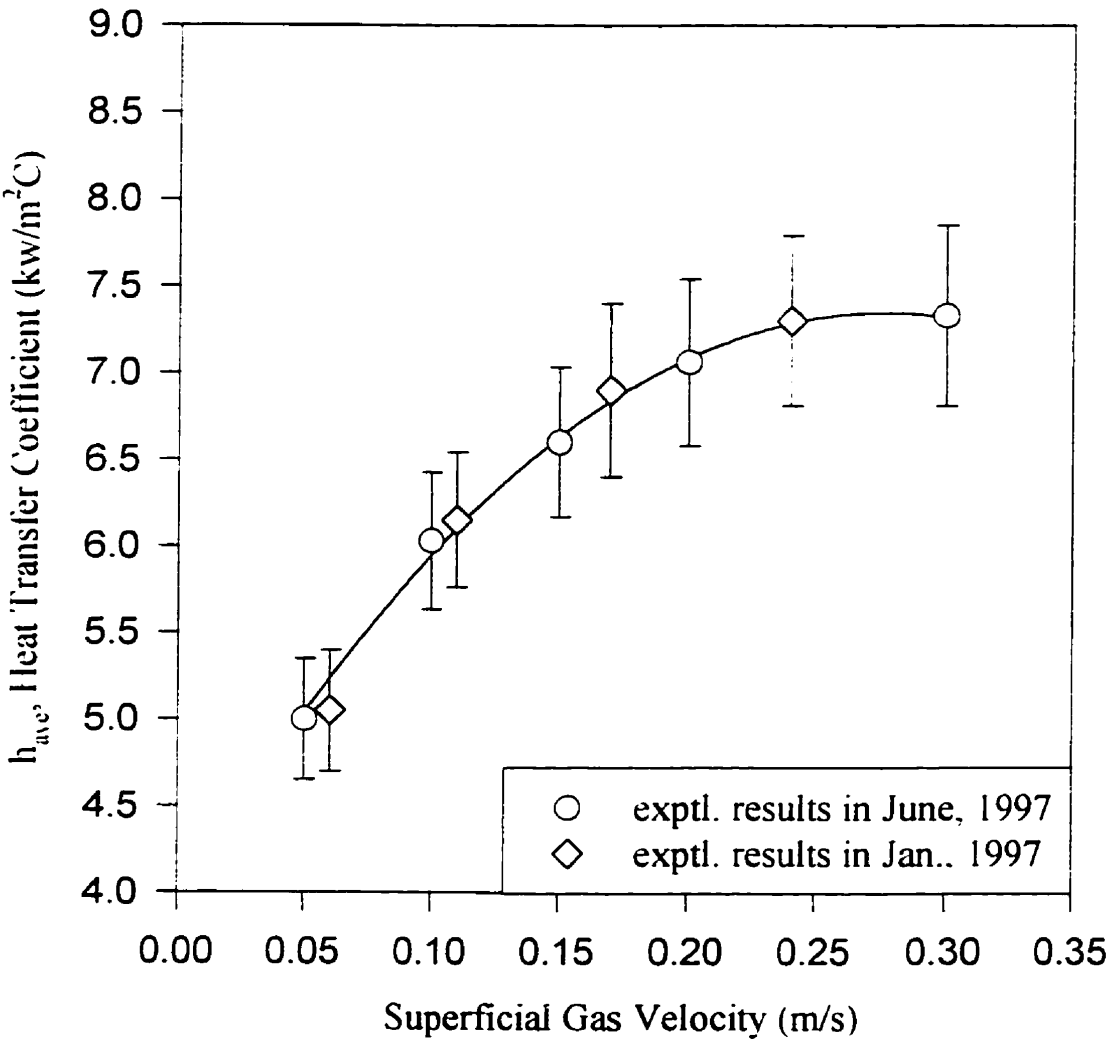

Figure 3.9 Average heat transfer coefficients in air-water system at column center (95% confidence intervals) (Data based on Appendix E2)

3.3.2 Phase Holdups

Phase holdups are important hydrodynamic parameters for designing a slurry bubble column. They are defined as the fractions of the bed volumes occupied by each phase.

In this study, phase holdups were obtained from measurements of pressure gradients and slurry sampling along column axis. In a three-phase slurry bubble column, the static pressure drop along the bed height is given as:

$$\Delta P = g(\rho_g \varepsilon_g + \rho_l \varepsilon_l + \rho_s \varepsilon_s)\Delta H \qquad (3.3)$$

where, ε_g, ε_l and ε_s are gas, liquid and solid phase holdups; ρ_g, ρ_l and ρ_s are gas, liquid and solid densities.

Moreover, the sum of the holdups must be equal to unity:

$$\varepsilon_g + \varepsilon_l + \varepsilon_s = 1 \qquad (3.4)$$

Liquid and solid phase holdups can also be defined as:

$$\varepsilon_l = \phi_l\ (\varepsilon_l + \varepsilon_s) = \phi_l (1 - \varepsilon_g) \qquad (3.5)$$

$$\varepsilon_s = \phi_s\ (\varepsilon_l + \varepsilon_s) = \phi_s (1 - \varepsilon_g) \qquad (3.6)$$

where ϕ_l and ϕ_s are volume fractions of liquid (water) and solids in bubble-free slurry phase, which are obtained from slurry samples collected by using sampling probe.

The concentration of slurry sample was measured using a pycnometric technique. The fraction of solid in slurry phase can be obtained by:

$$\phi_s = \frac{\rho_{sl} - \rho_l}{\rho_s - \rho_l} \tag{3.7}$$

where, slurry density, ρ_{sl}, was measured by weighing samples of known volume.

Substituting equations (3.4) - (3.6) into equation (3.3):

$$\begin{aligned}\frac{\Delta P}{\Delta H} &= g(\rho_g \varepsilon_g + \rho_l \phi_l (1-\varepsilon_g) + \rho_s \phi_s (1-\varepsilon_g)) \\ &= g(\rho_g \varepsilon_g + (\rho_l \phi_l + \rho_s \phi_s)(1-\varepsilon_g))\end{aligned} \tag{3.8}$$

Since ρ_g is negligibly small, the above equation becomes:

$$\Delta P = g(\rho_l \phi_l + \rho_s \phi_s)(1-\varepsilon_g)\Delta H \tag{3.9}$$

Therefore gas holdup can be obtained as:

$$\varepsilon_g = 1 - \frac{1}{g(\rho_l \phi_l + \rho_s \phi_s)} \frac{\Delta P}{\Delta H} \tag{3.10}$$

If ΔP is measured by means of a water manometer, ΔP can be expressed as:

$$\Delta P = \rho_w g \Delta h_m \tag{3.11}$$

where, Δh_m is the height difference measured in the water manometer. The gas holdup can be obtained as follow:

$$\varepsilon_g = 1 - \frac{1}{\rho_l \phi_l + \rho_s \phi_s} \frac{\rho_w \Delta h_m}{\Delta H} \tag{3.12}$$

The solids and liquid holdups can be then calculated by Equations 3.6 and 3.7.

Experiments conducted at different times were compared to verify the reproducibility of gas holdup measurements. Figure 3.10 compares the experimental results obtained over a six months period. The data points are plotted with 95 % confidence intervals. It can be seen that the results obtained are very close, verifying the reproducibility and stability of pressure transducers.

3.3.3 Dynamic Gas Disengagement

The dynamic gas disengagement technique is based on complete stoppage of gas phase entering the column at a given time. Before this moment, the inlet gas flowrate was kept at a constant value. A quick closing ball valve was used for stopping gas flow into column.

The data acquisition for measuring pressure started about 10 seconds before gas flow was shut down, so as to record the whole dynamic process of pressure variation. The whole process included three parts: steady operation, gas escaping after stoppage of gas flow, and gas free suspension.

As the gas inlet valve was closed, the instantaneous gas holdup was monitored by two pressure transducers, which provided instantaneous gas holdup defined as:

$$\varepsilon_g(t) = 1 - \frac{1}{\rho_l \phi_l + \rho_s \phi_s} \frac{dP(t)}{dH} \qquad (3.13)$$

This technique is based on the principle that different bubble classes in a gas-liquid dispersion can be distinguished if there are significant differences between their rise velocities. The rate at which the instantaneous gas holdup drops would depend on the fraction and rise velocity of the gas bubbles. Initially, when the fast rising larger bubbles

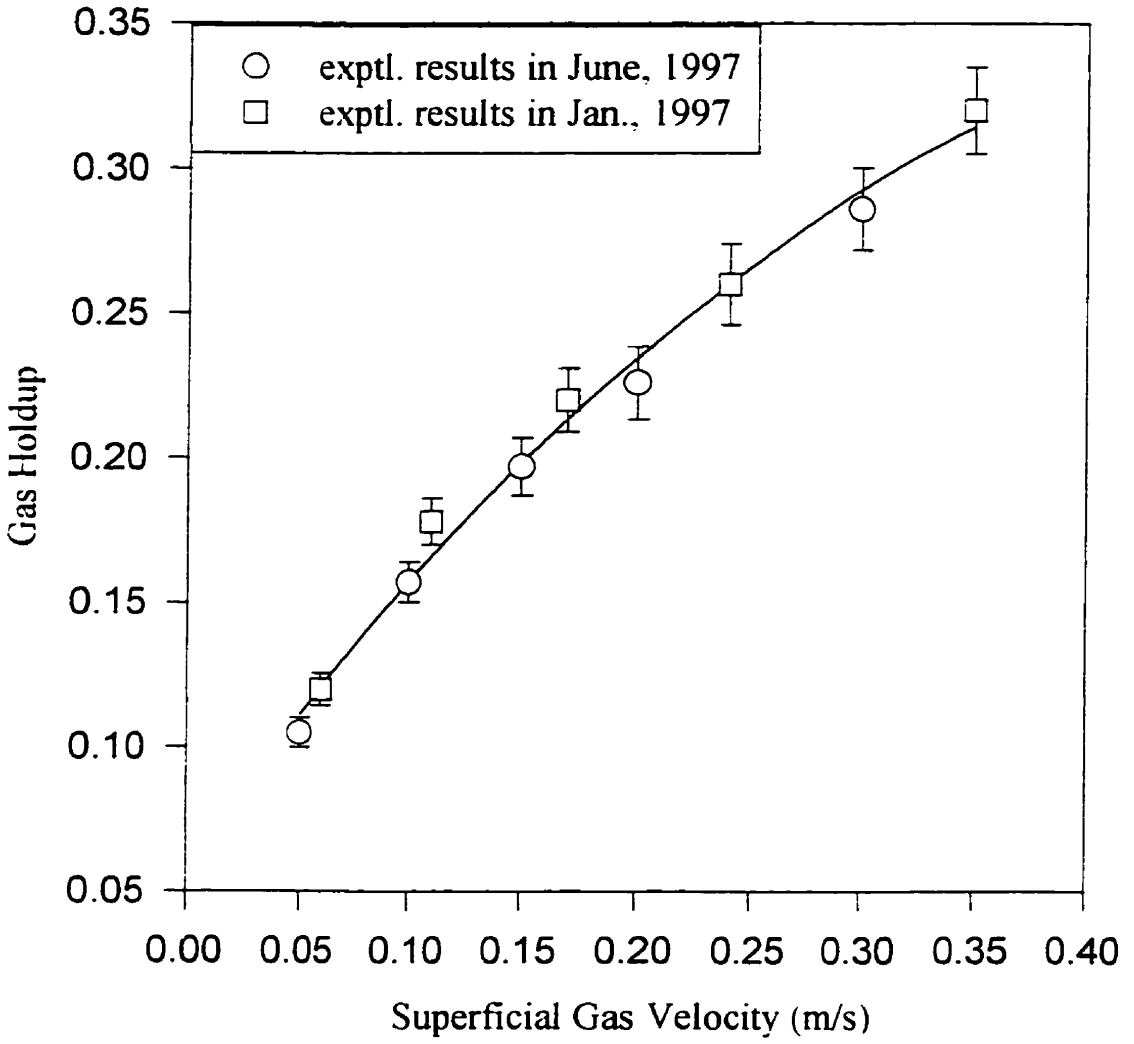

Figure 3.10 Gas holdup in air-water system (95% confidence intervals)
(Data based on Appendix E1)

are escaping, the drop of the instantaneous gas holdup would be fast. The rate of drop would, however, slow down when only small bubbles are escaping. This technique can provide reasonably approximate information if there are two distinct classes of bubbles. Various assumptions and sources of errors associated with the technique have been reviewed by Schumpe and Grund (1986). The main assumptions for this application are: 1) the holdup structure is not affected by the bubbles interactions after the gas supply is cut off; 2) the holdup structure is axially uniform. The gas holdup structure can be affected during the disengagement of larger bubbles, which can accelerate the smaller bubbles in their wake. Meanwhile, the gas holdup of smaller bubbles may be affected by the volume of sparger.

The gas holdups of larger and small bubbles are identified by observing instantaneous gas holdup during gas disengagement. Figure 3.11a shows instantaneous gas holdups during gas disengagement in an air-water system at different superficial gas velocities. At high superficial gas velocity, the instantaneous gas holdups have higher fluctuations and drop faster as gas is shut off, indicating larger bubbles escaping from the bed. This can be defined as first period. At the rear end of the larger bubble leaving out from the bed, only small bubbles disengage, when gas holdups drop smoothly. This can be defined as secondary period. At low superficial gas velocity (i.e. Vg=0.05 m/s), first period was not observed, indicating negligible amount of larger bubbles in the bed.

Figure 3.11b shows typical instantaneous gas holdup and behaviors of two classes of bubbles during disengagement. The initial gas holdup at t_0 is defined by ε_0. After stopping the gas supply, the instantaneous gas holdup drops fast, indicating larger bubbles escaping. At time t_1, the rear end of the larger bubble swarm reaches the dispersion level denoted by ε_2. In the second period, only small bubbles disengage and the slope is much smaller. Then at time t_2, the rear of the small bubble swarm leaves out from the liquid phase; at that time the gas holdup become zero. These two lines can be used for evaluating bubble rise velocity and gas holdup of the two bubble classes. The

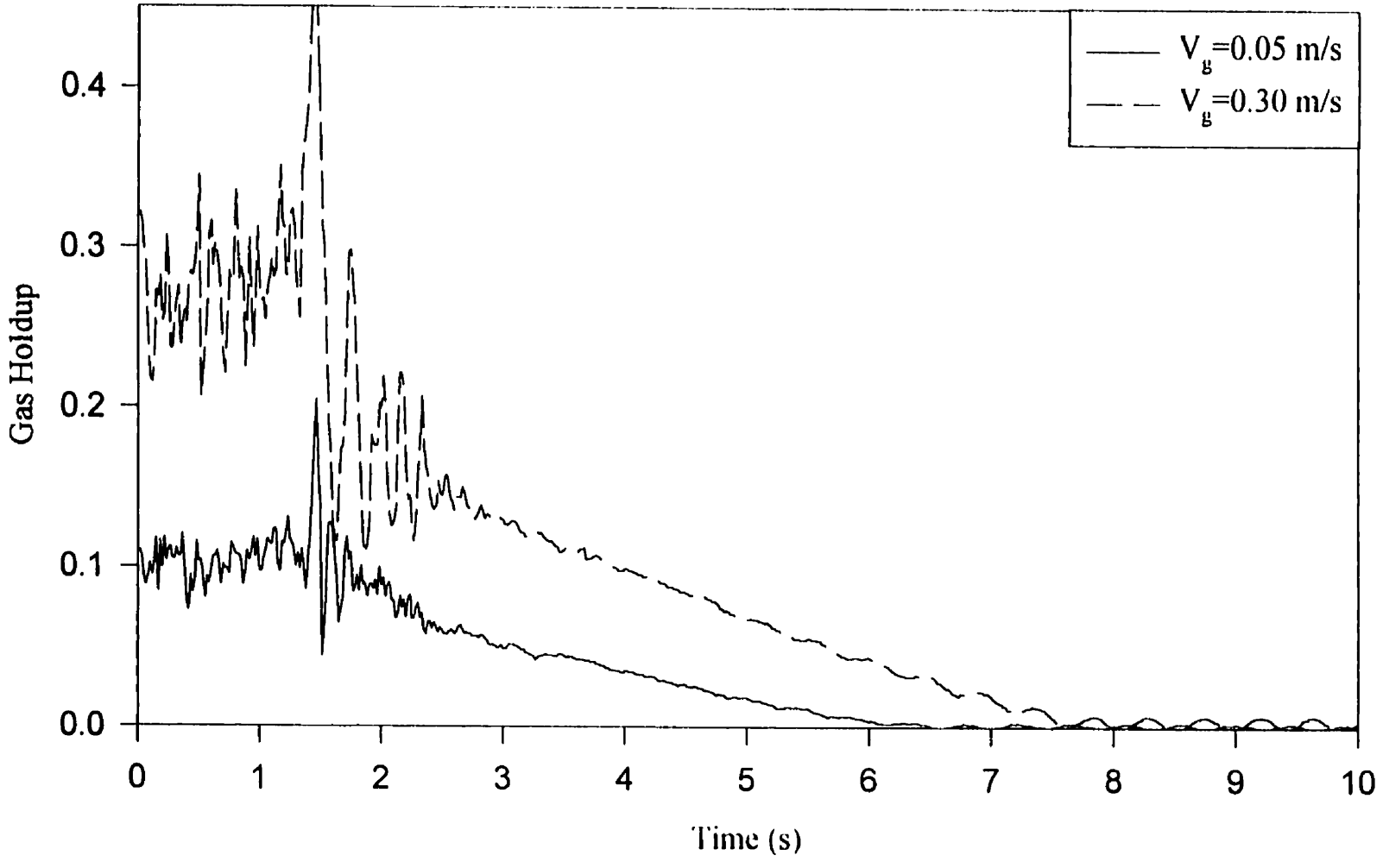

Figure 3.11a Gas disengagement in air-water systems

Figure 3.11b Gas disengagement in air-water systems (Vg = 0.30 m/s)

two linear equations were obtained by regression analysis. The two straight lines were considered separately only when their slopes were statistically different.

In the first period of the disengagement, the disengagement rate of small bubbles can be accelerated by the wakes of larger bubbles, while the liquid backflow due to bubble disengagement can slow their disengagement rate. These two effects can compensate for each other. Figure 3.11c shows two different expanded bed heights which can be used to estimate small bubbles properties. H_{d3} is the height which accounts for the disengagement of small bubbles during both periods. If small bubbles disengage at the same rate in both periods, $H_{d3}=H_{d1}$; if there is no disengagement of small bubbles during the first period, $H_{d3}=H_{d2}$. The true value may lie between these two extremes. Schumpe and Grund (1986) accounted for the effects of liquid backflow on the disengagement rate of the small bubbles during the first period and proposed the following procedure to obtain the dispersion height of small bubbles:

$$\left(dH_d/dt\right)_{l,s}=\left(dH_d/dt\right)_2\frac{(H_{d0}-H_{d3})(H_{d1}-H_s t_1/t_2)}{H_{d0}(H_{d1}-H_s)} \qquad (3.14)$$

$$H_{d3}=H_{d1}-t_1(dH_d/dt)_{l,s} \qquad (3.15)$$

where, H_{d0}, H_{d1}, H_{d2}, H_{d3} and H_{lel} are defined as Figure 3.13c.

The value of H_{d3} was obtained by an interactive procedure, using equations 3.14 and 3.15. Equations 3.14 and 3.15 require the initial and expanded height H_0, H_{d0}, H_{d1} and H_{d2}, which can be converted from corresponding gas holdups:

$$H_{di}=\frac{H_s}{1-\varepsilon_i}$$

where, H_s is static liquid height without bubbles.

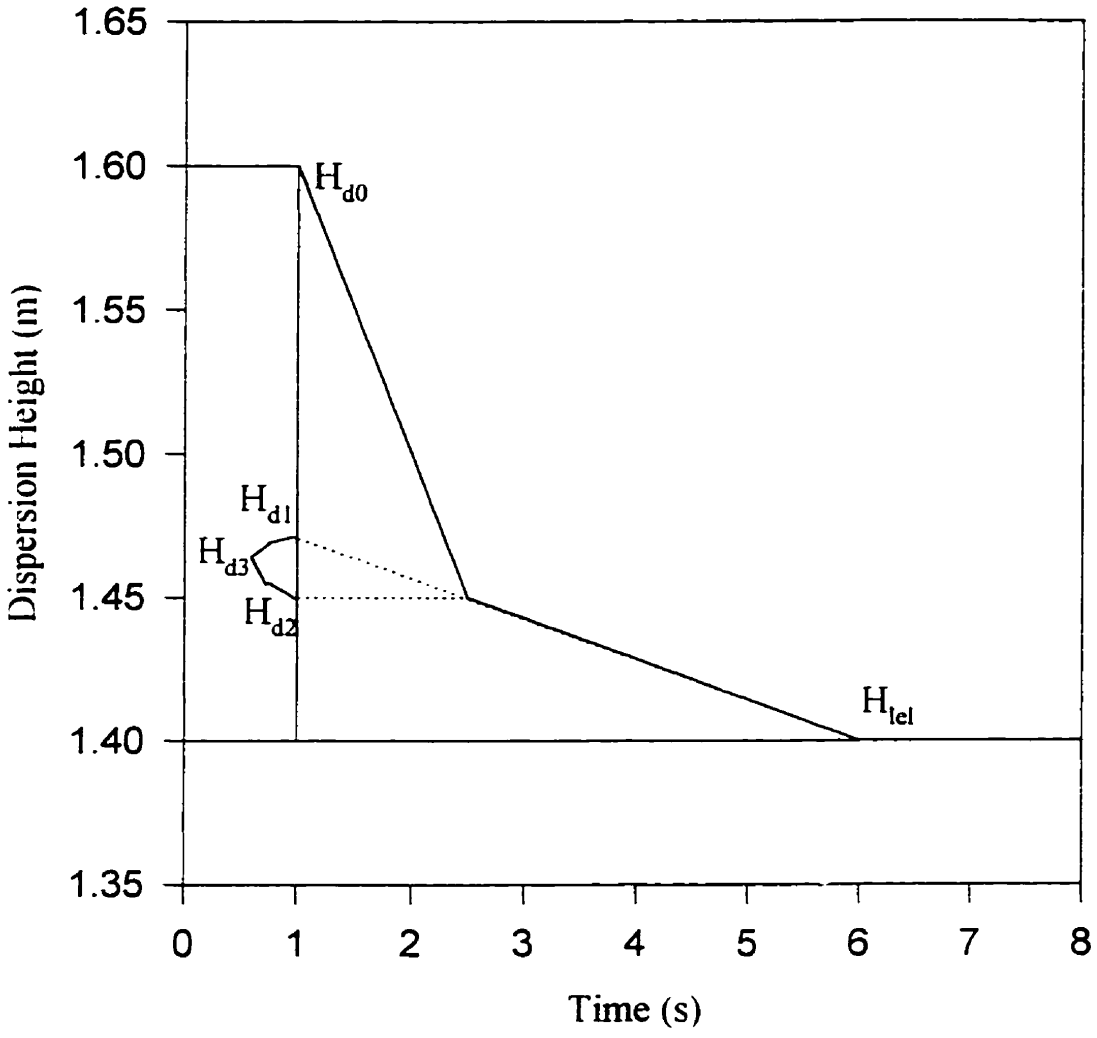

Figure 3.11c Plot of dispersion height as a function of time

Based on this calculation procedure, the values of H_{d3} were always found to be close to H_{d1} (within 3%). Thus, small bubbles disengage at the same rate in both periods. This indicated that in this experiment, the rise velocities of small bubbles at both periods were essentially the same and that the gas holdups of small bubbles is close to ε_1.

In this technique, another problem is the effect of sparger volume on small bubble gas holdup. Schumpe and Grund (1986) outlined a calculation procedure to correct the dispersion height of small bubbles if the volume of the sparger makes a contribution in this technique. Based on this correction, the effect of sparger volume on dispersion height of small bubbles in this study is negligible (< 1 %).

Based on mass balance during second period of disengagement, the amount of gas leaving due to small bubbles from the region between two probe should be equal to that of liquid flowing back in from the top, that is:

$$V_{g,s} = -\frac{d(\varepsilon(t)H_d)}{dt} \tag{3.16}$$

here, V_{gs} is superficial gas velocity associated with small bubbles; H_d is the height between two probes. Thus, the superficial gas velocity of small bubbles can be obtained from the slope of the second period of disengagement.

The individual gas holdups, the superficial gas velocities and the rise velocities for the two bubbles classes can be obtained using the following relations:

$$\varepsilon_{b,L} = \varepsilon_0 - \varepsilon_1 \tag{3.17}$$

$$\varepsilon_{b,s} = \varepsilon_1 \tag{3.18}$$

$$V_{g,l} = Vg - V_{g,s} \tag{3.19}$$

$$U_{b,L} = V_{g,l}/\varepsilon_{b,L} \tag{3.20}$$

$$U_{b,s} = V_{g,s} / \varepsilon_{b,s} \qquad (3.21)$$

3.4 General Operation Procedures

Experiments were carried out at five superficial gas velocities for each slurry concentration. When switching from a lower to a higher solids concentrations, instead of removing the entire slurry and replacing with fresh slurry, the liquid from the top of the column was removed and the desired mass of solids was added into the slurry bed.

For startup at higher concentration slurry systems (20 vol.% solids and higher), the bed of settled solids particles could not be dispersed by simply switching on the desired gas velocity. At these solids concentrations, solids plugs were forming and moving up along the column without solids dispersion. Air was first introduced by using the solids sampling probe located near the top of the settled bed. Therefore at high solids concentrations, the solids were dispersed stagewise. Once solids in the region beyond the first sampling probe were dispersed, the next sampling probe was used. This was continued until dispersion was completed by the gas sparger itself. The approximate time of dispersion was 1 hour for a 20 vol.% solids system and about 4 hours for a 40 vol.% solids system.

4.0 Results and Discussion

This chapter presents the results of the hydrodynamics and heat transfer measurements. The first section reviews the gas holdups, solid distribution data and gas disengagement results. Section 4.2 discusses local average and instantaneous heat transfer measurements at various superficial gas velocities and slurry concentrations in different regions of the column. Bubble wake behavior is analyzed based on instantaneous heat transfer coefficients.

4.1 Hydrodynamics

The results in this section are presented in three subsections. In subsection 4.1.1, gas holdups obtained in the bubble column and the slurry bubble column are presented. In subsection 4.1.2, measured axial solid concentrations are applied to the study of particle hindered settling velocity and solid dispersion coefficients. In subsection 4.1.3, gas disengagement data are analyzed to investigate bubble rise velocities and bubble size population.

4.1.1 Gas Holdups

The gas holdups obtained in air-water system based on pressure gradients are shown in Figure 4.1.1. The experimental results are also compared with literature studies (Goldbole et al., 1984; Saxena et al., 1989, 1990a). Goldbole et al. (1984) and Saxena et al. (1989, 1990a) measured gas holdups in column diameter of 0.305 m. It can be seen from Figure 4.1.1 that the gas holdups at gas velocities from 0.05 to 0.30 m/s are in good agreement with these literature studies. It can also be seen from Figure 4.1.1 that gas holdup was an increasing function of gas velocity.

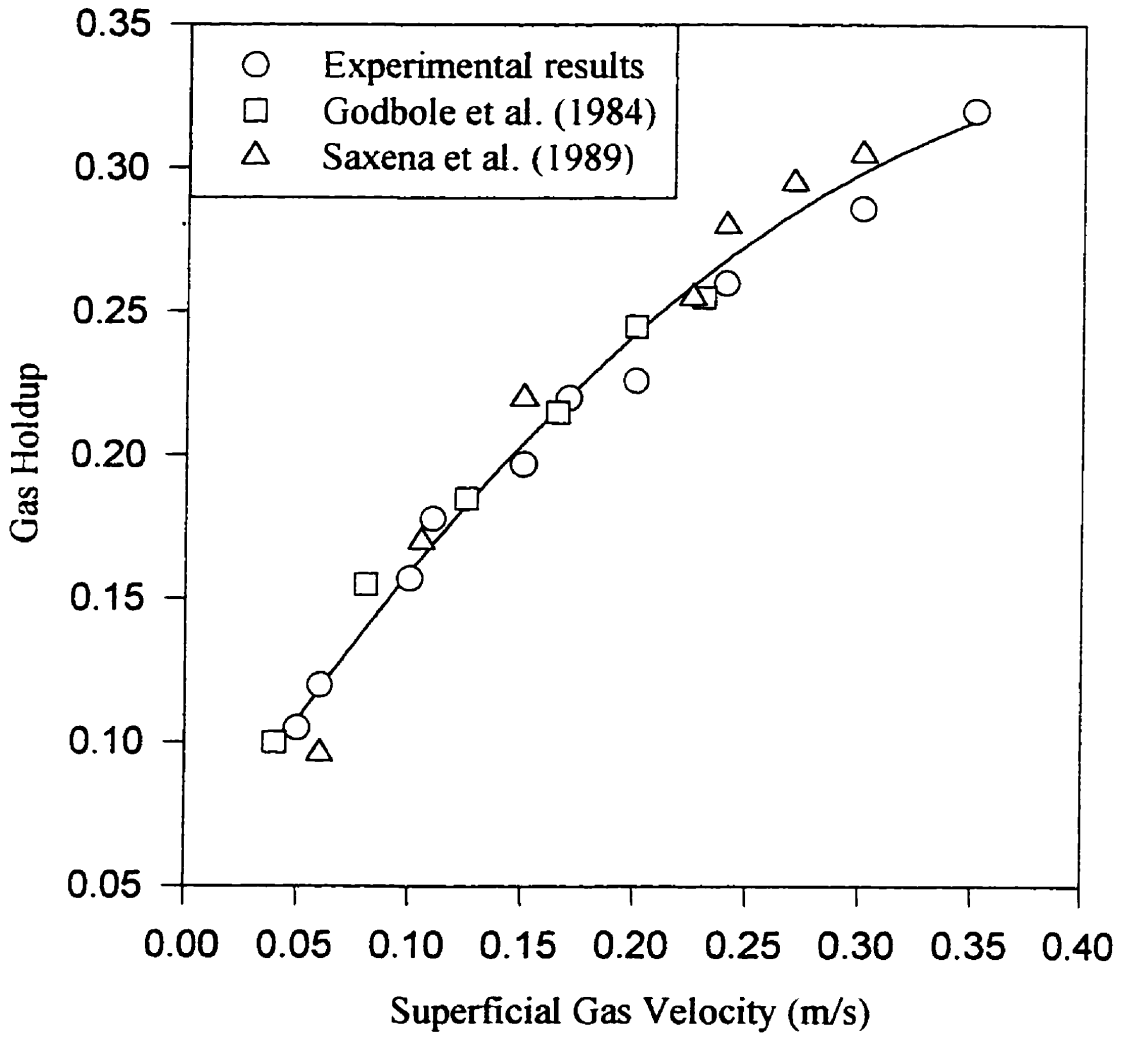

Figure 4.1.1 Gas holdup in air-water system
(Experimental results based on Appendix E1)

As fine particles are added into water, it becomes a slurry phase and its hydrodynamic behavior is changed. Figure 4.1.2 shows the dependence of gas holdup on gas velocity at various solids concentration. It can be seen from Figure 4.1.2 that the gas holdups increased with increasing gas velocity for all slurry concentrations. Figure 4.1.2 also indicates that the addition of solids into water reduced the gas holdup. However, the effects of high slurry concentrations on gas holdup are not clearly shown in Figure 4.1.2.

Figure 4.1.3 presents the variation for gas holdup with slurry concentration for constant gas velocities. It can be seen from Figure 4.1.3 that gas holdup initially decreased quickly with increasing slurry concentration up to slurry concentration of about 15 vol.%. For higher slurry concentrations, the rate of decrease slowed down. In fact there was a slight increase in gas holdup at high solids concentrations (> 25 vol. %). There were minimum gas holdups at slurry concentration around 25 vol. % for gas velocities from 0.05 to 0.30 m/s. This phenomenon has not been reported in literature so far.

It is interesting to note from Figure 4.1.3 that the decrease of gas holdup depends on gas velocity at slurry concentrations below 15 vol.%. It is seen from Figure 4.1.3 that the gas holdup at high gas velocities decreased more rapidly with increasing slurry concentration, compared with that at low gas velocities. The decrease in gas holdup with increasing slurry concentrations has been observed by other researchers (Kara et al., 1982; Koide et al., 1984; Sauer and Hempel, 1987). This phenomenon may be explained by an increase in bubble size due to the increase in slurry viscosity in presence of fine solids particles (Kara et al., 1982; Nigam and Schumpe, 1996). The gas holdup at a given gas velocity would decrease, due to higher rise velocity of larger bubbles formed. As solids particles are added into water, the apparent slurry viscosity would increase. The increase of bubble size can be attributed to either increasing rate of bubble coalescence or reduced rate of bubble-breakup. Fan (1989) attributed the drop in gas holdup to the promotion of bubble coalescence caused by increase in "pseudo-viscosity" of suspension. However, it is also important to consider effects of

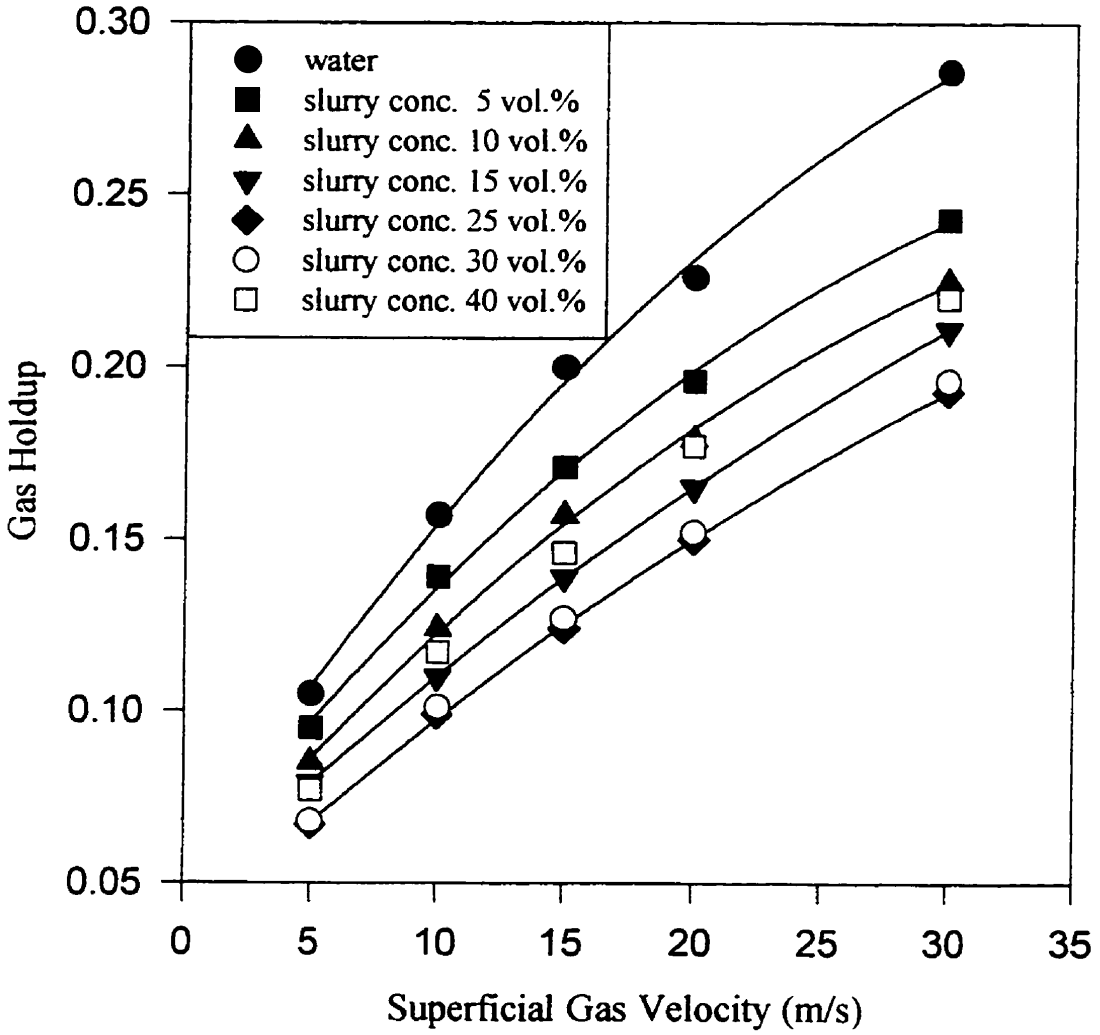

Figure 4.1.2 Gas holdup as a function of gas velocity at constant slurry concentrations
(Data based on Appendix E1)

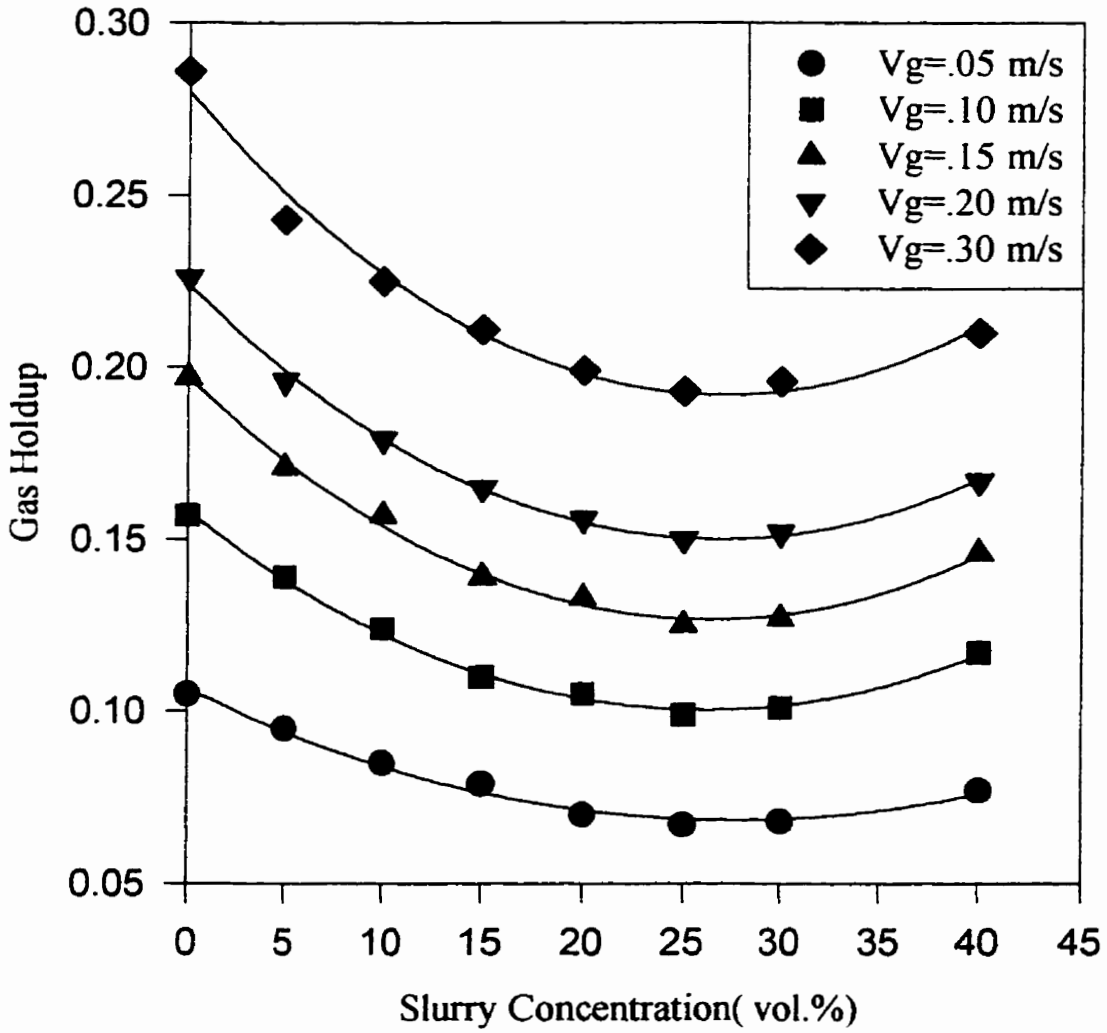

Figure 4.1.3 Gas holdup as a function of slurry concentration at a constant superficial gas velocity (Data based on Appendix E1)

fine particle suspension on bubble breakup rate. It is reasonable to explain this phenomenon by means of both bubble coalescence and bubble breakup. Bubble breakup occurs through bubbles interactions with turbulent eddies (Prince and Blanch, 1990) as large unstable bubble moves up from the tips of gas jets. High gas velocity will improve the turbulence of the slurry phase. The improved turbulence will improve the interactions between bubble and turbulent eddies, which result in an increase in the rate of bubble breakup. Therefore, high gas holdup at high gas velocity can be attributed to the high rate of bubble breakup. The addition of solids reduces the bubble breakup rate by increasing slurry pseudo viscosity of the continuous phase, which result in the larger size bubble. Therefore, gas holdup will decrease. It can be seen from Figure 4.1.3 that the rate of decrease of gas holdup with an increase in slurry concentration is much higher at higher gas velocity. This indicates that the addition of solids at high gas velocity more effectively reduces the rate of bubble breakup, which results in a fast increase in bubble size and in a fast decrease of gas holdup. At low gas velocity, the bubble breakup rate is expected to be low, therefore the rate of decrease of gas holdup with increasing slurry concentration is low for low air velocity.

For solids concentrations between 20 to 30 vol%, data on Figure 4.1.3 shows only a slight dependence of gas holdup on slurry concentration. Similar observations have been made by other researchers (Deckwer et al., 1980; Ying et al., 1980). Ying et al. (1980) found that gas holdup in silica-water system reduced up to solids concentration of about 16 wt% but thereafter no significant change was observed as slurry concentrations increased. This indicated that bubble size has reached a stable value of the coalesced bubble flow regime (Fan, 1989). In this flow regime, bubble size and rising velocity do not change significantly with an increase in solids concentration, which will result in a slight dependence of gas holdup on solids concentration.

Figure 4.1.3 also shows that the measured gas holdups increased slightly at the slurry concentrations higher than 25 vol.%. Such an increase in gas holdup with slurry concentration has not been reported in literature since most literature studies have

stayed below slurry concentrations of 20 vol.%. The observed increase in gas holdup at the high slurry concentration could be attributed to decrease in rise velocity of small bubbles due to significantly increased suspension viscosity and density. Literature studies have shown negligible effects of liquid properties (viscosity, density etc.) on the rise velocity of large spherical cap bubbles. The terminal velocity of small single bubbles in liquid phase has been investigated by many authors (Wallis,1974; Peebles and Garber, 1953). The terminal velocity of small single bubble depends on the liquid properties. Jamialahmadi et al. (1994) predicted terminal bubble rise velocity by the following equation:

$$U_\infty = \frac{U_\infty^{sp} U_\infty^{w}}{\sqrt{\left(U_\infty^{sp}\right)^2 + \left(U_\infty^{w}\right)^2}} \tag{4.1.1}$$

here, U_∞ is terminal bubble rise velocity. U_∞^{sp} and U_∞^{w} are rise velocities of small and larger bubbles, which are given by:

$$U_\infty^{sp} = \frac{1}{18}\frac{\rho_l - \rho_g}{\mu_l} g d_b^2 \tag{4.1.2}$$

$$U_\infty^{w} = \sqrt{\frac{2\sigma_l}{d_b(\rho_l + \rho_g)} + \frac{g d_b}{2}} \tag{4.1.3}$$

Slurry viscosity can be calculated by using correlation proposed by Vand (1948):

$$\mu_{sl} = \mu_L \exp\left[\frac{2.5\phi_s}{1 - 0.609\phi_s}\right] \tag{4.1.4}$$

The calculated terminal bubble velocities are shown in Figure 4.1.4. It is seen from Figure 4.1.4 that as slurry concentration increases from 25 vol% to 40%, the terminal bubble velocity of small bubble decreases, particularly for bubble size smaller than 4 mm. This will result in a longer residence time of small bubbles in the dispersion.

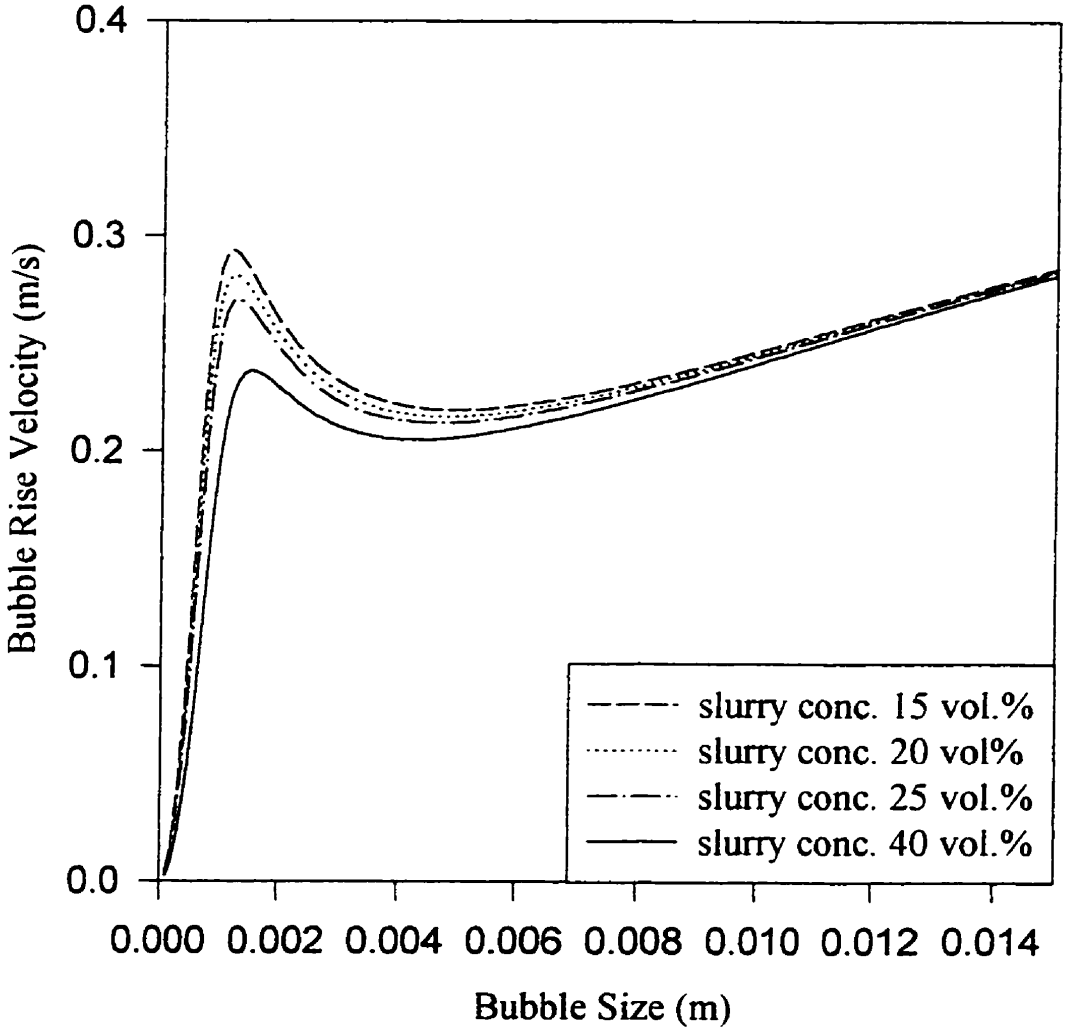

Figure 4.1.4 Single bubble terminal velocity at high slurry concentrations
(Calculations based on Jamialahmadi, 1994)

As slurry concentration increased from 25 vol.% to 40 vol.%, rise velocity of coalesced bubbles remained unchanged because the rise velocity of spherical cap large bubbles are independent of slurry properties (Fan, 1989; Jamialahmadi et al., 1994; Wallis, 1974). Thus the gas holdup of larger bubbles remained constant as slurry concentration increased from 25 vol.% to 40 vol.%. As calculated above, rise velocities of small bubbles are reduced. The reduced rise velocities of small bubbles will result in an increase in gas holdup. The detailed description of the effects of larger and smaller bubbles on gas holdups will discussed in section 4.1.3.

It may also be pointed out that pressure at the column bottom increased with increasing concentration of high density solid particles used in this study. Gas holdup has been found to increase with operating pressure (or gas density) by several literature studies (Idogawa et al., 1986; Wilkinson et al., 1990). At high slurry concentrations, the pressure at the column bottom will increase. However, based on the reported studies, the small pressure increase due to high slurry density cannot account for observed increases in gas holdups in this study.

The measured gas-holdup in two phase (air-water) and three phase (air-water-glass particles) are compared with the predictions by literature correlations. The various correlations for gas holdups which have been commonly used in bubble columns are listed in Table 4.1.1.

Figure 4.1.5 shows the comparison of experimental gas holdup with the various correlations in air-water system. It can be seen that the correlation proposed by Hikita et al. (1980) provides good predictions in air-water system. Prediction by Koide et al. (1984) are also close to experimental observation in air water system below gas velocity of 0.25 m/s. Predictions by correlations proposed by Smith et al. (1984) and Sauer and Hempel (1987) are lower than experimental results. The correlation proposed by Hikita et al. (1980) is based on the experimental data obtained in two phase system.

Table 4.1.1 Correlations for gas holdup in bubble column and slurry bubble column

Investigators	Correlation for Gas Holdup	System	Range of Variables
Hikita et al. (1980)	$\varepsilon_g = .672\left(\frac{V_g\mu_l}{\sigma}\right)^{.578}\left(\frac{\mu_l^4 g}{\rho_l\sigma^2}\right)^{.131}\left(\frac{\rho_g}{\rho_l}\right)^{.062}\left(\frac{\mu_g}{\mu_l}\right)^{.107}$	Gas : air, H_2 Liquid: water, methanol, n-butanol, 30%-50% sucrose solution (ring sparger)	D: 0.158, 0.23 m $0.25 < V_g < 0.28$ m/s $683 < \rho_l < 2960$ kg/m3 $.0004 < \mu_l < .05$ kg/ms $0.02 < \sigma < .073$ kg/s2
Smith et al.(1984)	$\varepsilon_g = \left[2.25 + \frac{0.379}{V_g}\left(\frac{\rho_{sl}}{72}\right)^{.031}\mu_{sl}^{.0016}\right]^{-1}$ $\mu_{sl} = \mu_l \exp\left[\frac{(5/3)\phi_s}{1-\phi_s}\right]$	Gas : nitrogen Liquid: water, silicone oil, ethylene glycol, ethanol solid: glass bead ($48.5 < d_p < 194$ μm) (multi orifice sparger)	D = 0.108 m $0.03 < V_g < 0.20$ m/s $820 < \rho_l < 1100$ kg/m3 ρ_s - 2500, 8770 kg/m^3
Koid et al. (1984)	$\frac{\varepsilon_g}{1-\varepsilon_g} = \frac{k_l\left(\frac{V_g\mu_l}{\sigma}\right)^{.918}\left(\frac{g\mu_l^4}{\rho_l\sigma_l^3}\right)}{1+4.35\phi_s^{.748}\left(\frac{\rho_s-\rho_l}{\rho_l}\right)^{.881}\left(\frac{DV_g\rho_l}{\mu_l}\right)^{-.168}}$	Gas : air Liquid: water, ethylene glycol, glycerol aqueous sln solid: glass & bronze spheres ($47.5 < d_p < 194$ μm) (perforated plate distributor)	$0.14 < D < 0.3$ m $0.01 < V_g < 0.18$ m/s $997 < \rho_l < 1178$kg/m3 ρ_s - 2500, 8770 kg/m^3
Sauer & Hempel	$\frac{\varepsilon_g}{1-\varepsilon_g} = .0277\left(\frac{V_g}{(\nu_{sl}gV_g)^{.25}}\right)^{.844}\left(\frac{\nu_{sl}}{\nu_{eff}}\right)^{.136}\left(\frac{C_s}{C_{so}}\right)^{.0392}$ $\nu_{sl} = \mu_l(1+2.5\phi_s+10.05\phi_s^2+.00273\exp(16.6\phi_s))/\rho_{sl}$ $\nu_{eff} = .011D_c\sqrt{gD}(V_g^3/g\nu_l)^{.18}$	Gas: air Liquid: water solid: sand, plastics ($110 < d_p < 2900$ μm) (perforated plate distributor)	D = 0.14 m $0.01 < V_g < 0.08$ m/s $1020 < \rho_s < 2780$ kg/m3

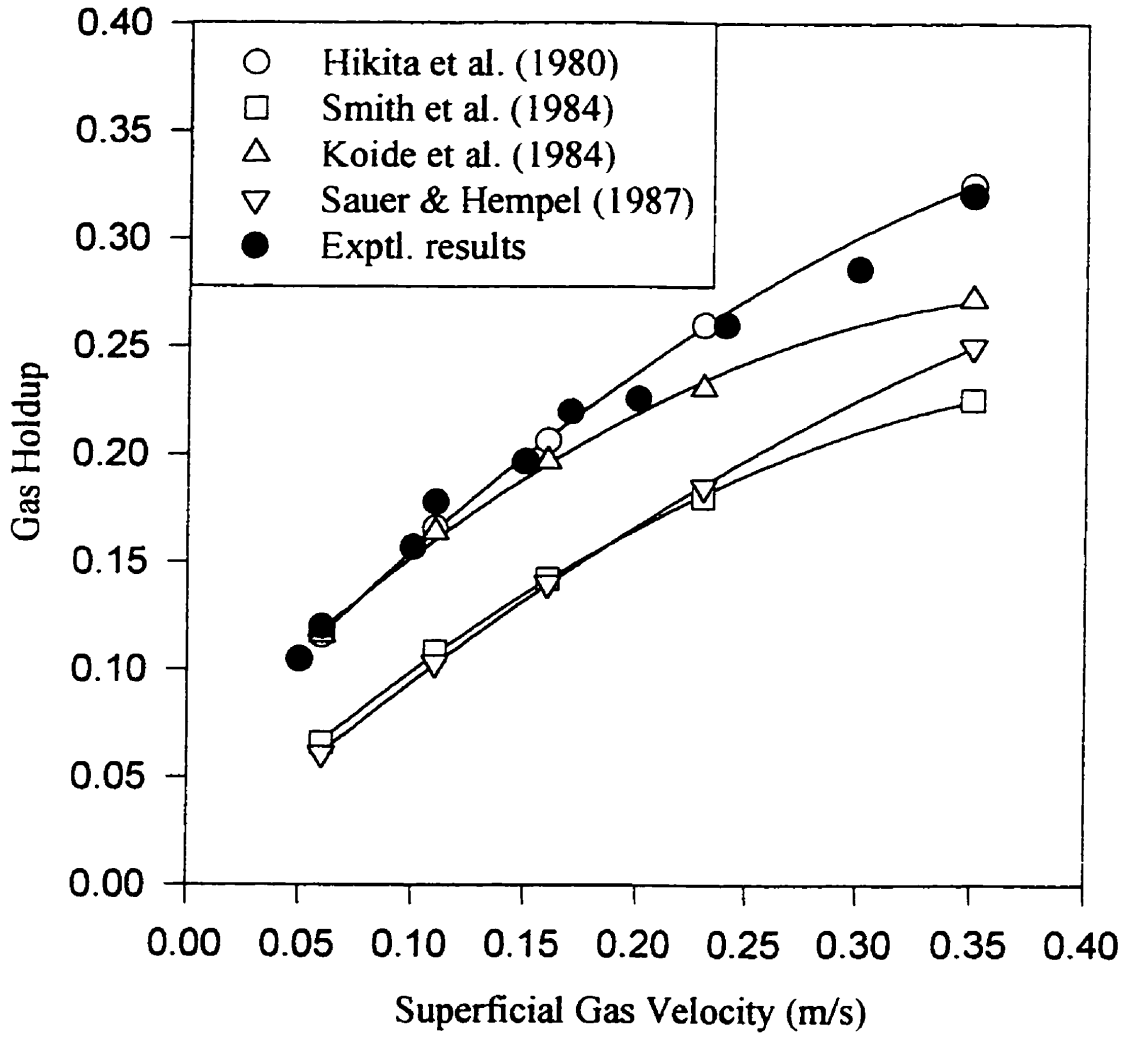

Figure 4.1.5 Comparison of measured gas holdup with literature correlations in air-water system
(Exptl. results based on Appendix E1)

Figures 4.1.6a through 4.1.6c compare various literature correlations (Koide et al., 1984; Smith et al., 1984; Sauer and Hempel, 1987) with experimental results in three phase systems. Table 4.1.2 presents average relative errors and maximum and minimum errors. Since the correlation proposed by Hikita et al. (1980) did not concern the effects of solids concentration, experimental results are not compared with correlations by Hikita et al. (1980). As shown in Figures 4.1.6a through 4.1.6c, the correlation proposed by Koide et al. (1984) was close to experimental results. The correlations proposed by Smith et al. (1984) and Sauer and Hempel (1987) overestimate experimental gas holdup. It may be pointed out that the correlation proposed by Koide et al. (1984) is based on data obtained in 0.30 m diameter column which is close to the column diameter used in present study. The correlations by Smith et al. (1984) and Sauer and Hempel (1987) were developed based on experimental data in column diameters of .108 and .14 m.

Table 4.1.2 Deviation and range of gas holdups

	average relative deviation (%)	maximum relative error (%)	minimum relative error (%)
Hikita et al.(1980) (air-water)	2.87	7.14	0.203
Koide et al. (1984) (air-water-glass beads)	16.92	51.9	0.35
Smith et al.(1984) (air-water-glass beads)	42.27	72.7	9.03
Sauer and Hemple(1987) (air-water-glass beads)	57.79	111	15.0

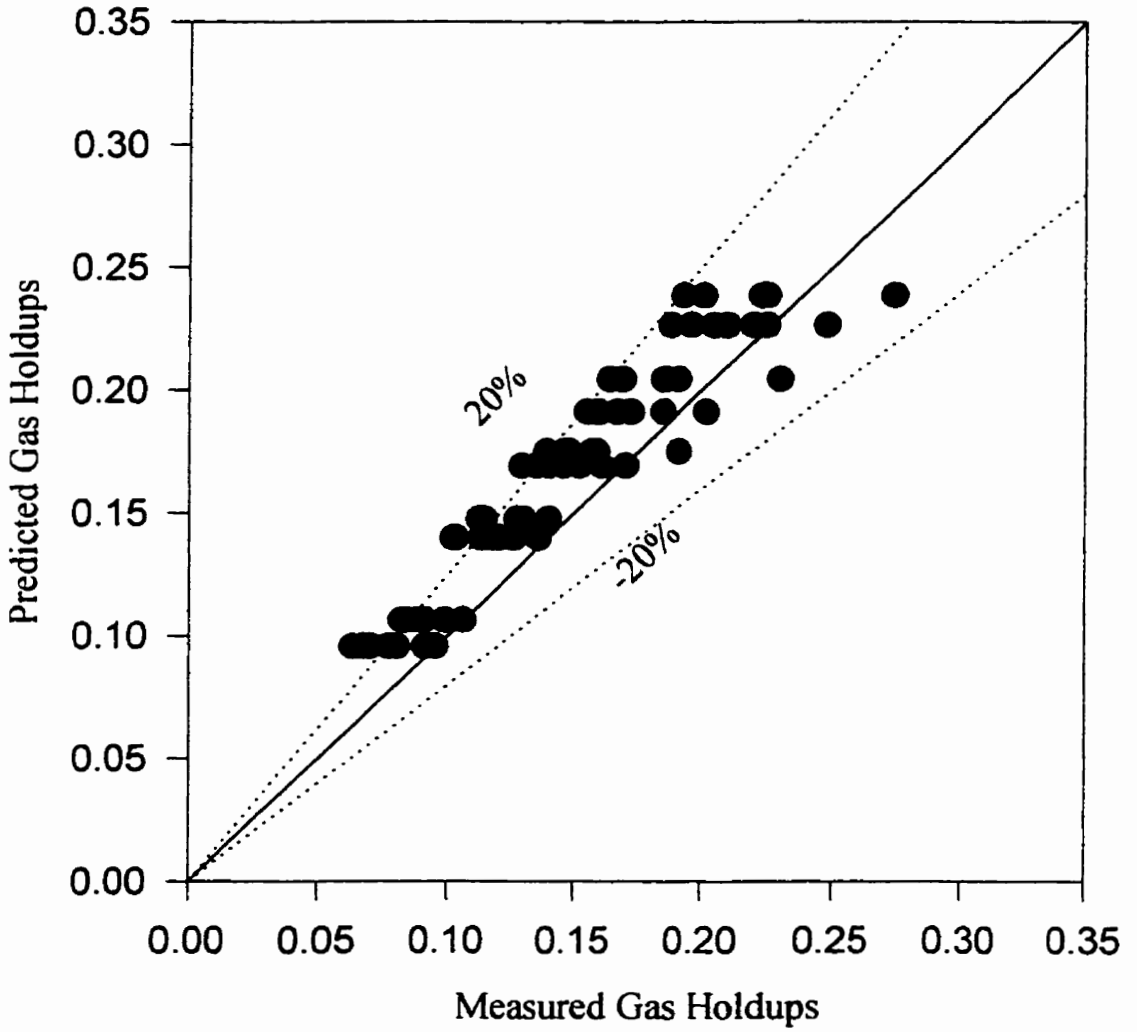

Figure 4.1.6a Comparison of Koide et al. (1984) correlation with experimental gas holdups in slurry bubble column (Data based on Appendix E1)

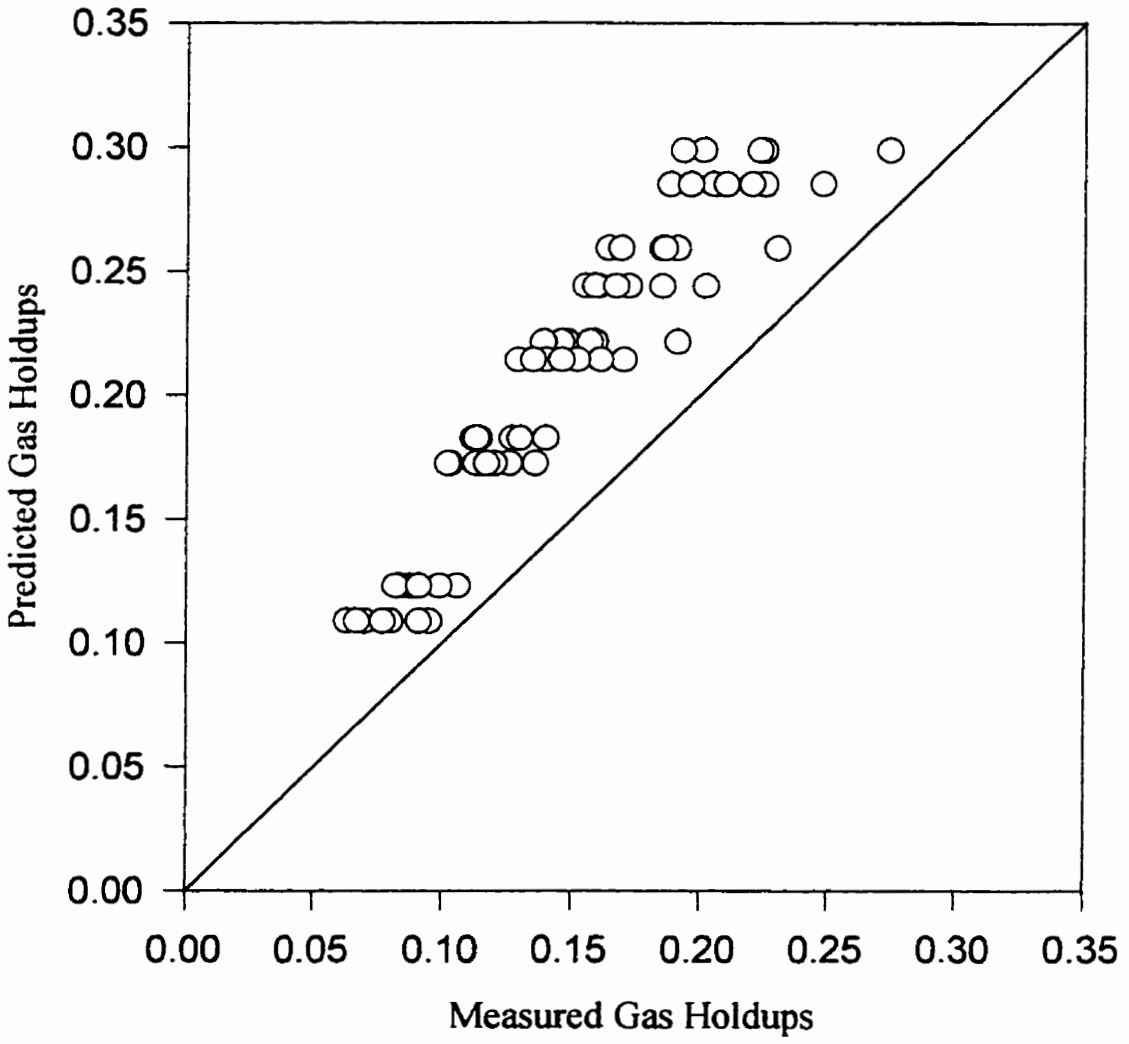

Figure 4.1.6b Comparison of Smith et al. (1984) correlation with experimental gas holdups in slurry bubble column (Data based on Appendix E1)

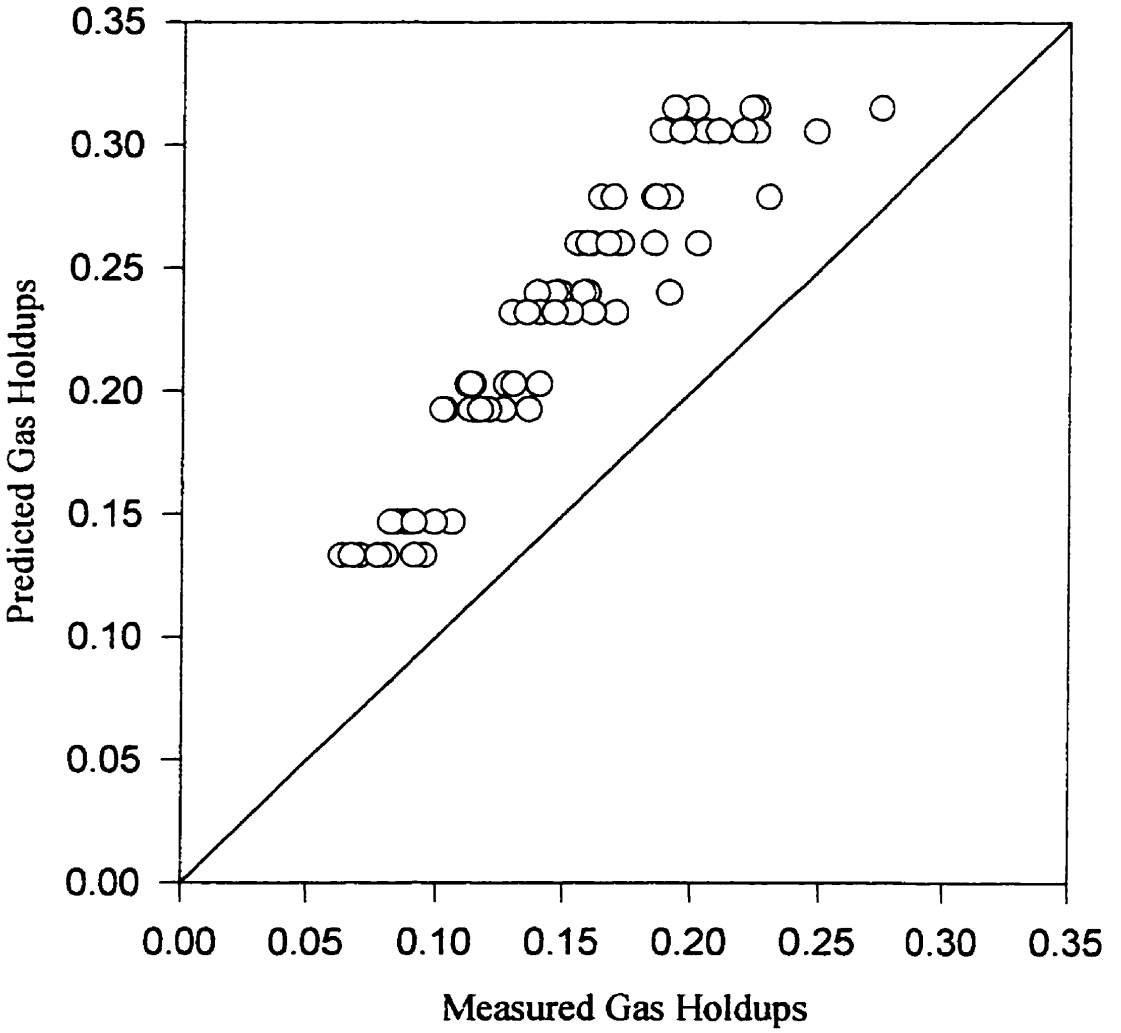

Figure 4.1.6c Comparison of Sauer and Hempel (1987) correlation with experimental gas holdups in slurry bubble column (Data based on Appendix E1)

Several literature studies have successfully modeled gas holdup in bubble column based on the drift velocity (V_0) concept of Nicklin (1962). Based on this approach, the gas holdup ε_g in a three phase system can be expressed in terms of the superficial gas velocity V_g, the superficial slurry velocity V_{sl}, and the drift velocity V_0:

$$\varepsilon_g = \frac{V_g}{V_g + V_{sl} + V_0} \tag{4.1.5}$$

For the churn turbulent regime, O'Dowd et al. (1987) assumed the drift velocity to be the sum of the superficial gas velocity and the characteristic terminal bubble rise velocity so that

$$V_0 = V_g + V_{b\infty} \tag{4.1.6}$$

where, $V_{b\infty}$ is characteristic terminal bubble rise velocity. Substituting V_0 in equation (4.1.5) gives:

$$\varepsilon_g = \frac{V_g}{2V_g + V_{sl} + V_{b\infty}} \tag{4.1.7}$$

In the present study, V_{sl} is zero since the slurry column was operated in the semi-batch mode. Thus, equation (4.1.7) is reduced to:

$$\varepsilon_g = \frac{V_g}{2V_g + V_{b\infty}} \tag{4.1.8}$$

The above derivation assumes the bubble terminal rise velocity in the fully developed churn-turbulent regime to be independent of superficial gas velocity for a fixed set of

operating conditions (i.e. solids type and loading, liquid properties, and column configuration). The fully developed churn turbulent regime is usually attained above a superficial gas velocity of about 0.08 m/s in bubble column (Shah et al., 1982). The bubble terminal rise velocities were calculated by using equation 4.1.8 and experimental gas holdups. The average bubble terminal rise velocities were then obtained for different slurry concentrations. By using the average bubble terminal rise velocities, the gas holdups at various gas velocities and slurry concentrations can be calculated by using equation (4.1.8). Figure 4.1.7 shows that the calculated gas holdups compare well with experimental values. This figure also lists values of terminal rise velocities. It can be seen that bubble terminal rise velocities increase with increasing slurry concentration up to slurry concentration of 25 vol.% but decrease for the high slurry concentration of 40 vol.%. As pointed by O'Dowd et al. (1987), the bubble terminal rise velocity essentially reflects the bubble size distribution and higher bubble terminal rise velocities indicate presence of larger bubbles.

The increase in bubble size with increasing slurry concentration can be attributed to an increase in apparent slurry viscosity, since higher apparent slurry viscosity promotes bubble coalescence rate. The correlations for prediction of apparent slurry viscosity were proposed by Vand (1948), Thoms (1965) and Barnea and Mizrahi (1973). These correlations, given below, were used to estimate the apparent suspension viscosity over the entire range of slurry concentration used in this study.

Vand (1948):

$$\mu_{sl} = \mu_L \exp\left[\frac{2.5\phi_s}{1-0.609\phi_s}\right] \qquad (4.1.4)$$

Thomas (1965):

$$\mu_{sl} = \mu_l \left(1 + 2.5\phi_s + 10.0\phi_s + 0.00273\exp(16.6\phi_s)\right) \qquad (4.1.9)$$

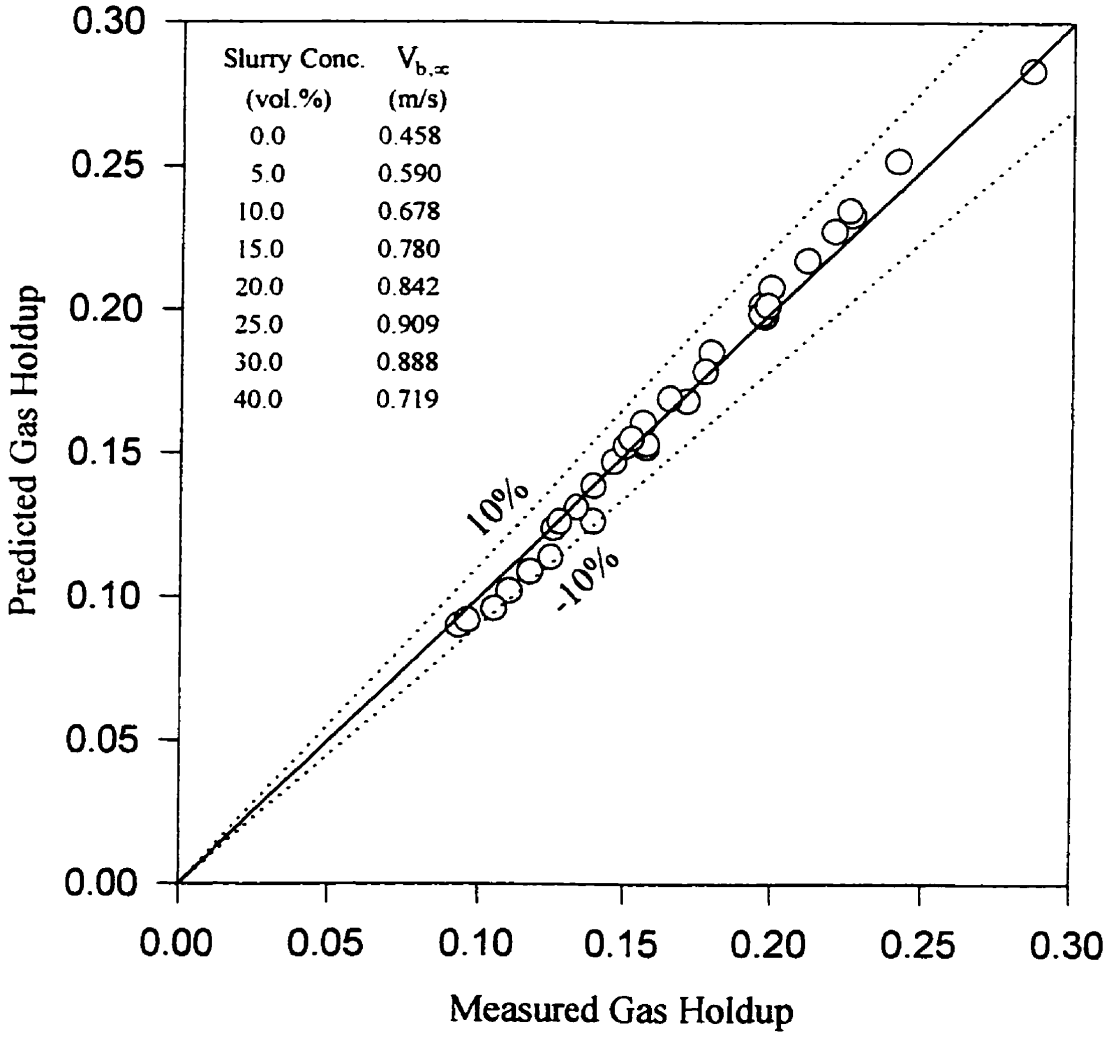

Figure 4.1.7 Comparison of predicted gas holdup with experimental values
(Experimental results based on Appendix E1)

Barnea and Mizrahi (1973):

$$\mu_{sl} = \mu_l \exp\left(\frac{(5/3)\phi_s}{1-\phi_s}\right) \qquad (4.1.10)$$

The calculated terminal rise velocities for different slurry concentrations were plotted against apparent suspension viscosity obtained with above correlations. Figure 4.1.8 shows the relationship between the characteristic bubble terminal rise velocity and slurry concentration. At low slurry concentration, the rise velocity increases with slurry concentration. At slurry concentration higher than 25 vol.%, the rise velocity decreases with slurry concentration. At the slurry concentration around 25 vol.%, the rise velocity reaches a maximum value. It can be found that the drop in the terminal rise velocity coincides with the steep increase in slurry viscosity predicted by three correlations at the high slurry concentrations. Even though the results from different correlations have different values, all the results provide similar trends.

Figure 4.1.3 shows that at various gas velocity, variation of gas holdup with slurry concentration has similar trends. Therefore, a normalized gas holdup can be used to generalize this trend. The normalized gas holdup is defined as the ratio of gas holdup in three-phase to gas holdup in air-water system at corresponding gas velocity.

Figure 4.1.9 shows the normalized gas holdup. Figure 4.1.9 indicates that the normalized gas holdups are relatively independent of gas velocity, and strongly dependent on slurry concentration. Meanwhile, at slurry concentration of 25 vol.%, there is a minimum normalized gas holdup. Based on those observations, an expression for normalized gas holdup can be suggested as follows:

$$\frac{\varepsilon_3}{\varepsilon_2} = \left.\frac{\varepsilon_3}{\varepsilon_2}\right|_{25\,\text{vol.\%}} + a(C_s - .25)^b \qquad (4.1.11)$$

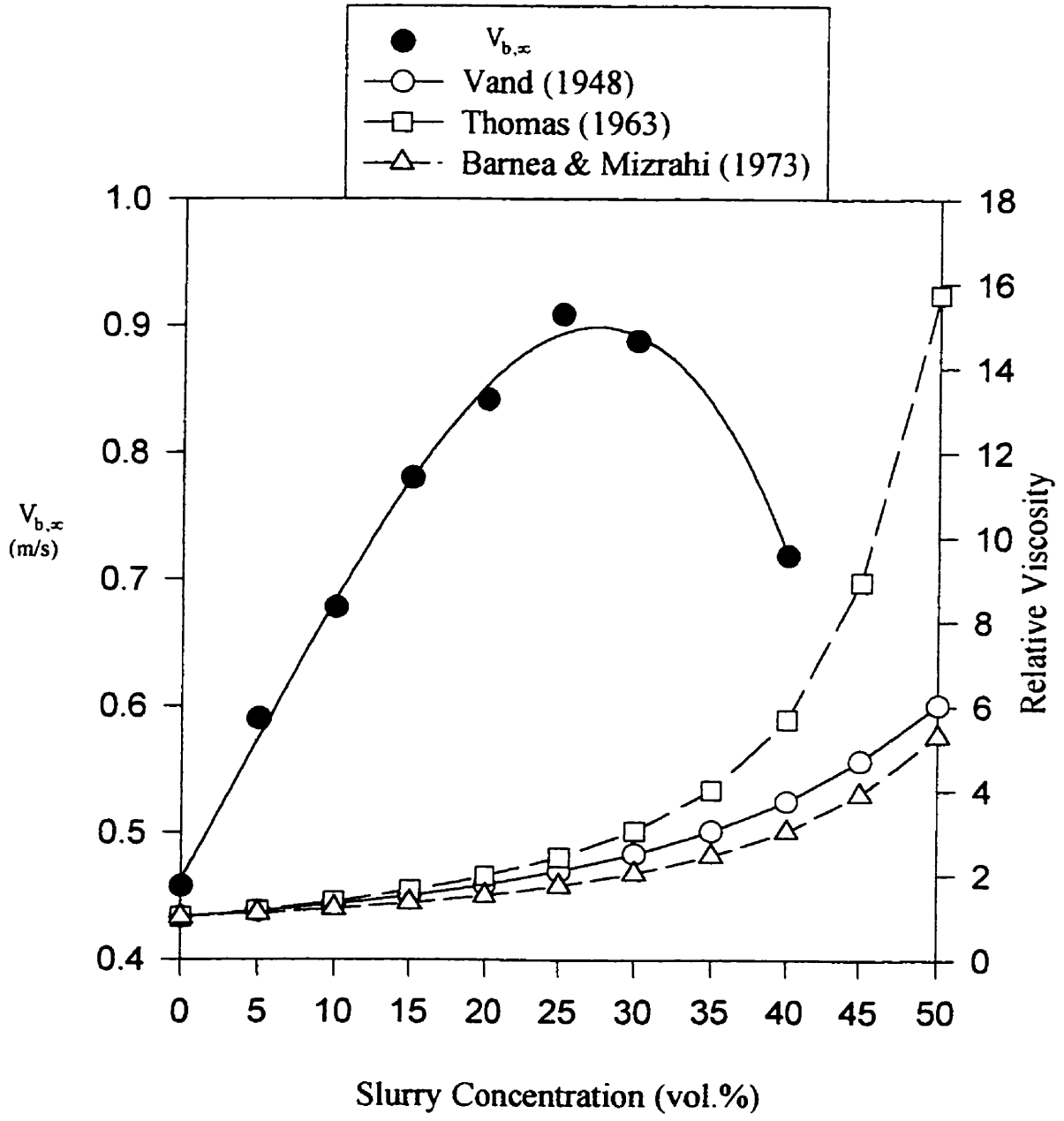

Figure 4.1.8 Variation of terminal rise velocity of the swarm of bubbles and relative viscosity with slurry concentration
(based on Figure 4.1.7)

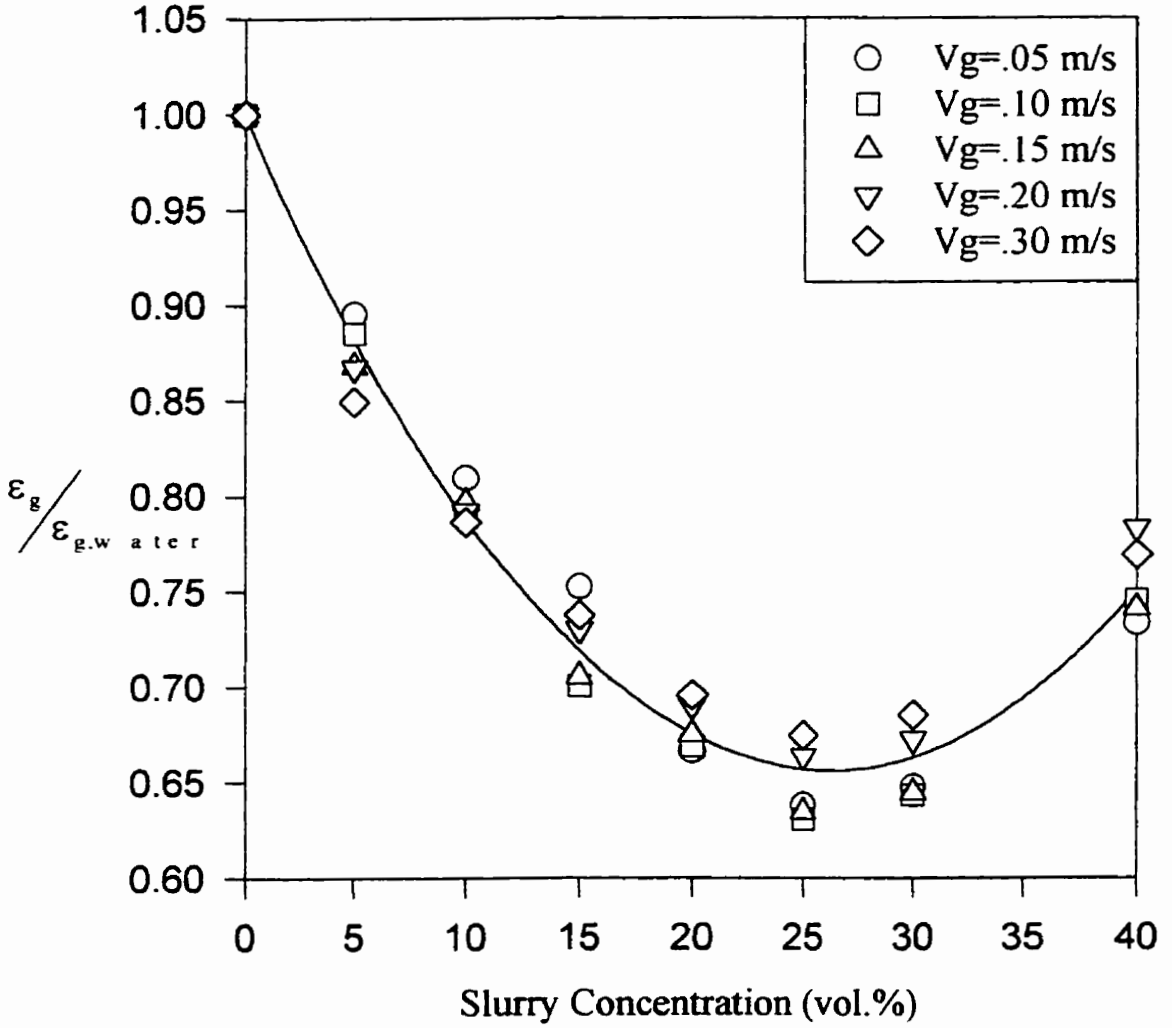

Figure 4.1.9 Ratio of gas holdup in slurry system to gas holdup in air-water system
(Data based on Appendix E1)

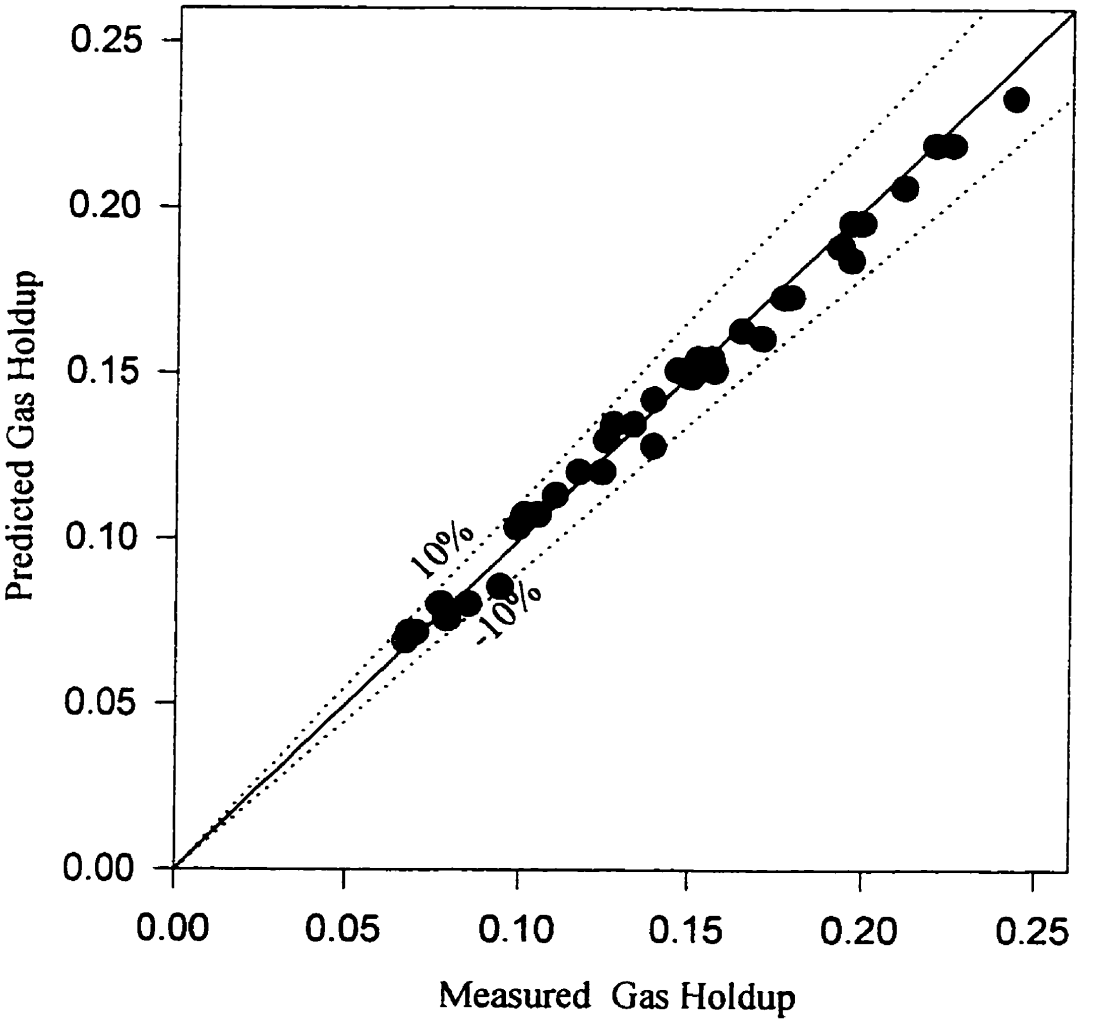

Figure 4.1.10 Comparison of predicted gas holdup in equation 4.1.11 with measured gas holdup
(Exptl. results based on Appendix E1)

By fitting the experimental results, parameters a and b are found to be

a= 1.322

b= 1.325

Figure 4.1.10 compares the calculated results with experimental results. Average relative error is 3.44%.

4.1.2 Solids Distribution Profiles

In this section, axial profiles of solid concentration at different gas velocities and slurry concentrations are presented. Particle hindered settling velocities and solid dispersion coefficients are obtained based on experimental axial solid concentration profiles. The axial solid concentration profiles, particle settling velocities and solid dispersion coefficients are compared with literature correlations.

4.2.2.1 Axial Solid Concentration Profiles

Axial profile of solids concentration at various slurry concentrations are presented in Figure 4.1.11a through 4.1.11d. In general, a downward sloping axial solids concentration profiles (gradient) were observed for various solids concentrations and gas velocities. The gradients are, however, higher at the low gas velocity of 0.06 m/s. For higher gas velocities, there is no significant effect of gas velocity on concentration gradients. The gradients can be explained by the settling effect of gravity on dense solids particles. However, due to the turbulence created by the flow of gas and liquid circulation, there is also an upward force acting on the particles. When the net upward force exceeds the gravity on particles, the particles are dispersed upwardly. The lift is a function of slurry kinetic energy which in turn is related to column turbulence and bubble wake phenomenon.

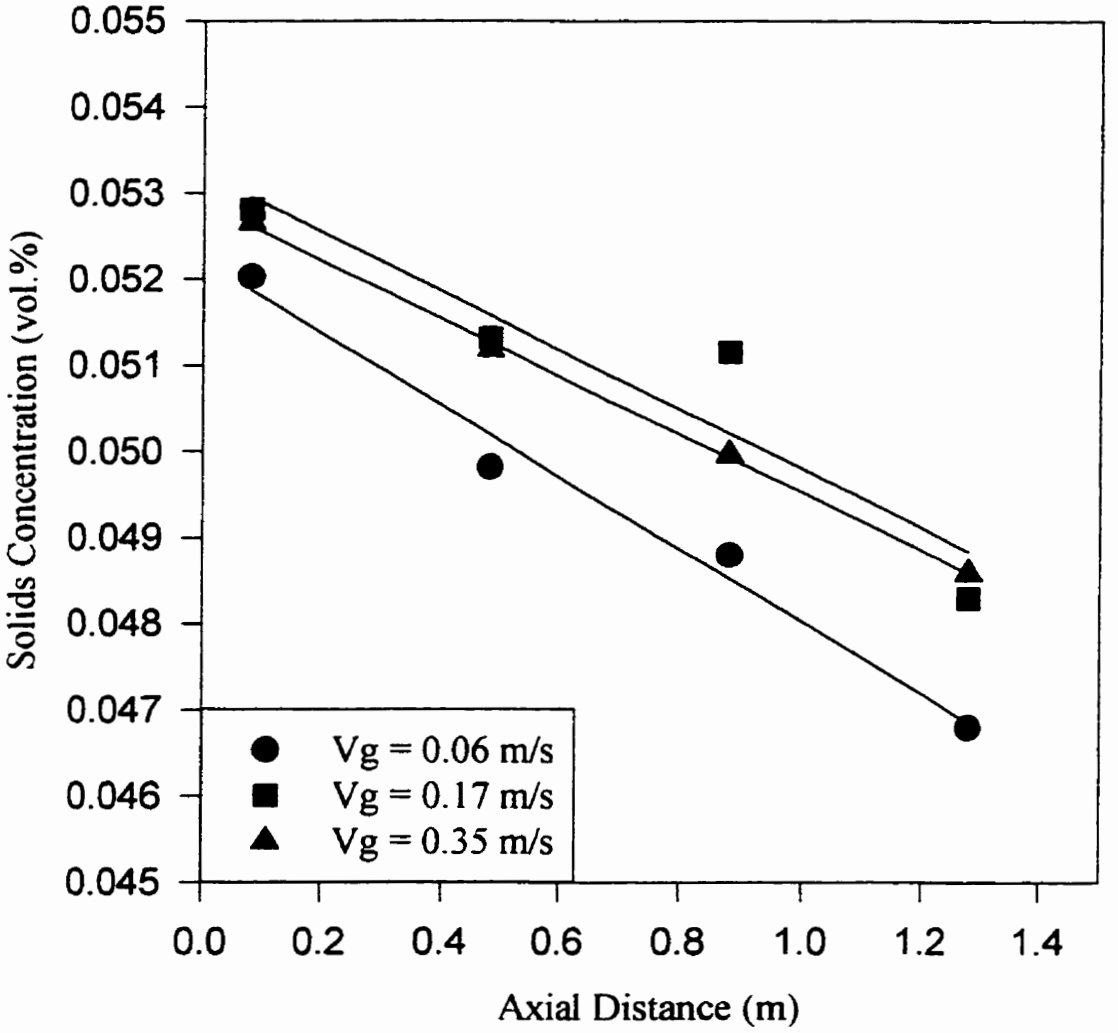

Figure 4.1.11a Axial distribution of solids concentration at slurry concentration of 5 vol%
(Data based on Appendix E11)

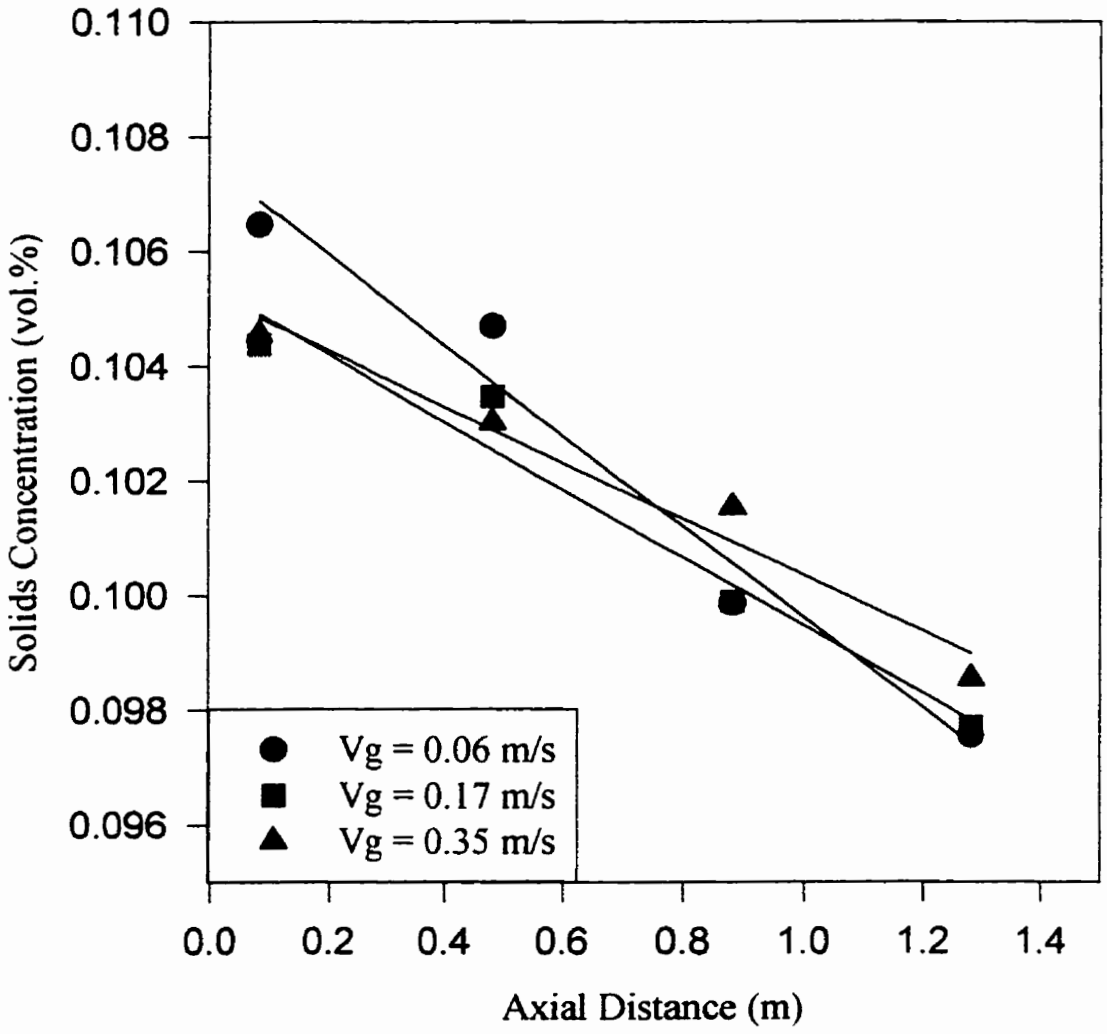

Figure 4.1.11b Axial distribution of solids concentration at slurry concentration of 10 vol%
(Data based on Appendix E11)

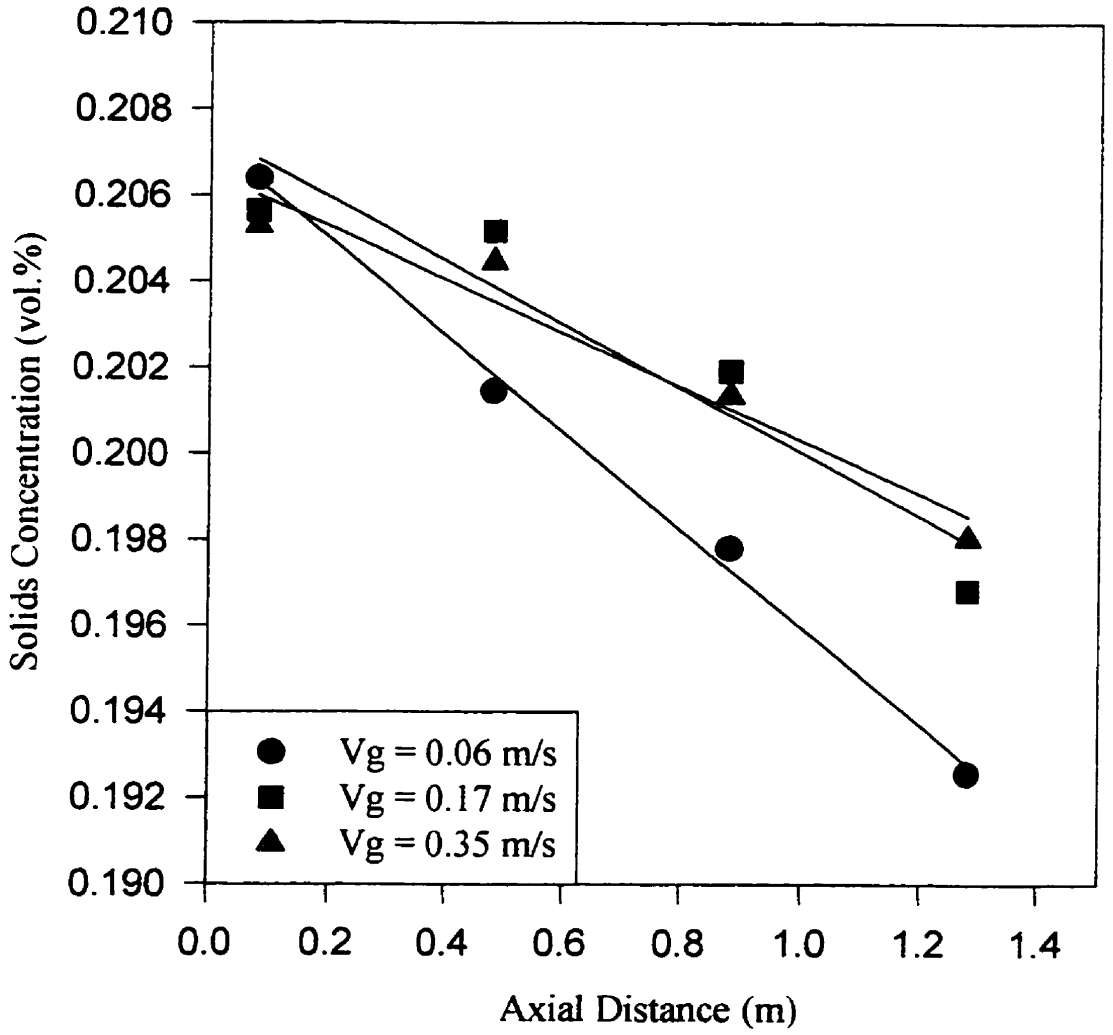

Figure 4.1.11c Axial distribution of solids concentration at slurry concentration of 20 vol%

(Data based on Appendix E11)

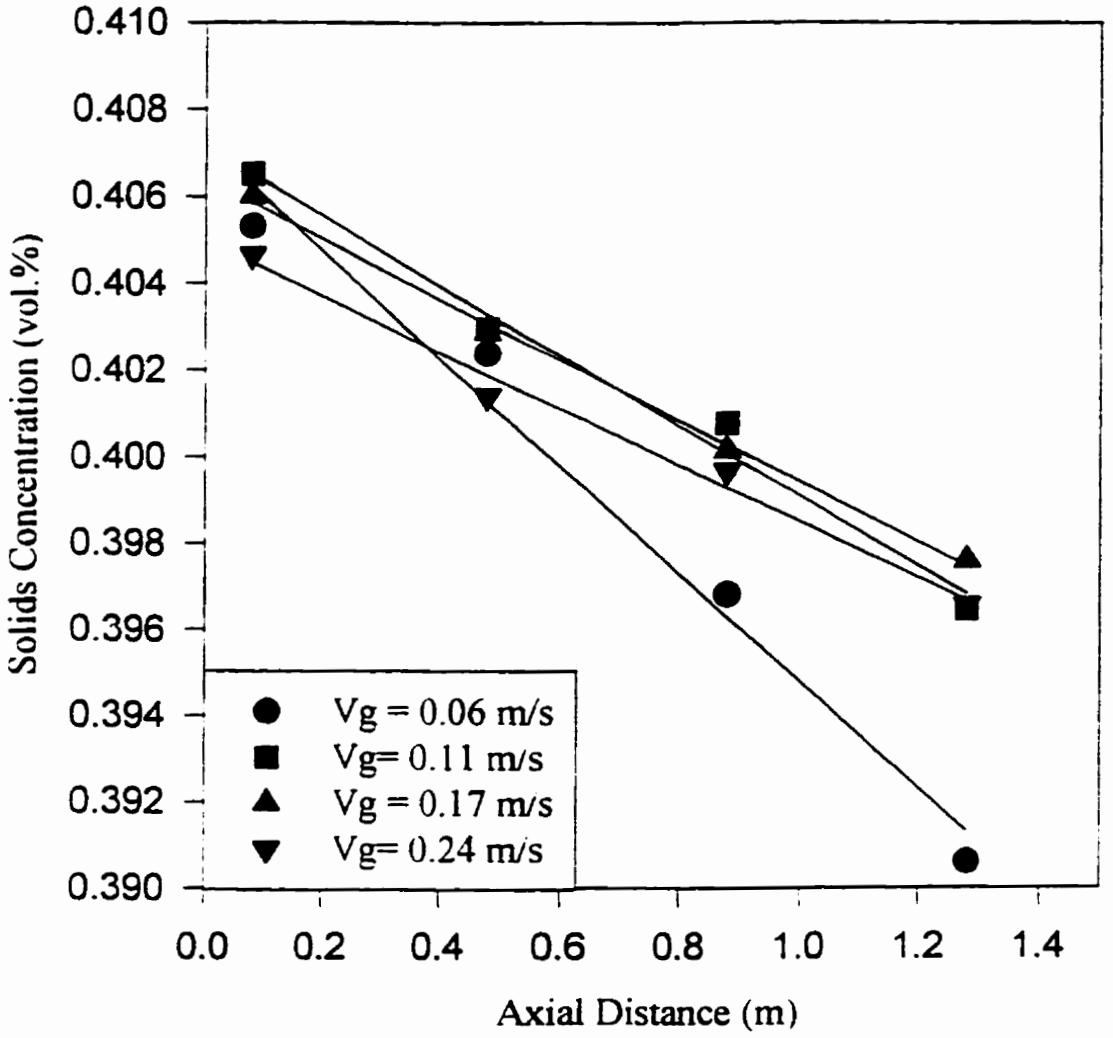

Figure 4.1.11d Axial distribution of solids concentration at slurry concentration of 40 vol%

(Data based on Appendix E11)

The effects of varying superficial gas velocities are further studied for different slurry concentrations. As gas velocity increases, the slope of axial solids concentration is generally lowered. This effect can be explained in terms of the potential energy required to keep particles in suspension. The incoming buoyant power, which is primarily a function of a gas volumetric flowrate, is used for the generation of bulk motion and can be calculated as follows (Lamont, 1958):

$$P_{in,g} = P_0 Q_{o,g} \ln \frac{P_o + \rho_{sl} g H_c}{P_o} \qquad (4.1.12)$$

Turbulence is generated as a result of this bulk motion and spread quickly throughout the reactor. As pointed out by Kleijintjens et al. (1994), a portion of the turbulent power generated is used to maintain the potential energy of the particles in suspension and the remainder maintains slurry motion (kinetic energy). Assuming uniform axial and radial distribution of particles, the energy input required to maintain the potential energy of suspended particles can be approximated as:

$$\frac{d E_{pot,p}}{dt} = V_r \varepsilon_s g (\rho_s - \rho_l) U_p \qquad (4.1.13)$$

For the range of gas flowrates in this study ($0.06 < Vg < 0.35$ m/s), the incoming power was calculated by the above correlation (4.1.12) to range from 50 W to 430 W. However, the corresponding potential energy required to keep particles in suspension was calculated to be less than 2.5 W. Thus, there is an abundant amount of energy available to keep particles in suspension. Since the particles are already in suspension at lower gas velocities, the effect of increasing gas velocity was small.

Figure 4.1.12a through 4.1.12c show the effect of different average solids concentrations. To clearly demonstrate the effect, the normalized concentration profile

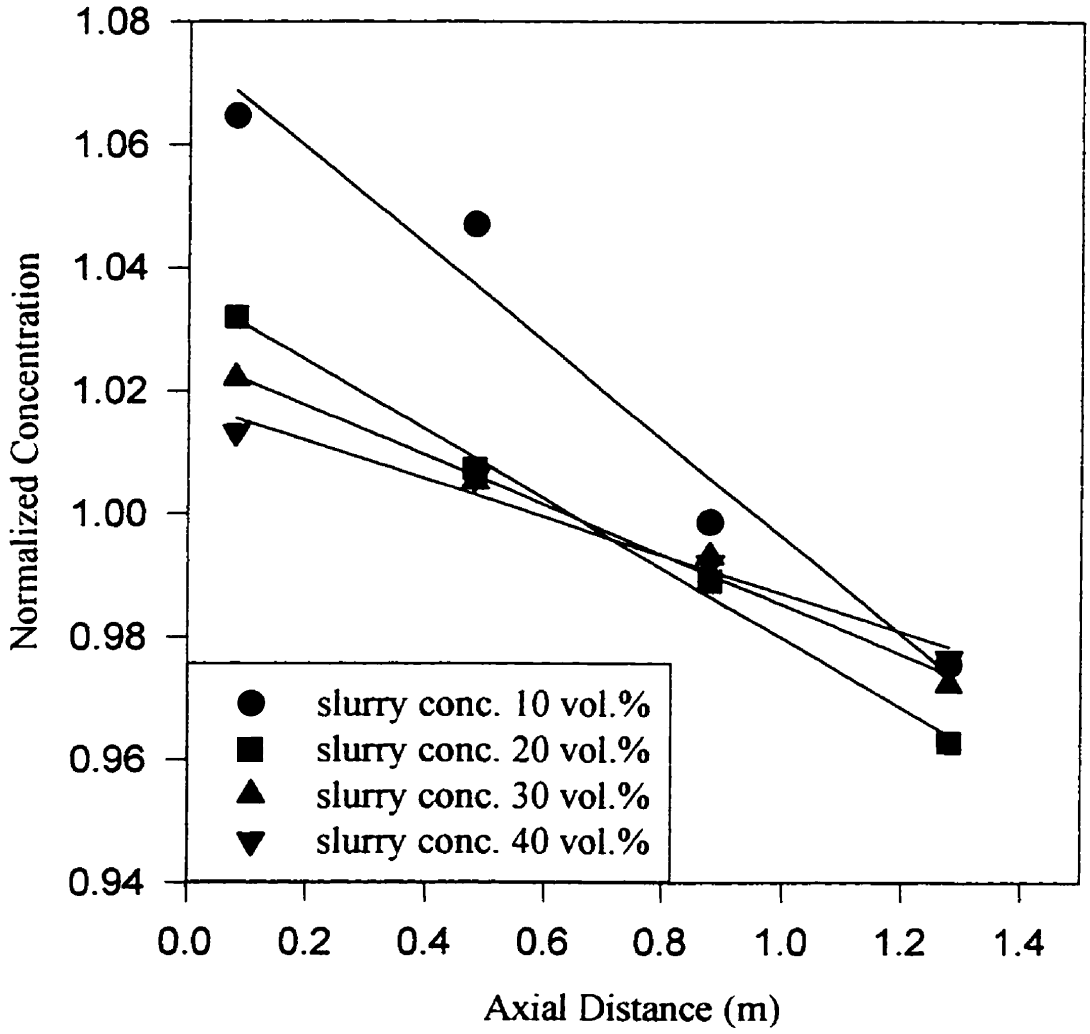

Figure 4.1.12a Normalized axial solid concentraion at a gas velocity of 0.06 m/s
(Data based on Appendix E11)

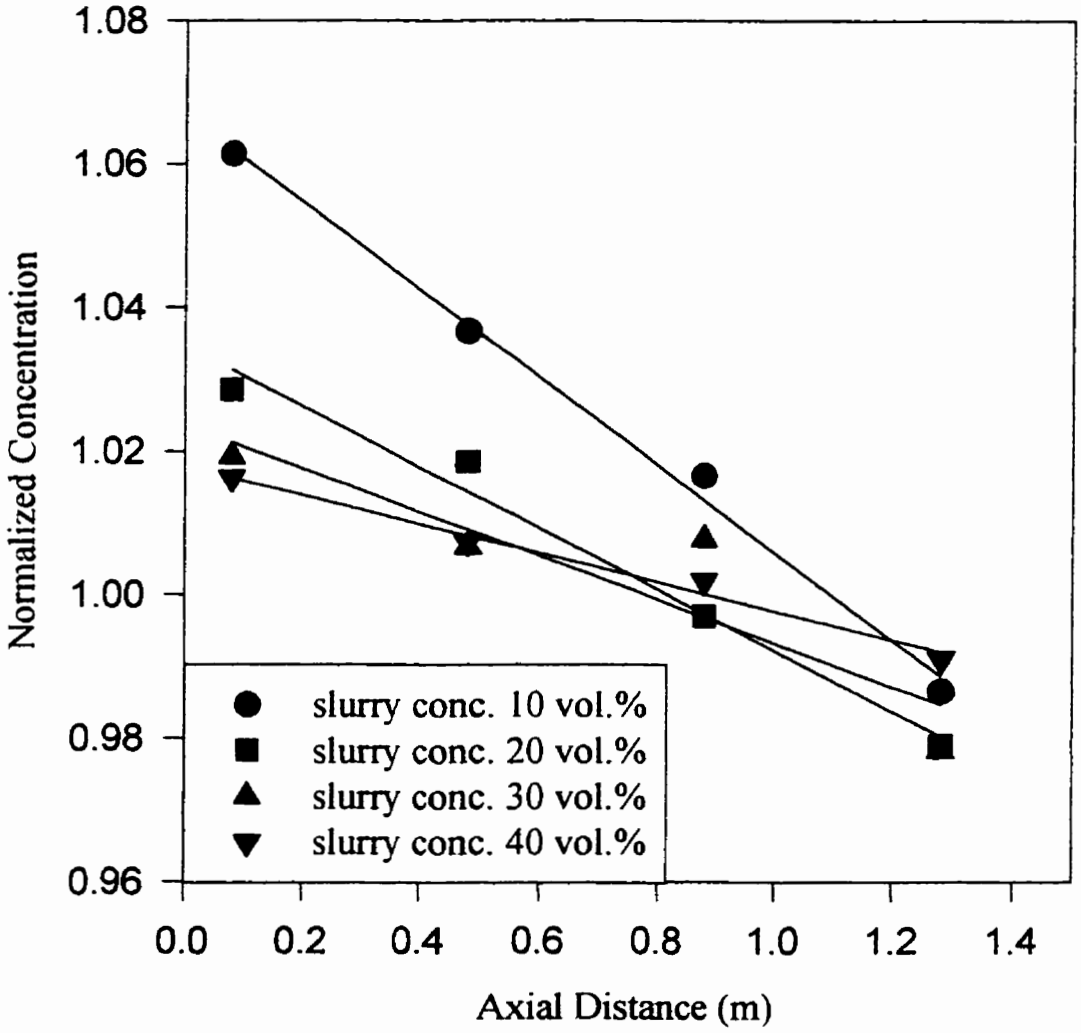

Figure 4.1.12b Normalized axial solid concentraion at a gas velocity of 0.11 m/s

(Data based on Appendix E11)

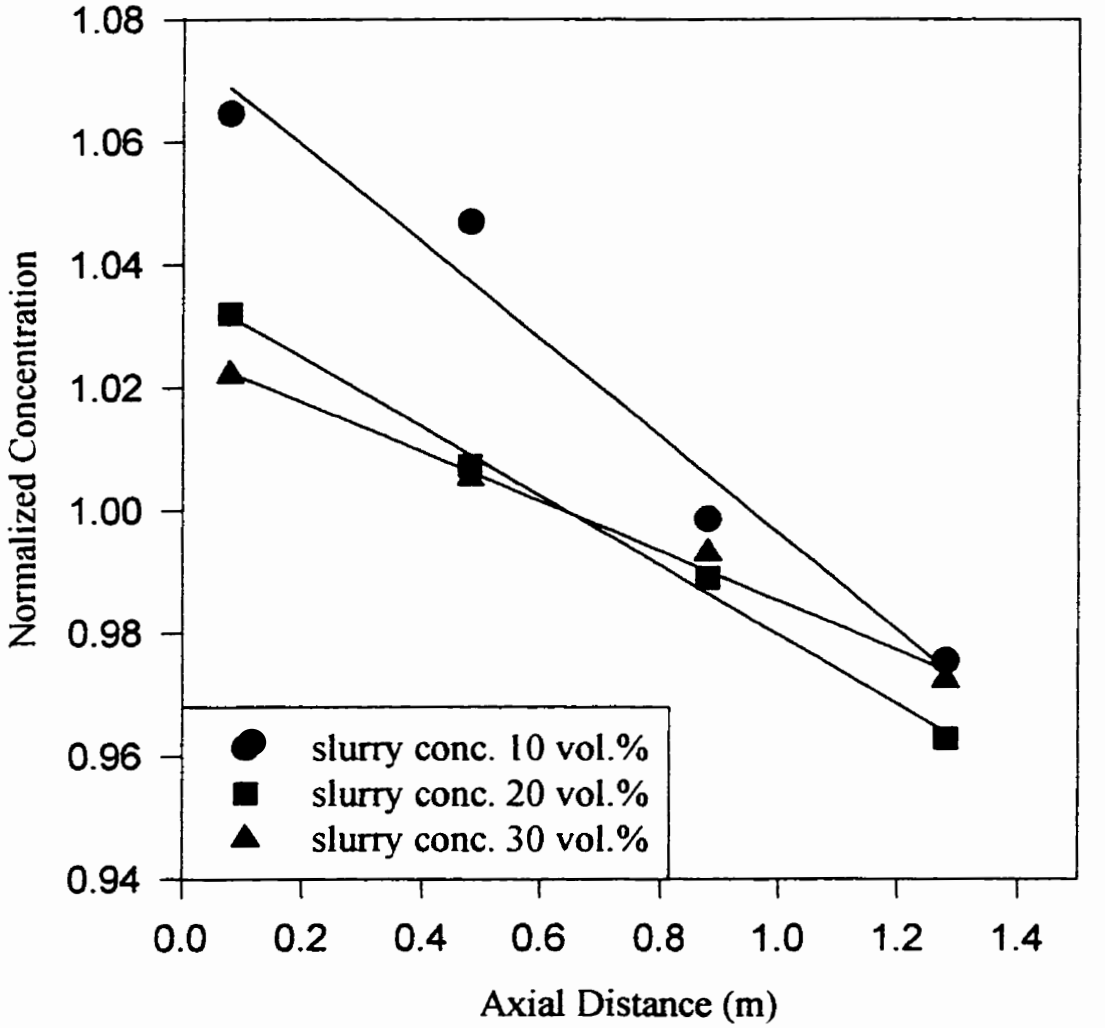

Figure 4.1.12c Normalized axial solid concentraion at a gas velocity of 0.35 m/s

(Data based on Appendix E11)

can be defined as the ratio of local slurry concentration to average slurry concentration. As shown in Figure 4.1.12a through 4.1.12c, the slope of normalized concentration profiles decreases as slurry concentration increases. Similar results have been reported by O'Dowd et al. (1987) and Gandhi et al. (1998). This can be attributed to a decrease in hindered settling velocity as slurry concentration increases. The regression result of hindered settling velocity from experimental data indicated this tendency. Higher slurry concentrations increase particle-particle interactions which reduces the hindered settling velocity.

4.1.2.2 Sedimentation-Dispersion Model

The one-dimensional sedimentation-dispersion model has been widely used to describe the axial solids concentration profiles for batch and continuous slurry bubble column systems. In this section, the sedimentation-dispersion model was used to estimate the axial profile of slurry concentration, the particle hindered settling velocity and the solid dispersion coefficient.

According to the sedimentation-dispersion model, the longitudinal movement of suspended solid particles is assumed to be caused by longitudinal dispersion and settling of solid particles and liquid flow, resulting in the concentration distribution of solid particles in the bubble column. The model was originally proposed by Cova (1966). The model was subsequently developed and simplified by other researchers (Kato et al., 1972; Smith and Ruether 1985).

The following assumptions have been made in formulating the sedimentation-dispersion model:

1. no radial gradients in solid particles concentration;
2. all solids particles have identical terminal velocity.
3. gas holdup, solids dispersion coefficient and settling velocity of solids are all constant along the column axis;

4. gas and liquid velocities are such that all solids particles are completely suspended in liquid.

If we consider a horizontal cross sectional element of a slurry bubble column having a thickness Δz, a differential mass balance in the vertical z-direction with respect to solids particles gives:

Rate of accumulation within volume element	=	Rate of (mass in - mass out) due to dispersion	+	Rate of (mass in - mass out) due to convective flow of slurry	+	Rate of (mass in - mass out) due to the settling of solids

The effects of gravitational and buoyant forces are taken into account in the last term on the right hand side of the above equation. The differential equation can be obtained as

$$\frac{\partial C_s}{\partial t} = -\frac{\partial n_d}{\partial z} - \frac{\partial}{\partial z}\left(\frac{V_{sl}}{1-\varepsilon_g} C_s\right) + \frac{\partial}{\partial z}(U_{st} C_s) \qquad (4.1.14)$$

where, U_{st} is the generalized solids settling velocity, and the flux of solids particles due to dispersion, n_d, is given by

$$n_d = -E_s \frac{\partial C_s}{\partial z} \qquad (4.1.15)$$

where, E_s is solids dispersion coefficient. Substituting eqn. (4.1.15) into eqn. (4.1.14) yields the sedimentation-dispersion model (Parulekar and Shah, 1980):

$$\frac{\partial C_s}{\partial t} = \frac{\partial}{\partial z}\left(E_s \frac{\partial C_s}{\partial z}\right) - \frac{\partial}{\partial z}\left(\frac{V_{sl}}{1-\varepsilon_g} - U_{st}\right) C_s \qquad (4.1.16)$$

At steady state and batch mode, eqn. (4.1.16) can be simplified to:

$$0 = \frac{\partial}{\partial z}\left(E_s \frac{\partial C_s}{\partial z}\right) - \frac{\partial}{\partial z}(U_{st} C_s) \qquad (4.1.17)$$

The term U_{st} can be interpreted as particle terminal velocity or as the hindered settling velocity of a swarm of particles. Smith and Ruether (1985) defined U_{st} as the solids hindered settling velocity relative to liquid (slurry). The sedimentation-dispersion model is then integrated as:

$$\frac{C_s}{C_0} = \exp(-\frac{\bar{\varphi}_l U_p}{E_s} z) \qquad (4.1.18a)$$

Kato et al. (1972) defined U_{st} as the solids hindered settling velocity relative to the column. The sedimentation-dispersion model is then integrated as:

$$\frac{C_s}{C_0} = \exp(-\frac{U_p}{E_s} z) \qquad (4.1.18b)$$

where, C_s and C_0 are slurry concentration at location of z and the bottom; U_p is hindered settling velocity of particles relatively to liquid phase in equation (4.1.18a), and relatively to the column in equation (4.1.18b); $\bar{\varphi}_l$ is liquid fraction in slurry phase.

Hindered settling velocity (U_p) and solid dispersion coefficient (E_s) in equation (4.1.18a) can be obtained by using measured axial profile of measured slurry concentration. Equation (4.1.18a) is a non-linear equation. Therefore, non-linear least squares regression is required to estimate U_p and E_s for each average slurry concentration profile measured at various gas velocity. The value of two parameters (U_p and E_s) are determined to minimize the residual sum of squares between the measured and calculated slurry concentration by using equation (4.1.18a). The objective function is then defined as:

$$F = \Sigma(C_s - C_s^{\circ} \exp(\frac{-\varphi U_p z}{E_s}))^2 \qquad (4.1.19)$$

Marquart method (Ahrendts and Baehr, 1981) was used to obtain the minimum value of the objective function F. The parameters U_p and E_s in equation (4.1.19) are obtained by minimizing objective function F.

4.1.2.3 Hindered Settling Velocity

Particle hindered settling velocity, U_p, represents the slip velocity between the solid and liquid phase in the slurry bubble column (Smith and Ruether, 1985). Figure 4.1.13 shows particle hindered settling velocity at various gas velocities and slurry concentrations.

As shown in Figure 4.1.13, the particle hindered settling velocity decreased as slurry concentration increased. Higher slurry concentration increases particle-particle interactions, which reduces the hindered settling velocity. Figure 4.1.13 also shows that the hindered settling velocity is strongly dependent on the solids concentration in the slurry, which implies a hindered effect. Similar observation were made by Kato et al. (1972) and Smith and Ruether (1985) in relatively dilute suspension (0.012 vol.%). The effect of high solids concentration on particle settling velocity has not been addressed in previous investigations. From experimental observation in this study, the hindrance effect on particle settling velocity continues as slurry concentration increases above 0.012 vol.%.

Figure 4.1.13 also shows variance of hindered settling velocity with gas velocity. Hindered settling velocity increases as gas velocity increases. Higher gas velocity improves global slurry recirculation, which will increase particle settling velocity. Smith et al. (1986) observed a similar tendency of variation of hindered settling velocity with gas velocity.

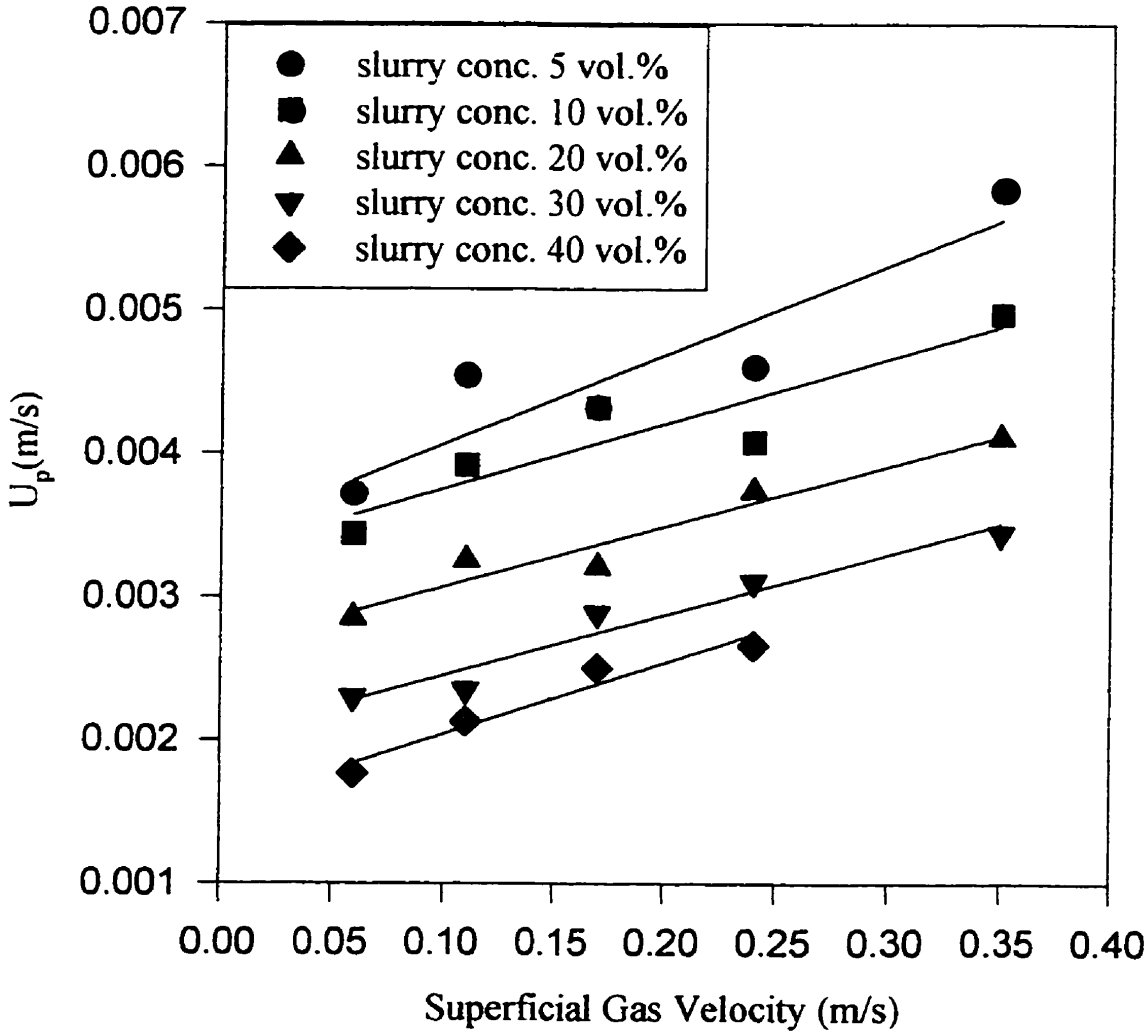

Figure 4.1.13 Particle hindered settling velocity obtained from experimental solids concentration profiles

(Data based on Appendix E11)

Correlations for hindered settling velocity have been proposed by several researchers (Kato et al., 1972; Smith and Ruether, 1985; O'Dowd et al., 1987). These correlations are presented in Table 2.4.1; where, φ_l is liquid volume fraction in slurry phase; V_g is the gas velocity; U_t is the terminal settling velocity of single particles, which can be calculated by using Stokes equation:

$$U_t = \frac{d_p^2 g (\rho_p - \rho_l)}{18 \mu} \qquad (4.1.20)$$

Figures 4.1.14a through 4.1.14c show the comparison of those correlation with experimental results. The average relative deviations and the ranges are list in Table 4.1.3. As shown in the Figures 4.1.14a, b, c and Table 4.1.3, the calculated hindered settling velocities from the correlations from Kato et al. (1972) and O'Dowd (1987) are close to that from the experimental observations. Thus, those correlations can be used to estimate the hindered settling velocity up to slurry concentrations of 40 vol.% and velocities up to 0.35 m/s.

Table 4.1.3 Deviation and range of particle hindered settling velocity

	average relative deviation (%)	maximum relative deviation (%)	minimum relative deviation (%)
Kato et al. (1972)	5.03	15.82	0.11
Smith and Ruether(1985)	32.58	66.02	1.05
O'Dowd et al. (1987)	5.57	15.93	0.42

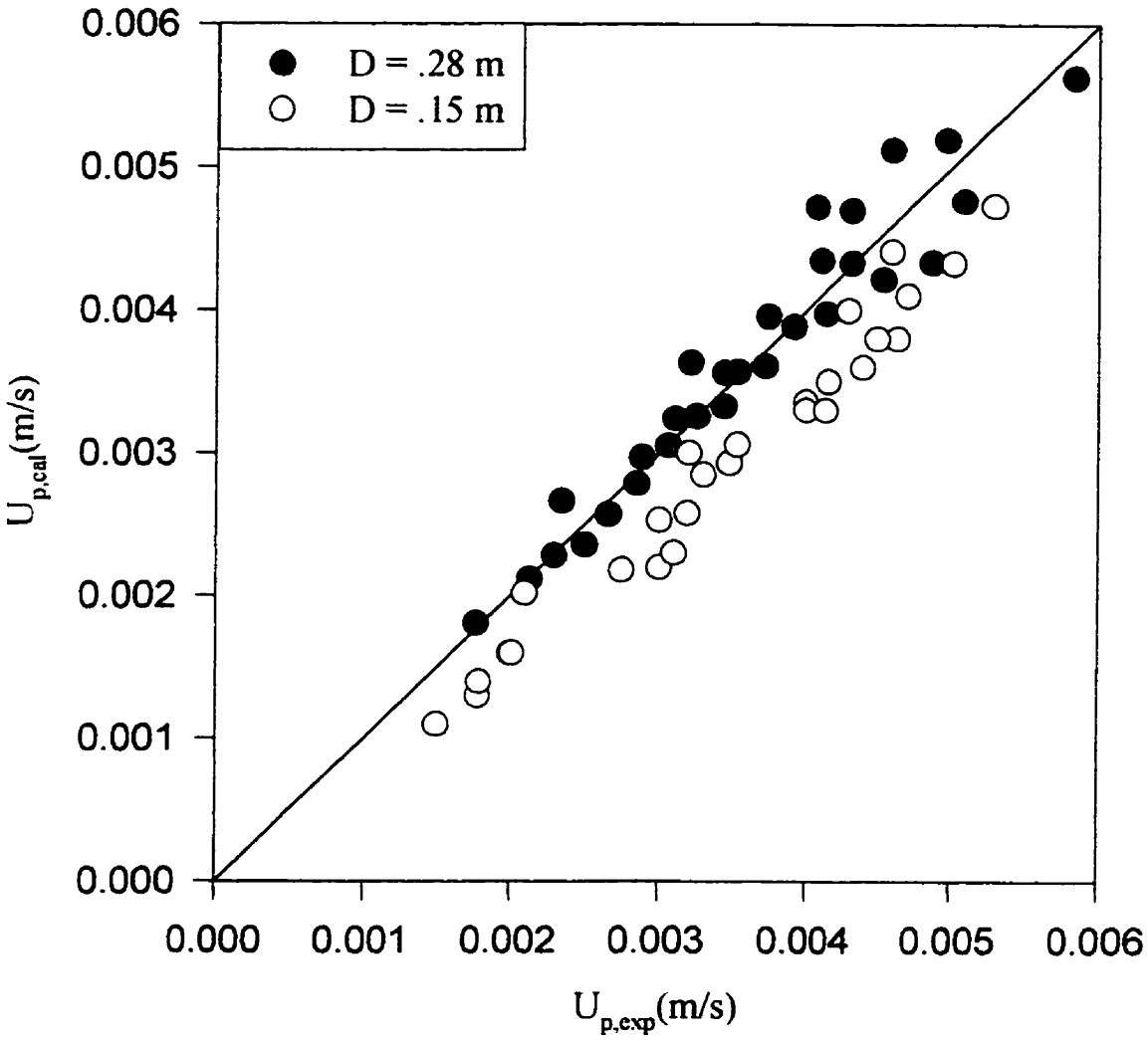

Figure 4.1.14a Comparison of Kato's correlation with measured particle hindered settling velocity
(Experimental data based on Appendix E11; calculation based on Kato et al., 1972)

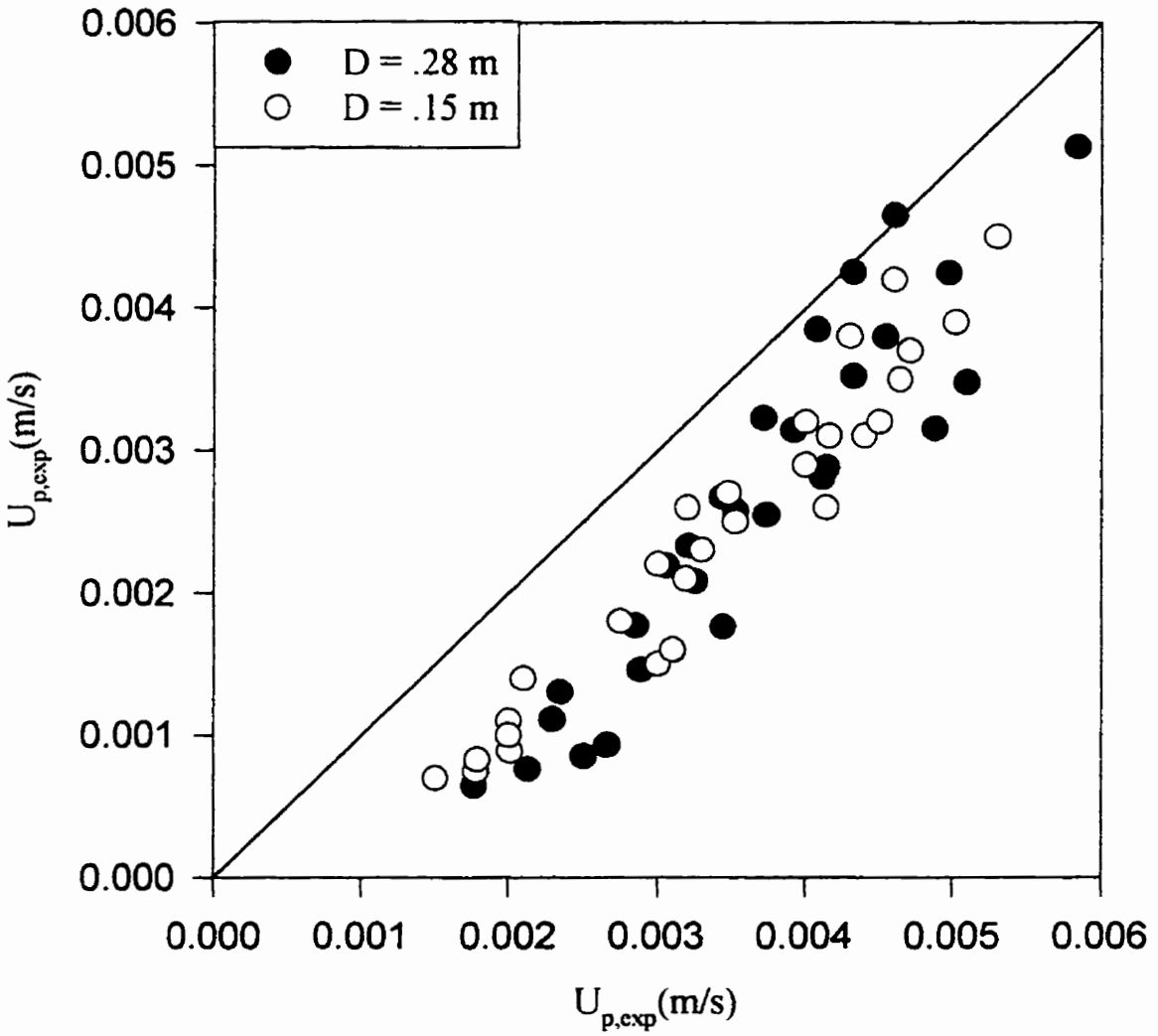

Figure 4.1.14b Comparison of Smith's correlation with measured particle hindered settling velocity

(Experimental data based on Appendix E11; calculation based on Smith and Ruether, 1985)

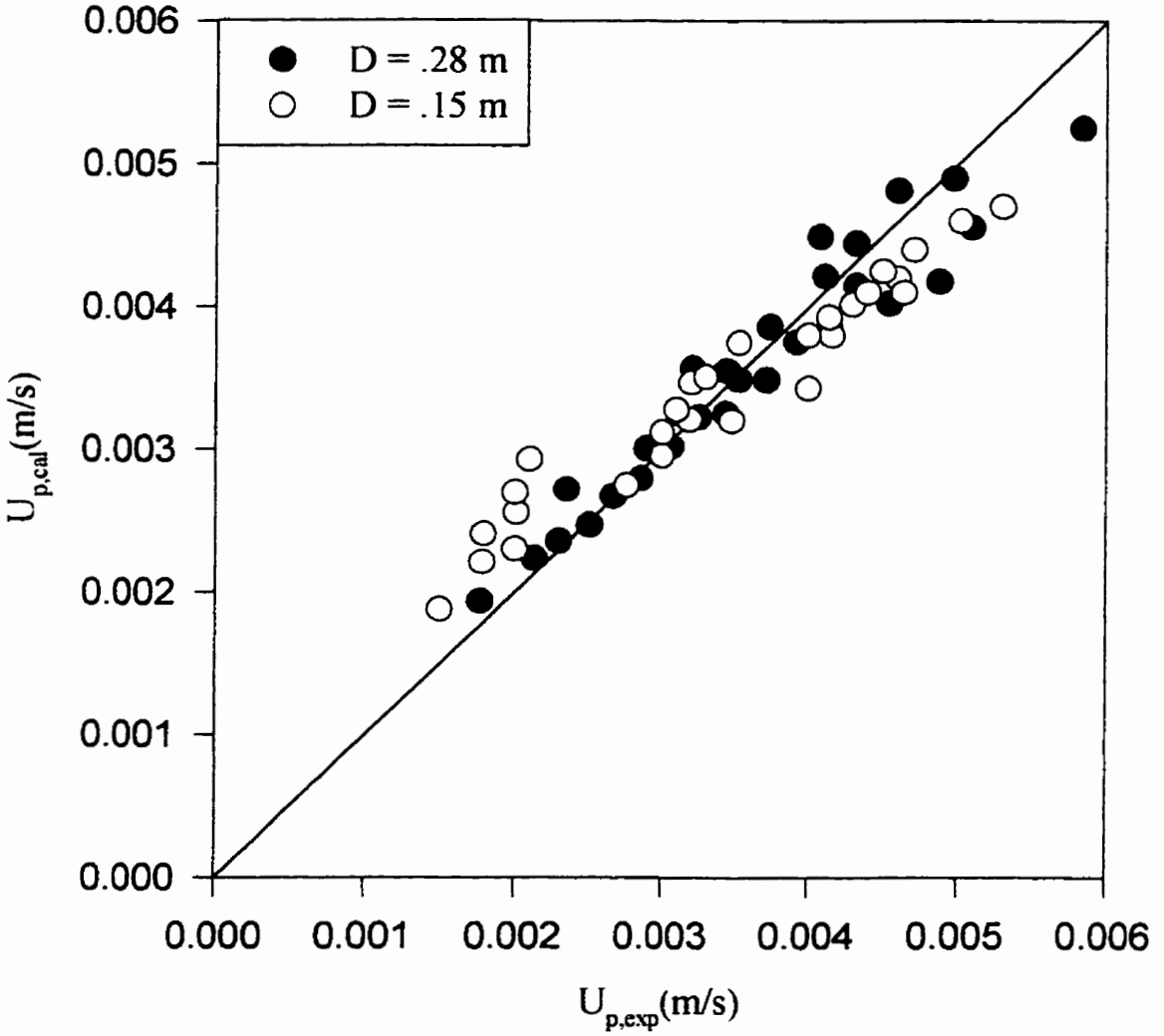

Figure 4.1.14c Comparison of O'Dowd's correlation with measured particle hindered settling velocity

(Experimental data based on Appendix E11; calculation based on O'Dowd et al., 1987)

4.1.2.4 Solids Dispersion Coefficient and Peclet Number

Axial solids backmixing or dispersion is another characteristic parameter of slurry bubble column. A quantitative description of the solids back mixing can be obtained from the solids dispersion coefficient. Solid dispersion coefficients at various gas velocities and slurry concentrations are shown in Figure 4.1.15a. As shown in Figure 4.1.15a, solid dispersion coefficient is an increasing function of gas velocity.

Figure 4.1.15b shows the effects of the column diameter on the solid dispersion coefficient. The solid dispersion coefficient for a column diameter of 0.15 m were obtained based on the axial profile of slurry concentration for a column diameter of 0.15 m from Gandhi (1997), who used same particles (35 μm glass beads) in his study. Generally, the solid dispersion coefficient is an increasing function of the column diameter, as shown in Figure 4.1.15b. These results are in agreement with Kato et al. (1972).

The correlation of the solid dispersion coefficients have been proposed by several researchers (Kato et al., 1972; Smith and Ruether, 1985; O'Dowd et al, 1987). These correlations are shown in Table 2.4.1. The correlations in Table 2.4.1 are expressed by solids Peclet number as a function of the Froude number, gas Reynolds number, and particle Reynolds number. Those dimensional variables are defined as follows:

$$Pe_p = \frac{V_g D}{E_s} \tag{4.1.21}$$

$$Re_g = \frac{V_g D \rho_{sl}}{\mu_{sl}} \tag{4.1.22}$$

$$Fr_g = \frac{V_g}{\sqrt{gD}} \tag{4.1.23}$$

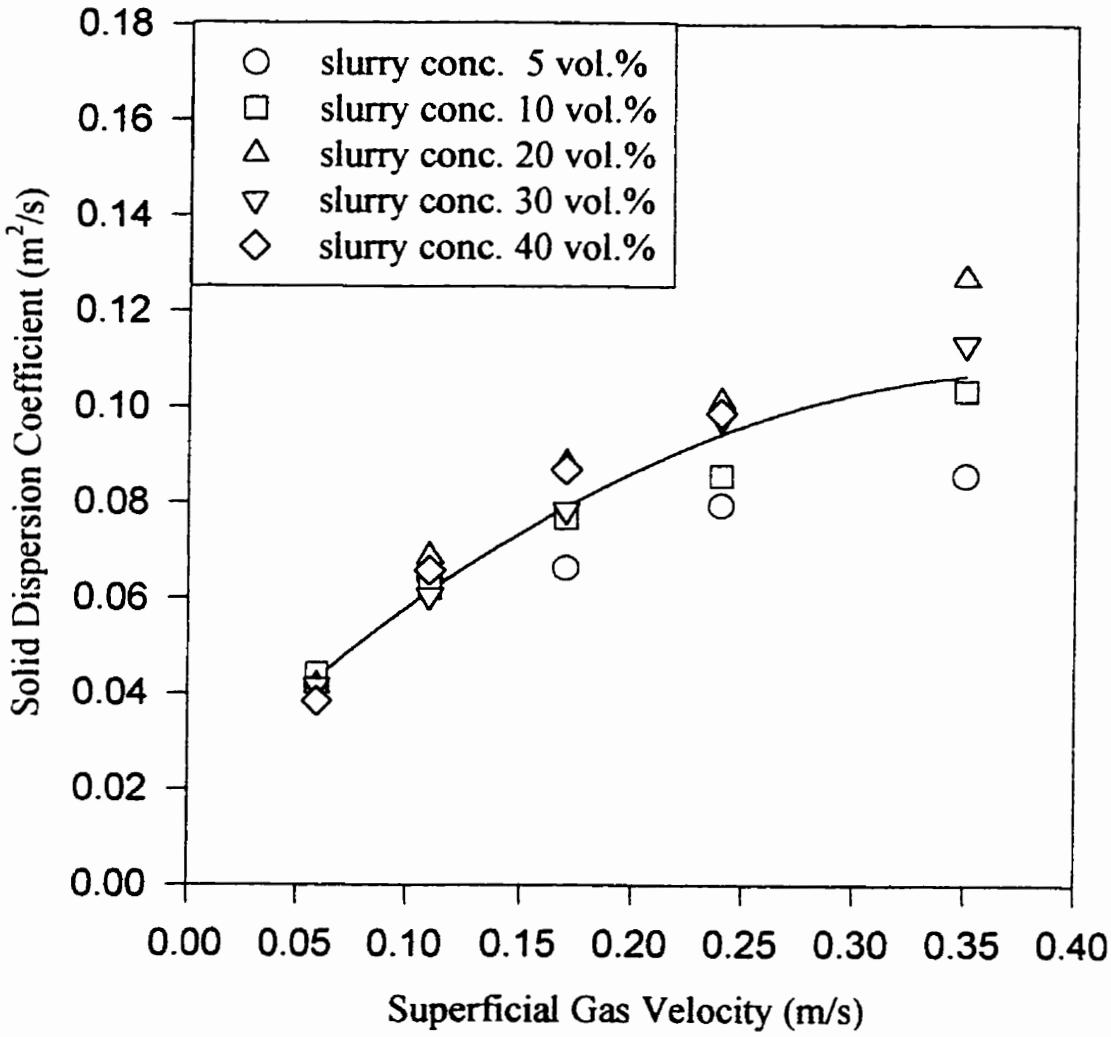

Figure 4.1.15a Variation of the solids dispersion coefficient with gas velocity based on data of this study

(Data based on Appendix E11)

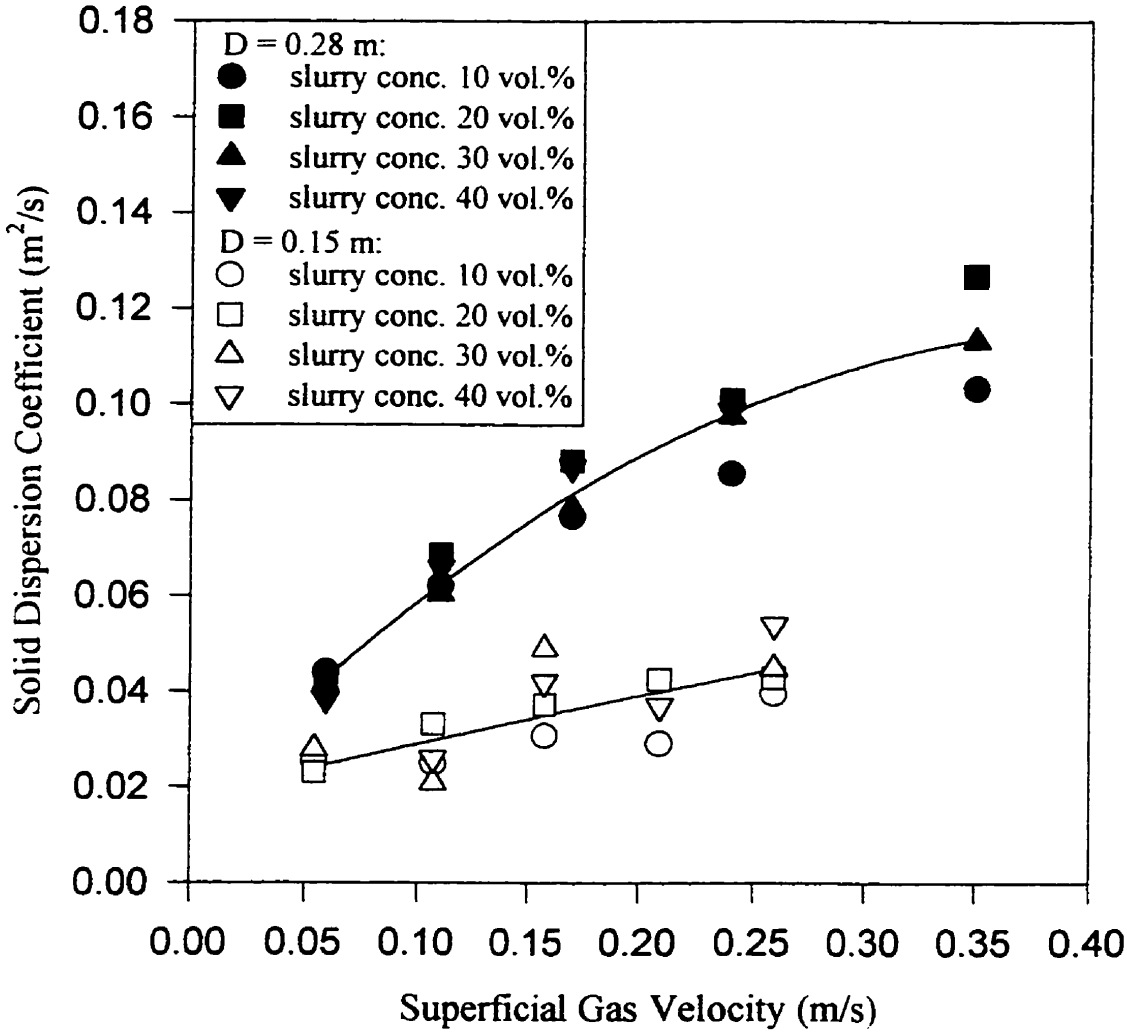

Figure 4.1.15b Solid dispersion coefficients at different column diameters
(Data based on Appendix E11)

$$Re_p = \frac{U_t d_p \rho_{sl}}{\mu_{sl}} \qquad (4.1.24)$$

Table 4.1.4 presents the average relative deviation and range of error. The predictions of the correlations of Kato et al. (1972) and Smith and Ruether (1985) are within 15 % of experimental values. Therefore, either of these correlations can be used for high slurry concentrations.

Peclet numbers computed by correlations shown in Table 2.4.1 are compared with experimental Peclet numbers. The Peclet number from experiment was defined in equation (4.1.21), in which E_s was used from experimental results. Table 4.1.5 list the relative deviation and error range. Again predictions by correlations of Kato et al. (1972) and Smith and Ruether (1985) are within 15 % of experimental data.

Table 4.1.4 Deviation and range of solid dispersion coefficient

	average relative deviation (%)	maximum relative deviation (%)	minimum relative deviation (%)
Kato et al. (1972)	12.38	36.45	0.48
Smith and Ruether(1985)	11.60	25.31	0.21
O'Dowd et al. (1987)	15.82	31.23	1.87

Table 4.1.5 Deviation and range of Peclet number

	average relative deviation (%)	maximum relative deviation (%)	minimum relative deviation (%)
Kato et al. (1972)	11.61	28.07	0.48
Smith and Ruether(1985)	12.86	33.88	0.21
O'Dowd et al. (1987)	19.83	45.42	1.83

4.1.2.5 Prediction of Axial Solids Concentration Distribution

The experimental data of axial solids concentrations were compared with the predictions by various literature correlations (Kato et al., 1972; Smith and Ruether, 1985; O'Dowd et al., 1987). In all three correlations, U_p and E_s can be obtained by using corresponding correlations. The obtained U_p and E_s are used in calculation of solids axial profile by using sedimentation-dispersion model (equation 4.1.18a or equation 4.1.18b).

Comparisons of literature correlations with axial profile of measured solids concentrations are shown in Figures 4.1.16a through 4.1.16c. The comparisons are also listed in Table 4.1.6. From Figures 4.1.16a, b, c and Table 4.1.6, it can be seen that any of the correlations can be used to predict axial solids concentration with good results.

Table 4.1.6 Deviation and range of axial solids concentration

	average relative deviation (%)	maximum relative deviation (%)	minimum relative deviation (%)
Kato et al. (1972)	.896	4.58	0.00
Smith and Ruether(1985)	1.100	4.64	0.00
O'Dowd et al. (1987)	.896	4.49	0.00

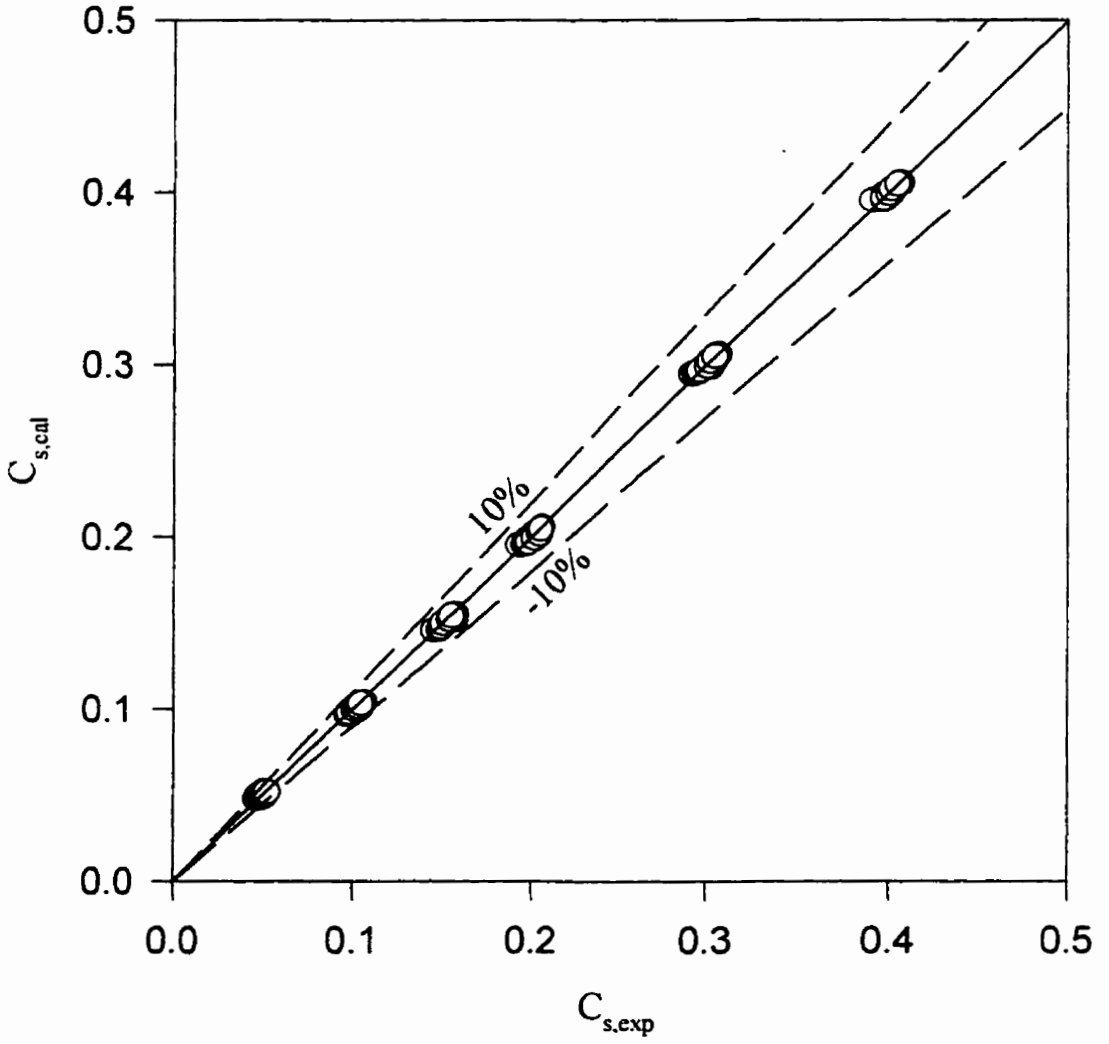

Figure 4.1.16a Comparison of Kato's correlation with measured solids concentration

(Experimental data based on Appendix E11; calculation based on Kato et al., 1972)

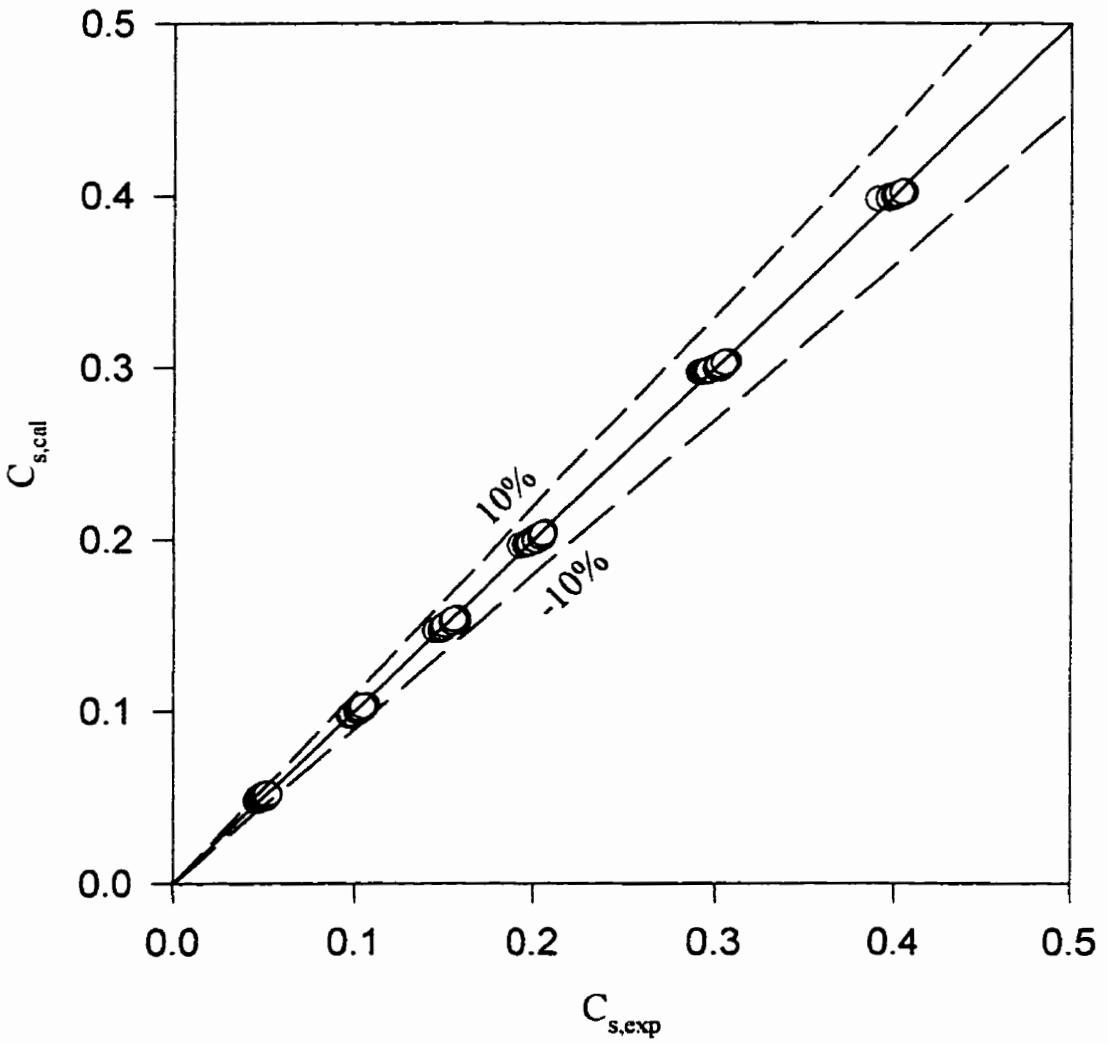

Figure 4.1.16b Comparison of Smith's correlation with measured solids concentration

(Experimental data based on Appendix E11; calculation based on Smith and Ruether, 1985)

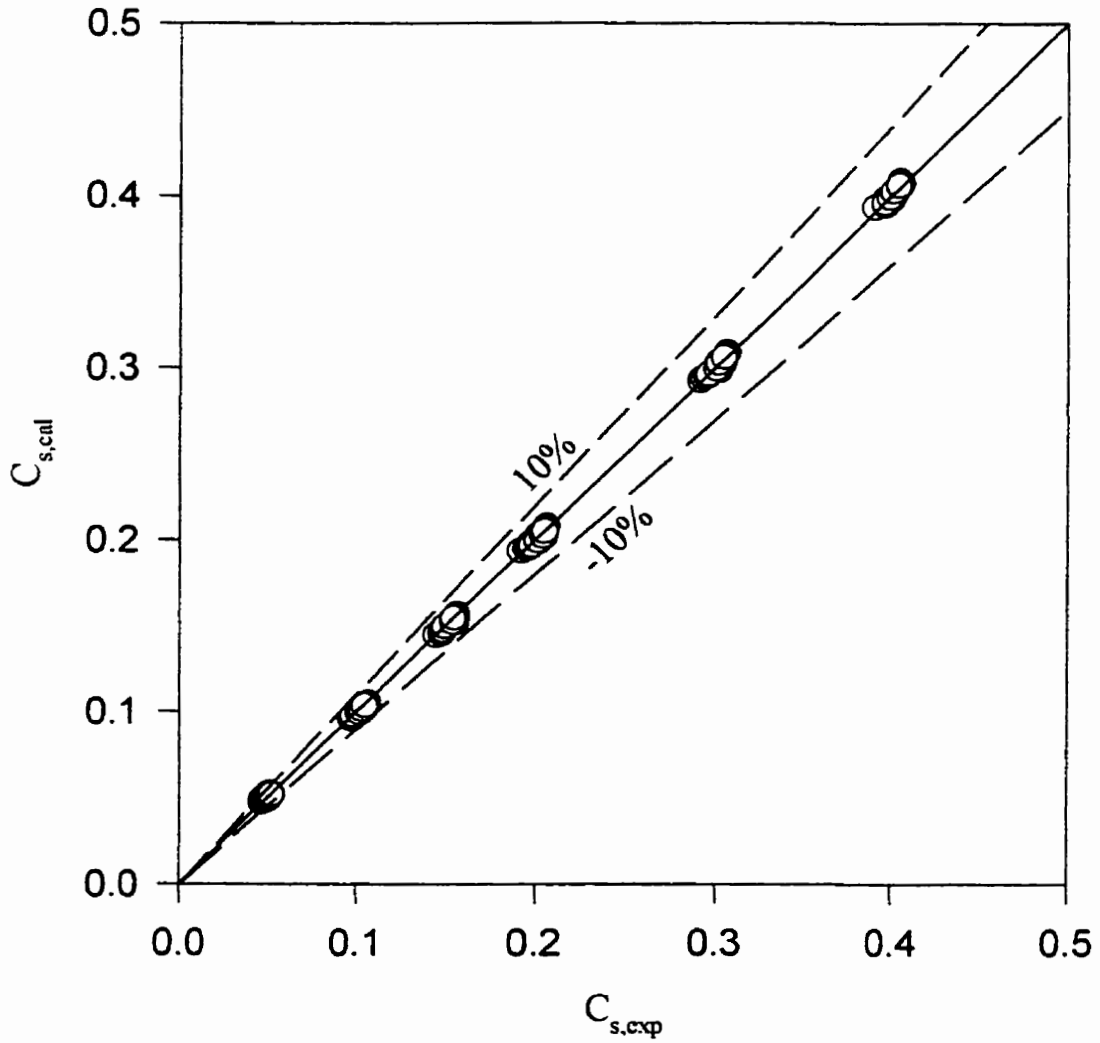

Figure 4.1.16c Comparison of O'Dowd's correlation with measured solids concentration

(Experimental data based on Appendix E11; calculation based on O'Dowd et al, 1987)

4.1.3 Gas Disengagement and Bubble Population

Gas holdup structure and bubble size distribution are important for a proper analysis of the bubble column reactor performance. The dynamic gas disengagement technique was used to obtain information on the fractions of larger and small bubble populations in the dispersion. The corresponding rise velocities of bubble classes were also estimated (sec. 3.3.5).

Figure 4.1.17 show the gas holdup distribution of larger bubbles and small bubbles in air-water system. As shown in Figure 4.1.17, the gas holdups due to both smaller and larger bubbles increased as gas velocity increased. It can be seen that holdups due to larger bubbles were generally lower than that of small bubbles, indicating more fraction of gas taken by small bubbles. The difference decreased as gas velocity increased, indicating more small bubbles coalescing into larger bubbles.

The effect of slurry concentration on gas holdup and bubble rise velocity, the relative gas holdup and relative rise velocity are discussed below. The relative variable is defined as the ratio of gas holdup or rise velocity in slurry phase to that in air-water system at same superficial gas velocity.

Figures 4.1.18a and 4.1.18b compare the gas holdup of small bubbles at different superficial gas velocities and slurry concentration. As the slurry concentration increases, the gas holdup of small bubbles decreased up to a slurry concentration of 25 vol.%. Above slurry concentrations of 25 vol.%, the gas holdup of small bubbles increased slightly, which can be attributed to reduced rise velocity of small bubbles, as shown in Figure 4.1.21.

Figures 4.1.19a and 4.1.19b compare the gas holdup due to larger bubbles at different slurry concentrations. The gas holdups slightly decreased with increase of slurry concentrations. As slurry concentration increases, coalesced larger bubble size

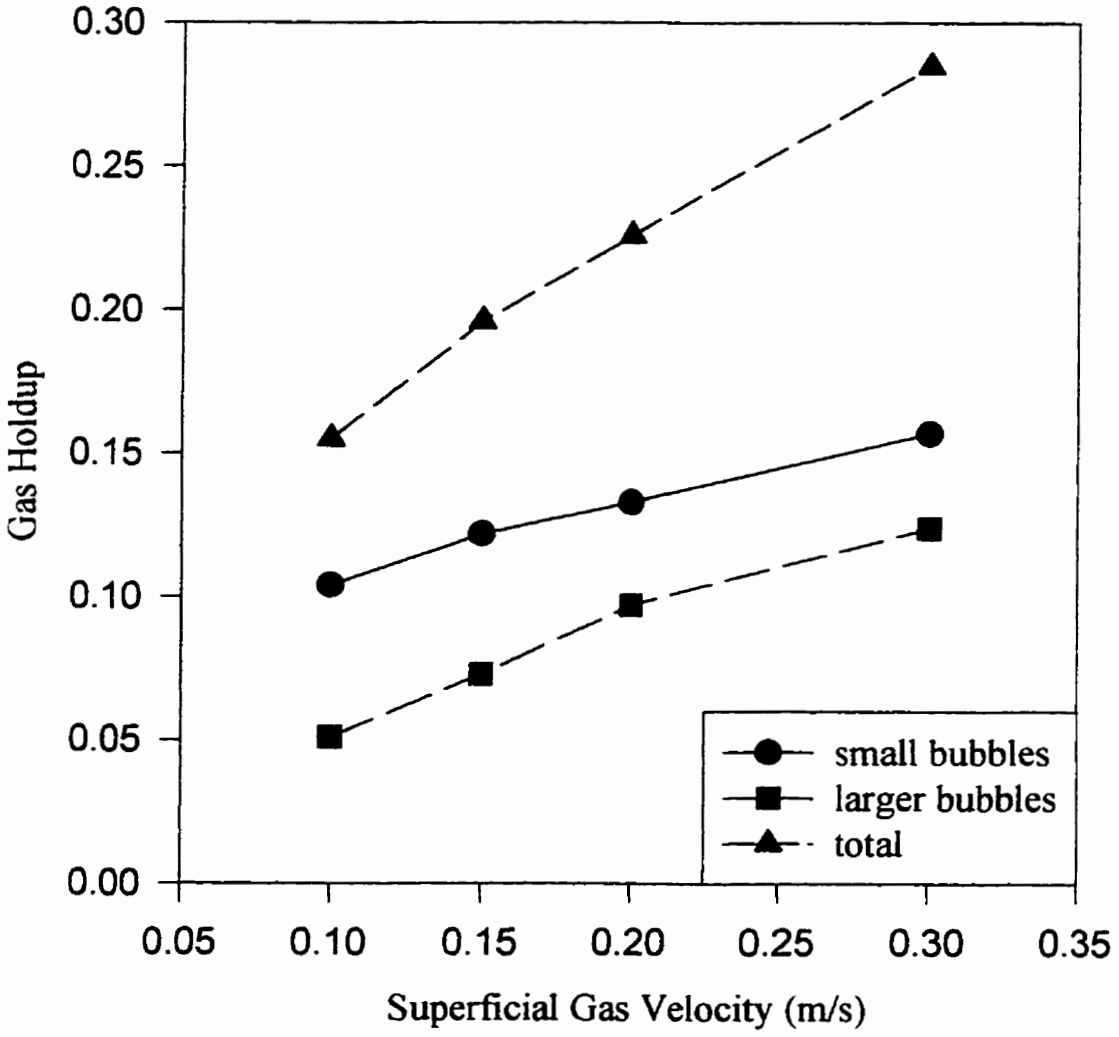

Figure 4.1.17 Gas holdup in air-water system

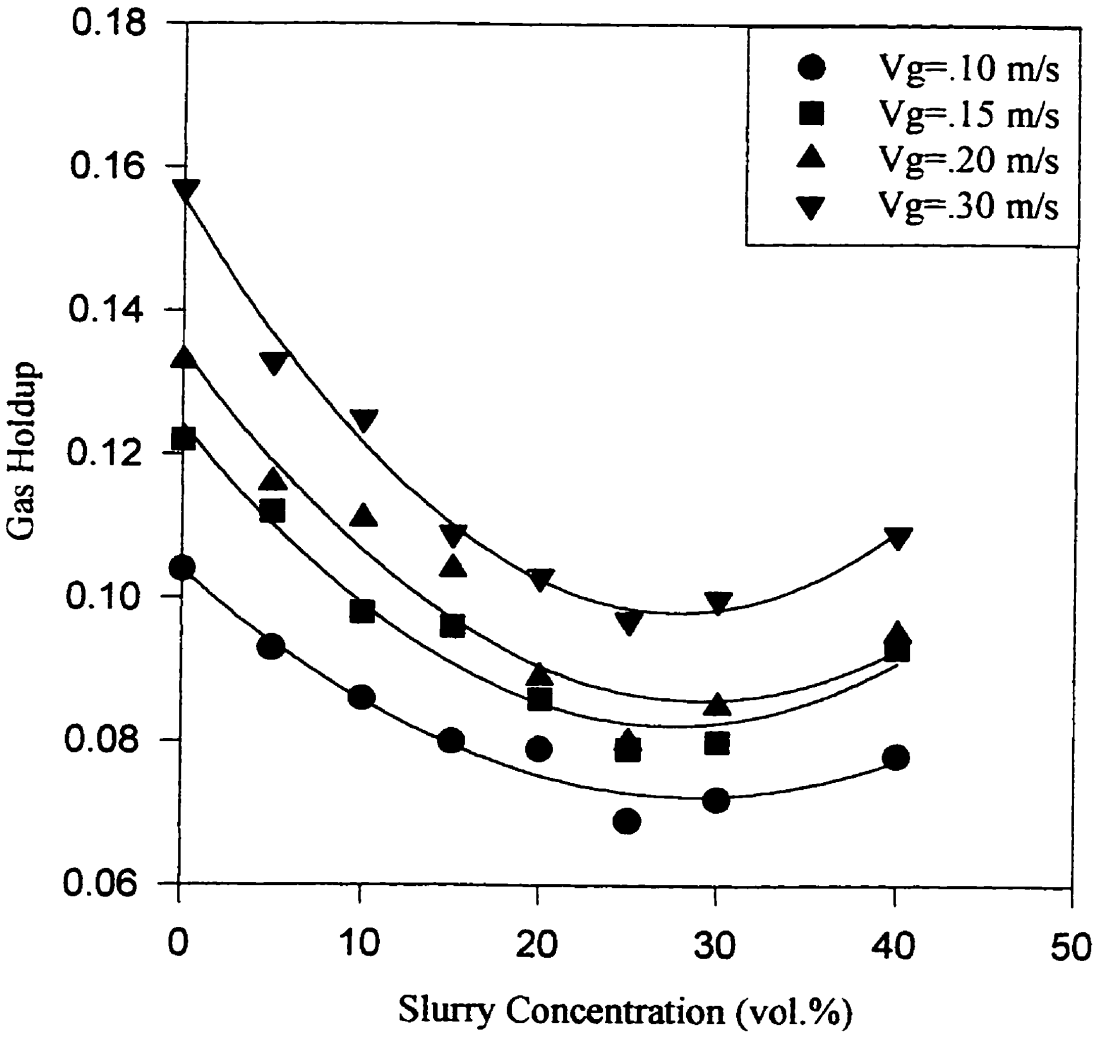

Figure 4.1.18a Small bubbles gas holdup

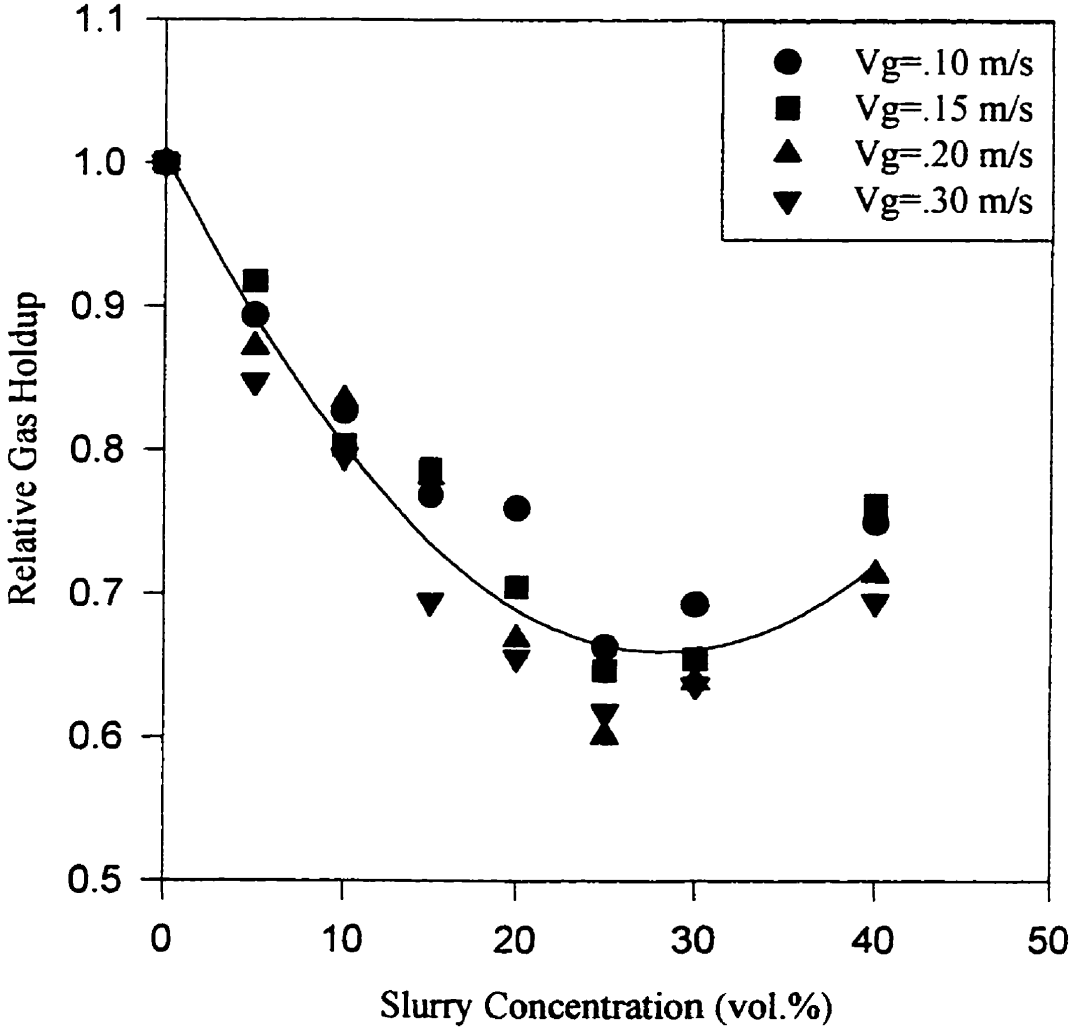

Figure 4.1.18b Relative small bubble gas holdup

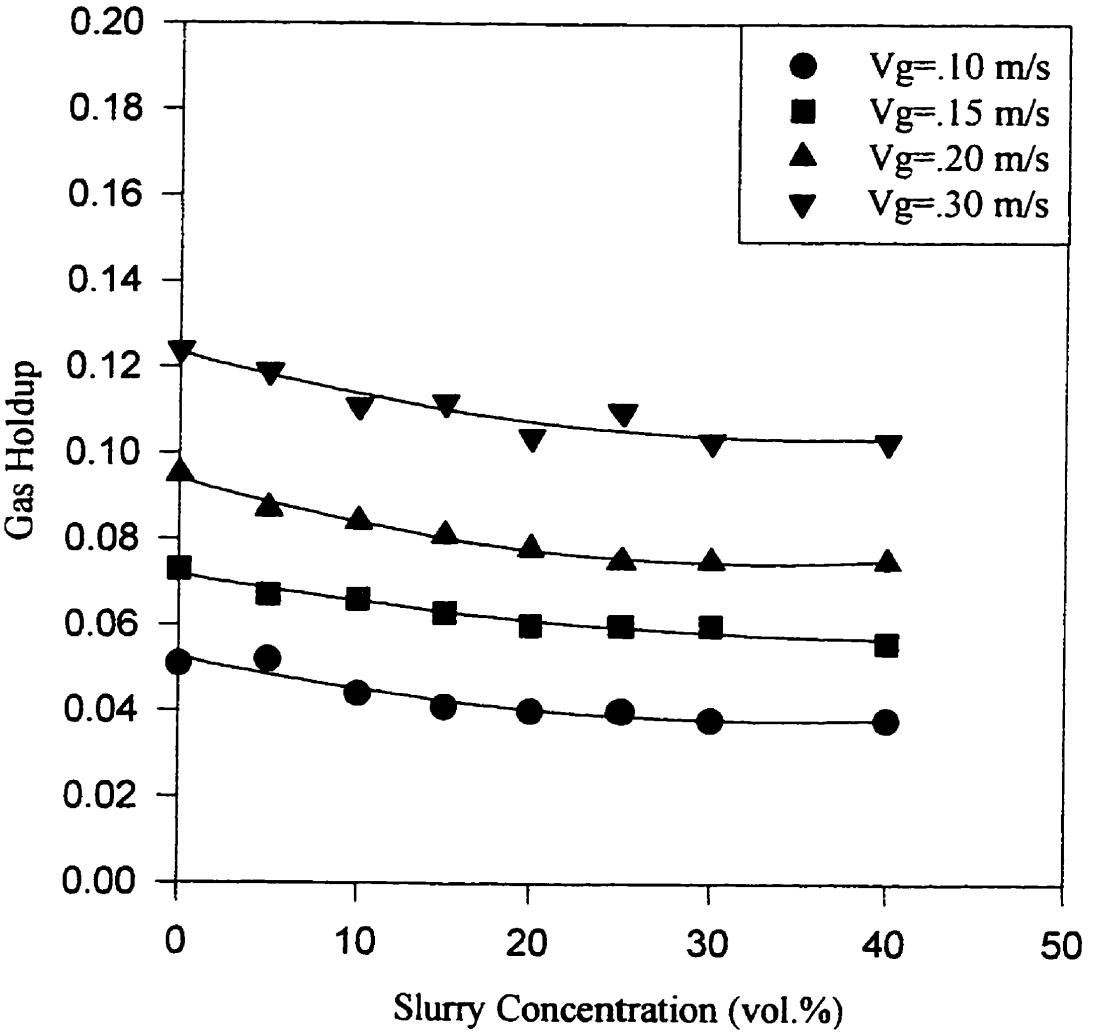

Figure 4.1.19a Larger bubble gas holdup

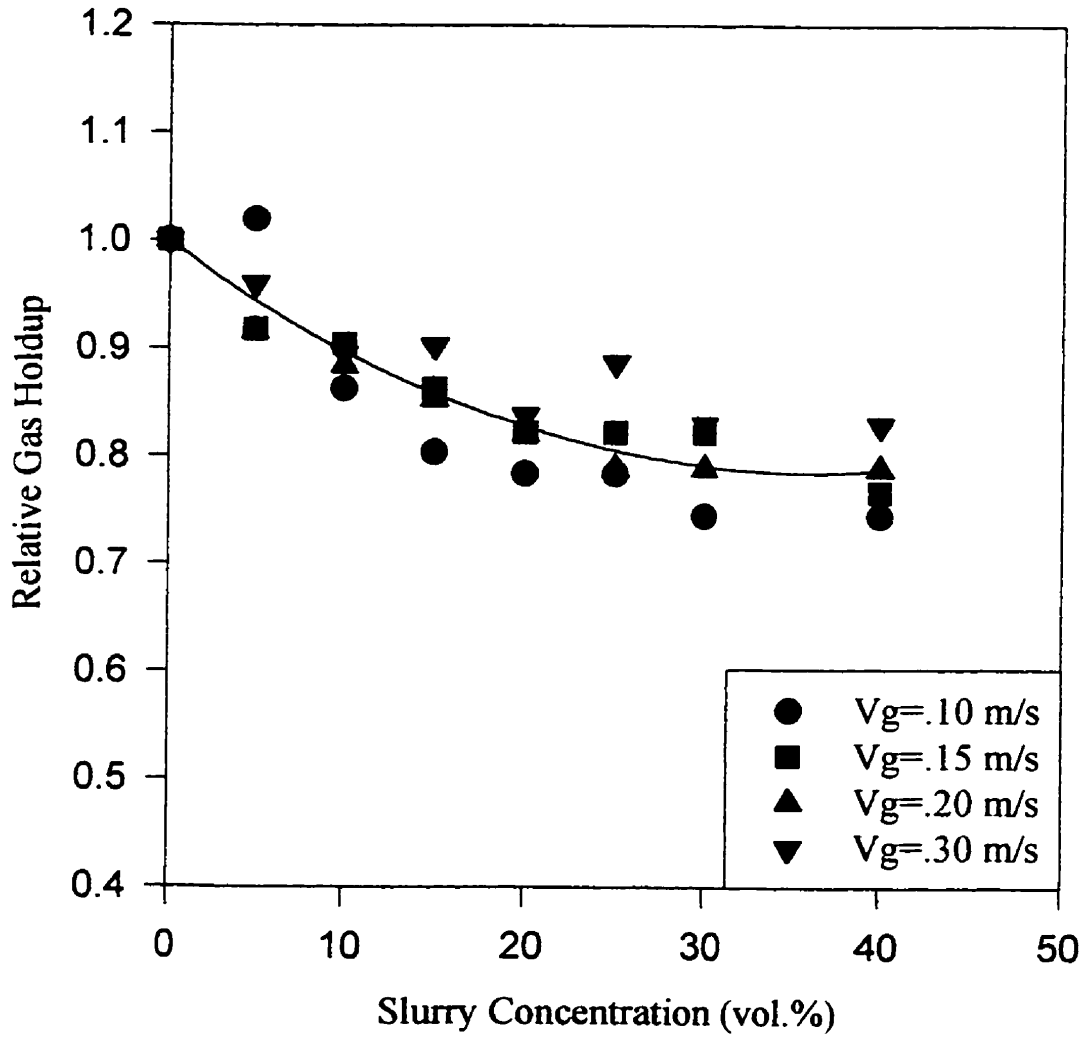

Figure 4.1.19b Relative larger bubble gas holdup

increases and the rise velocity of larger bubbles increases, resulting in a slightly reduced gas holdup.

Figure 4.1.20 shows the variation of rise velocity of small and larger bubbles as a function of gas velocity in air-water system. It can be seen that the rise velocity of larger bubbles increased with an increase in superficial gas velocity, due to the formation of coalesced larger bubbles. The rise velocity of small bubbles slightly decreased with an increase in gas velocity. Schumpe and Grund (1986) observed similar trend in air-water system. The rise velocity of small bubbles was found to be constant around 0.21 m/s. In the present study, rise velocity of small bubbles is 19 cm/s. The rise velocities of larger bubbles in this study are systematically higher than those observed by Schumpe and Grund (1986). This can be attributed to the procedure used. Schumpe and Grund (1986) measured gas holdup by observing dispersion height, which would have included the foam layer on the top of the column. The experimental result from this experiment, however, are based on observation by measuring pressure drop between two pressure transducers, in which the foam layer is not included.

Figures 4.1.21a and 4.1.21b show the effect of slurry concentration on the rise velocity of smaller bubbles. As shown in Figures 4.1.21a and 4.1.21b, the rise velocity of smaller bubbles increased with increase in slurry concentration up to slurry concentrations of 20 vol.%. Above slurry concentrations of 20 vol.%, the rise velocity of smaller bubbles decreased slightly. The increase in rise velocity of the small bubble population can be attributed to an increase in average bubble size with increasing slurry concentration. As discussed earlier, bubble breakup rate would be reduced with increasing slurry concentrations, leading to higher average bubble size. The slight drop in rise velocity of small bubbles above slurry concentrations of 25 vol.% can be attributed to an increase in apparent suspension viscosity.

Figure 4.1.22a and 4.1.22b show the effect of slurry concentration on the rise velocity of larger bubbles. The rise velocity of larger bubbles increased with increasing slurry

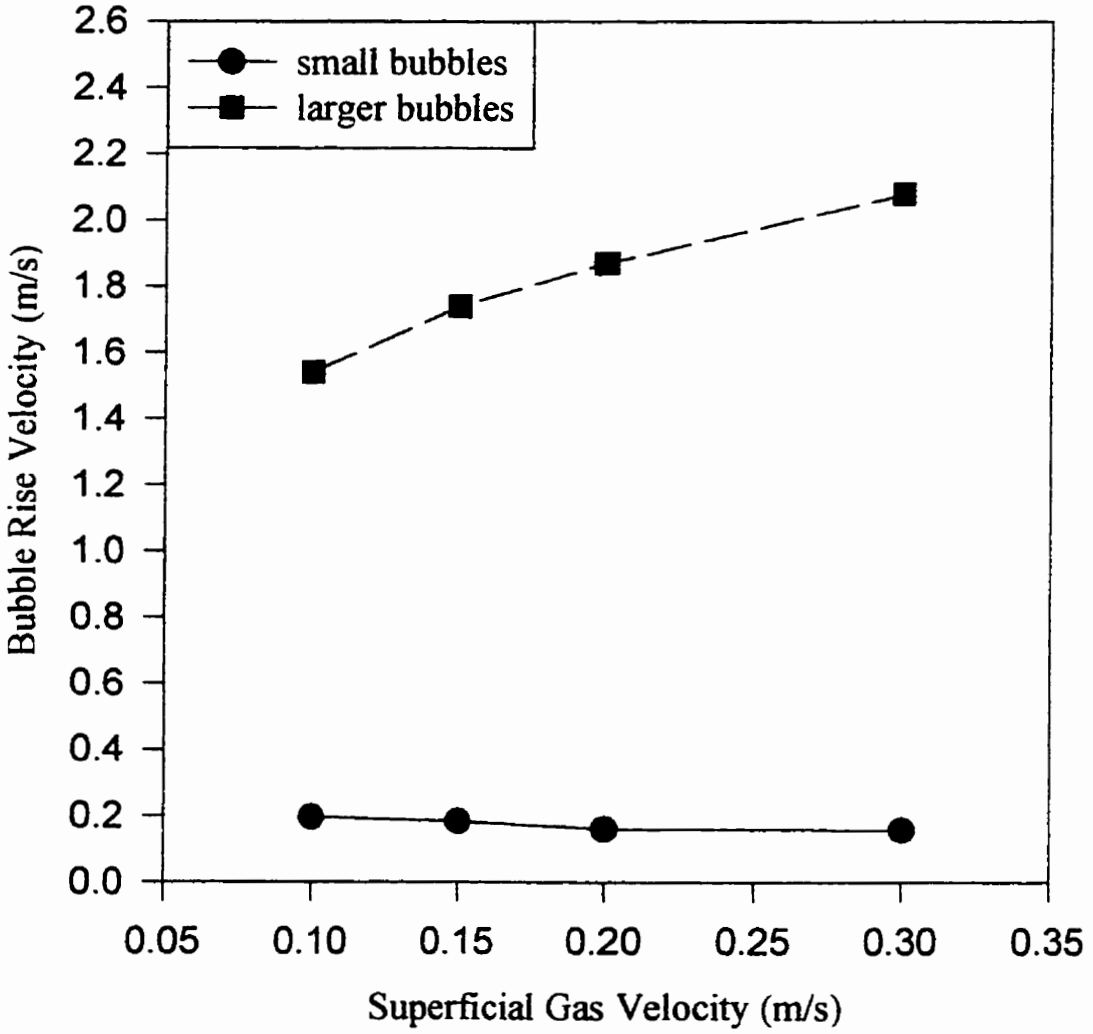

Figure 4.1.20 Bubble rise velocity in air water system

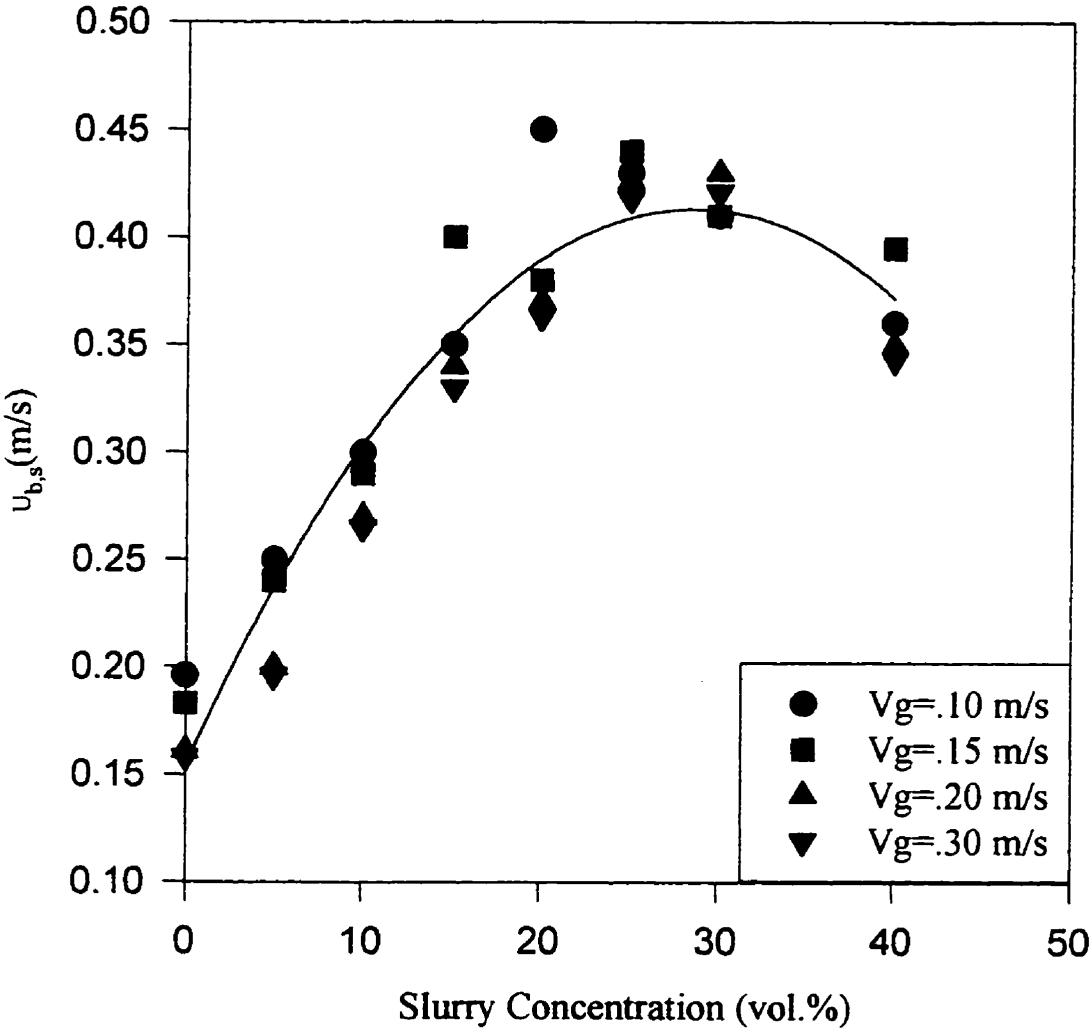

Figure 4.1.21a Rise velocity of small bubbles

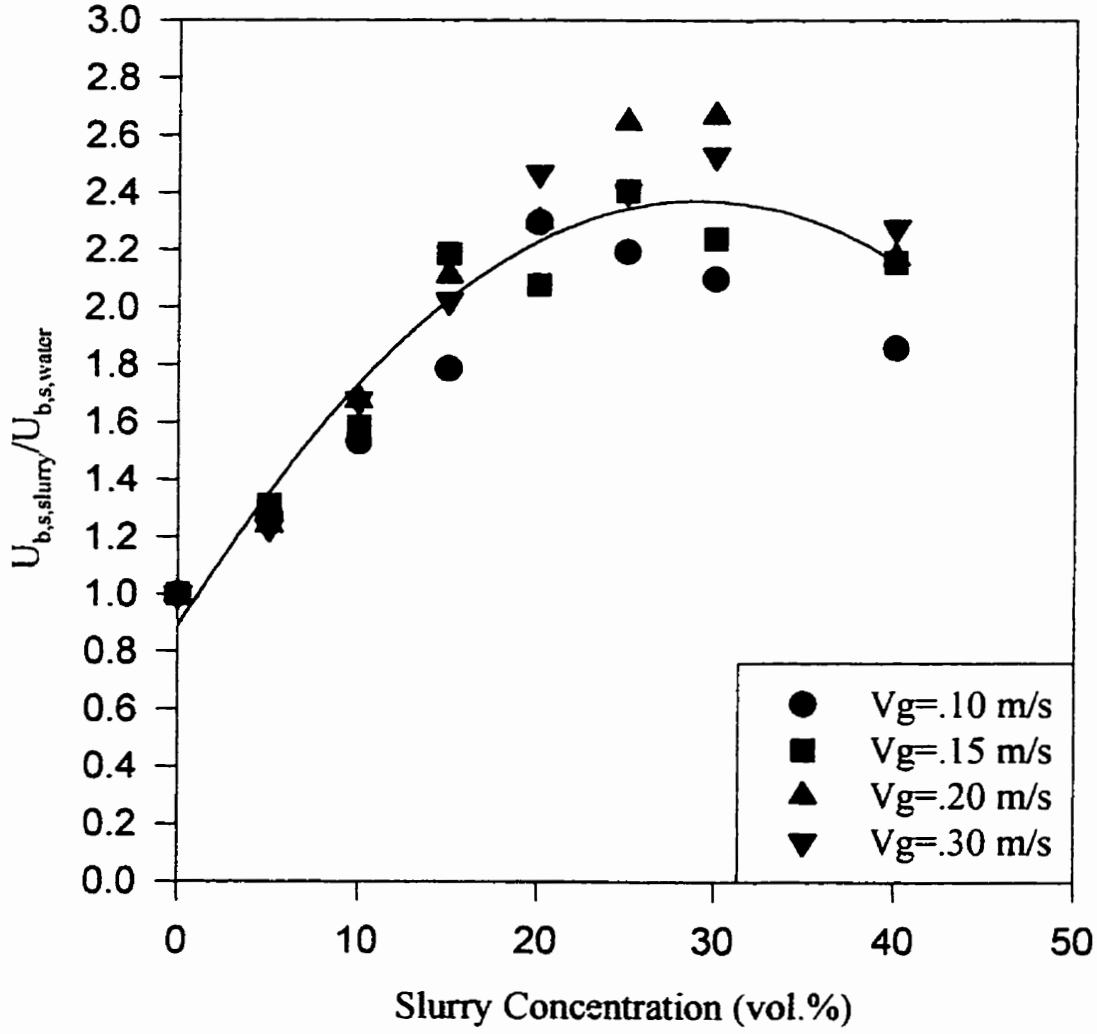

Figure 4.1.21b Relative rise velocity of small bubbles as a function of slurry concentration

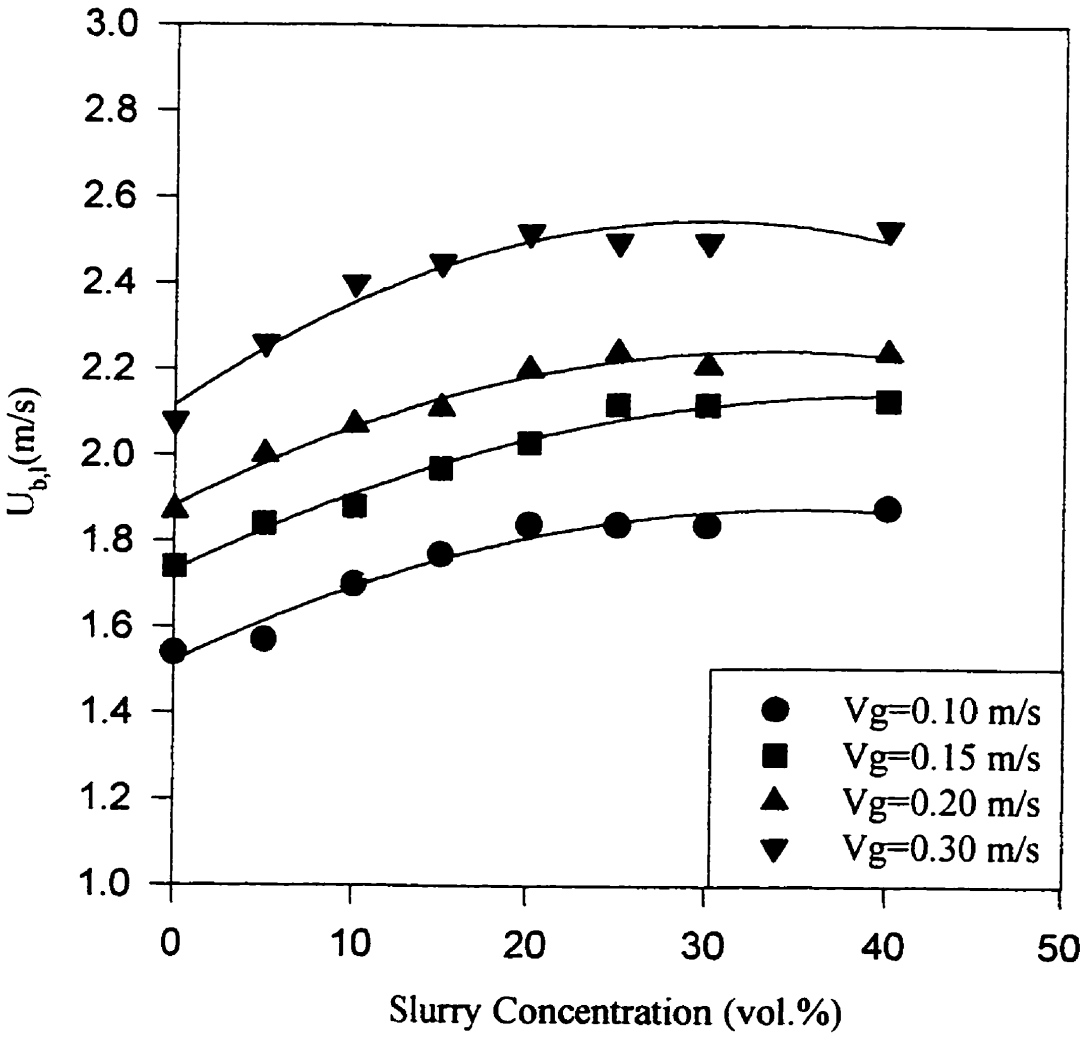

Figure 4.1.22a Larger bubble rise velocity as a function of slurry concentration

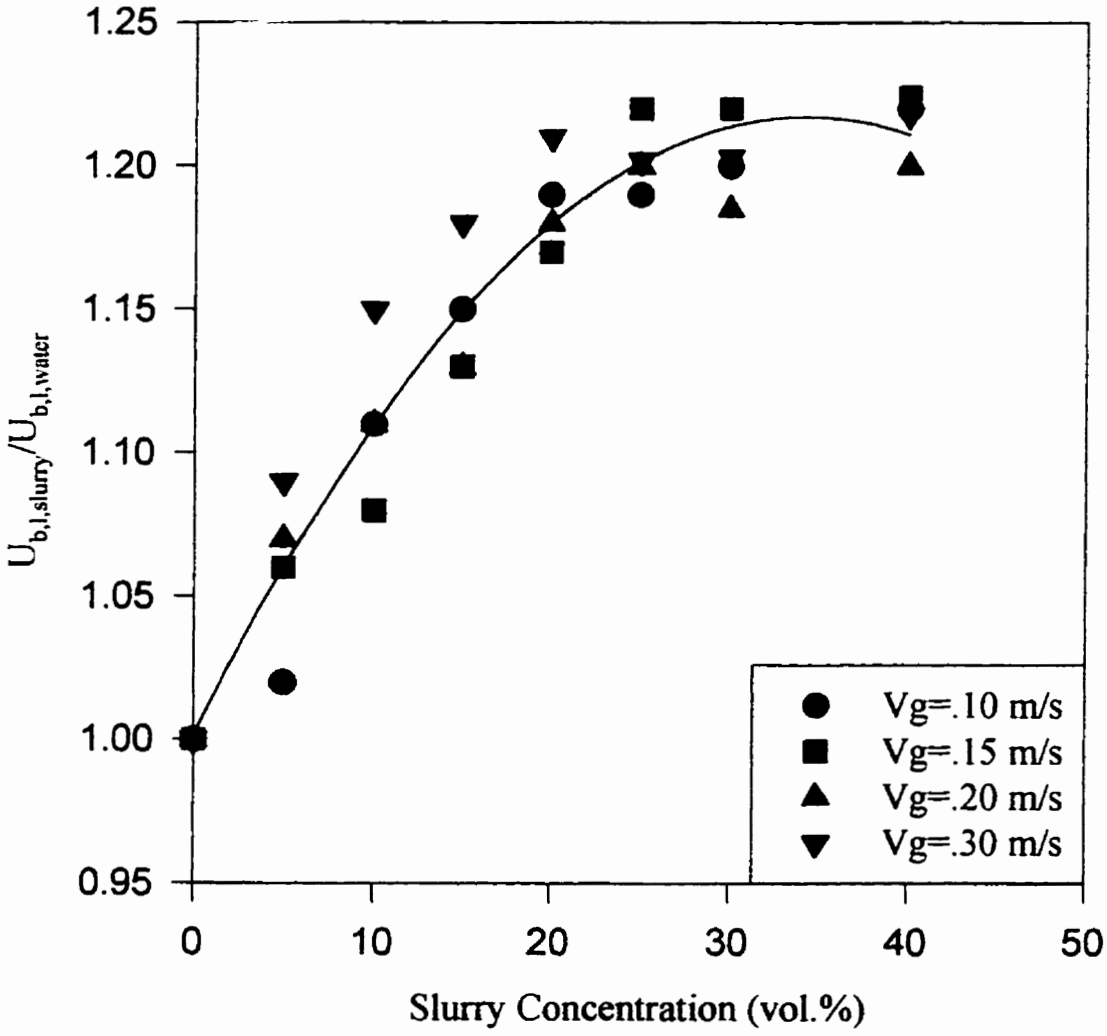

Figure 4.1.22b Relative larger bubble rise velocity as a function of slurry concentration

concentrations, due to the formation of coalesced larger bubbles. Above slurry concentrations of 20 vol.%, the larger bubble rise velocity increases only slightly, indicating formation of a more stable bubble size.

In the experimental observation described above, the effect of slurry concentrations on bubble population and rise velocities has not been reported in literature so far.

4.2 Heat Transfer Measurements

The local average and instantaneous heat transfer data are analyzed to investigate the effects of gas velocity and slurry concentrations in different regions of the slurry bubble column. The measured values are compared with literature correlations and models. Their applicabilities and limitations are pointed out. The heat transfer measurements at different axial, radial positions and for different probe orientations have provided insights into flow pattern in a slurry bubble column. The analysis of instantaneous heat transfer coefficients has provided insight into bubble wake behavior and bubble dynamics.

4.2.1 Local Average Heat Transfer Coefficients

Figure 4.2.1 shows that average heat transfer coefficients increased with increasing gas velocity in both the central and wall regions of the column for different slurry concentrations. The heat transfer coefficients in the wall region are always lower than in the central regions of the column. Based on instantaneous heat transfer measurements it is shown (Figure 4.2.2) that larger bubbles pass in the central region and enhance heat transfer, compared to that near the wall. As discussed in section 4.2.2, the higher heat transfer coefficient in the central region of the column is attributed to faster rising bubbles along the column axis. Thus, the average heat transfer coefficient in the center is systematically higher than at the wall.

The rate of increase in heat transfer is high up to a gas velocity of about 0.25 m/s and then decreases thereafter (Figure 4.2.1). This trend can be observed in both central and wall regions of the column. With increasing gas velocity, turbulence in the column increases due to the formation of faster rising gas bubbles which carry a turbulent wake behind them (Tsuchiya and Fan, 1988; Chen et al., 1994). This enhanced bubble-wake-turbulence reduces the heat transfer film on the surface of the probe resulting in a higher heat transfer rate. The heat transfer rate decreased with increasing slurry concentrations.

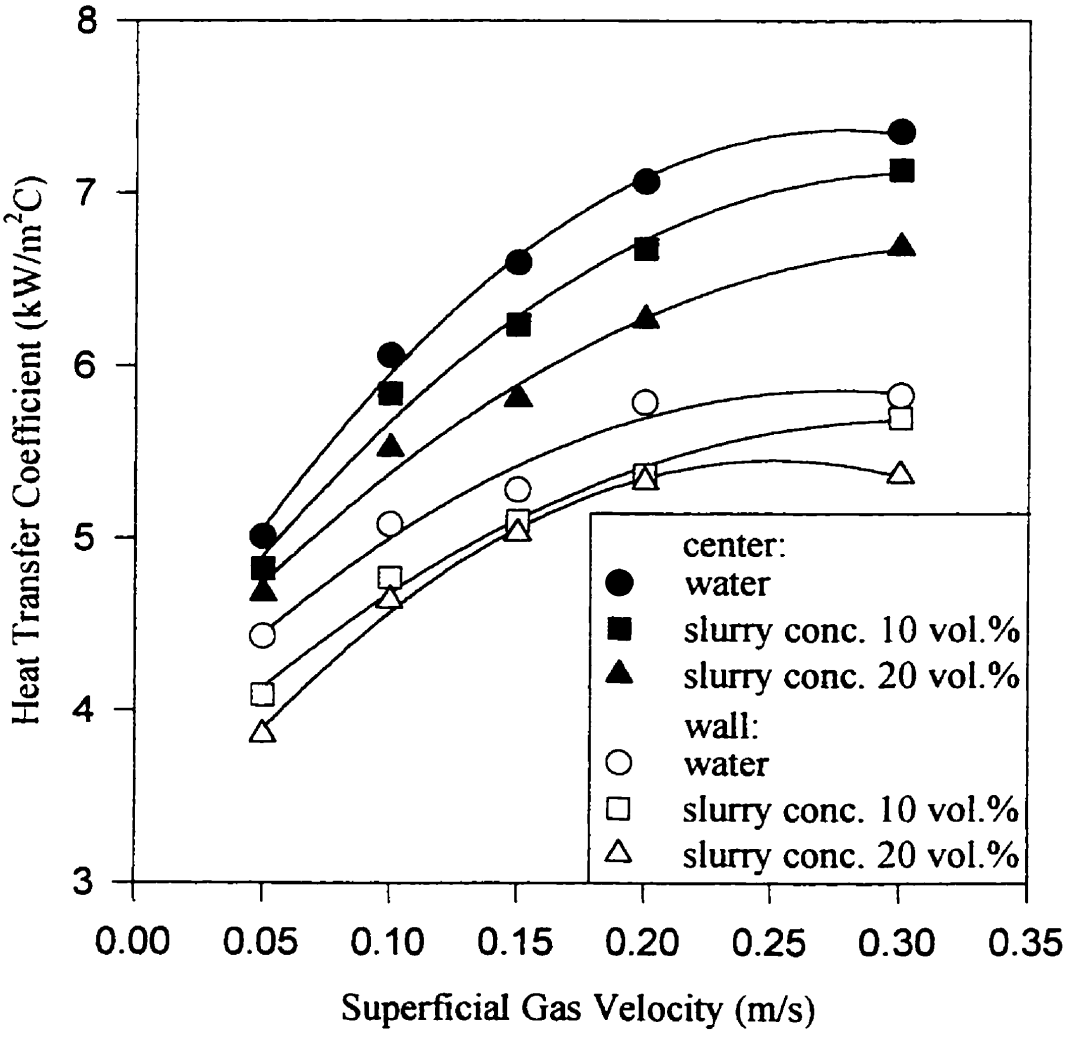

Figure 4.2.1 Variation of average heat transfer coefficient with gas velocity
(Data based on Appendix E2 and E6)

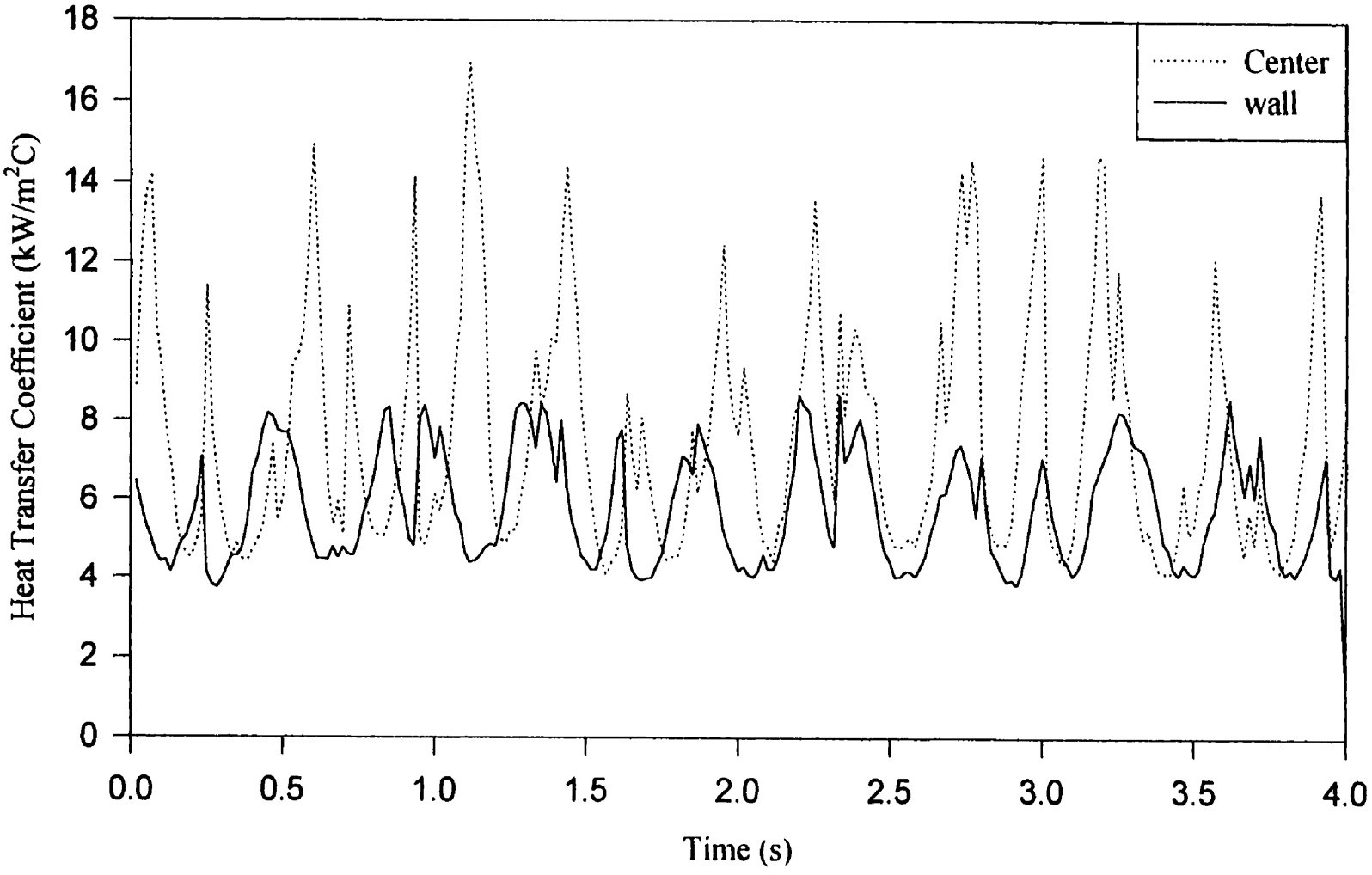

Figure 4.2.2 Instantaneous heat transfer coefficient at different location in bulk region (z=1.28m)

Figures 4.2.3 and 4.2.4 present the effects of increasing slurry concentrations in the central and wall regions of the column. It may be noted from these figures that for slurry concentrations below 10 vol.%, the rate of decrease of heat transfer is low for gas velocities higher than 0.1 m/s. However for higher slurry concentrations, the heat transfer rate decreases with increasing slurry concentrations for all gas velocities. In the wall region, the heat transfer rate decreases more rapidly for low gas velocities (Figure 4.2.4). This can be attributed to low turbulence in the wall region and higher local slurry concentrations. Heat transfer in slurry bubble columns has been investigated by several researchers (Deckwer et al., 1980; Saxena et al., 1989, 1990, 1992a). Generally a weak dependence of the heat transfer coefficient on the slurry concentration has been observed. Most of the literature studies, however, are limited to slurry concentrations below 20 vol.%. A comparison of heat transfer data of this study with literature correlations and models is presented below.

The measurements of heat transfer in particulate multiphase systems can be divided into object-to-bed (Deckwer et al., 1980; Saxena et al., 1989 and 1990a) or wall-to-bed heat transfer (Chiu and Ziegler, 1983; Saberian-Broudjenni et al., 1985). In this study, the measurements of heat transfer coefficients belong to object-to-bed heat transfer. Various correlations proposed in literature for heat transfer coefficients in these systems were reviewed in section 2.5.2. The correlations proposed by Deckwer et al., 1980, Kim et al., 1986 and Suh and Deckwer, 1989 are generally based on large amount of experimental data. These correlations were tested first against the data of this study.

The semi-theoretical correlation of Deckwer et al. (1980) is derived from Higbie's surface renewal theory and assumption of isotropic turbulence in bubble columns. This equation can be expressed as given below in terms of energy dissipation per unit volume P_v ($U_g \rho_{sl} g$) in a three-phase slurry bubble column:

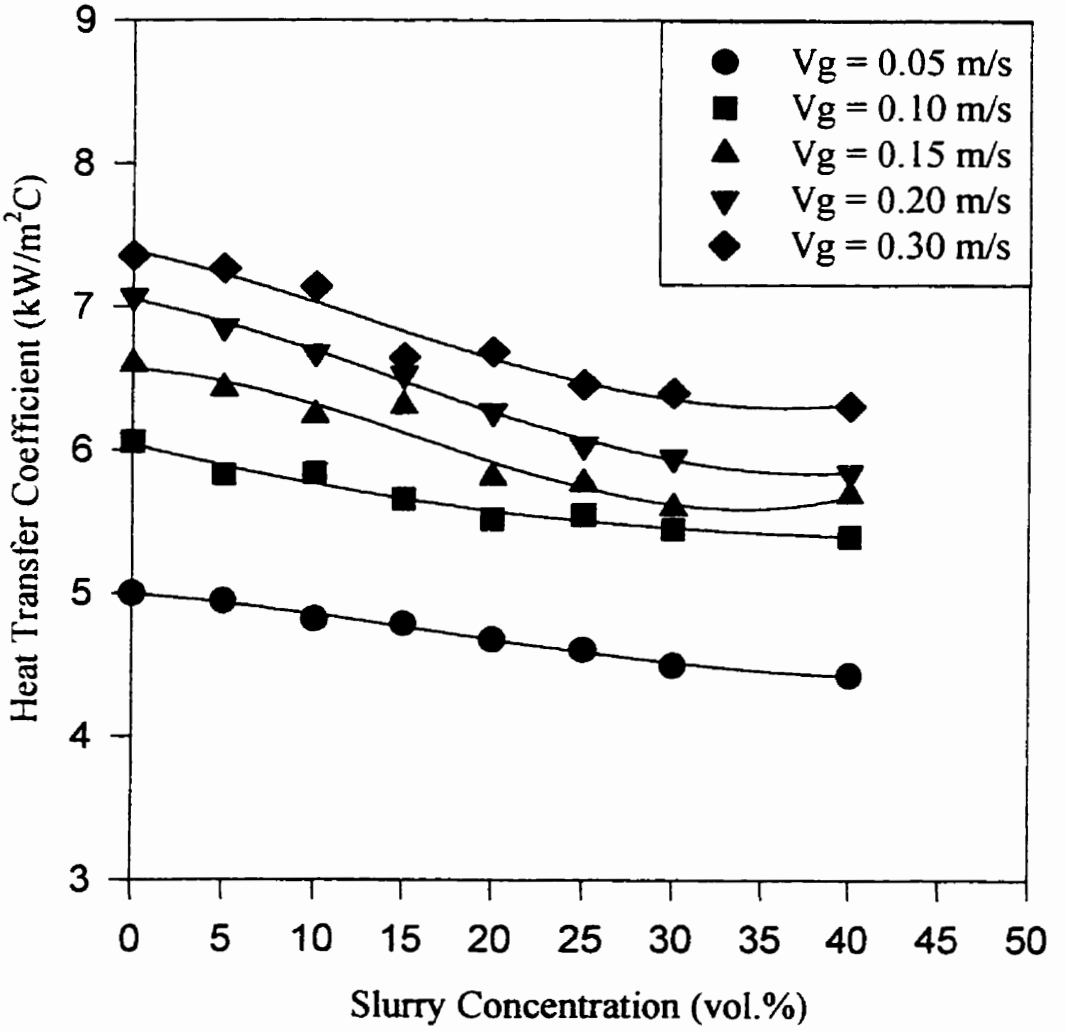

Figure 4.2.3 Average heat transfer coefficients as a function of slurry concentration in the central region (z=1.28m) (Data based on Appendix E2)

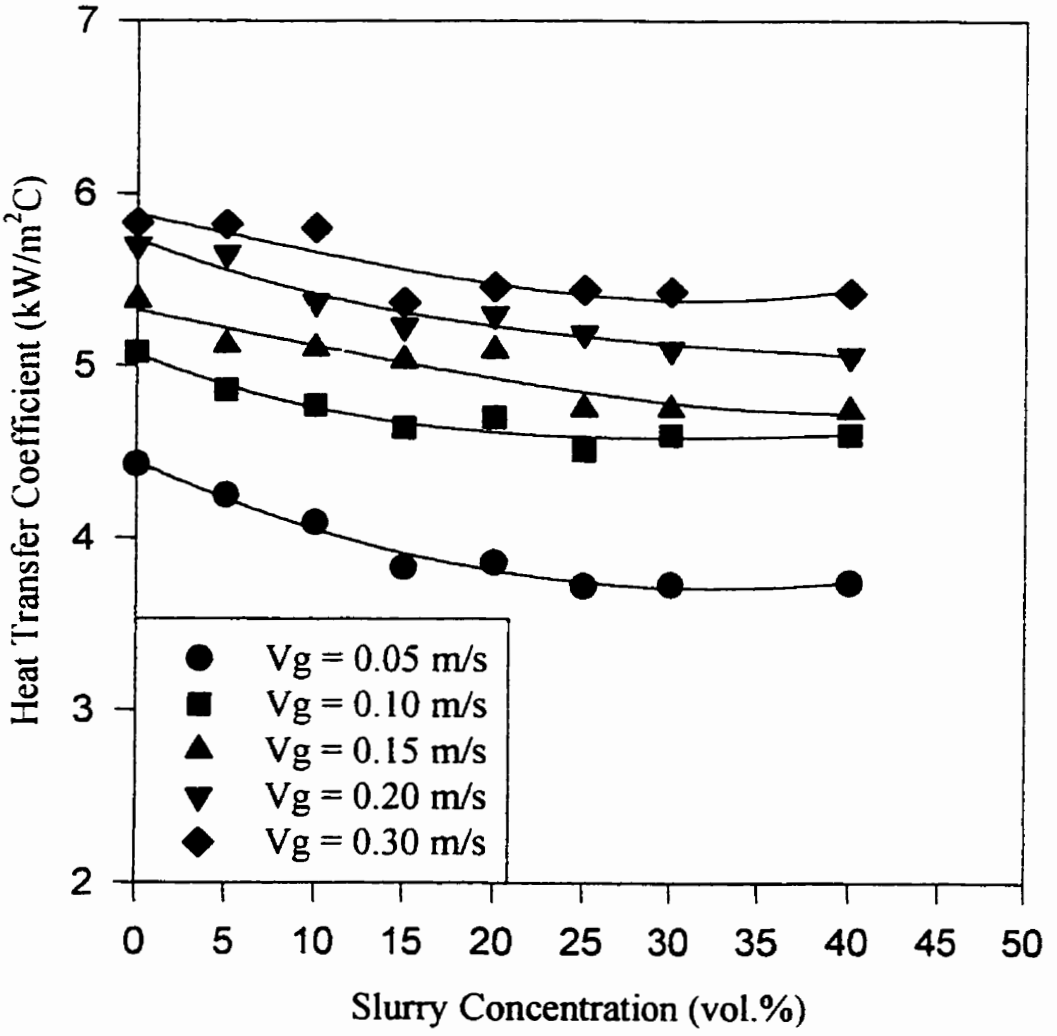

Figure 4.2.4 Average heat transfer coefficients as a function of slurry concentration in the wall region (z=1.28 m) (Data based on Appendix E6)

$$h = 0.1\left[k_{sl}\rho_{sl}C_{p,sl}\left(\frac{P_v}{\mu_{sl}}\right)^{0.5}\right]^{0.5} \qquad (2.5.23)$$

where, ρ_{sl}, $C_{p,sl}$ and k_{sl} are suspension density, specific heat and thermal conductivity respectively. The physical properties of the suspension were estimated from liquid and solid properties according to the following relations:

$$\rho_{sl} = \phi_s\rho_s + (1-\phi_s)\rho_l \qquad (4.2.1)$$

$$k_{sl} = k_l\frac{2k_l + k_s - 2\phi_s(k_l - k_s)}{2k_l + k_s - \phi_s(k_l - k_s)} \qquad (4.2.2)$$

$$C_{p,sl} = w_sC_{ps} + w_lC_{pl} \qquad (4.2.3)$$

For estimating of slurry viscosity, Deckwer et al. (1980) proposed Einstein's equation which is found to be applicable for dilute slurries (< 5 vol.%).

$$\mu_{sl} = \mu_l(1 + 4.5\phi_s) \qquad (4.2.4)$$

For the high slurry concentrations used in this study other equations were considered (sec. 4.1.1). The widely tested semi-theoretical correlation of Vand (1948) and the correlation proposed by Barnea and Mizrahi (1973) provided similar estimates of apparent slurry viscosity. Based on their analysis of heat transfer coefficients in three-phase fluidized beds, Suh and Deckwer (1989) also recommended the equation of Vand (1948) for estimation of bed viscosity. This equation was therefore selected to estimate apparent slurry viscosity in the present study.

$$\mu_{sl} = \mu_L\exp\left[\frac{2.5\phi_s}{1 - 0.609\phi_s}\right] \qquad (4.1.4)$$

For three-phase fluidized column with no liquid flow, the correlation of Suh and Deckwer (1989) can be written as:

$$h = 0.1(k_L \rho_L C_{pl} \{\frac{V_g(\varepsilon_g \rho_g + \varepsilon_L \rho_L + \varepsilon_s \rho_s)g}{\varepsilon_L \mu_{sl}}\}^{0.5})^{0.5} \qquad (4.2.5)$$

In this equation, the term in the inner bracket represents energy dissipation rate per unit volume of liquid:

$$P_v = \frac{V_g(\varepsilon_g \rho_g + \varepsilon_L \rho_L + \varepsilon_s \rho_s)g}{\varepsilon_L} \qquad (4.2.6)$$

The correlation proposed by Kim et al. (1986) is based on about thousand data points obtained in three-phase slurry-fluidized beds. For a slurry bubble column reactor this correlation is given as:

$$h = 0.0722(k_{sL} \rho_{sL} C_{psl} \{\frac{[(V_g)(\varepsilon_g \rho_g + \varepsilon_{sL} \rho_{sL} + \varepsilon_s \rho_s)]g}{\varepsilon_{sL} \mu_{sL}}\}^{0.5})^{0.5} \qquad (4.2.7)$$

Kim et al. (1986) used slurry viscosity for their correlation while Suh and Deckwer (1989) proposed the use of bed viscosity term. Moreover, the constant term in the correlation of Suh and Deckwer (1989) is higher than in Kim et al. (1986) correlation.

The values obtained with above correlations and experimental results from this study are compared in Figures 4.2.5a to e. It can be seen that the predictions by Deckwer et al. (1980) correlation are generally closer to measured heat transfer coefficients in the wall region of column up to slurry concentrations of 30 vol.% and gas velocity below 0.3 m/s. The predicted values are, however, significantly lower than measured values of heat transfer coefficients in the center. Figure 4.2.5a to 4.2.5e also show that the computed values based on Suh and Deckwer (1989) correlation are generally in between the measured values at the wall and at the center. It may be pointed out that the power input in Suh and Deckwer (1989) correlation is based on per unit liquid volume while in Deckwer et al. (1980) model it is based on per unit slurry volume. The calculated results

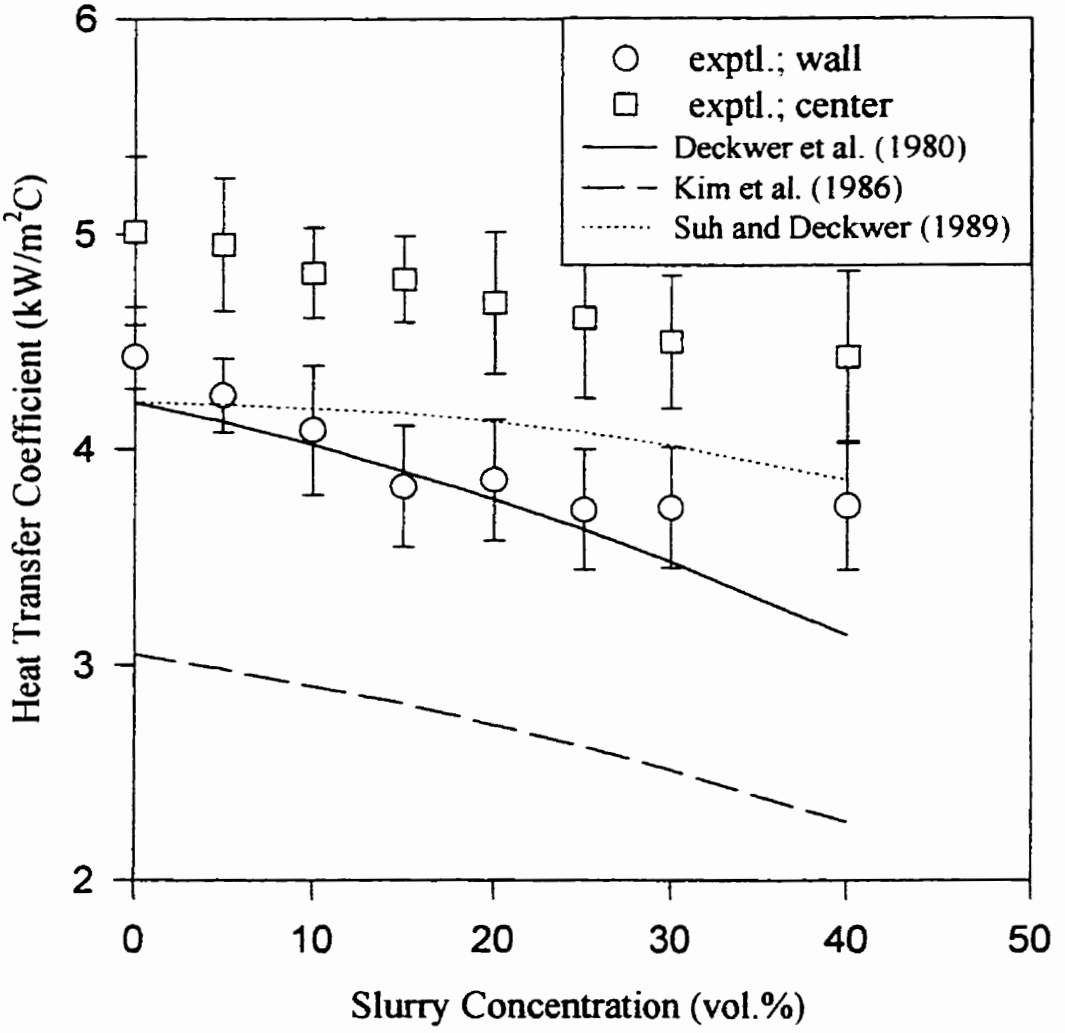

Figure 4.2.5a Comparison of measured heat transfer coefficients with literature correlations at Vg = 0.05 m/s (z=1.28 m)
(Data based on Appendix E2 and E6)

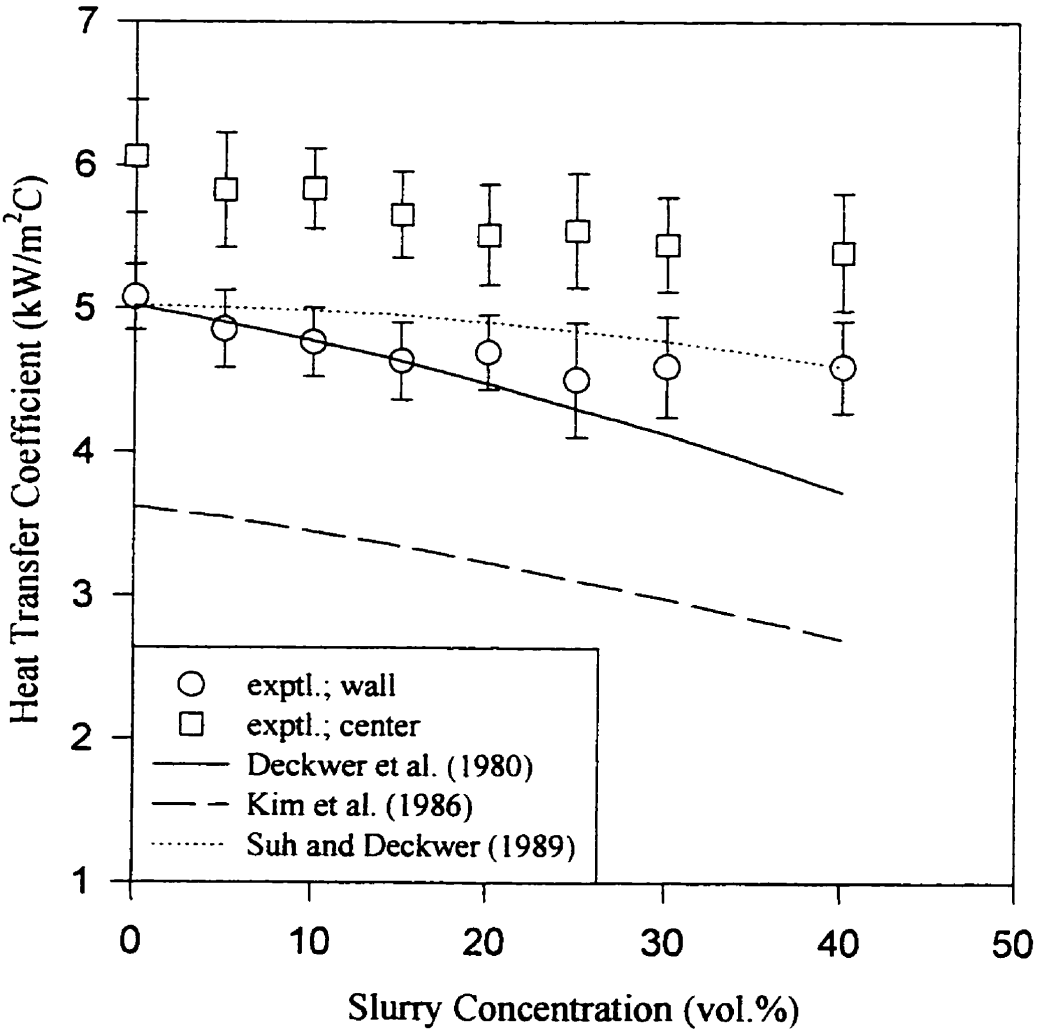

Figure 4.2.5b Comparison of measured heat transfer coefficients with literature correlations at Vg = 0.10 m/s (z=1.28 m) (Data based on Appendix E2 and E6)

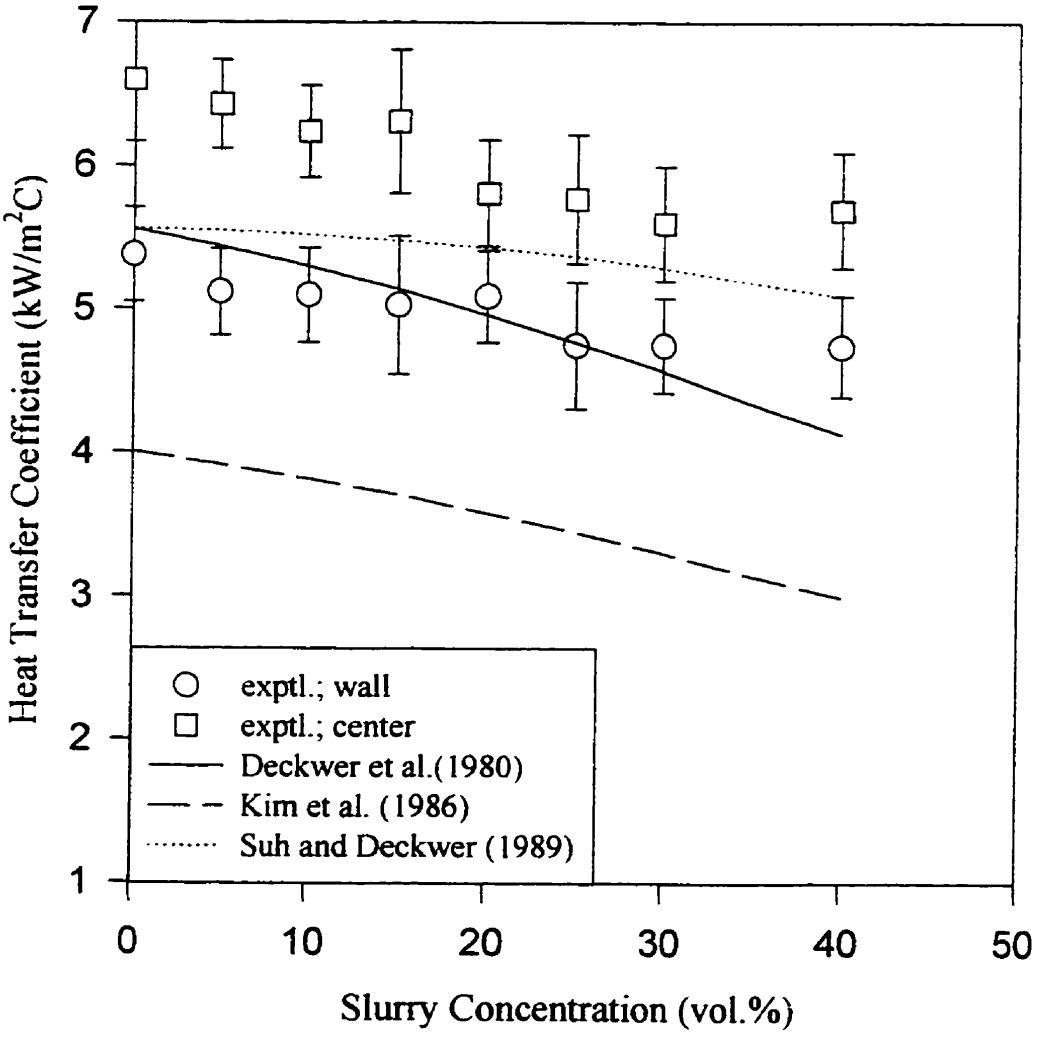

Figure 4.2.5c Comparison of measured heat transfer coefficients with literature correlations at Vg = 0.15 m/s (z=1.28 m)
(Data based on Appendix E2 and E6)

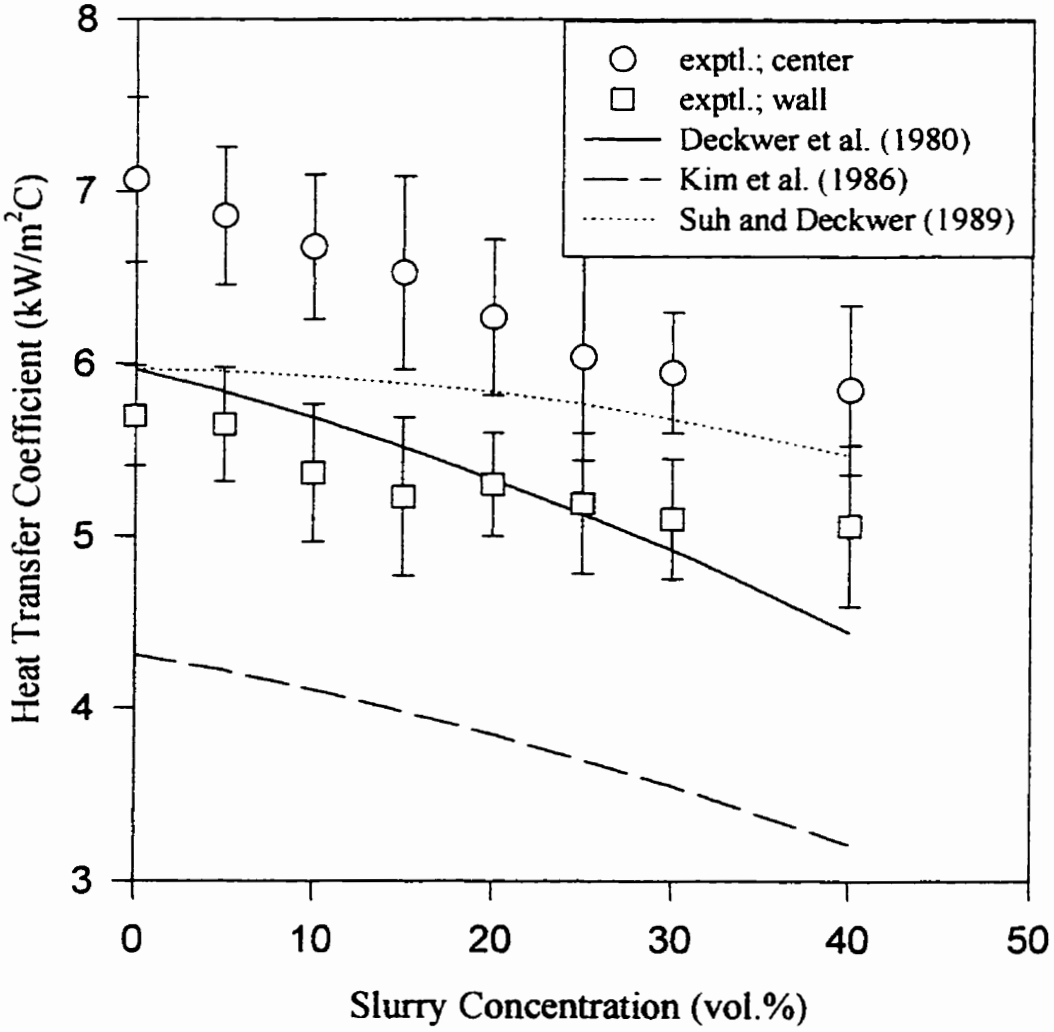

Figure 4.2.5d Comparison of measured heat transfer coefficient with literature correlations at Vg = 0.20 m/s (z=1.28 m) (Data based on Appendix E2 and E6)

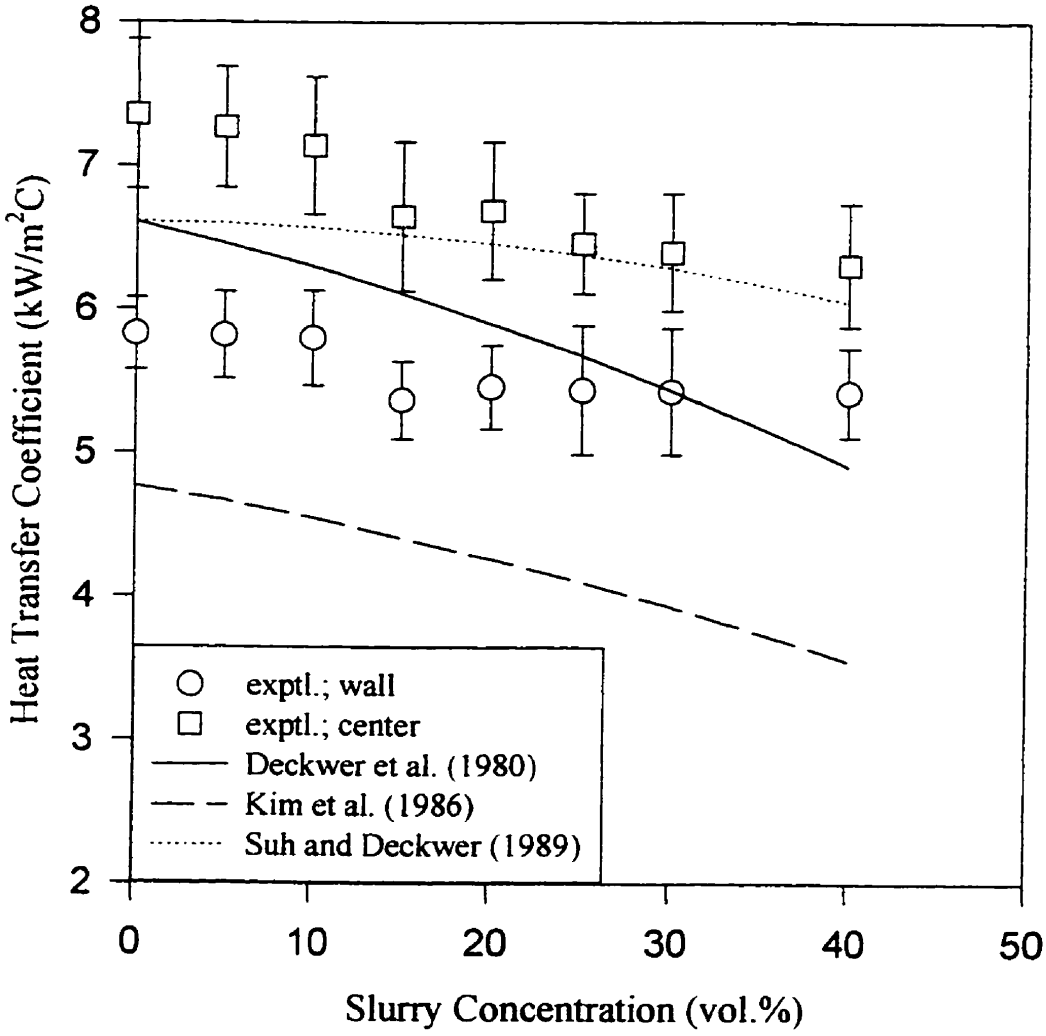

Figure 4.2.5e Comparison of measured heat transfer coefficient with literature correlations at Vg = 0.30 m/s (z=1.28 m) (Data based on Appendix E2 and E6)

by the Kim et al.(1986) correlation underestimate the measured heat transfer coefficients at all gas velocities and slurry concentrations

Figure 4.2.6 compares the predictions by Deckwer et al. (1980) correlation with all the experimental data in the wall region. It can be seen that while most points are within ± 10% of predicted values, a few points are not well predicted. The outliers belong to slurry concentrations above 30 vol.% and gas velocities above 0.2 m/s. Figure 4.2.7 shows that predicted values are within 10% of measured values when data points for high slurry concentrations (> 30 vol.%) and high gas velocities are removed. It is observed from Figure 4.2.5a to 4.2.5e that there is no significant change in measured heat transfer coefficients as slurry concentration is increased from 30 to 40 vol.% for all gas velocities. Therefore for a given gas velocity, the predicted values at the slurry concentration of 30 vol.% should provide an adequate estimate of heat transfer coefficients at 40 vol.%. Moreover, increase in measured heat transfer coefficients are relatively small as the gas velocity is increased from 0.2 to 0.3 m/s.

As observed from Figures 4.2.5a to 4.2.5e, the measured heat transfer coefficients in the central region are significantly higher than the predictions by Deckwer et al. (1980) correlation. Figure 4.2.8 compares the predicted values with the measured values in the central region. It can be seen that the measured values are higher by about 20% and the percent difference is within a narrow range (15 to 20%). This indicates that the basic assumptions of the semi-theoretical equation do not apply to the heat transfer mechanism in the central region of the column for the conditions of this study. In the derivation of their model, Deckwer et al. (1980) assumed energy dissipation by the micro scale eddies to be locally isotropic based on Kolmogoroff's theory (Hinze,1958). This assumption may be reasonable for the relatively low gas velocities (≤ 0.05 m/s) and fine gas distributor (sintered plates with mean pore diameter 75 μ m) used by Deckwer et al. (1980). These conditions would result in a uniform bubble distribution with relatively small average bubble size and high gas holdups (homogeneous flow regime). From instantaneous heat transfer measurements (Figure 4.2.2), it is observed that fluctuations

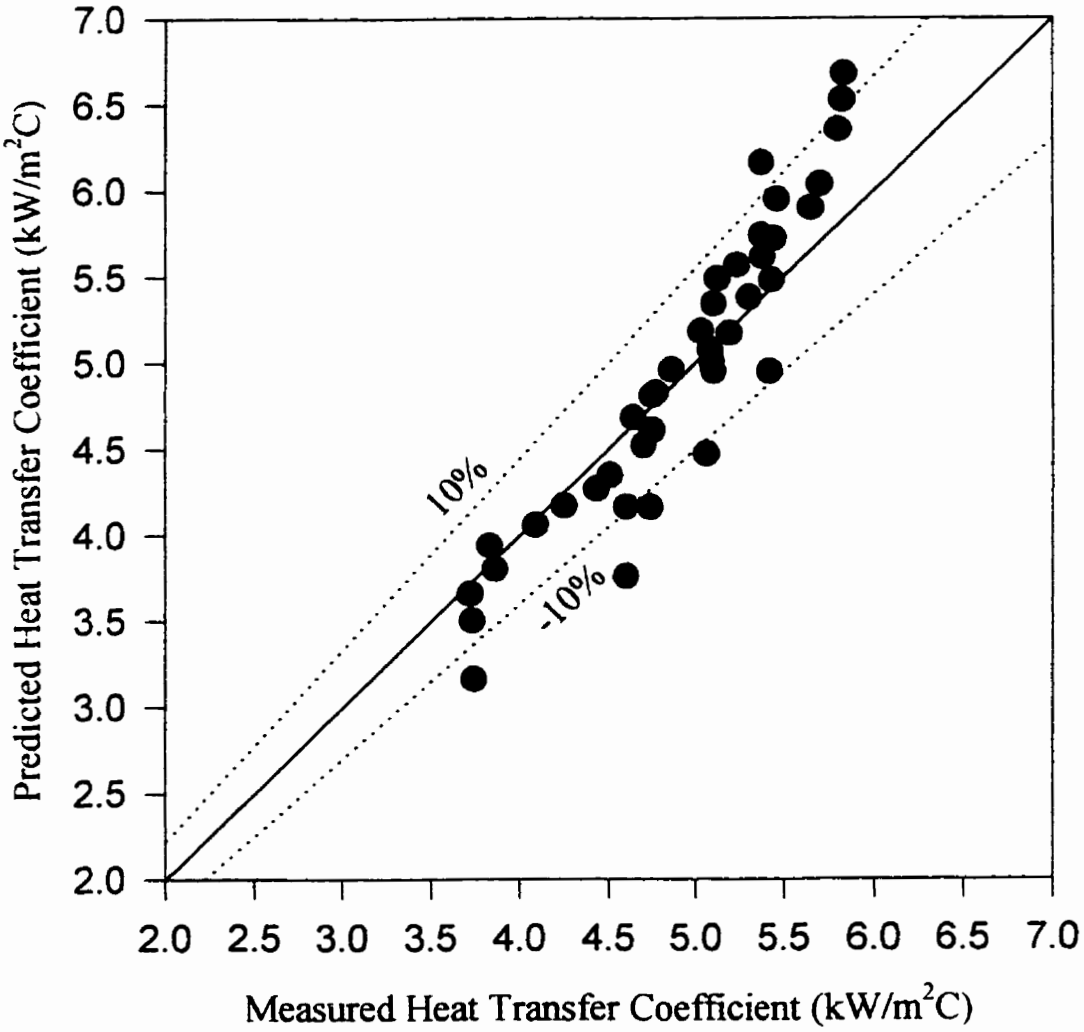

Figure 4.2.6 Comparison of predictions by Deckwer et al. (1980) model with measured heat transfer coefficient in the wall region (all data)
(Data based on Appendix E6)

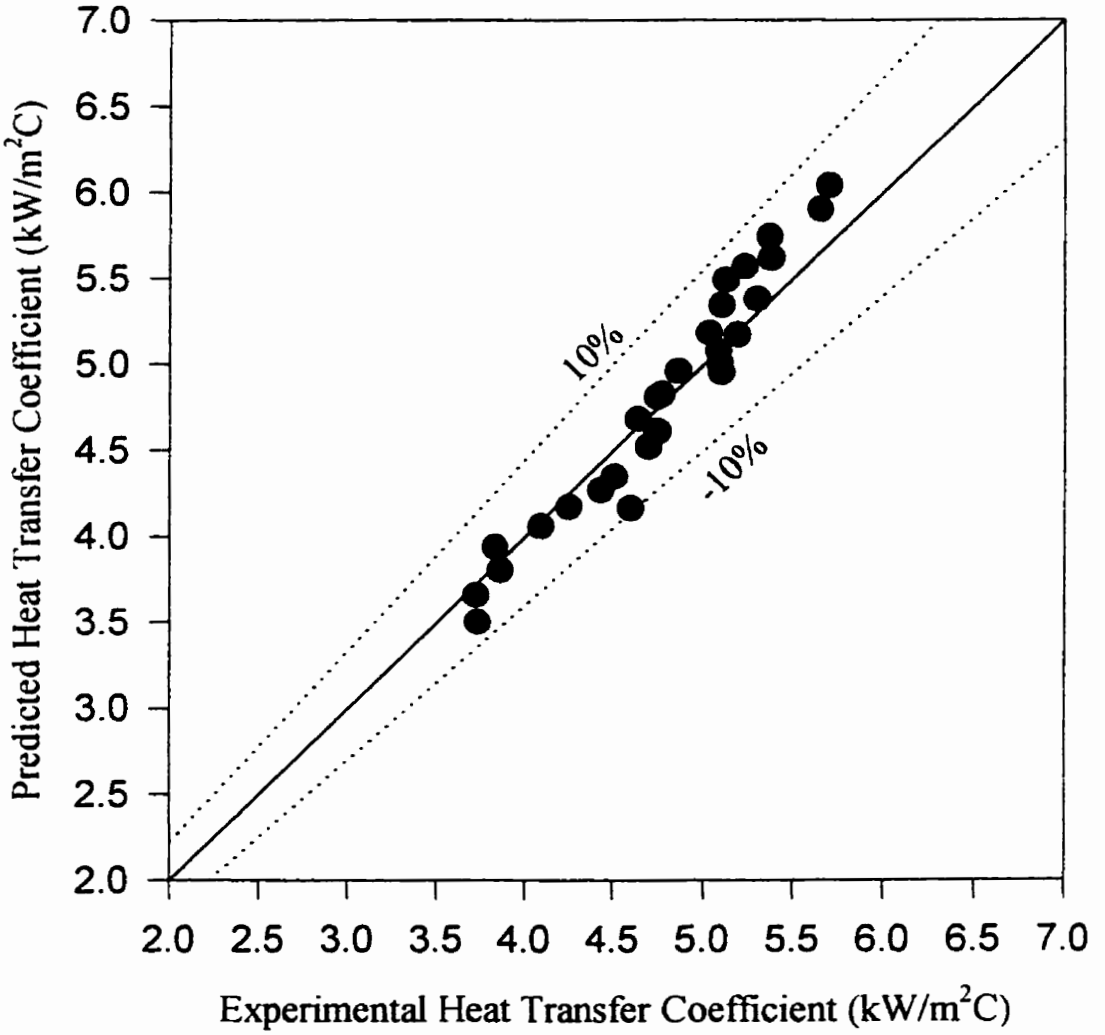

Figure 4.2.7 Comparison of predictions by Deckwer et al. (1980) model with measured heat transfer coefficients in the wall region (slurry conc. < 30 vol.% and Vg < 0.2 m/s)
(Data based on Appendix E6)

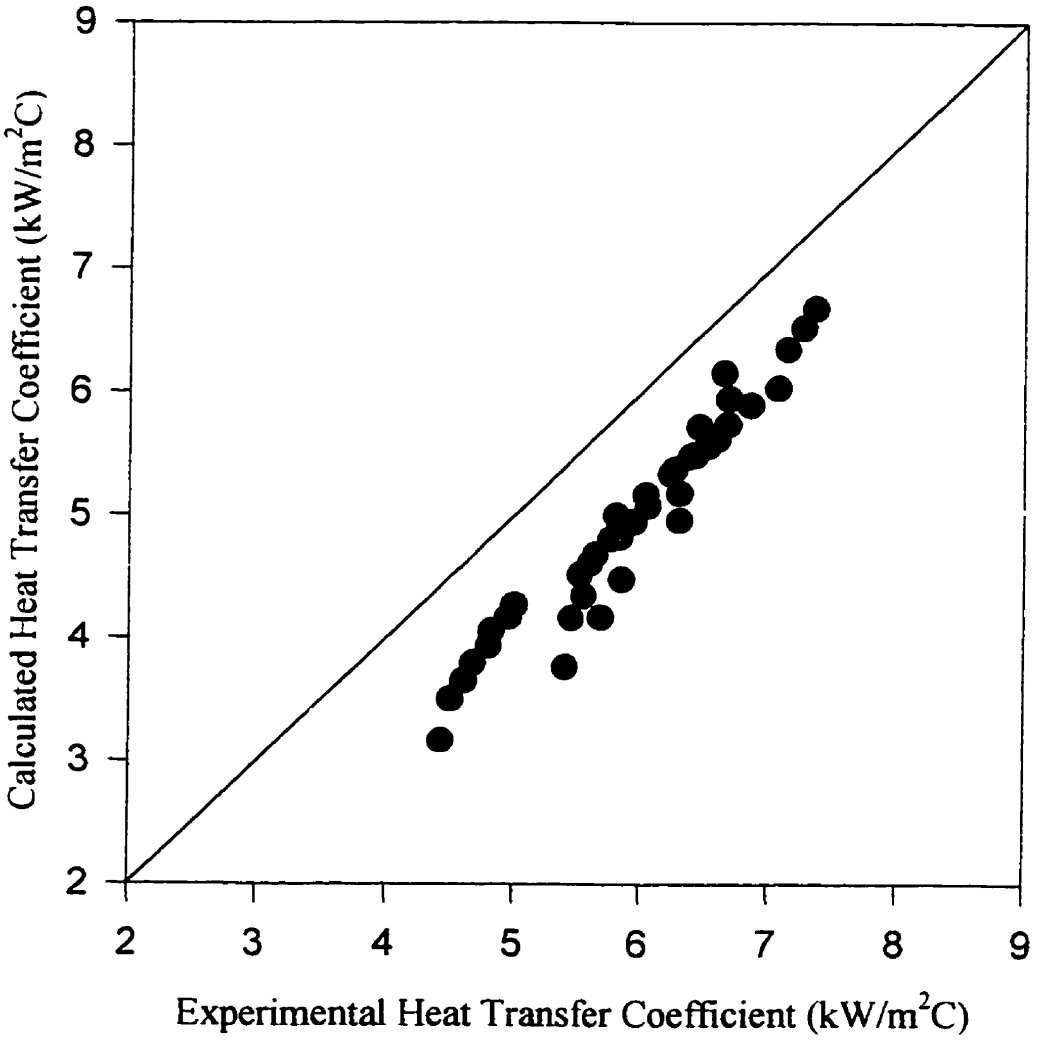

Figure 4.2.8 Predictions by Deckwer et al. (1980) correlation for central region of the column.
(Data based on Appendix E2)

in the wall region are much smaller compared to the central region of the column. The intensity of fluctuations can be related to the average bubble size in the region. The smaller bubbles in the wall region give rise to smaller fluctuations than the larger bubble of central region. There is an enhancement of heat transfer in the central region due to large wakes associated with larger bubbles. This enhancement is not accounted for by the Deckwer et al. (1980) correlation.

Saxena et al. (1992a) also concluded that the correlation of Deckwer et al. (1980) failed to predict the heat transfer coefficients measured in the central region of a slurry bubble column. Saxena et al. (1992a), however, made no measurements in the wall region of their column. Based on the data of their study, Saxena et al. (1992a) modified the Deckwer et al. (1980) correlation to predict heat transfer coefficients in a slurry bubble column:

$$h = 0.0035(k_{sl}\rho_{sl}C_{p,sl})^{0.5}(\rho_{sl}g/\mu_{sl})^{0.47}V_g^{0.25} \qquad (2.5.24)$$

This correlation is based on the experimental results of gas velocities up to 0.15 m/s, temperature between 297 and 343 K, and slurry concentrations up to 5 vol.% in air-water-sand system. Figure 4.2.9 compares experimental results with the above correlation. It can be seen that both experimental and predicted results are close at low slurry concentration and gas velocity up to 0.20 m/s. However, the correlation underestimates heat transfer coefficients at the higher slurry concentrations of this study.

It is observed from Figure 4.2.8 that the differences between heat transfer coefficients in the wall and central regions are relatively constant. Therefore reasonable estimates of heat transfer coefficients in the central region could be obtained from the values in the wall region by multiplying them with a suitable enhancement factor. Therefore, for the central region, the correlation of Deckwer et al. (1980) was modified as:

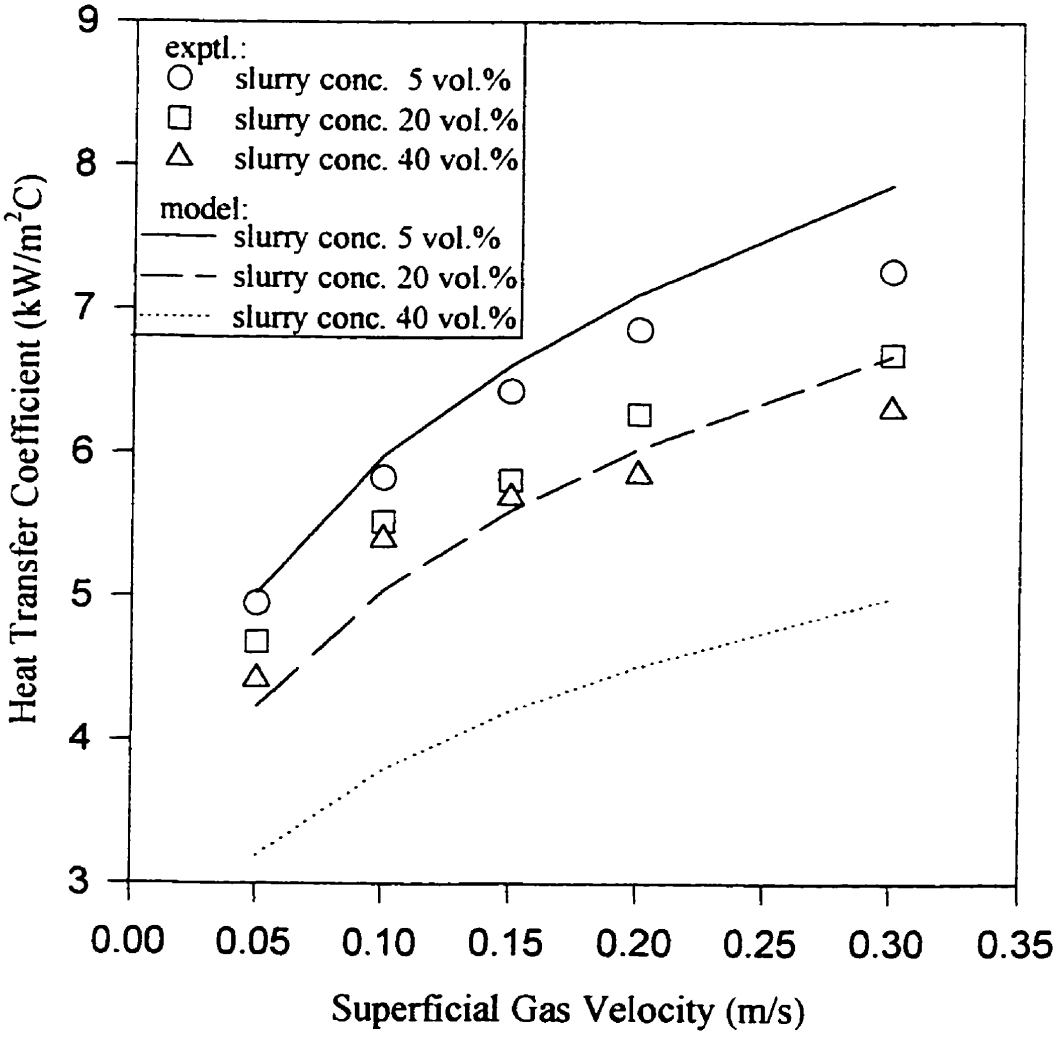

Figure 4.2.9 Comparison of measured heat transfer coefficients with model of Saxena et al. (1992a)
(Data based on Appendix E2)

$$h_o = 0.1217\left[k_{sl}\rho_{sl}C_{p,sl}\left(\frac{P_v}{\mu_{sl}}\right)^{0.5}\right]^{0.5} \qquad (4.2.8)$$

Figure 4.2.10 presents a parity plot of the experimental and predicted values in the central region. It can be seen that the predicted values are within 10% of experimental values. It can be seen from Equation 4.2.8. that the coefficient in the central region is about 22% higher than the original Deckwer et al. (1980) correlation. The Deckwer et al. (1980) correlation is based on the assumption of isotropic turbulence in which micro-eddies contribute to surface renewal. In the central region, however, the bubble wake behind larger bubbles also contributes to surface renewal. The contribution due to bubble wake can be defined as a bubble wake enhancement factor (E_{wk}). Equation 4.2.8 can be written as:

$$h_o = 0.1(1.+E_{wk})\left[k_{sl}\rho_{sl}C_{p,sl}\left(\frac{P_v}{\mu_{sl}}\right)^{0.5}\right]^{0.5} \qquad (4.2.9)$$

where E_{wk} is the bubble wake enhancement factor with a value of 0.217.

4.2.1.1 Modeling Heat Transfer Based on Consecutive Film and Surface-Renewal Theory

The heat transfer mechanism in the slurry bubble column was further analyzed based on consecutive film and surface-renewal theory originally proposed by Wasan and Ahluwalia(1969) for gas-solid and liquid-solid systems. This theory was applied by Kumar and Fan (1994) and Luo et al. (1997) to examine the heat transfer behavior in three-phase fluidized beds using a flat surface probe. This model assumes that a thin liquid film of thickness δ exists surrounding the heating surface, through which the heat transfer takes place by conduction. The outer surface of the film is continuously renewed with fluid elements induced by the bubble wake. During the contact, the heat is

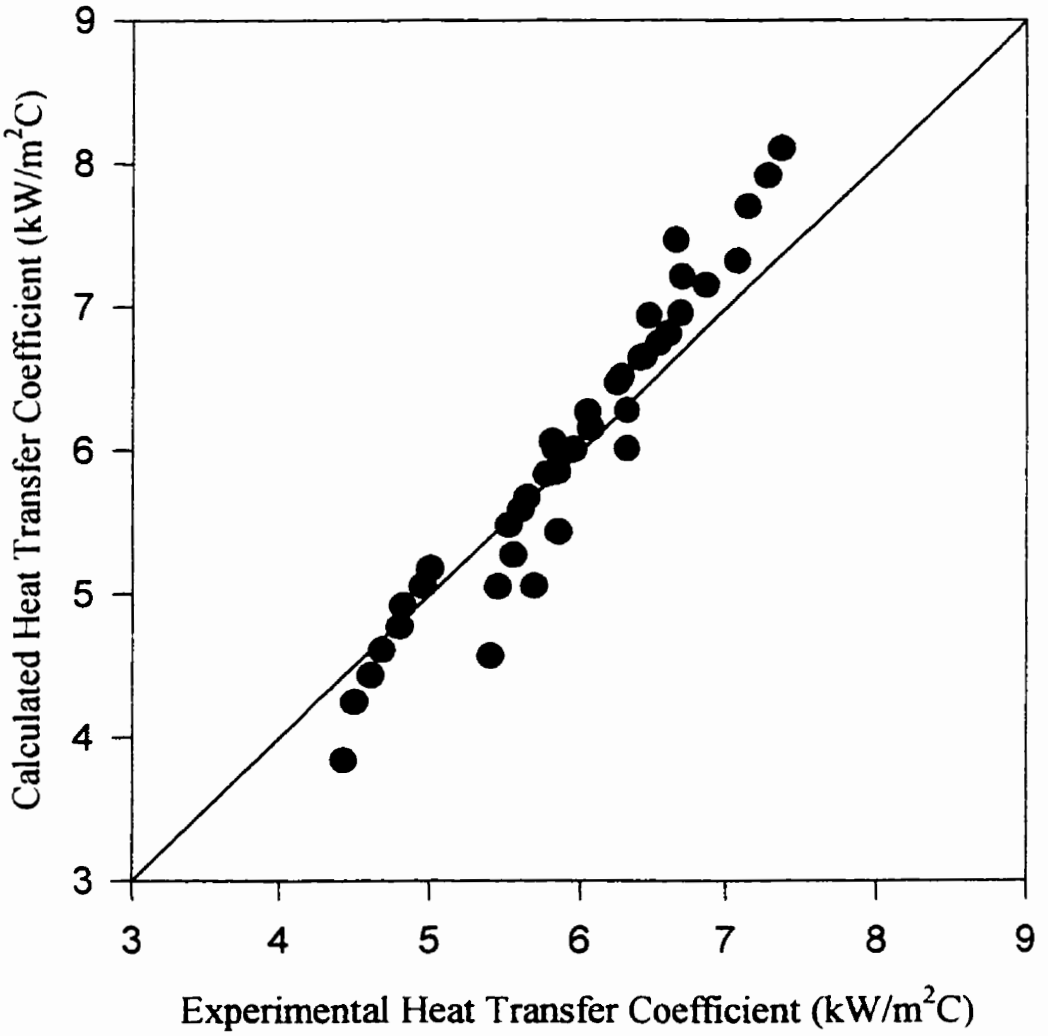

Figure 4.2.10 Prediction of heat transfer coefficients in the central region by modified Deckwer et al. (1980) correlation (Data based on Appendix E2)

transferred by the elements through unsteady-state conduction. The temperature of the fluid element sweeping the outer surface of the film is assumed to be uniform and equal to the bulk temperature. Thus the heat transfer phenomenon is a sequential process of diffusion followed by convection. The time average heat transfer coefficient from the heating surface to the bed can be expressed by physical properties of the liquid, the film thickness (δ) and the contact time between the liquid elements and the film (θ_c) as:

$$h = \frac{2k_l}{\sqrt{\pi\alpha\theta_c}} + \frac{k_l\delta}{\alpha\theta_c}\left\{\left[1-\mathrm{erf}\left(\frac{\sqrt{\alpha\theta_c}}{\delta}\right)\right]\exp\left(\frac{\alpha\theta_c}{\delta^2}\right)-1\right\} \qquad (4.2.10)$$

the term $(\sqrt{\alpha\theta_c}/\delta)$ accounts for the contribution of film resistance to heat transfer (Luo, 1997).

The contact time θ_c can be estimated by applying Kolmogoroff's concept of isotropic turbulence for evaluating the contact time of turbulent eddies at the heat exchange surface (Deckwer, 1980):

$$\theta_c = \left(\frac{\nu_{sl}}{P_v}\right)^{1/2} = \left\{\frac{\mu_{sl}}{V_g\rho_{sl}g}\right\}^{1/2} \qquad (4.2.11)$$

The thickness of laminar viscous sublayer is depends on the geography of the surface of heat transfer source. For the cylindrical probe used in this study, the thickness of laminar viscous sublayer at different angular locations with respect to the point of incidence can be expressed as (Schlichting, 1960):

$$\delta_o = \frac{A_p R_p}{Re_c^{1/2}} \qquad (4.2.12)$$

here, R_p is the radius of the cylindrical probe, parameter A_p depends on angular location on probe (Schlichting, 1960) and Re_c is Reynolds number based on probe radius. The bulk fluid is velocity assumed to be average bubble rise velocity (Luo, 1997), expressed as:

$$U_{b,avg} = \frac{V_g}{\varepsilon_g} \tag{4.2.13}$$

This approximation is reasonable in view of the assumption of isotropic process in which micro-eddies contributes to surface renewal at the heat transfer surface. The thickness of laminar sublayer is normally defined as the distance from solid surface while velocity inside laminar layer is larger than 0.99 of bulk velocity, u_∞. The heat flux sensor was located at an angle of 90° in front of liquid flow. The parameter A_p in equation (4.2.12) is found to be 2.5 (Schlichting, 1960).

The film thickness of thermal conduction δ is equivalent to the thickness of the diffusion sublayer and is related to the laminar viscous sublayer, δ_o as:

$$\delta = \frac{\delta_o}{Pr^{1/3}} \tag{4.2.14}$$

Thus, the film thickness can be calculated by combing equations 4.2.12 and 4.2.14, expressed as:

$$\delta = \frac{2.5R_p}{Re_p^{1/2}} Pr^{-1/3} \tag{4.2.15}$$

As before, apparent slurry viscosity was computed by expression of Vand (1948). Figure 4.2.11 shows that experimental values in the wall region are well predicted by the above procedure. This procedure had to be modified for the central region, since the

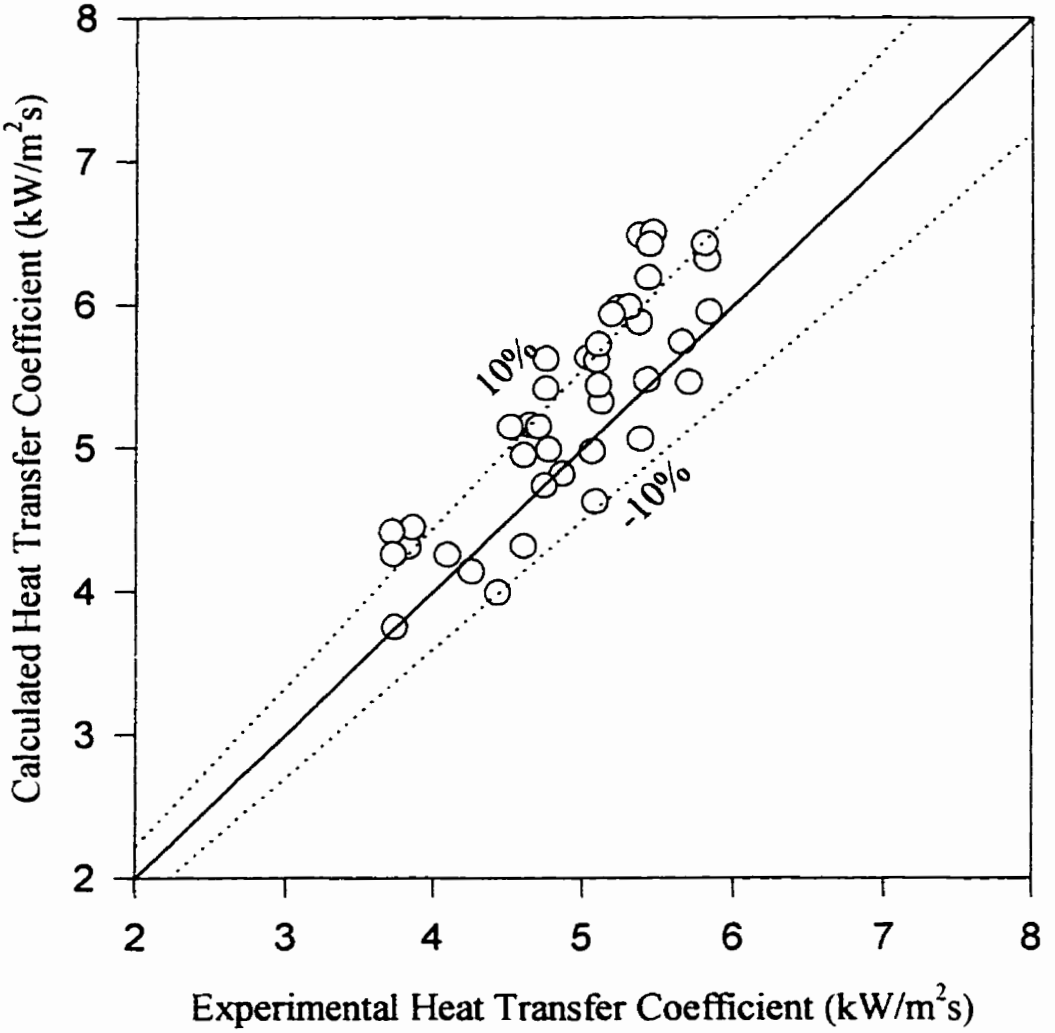

Figure 4.2.11 Comparison of predicted heat transfer coefficients with experimental results in the wall region (Data based on Appendix E6)

experimental values in the central region are about 20% higher than the wall region. The bubble rise velocity calculated by Equation 4.2.13 is an average bubble rise velocity. In the central region, however, bubble rise velocity is higher than the average bubble rise velocity. The relationship between bubble rise velocity in the center and average one can be expressed as:

$$U_{b,o} = c_b U_{b,avg} \qquad (4.2.16)$$

here $c_b > 1$. Table 4.2.1 gives average absolute relative deviation, and minimum and maximum relative deviations, calculated based on variation of c_b from 1 to 1.4

Table 4.2.1 Error analysis based on predictions of central region heat transfer coefficients for different ratios of mean to central region bubble rise velocities

$U_{b,o} / U_{b,avg}$	1.0	1.1	1.2	1.217	1.3	1.4
Avg. Relative Dev. (%)	10.8	7.64	6.50	6.39	6.39	10.05
Min. Relative Dev. (%)	0.58	0.034	0.53	0.10	0.44	0.23
Max. Relative Dev. (%)	23.62	20.12	16.90	16.31	13.71	20.50

It can be seen that minimum average relative deviation is obtained for a value of c_b of 1.3. Further examination showed that average relative errors are same for c_b values of 1.217 and 1.3; however maximum relative error is slightly higher at c_b value of 1.217. It was found earlier that heat transfer coefficients at the center are generally higher by this factor than the values at wall. Figure 4.2.12 compares the experimental heat transfer coefficients at the center with predicted values for $c_b = 1.217$. It can be seen that most of the data lies within ±10% error lines. The outliers belong to air-water system at gas

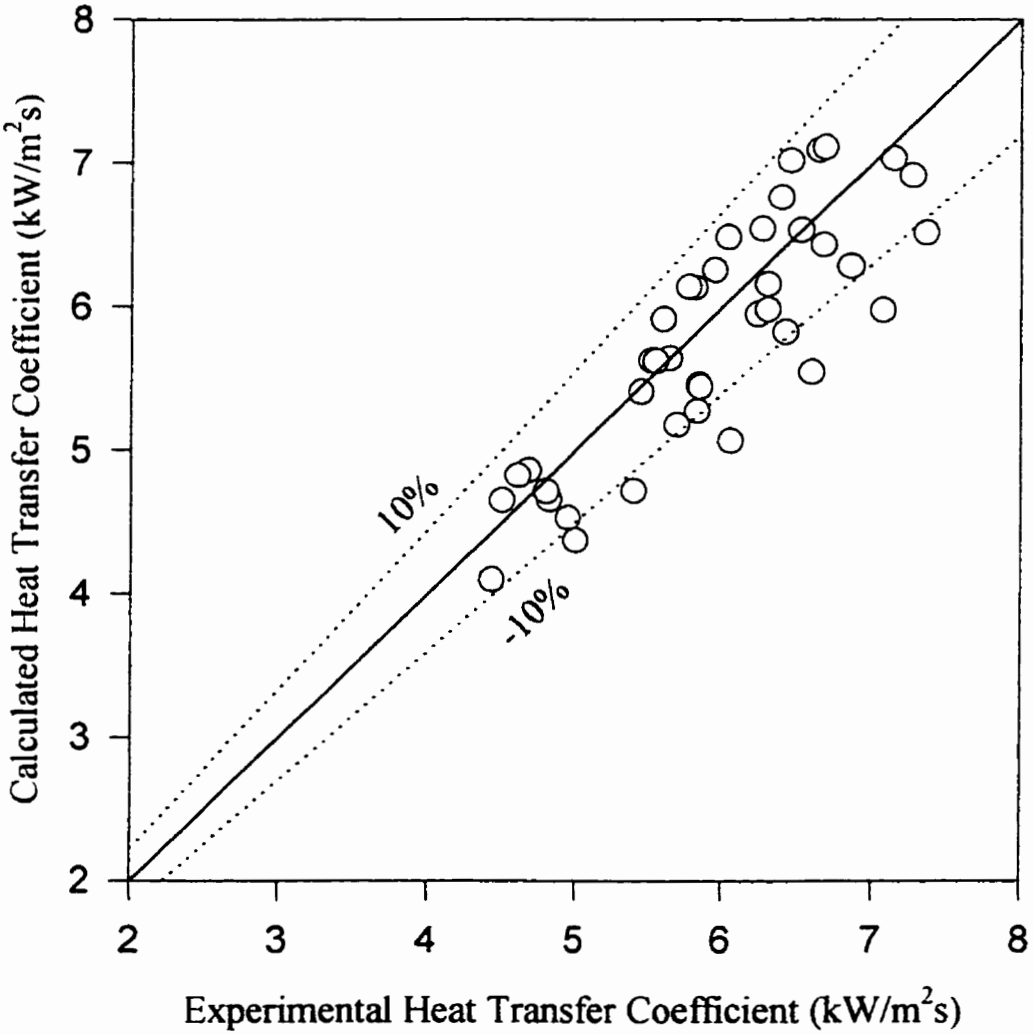

Figure 4.2.12 Comparison of predicted heat transfer coefficients with experimental results in central region ($U_{b,o}$=1.217$U_{b,ave}$)
(Data based on Appendix E2)

velocities ≥ 0.1 m/s. It is observed in the following section that radial profiles of heat transfer coefficients are steeper for air-water system compared to slurry systems.

4.2.1.2 Radial Profiles of Heat Transfer Coefficients

Radial profiles of heat transfer coefficients were obtained to further investigate heat transfer variations in the radial direction. Figures 4.2.13a to 4.2.13c present radial profiles of heat transfer coefficients in the bulk region of the column for gas velocities of 0.05, 0.15 and 0.3 m/s. It can be seen, from these figures, that as slurry concentration increases, radial profile generally becomes flatter in the central region. This can be attributed to formation of larger bubbles with increasing slurry concentrations (sec. 4.1.3). Larger bubbles rise in the central region of the column (Chen et al., 1994). Thus cross sectional area of the column occupied by larger bubbles will be expanded as slurry concentration increases resulting in flatter profiles. In the region near the wall, the slope of the radial profile of heat transfer coefficient generally became sharper as slurry concentration increased indicating a reduction in the wall region with increasing slurry concentration. This can again be attributed to expanded central region with increasing slurry concentration.

To quantitatively describe the radial profile of the heat transfer coefficient at various slurry concentrations, normalized heat transfer coefficients, defined below, were plotted as a function of dimensionless radius (r/R).

$$\Theta_h = \frac{h - h_w}{h_o - h_w} \qquad (4.2.17)$$

here, h_o and h_w are heat transfer coefficients in the center and near the wall.

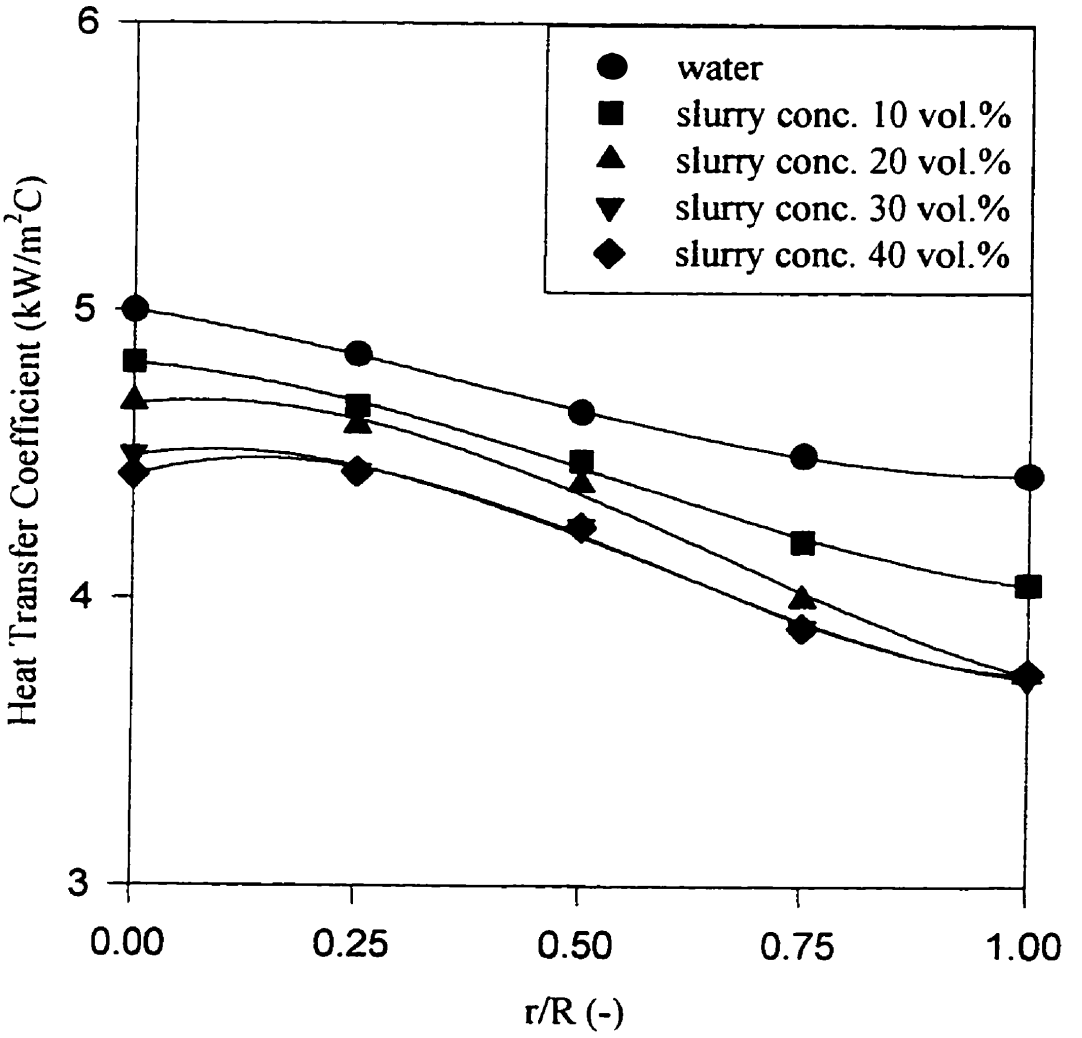

Figure 4.2.13a Radial profile of heat transfer coefficient at superficial gas velocity of 0.05 m/s (Data based on Appendix E2~E6)

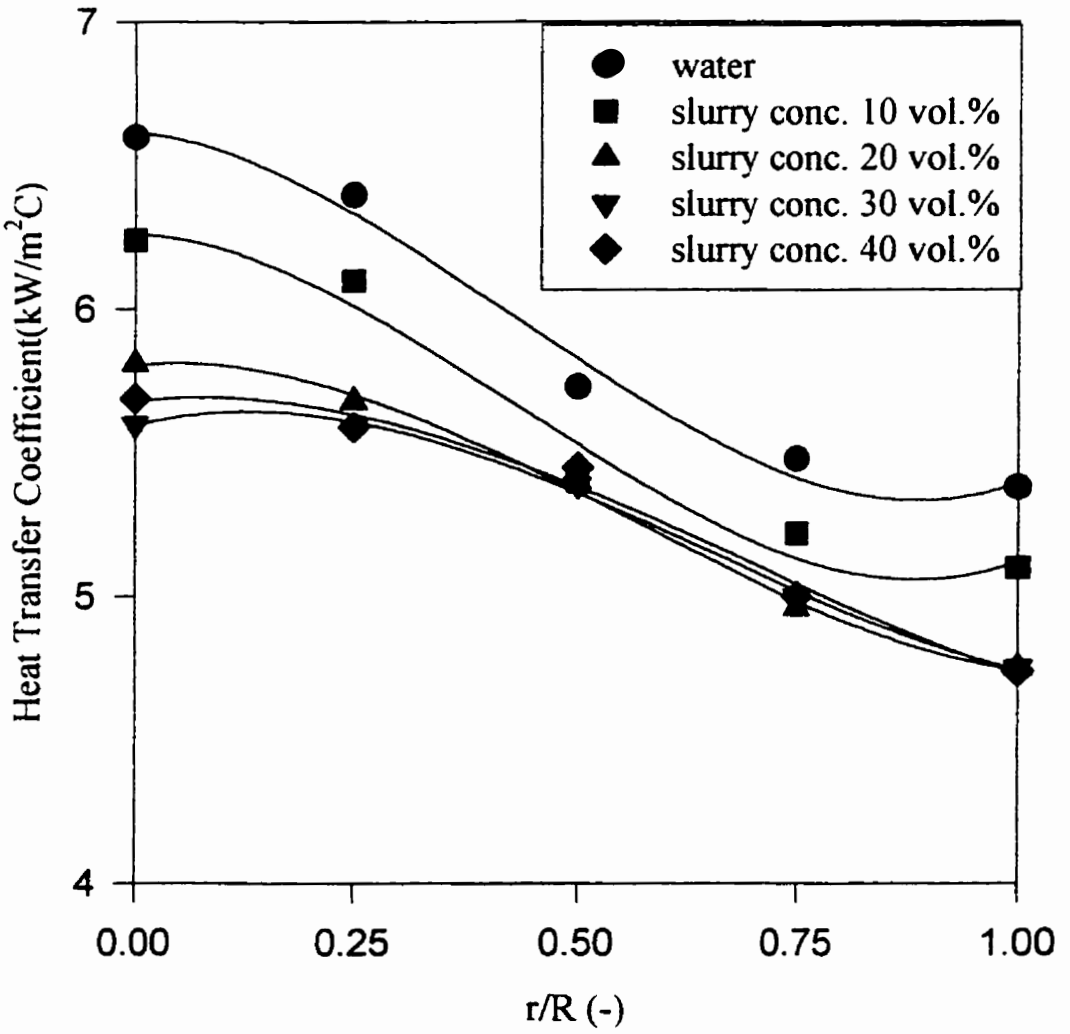

Figure 4.2.13b Radial profile of heat transfer coefficient
at superficial gas velocity of 0.15 m/s
(Data based on Appendix E2~E6)

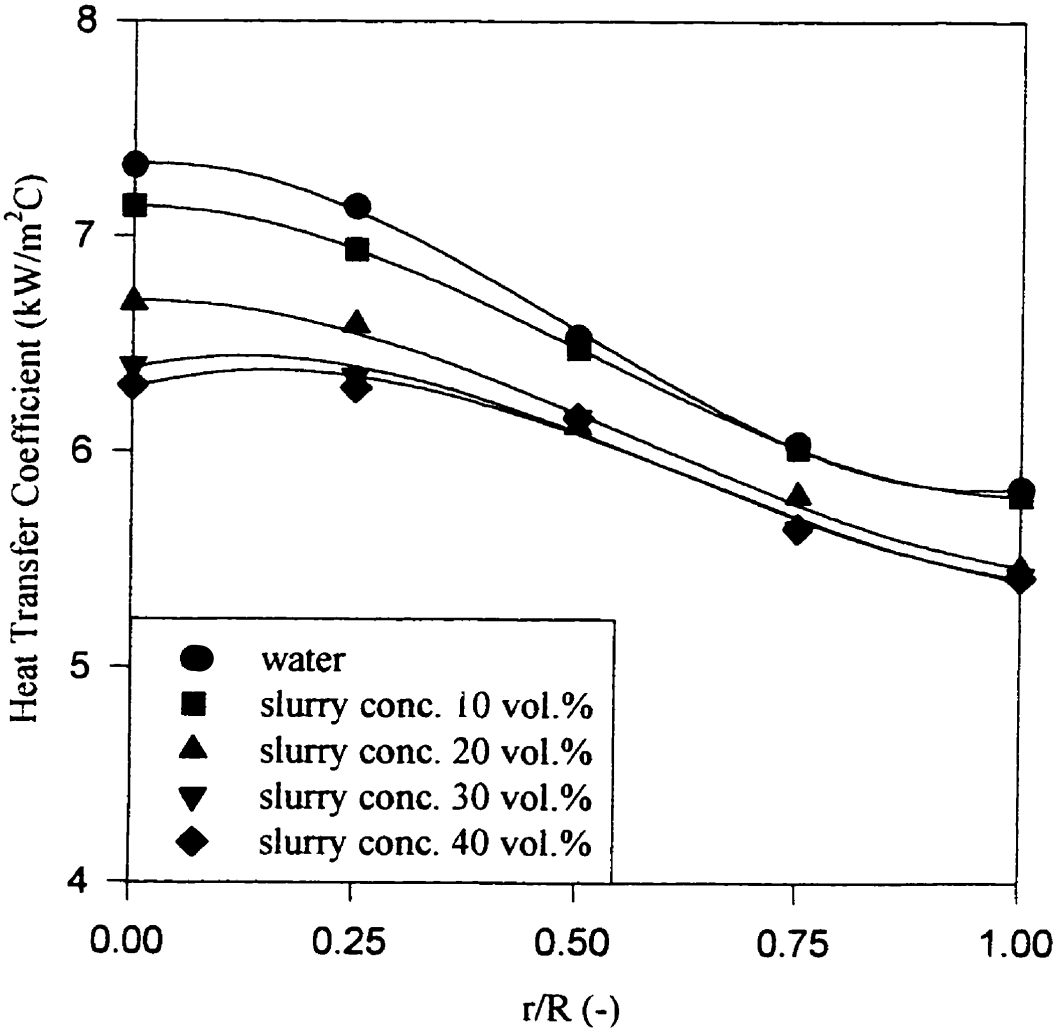

Figure 4.2.13c Rradial profile of heat transfer coefficient at superficial gas velocity of 0.30 m/s (Data based on Appendix E2~E6)

It can be seen from Figures 4.2.14a to c that the s-shaped profiles can be roughly divided into two main parts around the half way point between center and wall. Based on this feature, two curves can be fitted to describe the radial profile of the heat transfer coefficient in the two regions. The two curves are defined as follows:

Region of r/R = 0~0.5:

$$\Theta_h = 1.0 - c_1\left(\frac{r}{R}\right)^{c_2} \qquad (4.2.18a)$$

Region of r/R = 0.5~1:

$$\Theta_h = c_3\left(1 - \frac{r}{R}\right)^{c_4} \qquad (4.2.18b)$$

Figure 4.2.14a to c show the experimental results and fitting results based on above equations. At r/R=0.5, calculated values from Equations (4.2.18a) and (4.2.18b) will result in a small difference. The average of two values was used for estimating normalized heat transfer coefficients at r/R=0.5.

Figure 4.2.15 shows the radial profile of normalized heat transfer coefficient based on calculated results from both Equations(4.2.18a) and (4.2.18b). The parameters c_1-c_4 used in the equations are listed in Table 4.2.2. It is seen from Table 4.2.2 that parameter c_2 increases as slurry concentration increases, which indicates more uniform radial profile of normalized heat transfer coefficient in the central region. It also indicates that the central region becomes larger as slurry concentration increases. It is also seen from Table 4.2.2 that parameter c_4 becomes small as slurry concentration increases, indicating that the wall region become smaller with increasing slurry concentrations.

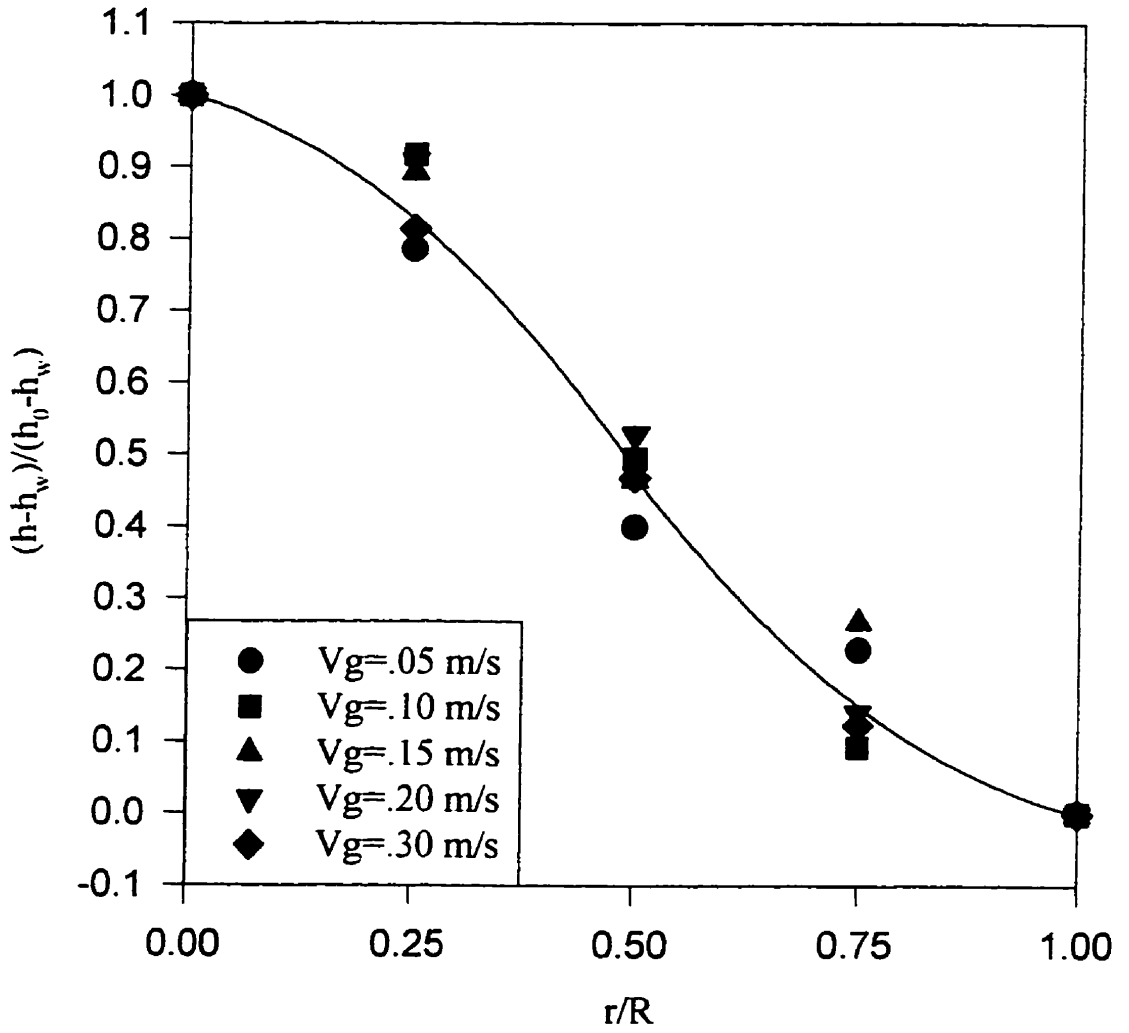

Figure 4.2.14a Radial profile of heat transfer coefficient
in 5 vol.% slurry system
(Data based on Appendix E2~E6)

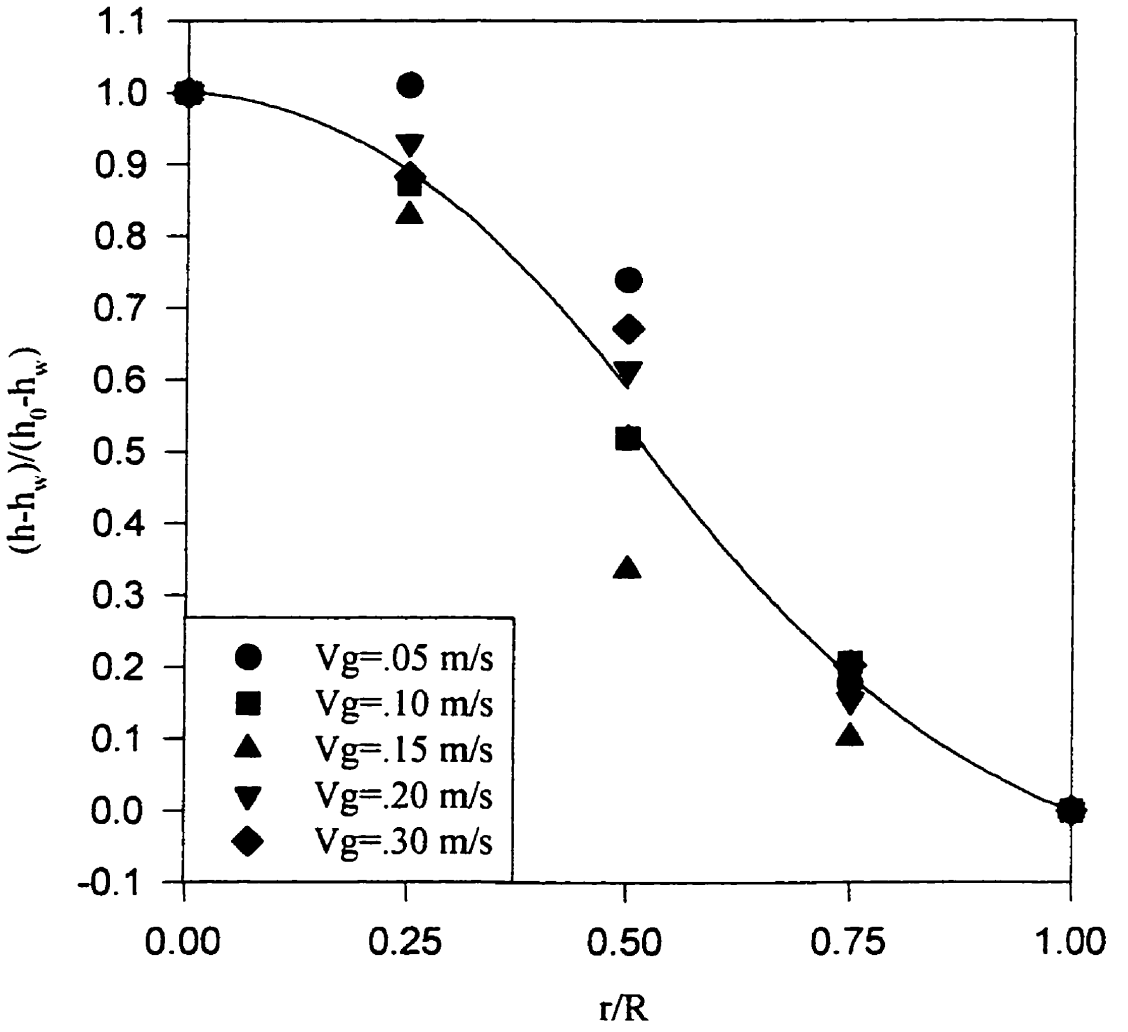

Figure 4.2.14b Radial profile of heat transfer coefficient
in 15 vol.% slurry system
(Data based on Appendix E2~E6)

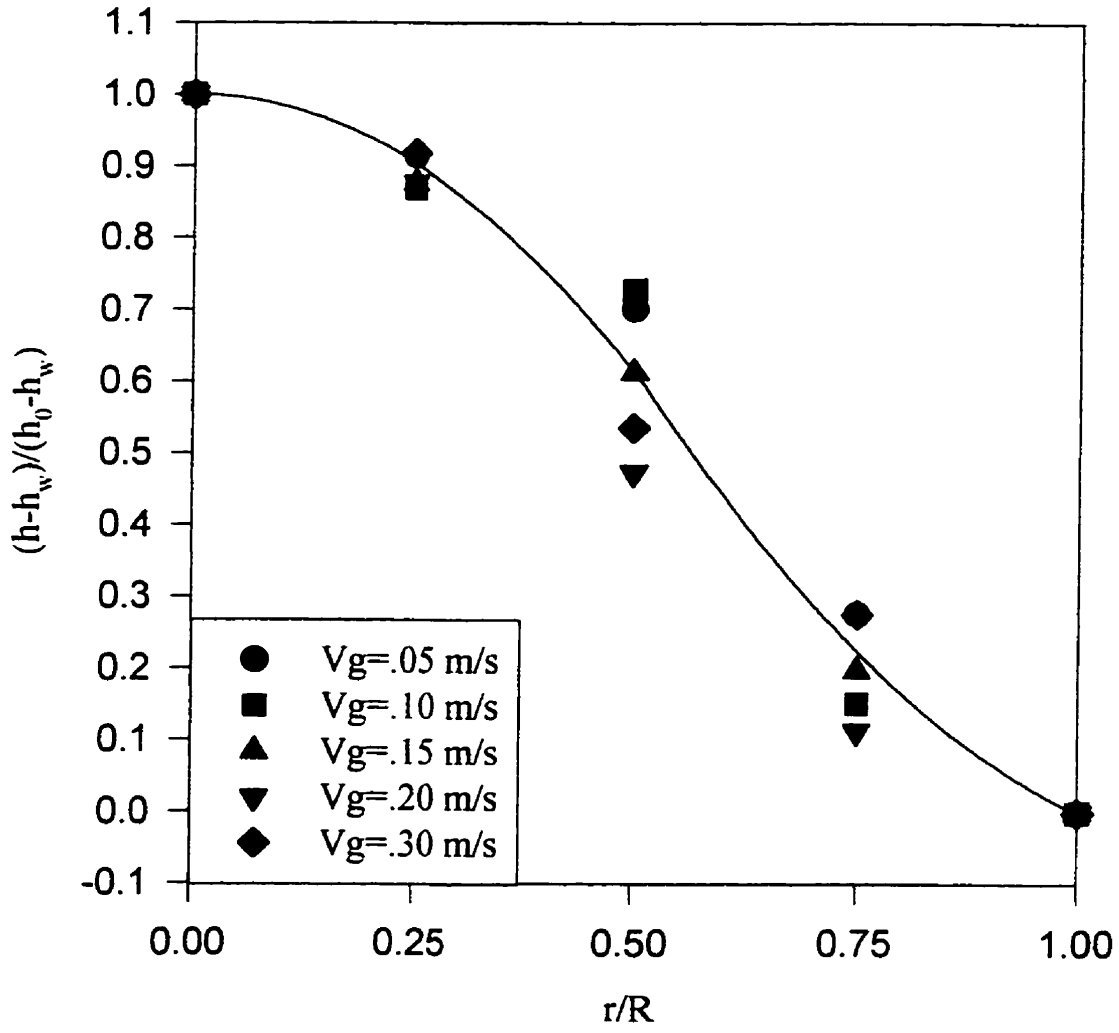

Figure 4.2.14c Radial profile of heat transfer coefficient
in 20 vol.% slurry system
(Data based on Appendix E2~E6)

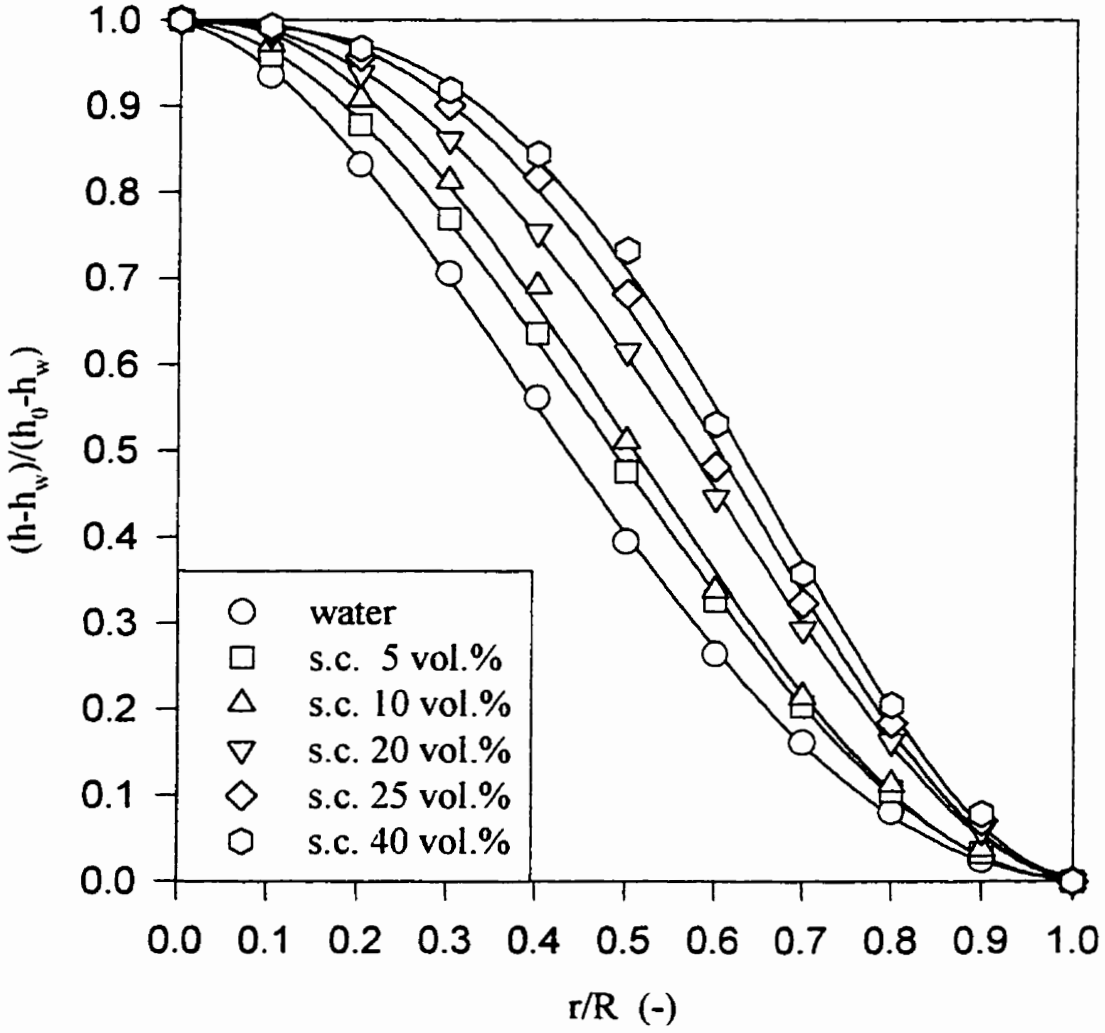

Figure 4.2.15 Effect of slurry concentration on radial profile of heat transfer coefficient
(Data based on Appendix E2~E6)

Table 4.2.2 Values of parameters in equations 4.2.18a and 4.2.18b for different slurry concentrations

	c_1	c_2	c_3	c_4
water	1.5884	1.3850	1.2568	1.7020
5 vol.%	1.5508	1.5829	1.4642	1.6396
10 vol.%	1.5444	1.7557	1.4299	1.5741
15 vol.%	1.5429	1.9080	1.5416	1.5168
20 vol.%	1.5419	2.0013	1.6884	1.4527
25 vol.%	1.2880	2.1349	1.7221	1.3884
30 vol.%	1.2866	2.1982	1.7785	1.3784
40 vol.%	1.2295	2.2583	1.8731	1.3743

Radial distribution of liquid velocity and gas holdups has been investigated in bubble columns (Hill, 1974; Ueyama and Miyauchi, 1979). Results of these studies indicate that the radial profiles of gas holdup and liquid velocity are similar to the heat transfer profiles of this study. The liquid flow was highest at the center. The direction of liquid flow was upward up to r/R of about 0.7. In the region from r/R = 0.7 to r/R = 1, there was a downward flow of liquid (Figure 4.2.16). Between these two regions, the liquid velocity decreased sharply. The absolute liquid velocity in the downward direction was significantly lower than in the upward direction. The observations of heat transfer profiles in the present study are in agreement with the radial profile of liquid velocity in a bubble column. Like the liquid velocities, the heat transfer coefficients are highest at the center and lowest near the wall with a sharp decrease in the transition region between the center and wall.

The heat transfer coefficient at a given radial position can be estimated as follows. The heat transfer coefficient near the wall (h_w) can be estimated by using Deckwer et al. (1980) correlation. The heat transfer coefficient at the center (h_o) can be estimated by

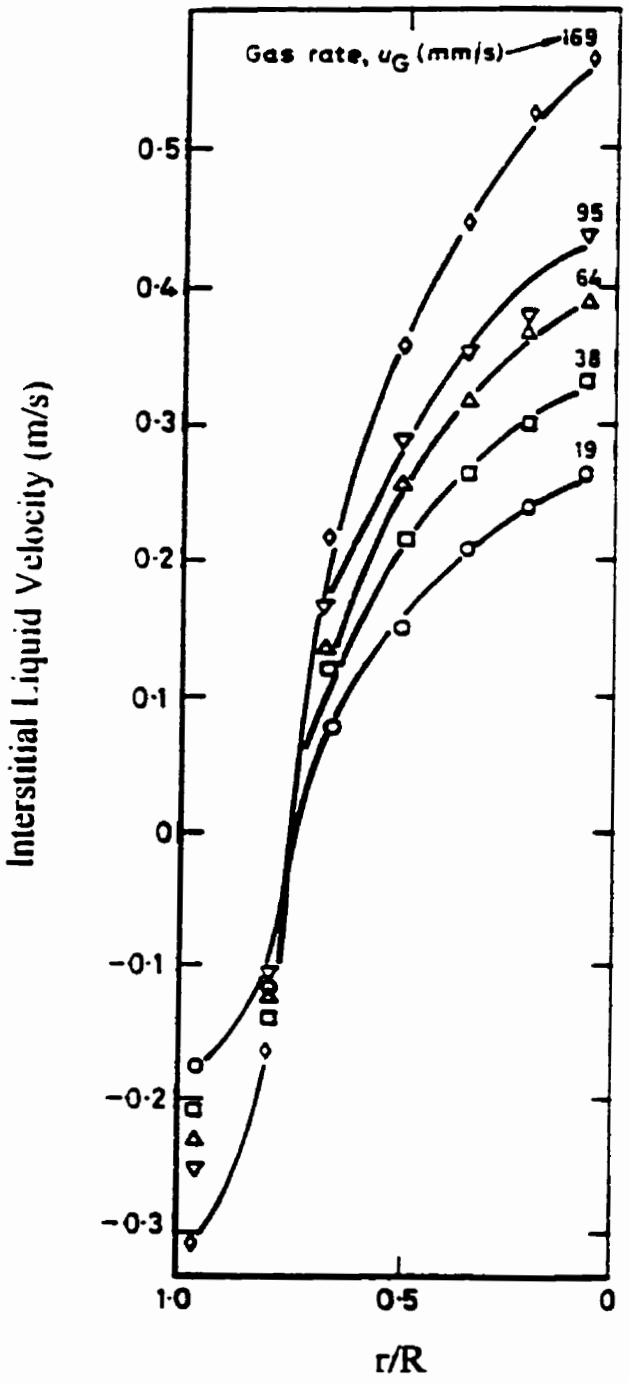

Figure 4.2.16 Radial profiles of liquid velocity in bubble column (Hill, 1974)

using corrected correlation for the central region (Eq. 4.2.8). Then use equation 4.2.18a or 4.2.18b to obtain the heat transfer coefficient at the desired radial location.

4.2.1.3 Heat Transfer Coefficients at Different Axial Locations

Figure 4.2.17 compares the heat transfer coefficients in the bulk and distributor regions at the wall and half way between wall and center. It can be observed that heat transfer coefficients in the bulk region are significantly higher than in the distributor region at both radial locations indicating higher turbulence in the bulk region of column. This is confirmed by the instantaneous heat transfer measurements shown in Figure 4.2.18. The fluctuations in the bulk region are significantly higher than in the distributor region.

It is also observed from Figure 4.2.17 that the heat transfer coefficients in the distributor region near the wall are systematically higher than that in the halfway position. This observation in the distributor region is reverse of that in the bulk region. This phenomenon can be attributed to sparger design and the locations of the heat transfer probe. As shown in Figure 4.2.19, each sparger arm had four orifices and three of these orifices were close to the wall while one was around halfway of the column. The positions of orifices on the sparger arm were based on criteria for uniform distribution of gas per unit cross-sectional area (section 3.2.1). The heat transfer probe was located just below the sparger arm. More gas bubbles were generated from three holes near the wall (thus providing more agitation) than from one hole in the halfway location. It was visually observed that the downward gas jets leaving from three holes near the wall tended to coalesce due to short distances between them. Thus, local slurry mixing near the wall was stronger than that in the halfway region. This resulted in a higher average heat transfer coefficients near the wall. The difference between the average heat transfer coefficients near the wall and in the halfway location is larger at low gas velocity. The gas jet penetration at low gas velocity is expected to be low due to low gas jet momentum. The bubbles leaving the sparger holes were observed to go quickly up and beyond the arm of sparger. These gas bubbles thus provided local agitation in the region

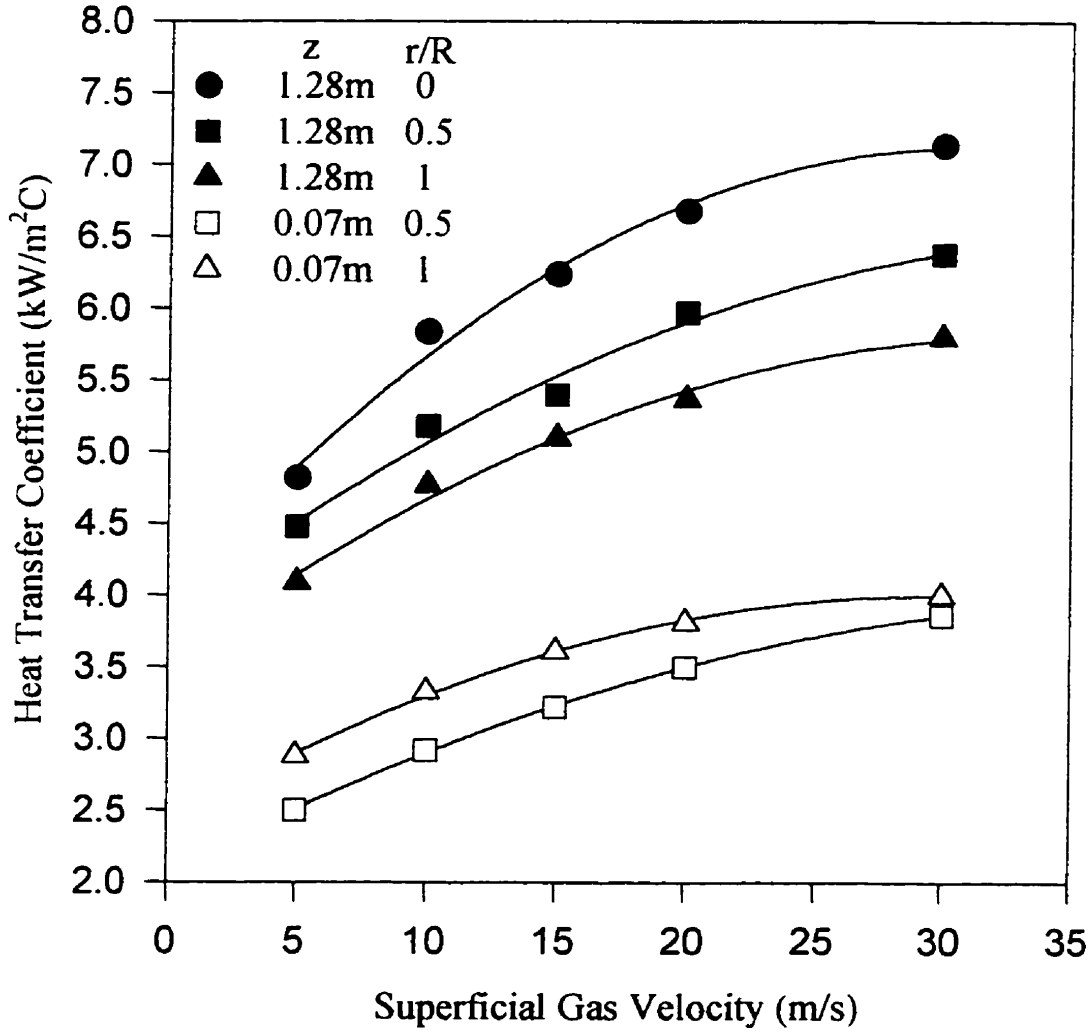

Figure 4.2.17 Variation of heat transfer coefficient with gas velocity at different axial and radial locations
(slurry conc.=10 vol.%)
(Data based on Appendix E9)

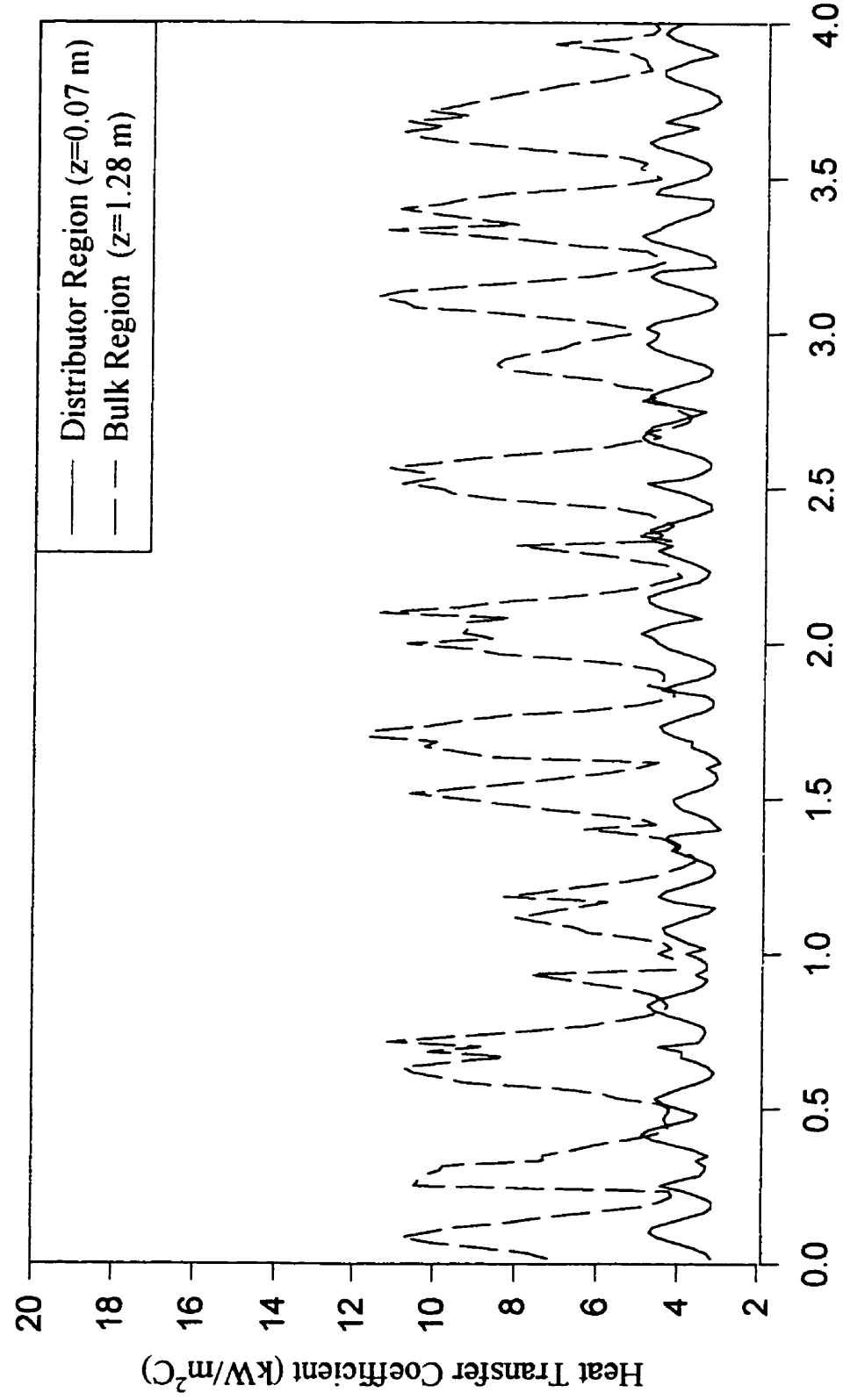

Figure 4.2.18 Instantaneous heat transfer in bulk and distributor regions
(r/R=0.5; V_g = 0.3 m/s; slurry conc. = 10 vol.%)

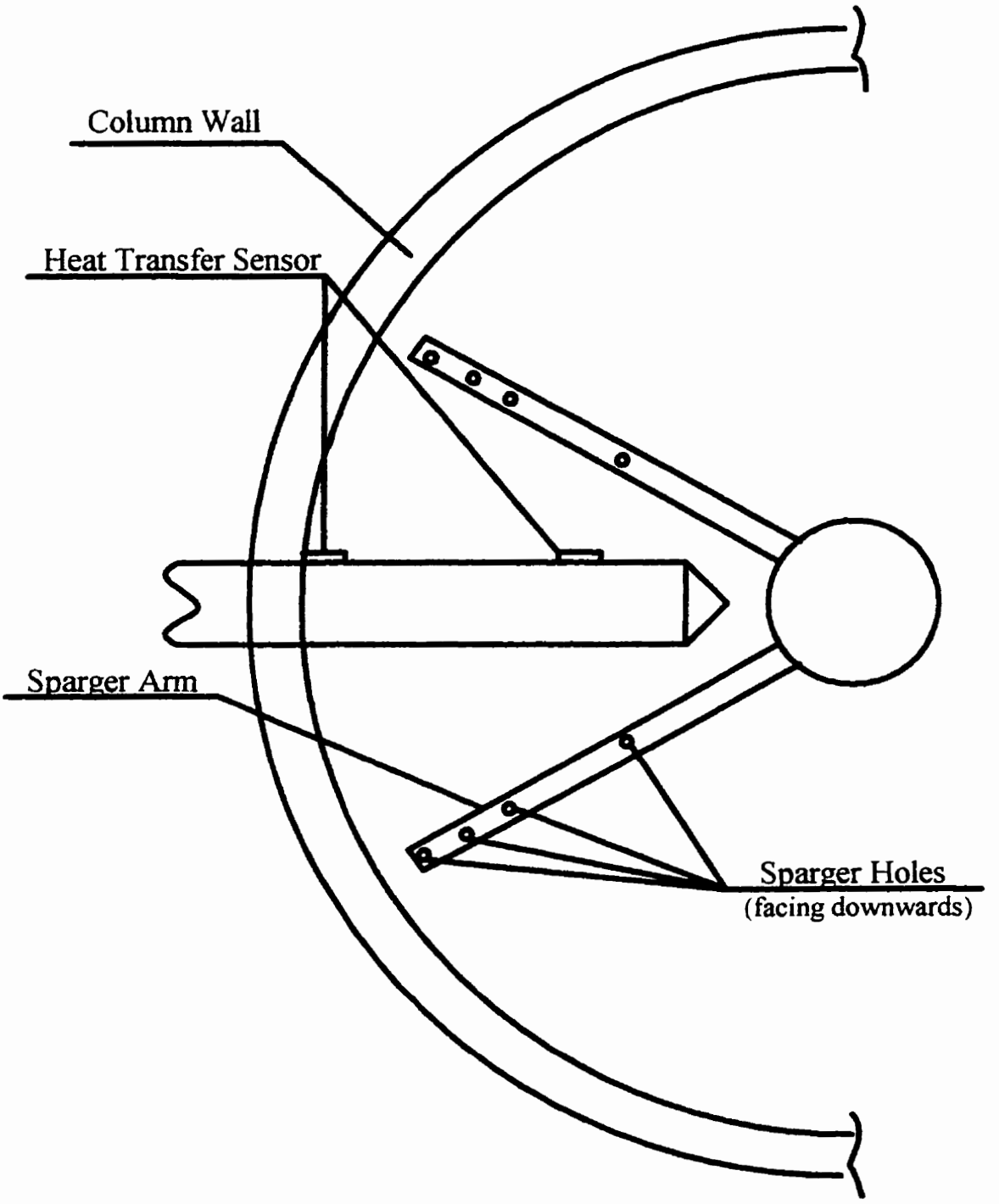

Figure 4.2.19 Relative locations of heat transfer sensors and sparger holes

resulting in a non-uniform mixing in the region. This non uniform mixing in the region at the bottom of the column resulted in the higher difference in the average heat transfer coefficients as shown in Figure 4.2.17. As the gas velocity increased, the difference in average heat transfer coefficients became smaller, indicating a more uniform mixing in the region. Jet momentum and length will increase with increasing gas velocity which should improve local agitation and mixing thus reducing the difference between heat transfer coefficients at two locations.

Heat transfer coefficients obtained in the central region above the gas distributor are compared in Figure 4.2.20. The probes were located at 0.52, 0.9 and 1.28 m above the column bottom. These results show that the heat transfer coefficients are generally close at the axial positions of 0.9 and 1.28m. However, the values are systematically higher (about 12%) at the height of 0.9 m (or 1.28m) compared to 0.52 m. This may be attributed to increasing bubble size along axial location due to bubble coalescence. Bubbles from the distributor region rise up and move toward the center to form larger bubbles with increasing height from the bottom. The influence of the distributor region usually extends up to 3 to 4 times the column diameter depending on column diameter, sparger design and physical properties of liquid phase (Yamashita, 1985; Haque et al., 1986). The height of 0.52 m from bottom is less than two times the column diameter which would be a developing region for bubble growth and liquid phase flow patterns. There is practically no difference between the heat transfer coefficients at the axial positions of 0.9 and 1.28m. This indicates that both positions are in fully developed bulk region of the column. Therefore it can be concluded that the distributor region effect extended between two to three times the column diameter in this study. The variation of heat transfer coefficients in axial direction was also investigated by Saxena et al.(1992a). The measurements were made in a 0.305 m diameter slurry bubble column at elevations of 0.52 m and 2.19 m from the distributor. It was observed that the average heat transfer coefficient at higher elevation (bulk region) was systematically higher (about 11%) than the lower region. These results are similar to the data of this study, which heat transfer

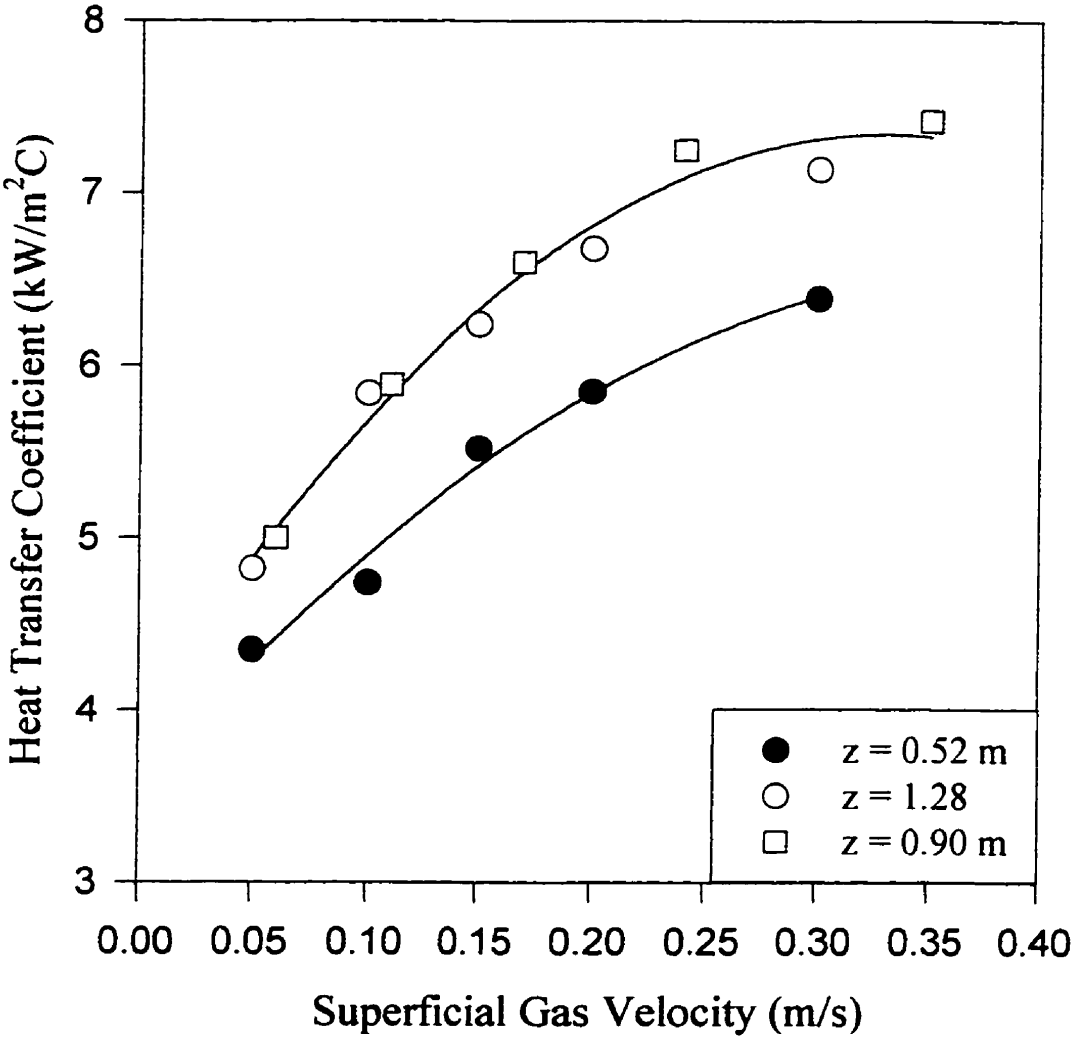

Figure 4.2.20 Heat transfer coefficient in the central region at different axial locations (slurry conc. 10 vol.%) (Data based on Appendix E9)

coefficients at higher elevation (bulk region) was systematically higher (about 12%) than the lower region.

Figure 4.2.21 compares the heat transfer coefficients at different axial locations for the wall region. It can be observed that heat transfer coefficients in the distributor region are significantly lower compared to the region above the distributor. This again shows that the mixing patterns in the distributor region are significantly different from the bulk region.

Moreover, the small differences between heat transfer coefficients at elevations of 0.52 and 0.9 m (and 1.28 m) became negligible with increasing gas velocities. This indicates that recirculating liquid flow in the wall region extends to lower axial positions with increasing gas velocity; however, it does not reach below the distributor.

The influence of slurry concentrations on local heat transfer coefficients in the distributor and bulk regions are shown in Figures 4.2.22 and 4.2.23 respectively. It is observed from Figure 4.2.22 that at low gas velocities (0.05 and 0.15 m/s) the difference between the two radial positions are significant for slurry concentrations below 30 vol.%. The differences, however, decrease with increasing slurry concentrations. For the highest gas velocity (0.3 m/s), the differences between the two radial locations are small and relatively constant for all slurry concentrations. However, in the bulk region, a significant difference remains between the wall and center values even at highest slurry concentration and gas velocity. This observation again suggests different mixing patterns in the distributor and bulk regions of the column. The mixing in the distributor region can be attributed mainly to agitation induced by gas jets and their break-up into bubbles. The agitation due to gas jets would increase with increasing gas velocities resulting in a more uniform mixing in the region. In the bulk region mixing is mainly caused by the wake region of large bubbles in the central region and a circulating flow of liquid in the wall region. The turbulence intensity of the wake region is controlled by bubble size which increases with slurry concentration (sec. 4.1.3). As observed in Figure 4.2.23, the

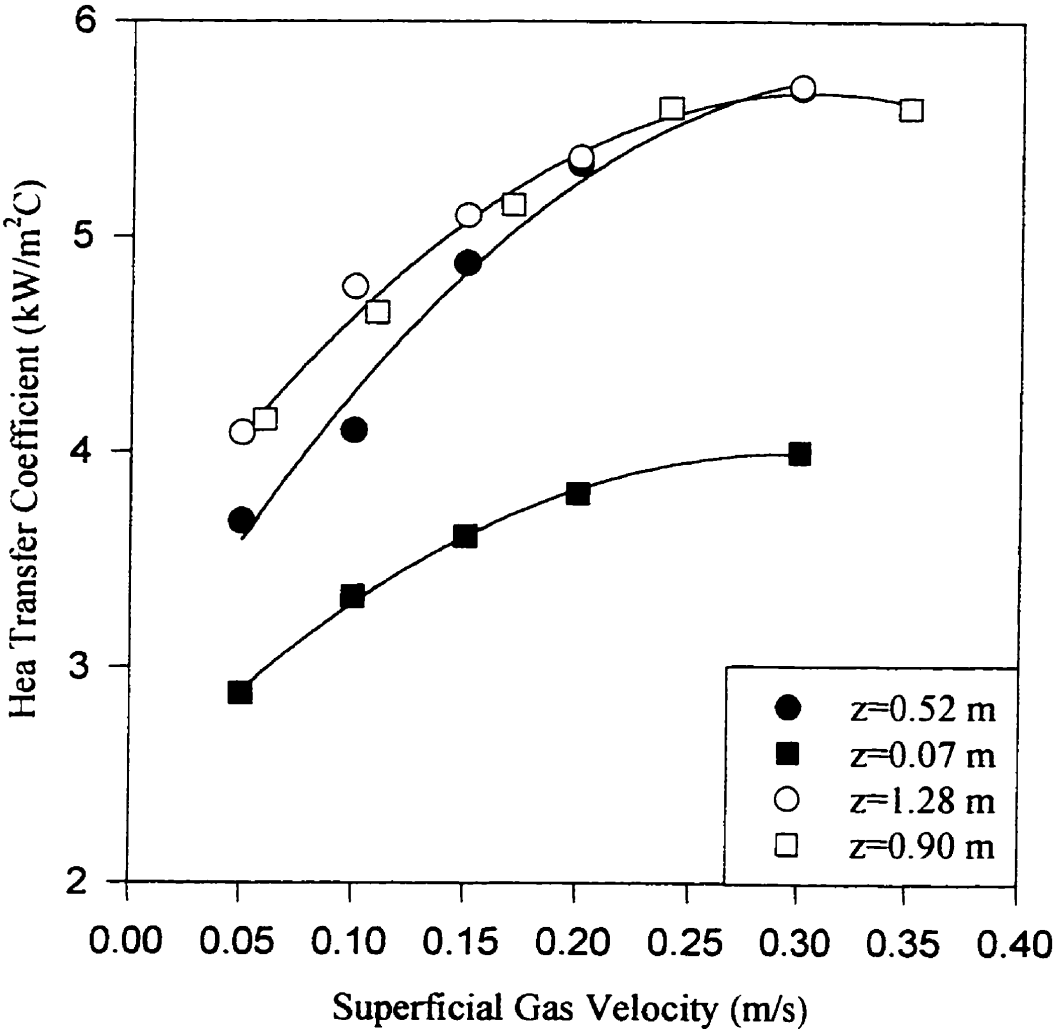

Figure 4.2.21 Comparison of heat transfer coefficient at different axial locations near wall (slurry conc. 10 vol.%) (Data based on Appendix E9)

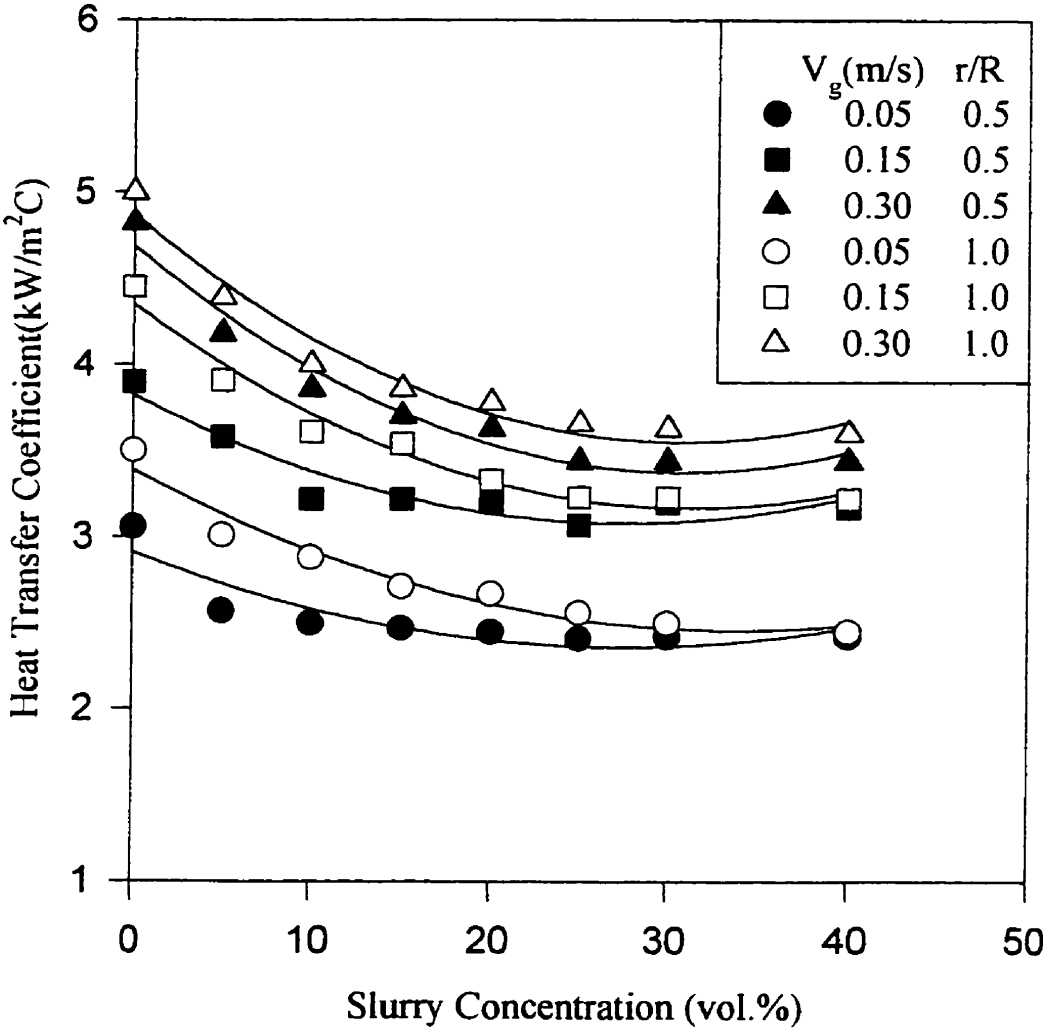

Figure 4.2.22 Variation of heat transfer coefficients with slurry concentration in distributor region (Data based on Appendix E7 and E8)

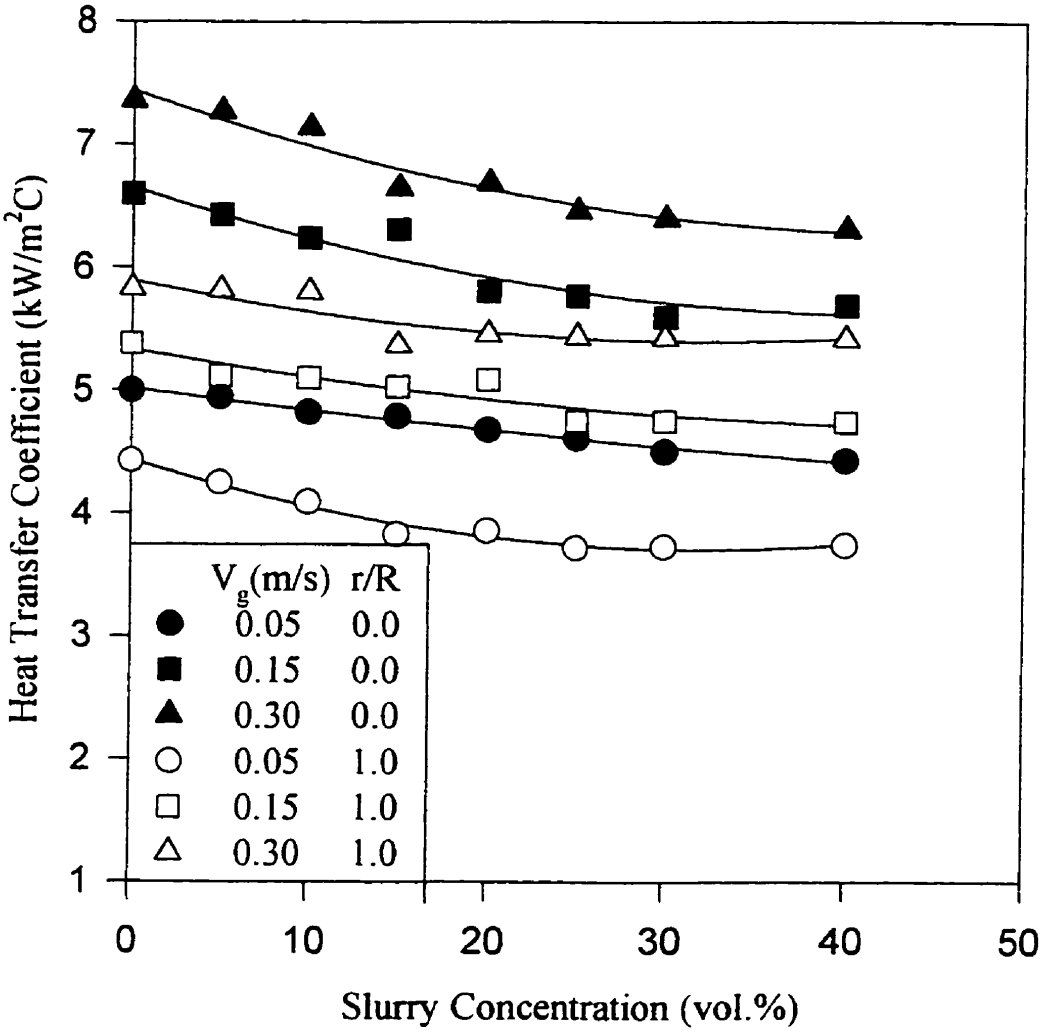

Figure 4.2.23 Variation of heat transfer coefficients in bulk region for different slurry concentrations (Data based on Appendix E2 and E6)

differences between wall and central region heat transfer coefficients are affected to a smaller extent by the increasing slurry concentration at all gas velocities.

4.2.1.4 Effect of Probe Orientations on Heat Transfer Coefficients

Local heat transfer coefficients were also measured for three probe orientations: downward (0°), side-way (90°) and upward (180°) orientation (Figure 4.2.24). Figures 4.2.25a and b show experimental results obtained in air-water and 10 vol.% slurry system in the central region and near the wall. In the central region, heat transfer coefficient in the downward orientation is higher than that in the upward orientation. At the wall, heat transfer coefficients in upward orientation is higher than that in the downward orientation (opposite of central region). The heat transfer coefficients in side orientation is between upward and downward (Figures 4.2.25a & b). These observations can be explained based on formation of boundary layer along the cylindrical probe surface. A boundary layer is formed when a fluid flows past a solid surface since the fluid velocity at the surface is zero. Boundary layer is generally defined as the region of fluid close to the solid surface whose velocity is less than 1% of the free stream velocity (Brodkey and Hershey, 1988). For flow past a cylinder, the development of boundary layer begins with a stagnation point in front of flow and reach a maximum thickness until a favorable pressure gradient exists in the direction of flow. The boundary layer can separate at the rear end of the probe due to an adverse pressure gradient (i.e. pressure is increasing in the direction of flow). The thickness of the thermal boundary layer is smallest in front (near stagnation point) due to the beginning of formation of the thermal layer. The heat transfer coefficient is highest in the downward orientation in the central region (Figure 4.2.25a), indicating an upward fluid flow. The cold water or slurry first arrive at the downside of the heat transfer probe associated with bubble wake. Thus the downside of the probe is in front of the incoming flow and it is more frequently renewed by the cold fluid in the bubble wake. At the lateral orientation (90°) of the probe a larger boundary layer thickness is formed resulting in a lower heat transfer coefficient. As shown in Figure 4.2.25a and b, the heat transfer coefficients at 90° orientation are systematically

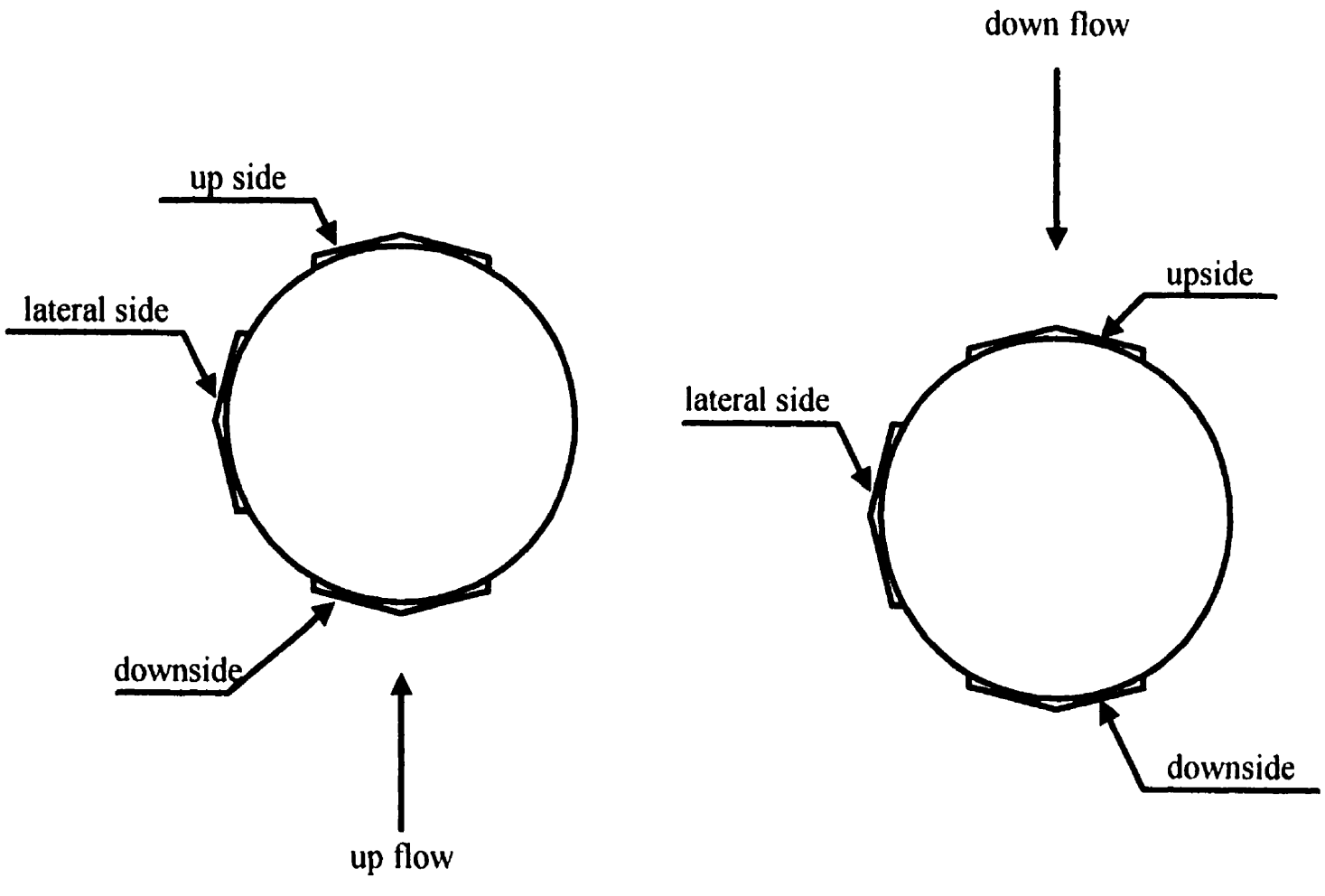

At the center

Near the wall

Figure 4.2.24 Position of heat flux sensor and direction of flow in center and at the wall

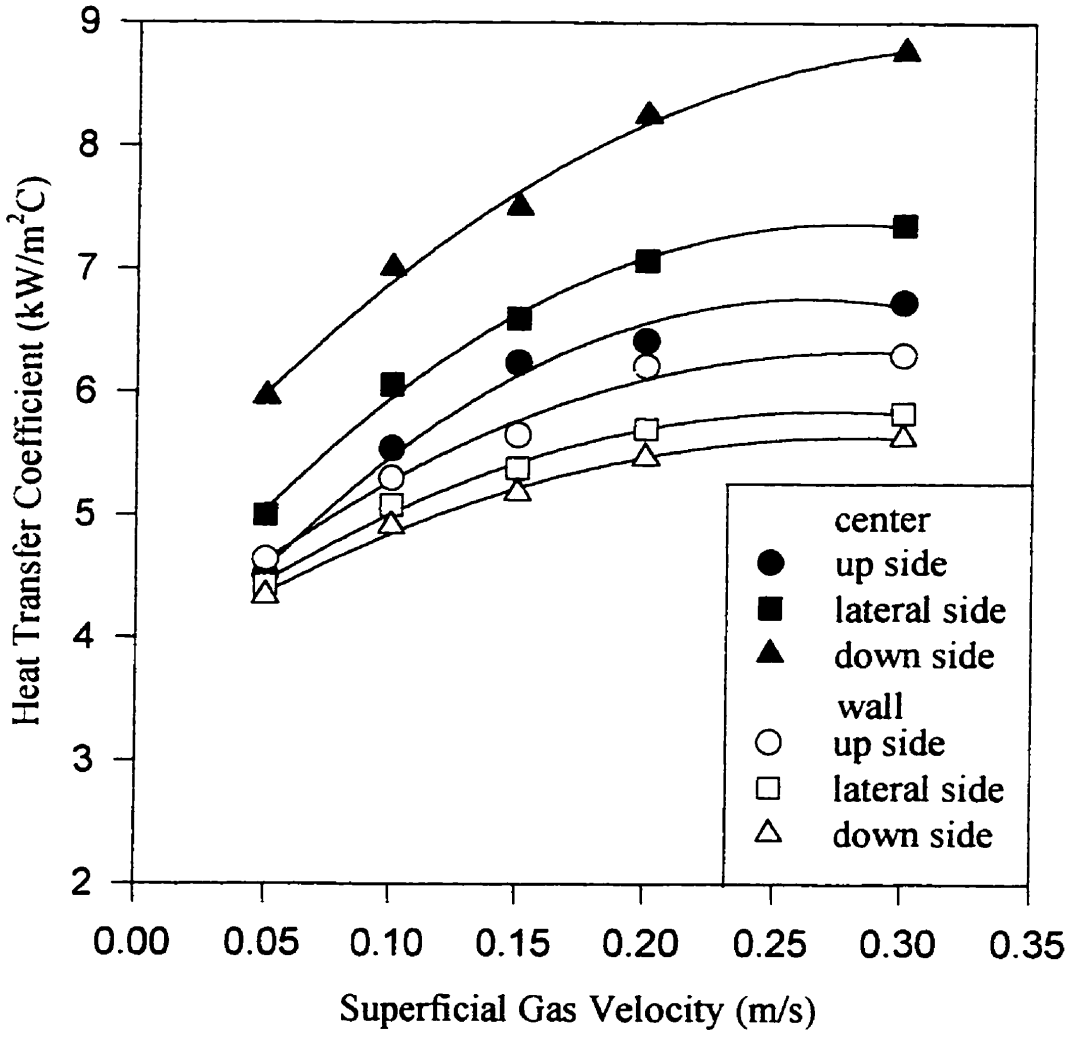

Figure 4.2.25a Heat transfer coefficient at different probe orietion in air-water system
(Data based on Appendix E10)

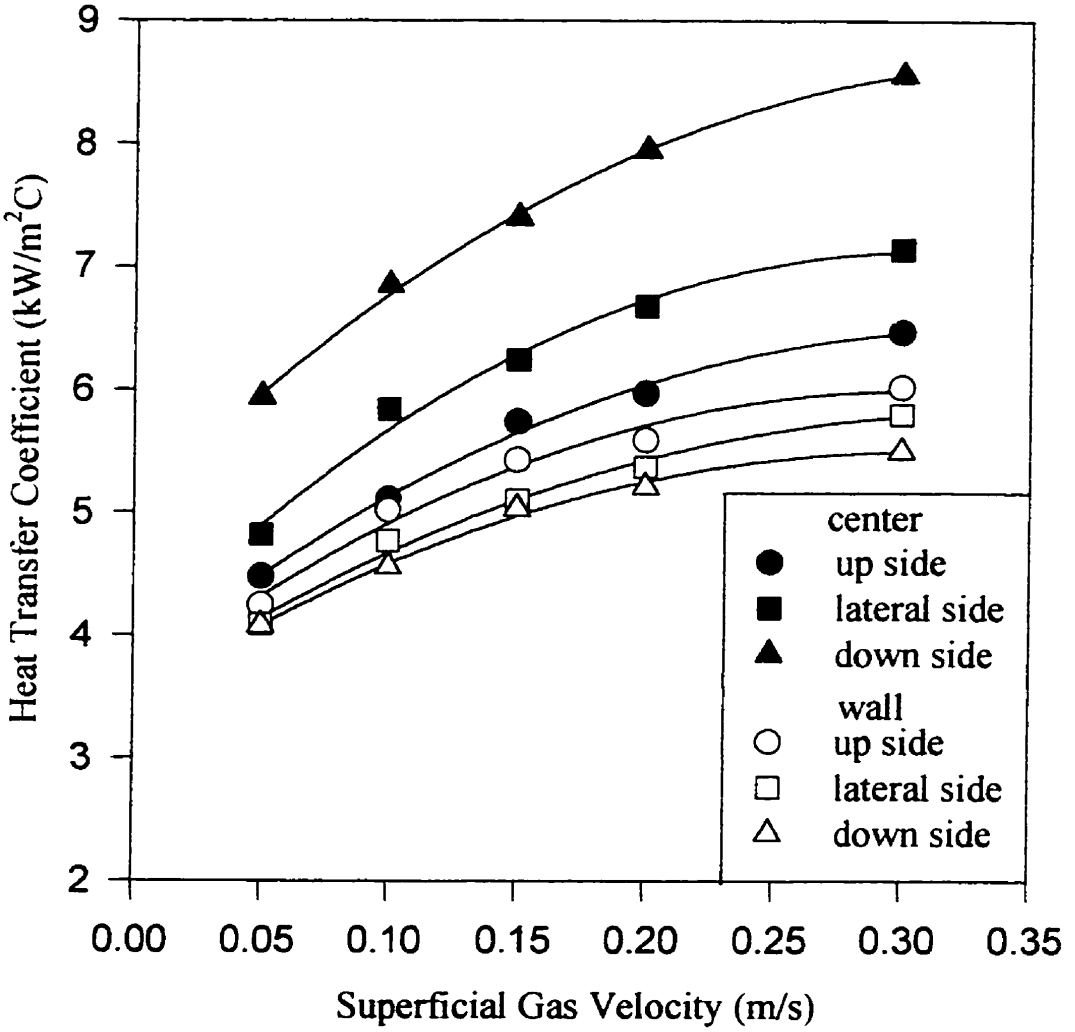

Figure 4.2.25b Heat transfer coefficients at different probe orientations in slurry concentration of 10 vol.% (Data based on Appendix E10)

lower than that in downside orientation. The heat transfer coefficients in the upward orientation is the lowest where the boundary layer separation effects could affect the heat removal rate.

At the wall, the heat transfer coefficient is highest when the probe is facing upwards indicating that flow of water (or slurry) is downward. The downward flow of liquid in the wall region of a bubble column has been recorded in literature (Hill, 1974 and Ueyama and Miyauchi, 1979). These observations show that by measuring heat transfer coefficient at different orientations, the direction of flow of fluid can be identified in the column thus providing further information on flow patterns.

4.2.2 Instantaneous Heat Transfer Coefficient

The measurement of the instantaneous heat transfer rate provides time dependent variations of the heat exchange process in different locations of the column for different gas velocities and slurry concentrations. As a bubble passes over the surface of the probe, heat transfer rate is enhanced due to its turbulent wake region. The bubble wake enhanced heat transfer is an important event which could be recorded by the fast response probe used in this study.

4.2.2.1 Air-Water System

Figure 4.2.26 compares the variation of the instantaneous heat transfer coefficient at the central in air-water system for low and high gas velocities. It can be seen that peaks are significantly higher for the higher gas velocity. As gas velocity increases, larger coalesced bubbles generate stronger bubble-wake-induced turbulence, resulting in higher heat transfer rate. It was observed in section 4.1.3 that the concentrations of both small and large bubbles increase with increasing gas velocities. However, rise velocities of larger bubbles population increase faster compared to small bubbles population. Increase in bubble size with gas velocity has been reported in literature in both gas-liquid and gas-liquid-solid system (Rigby et al., 1970; Kim et al., 1977; Han and Kim, 1990).

Variations of instantaneous heat transfer coefficients at center and at wall are presented in Figure 4.2.27 for air-water system at gas velocity of 0.05 m/s. It can be seen that the peaks at the wall are significantly smaller than that at the center. This indicates that the wall region is relatively free of larger bubbles or faster moving bubble chain. Higher bubble-wake-induced turbulence in the center is due to faster moving larger bubbles in the central region of the column. Smaller peaks of instantaneous heat transfer coefficient and absence of sharp peaks at the wall region indicate small bubbles passing at the wall

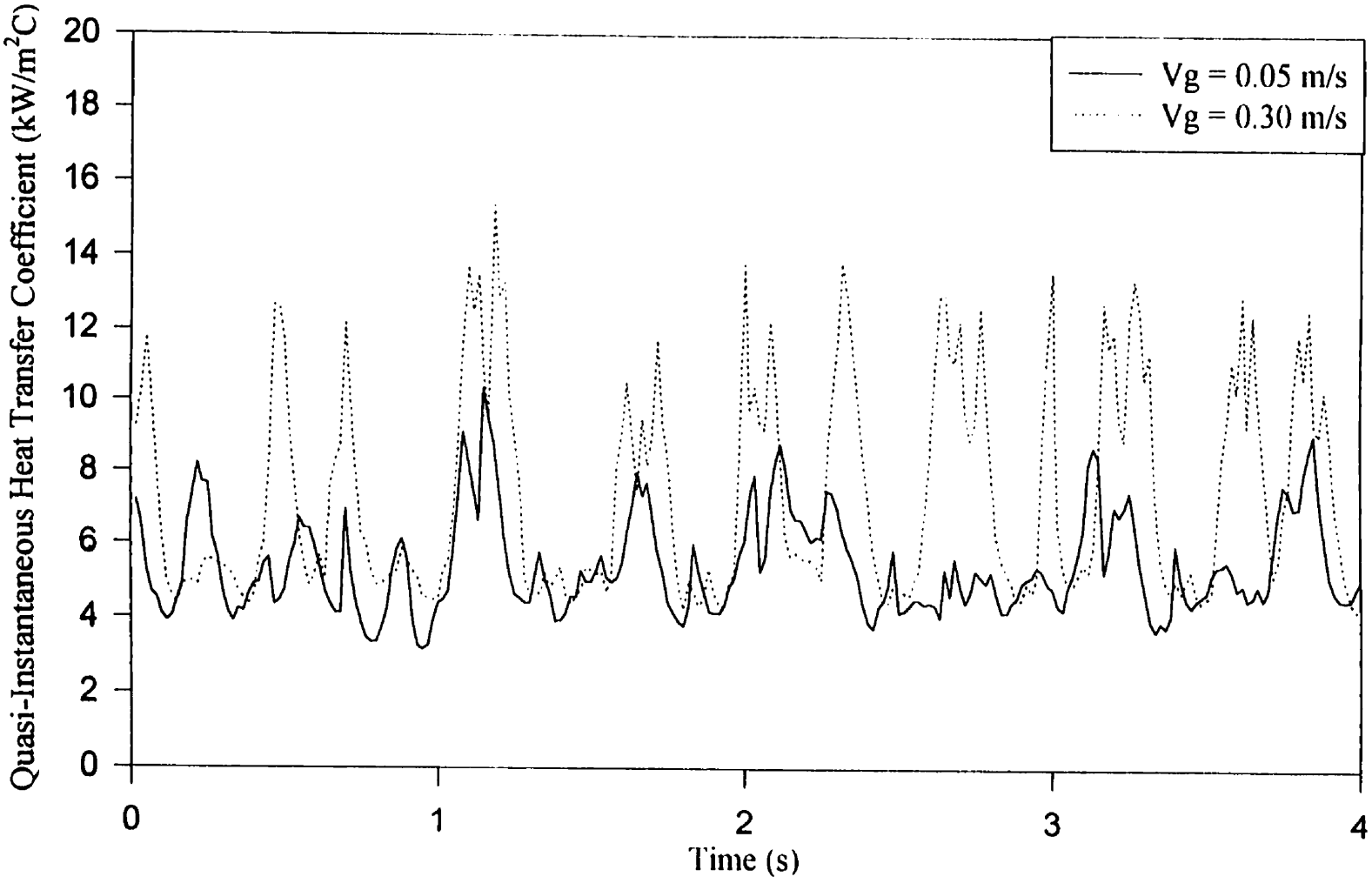

Figure 4.2.26 Instantaneous heat transfer coefficient (air-water; center)

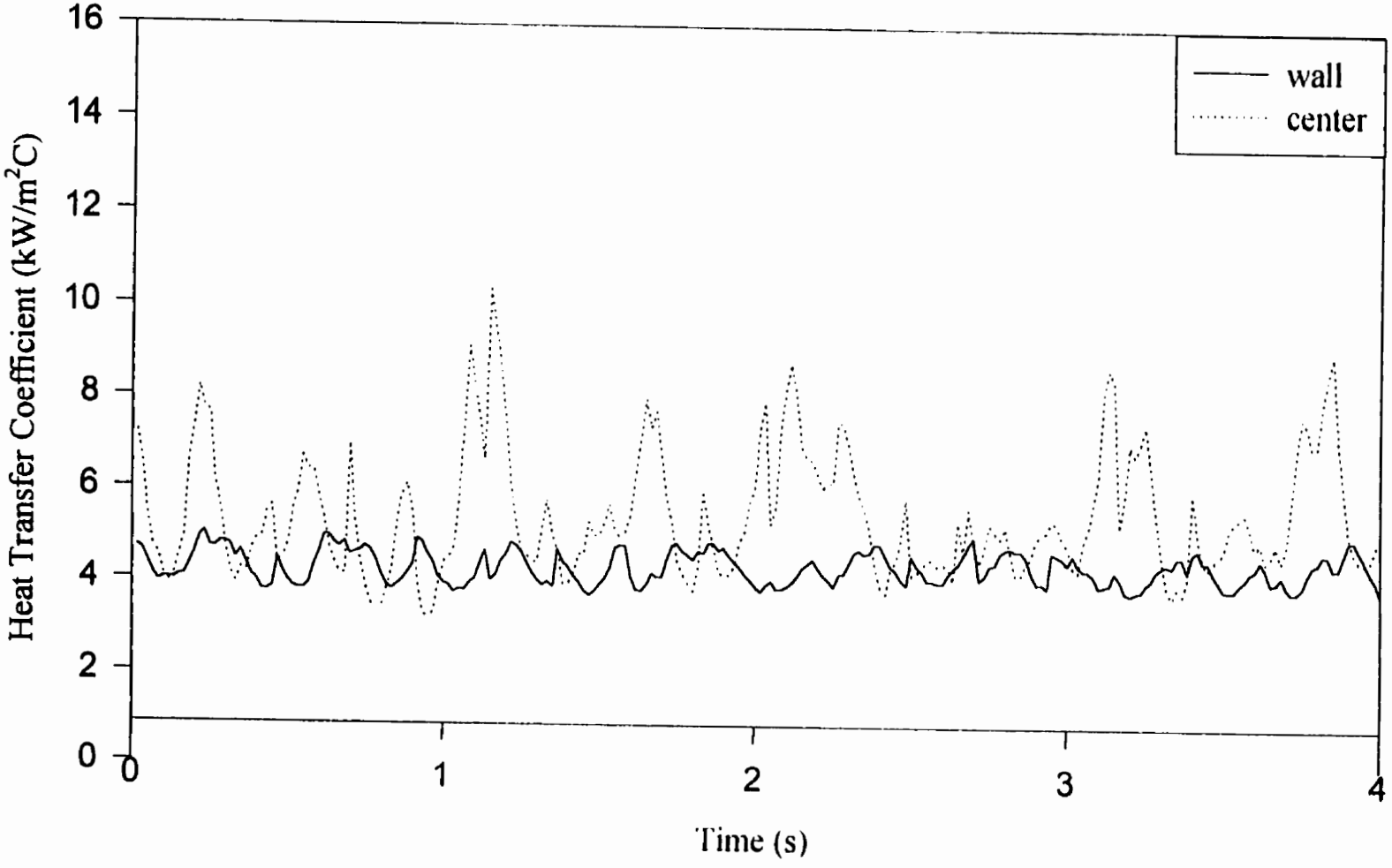

Figure 4.2.27 Comparison of instantaneous heat transfer coefficients at center and wall (air-water; Vg=0.05 m/s)

region of the column. The bubbles with the smaller diameter near the wall would have smaller bubble-wakes, resulting in smaller peaks of local heat transfer coefficients.

These observations can be compared with reported radial profiles of bubble size distribution and gas holdup in bubble column (Yasunishi et al., 1986; O'Dowd et al., 1987; Yu and Kim, 1988; Chen et al., 1994; Kwon et al., 1994). These studies have shown that average bubble diameter is smaller near the wall and larger in the central region of the bubble column. The experimental observation of instantaneous heat transfer coefficients of this study shows similar trends. Higher peaks of heat transfer coefficients are found in the central region and smaller peaks at the wall, indicating larger bubbles in the central region and smaller bubbles in the wall region..

4.2.2.2 Effect of Solid Addition

Figure 4.2.28 compares quasi-instantaneous heat transfer coefficients in the air-water system with the air-water-glass particles system for a solids concentration of 5 vol.% in the central regions. It can be seen from Figure 4.2.28 that the addition of solids particles significantly reduces the peak height (or intensity) of instantaneous heat transfer coefficients. Reduced peak height indicates lower turbulence intensity generated by bubble wakes. The change in instantaneous heat transfer coefficient with the addition of solids is a net result of two opposing factors. As solids are added into water, gas holdups decrease and bubble rise velocities increase (sec. 4.1.3) indicating formation of larger bubbles. This should lead to larger bubble wakes and higher peak intensities. However, with addition of solids, the apparent suspension viscosity also increases which would have a dampening effect on turbulence intensity. Kumar and Fan (1994) studied the effects of liquid viscosity on instantaneous heat transfer coefficients. It was observed that the increase of the liquid viscosity lowered the local maximum heat transfer coefficient behind bubbles. This can be attributed to reduction of circulation strength of the bubble wake caused by higher dissipation of vorticity. The addition of solids into the

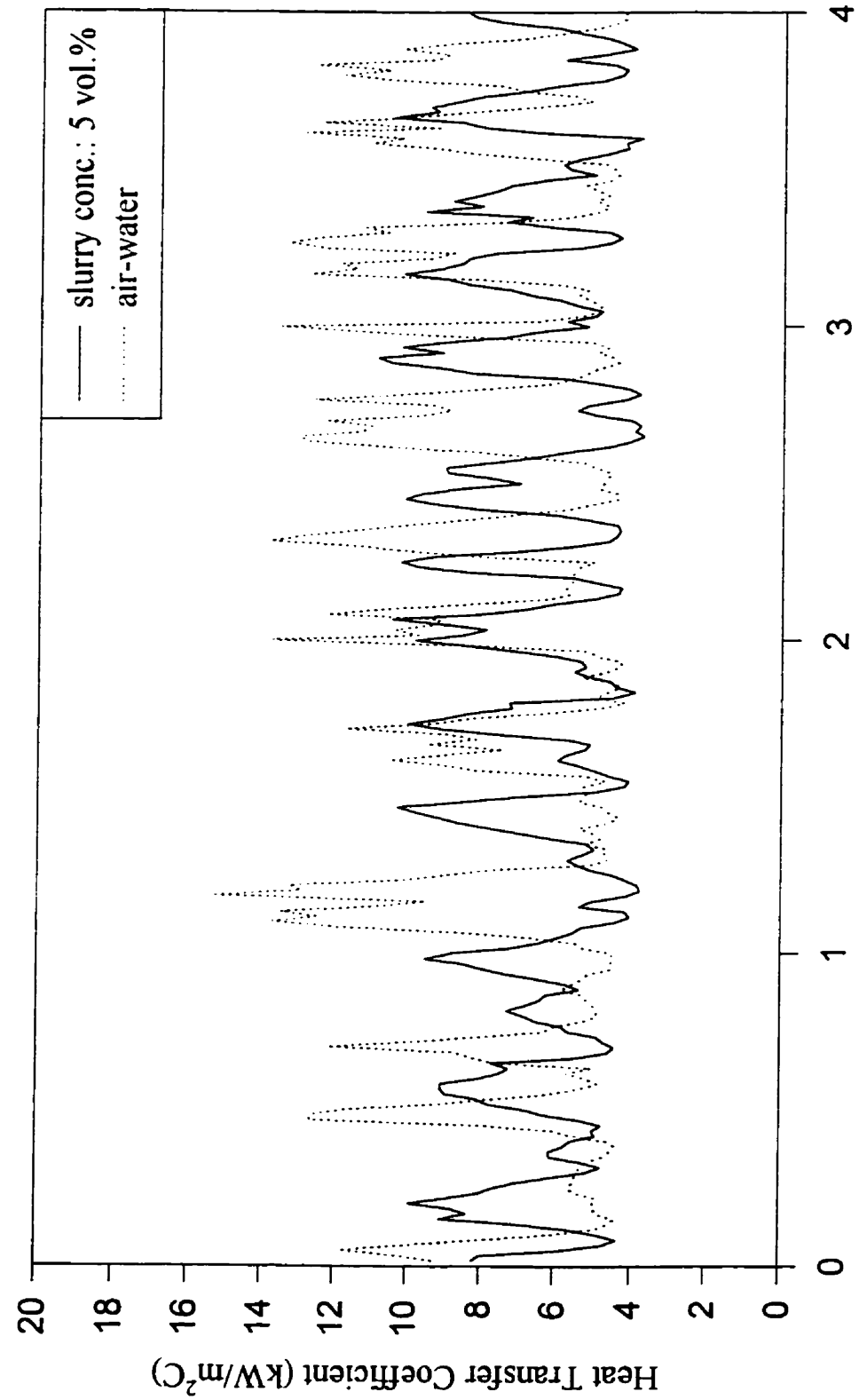

Figure 4.2.28 Effect of solids addition on heat transfer probe response (center; Vg=0.30 m/s)

bubble wake destroy an ordered motion/ circulation, resulting in reduced vortical strength in the water inside the bubble wake (Raghnathan et al., 1992).

Instantaneous heat transfer coefficients for increasing slurry concentrations are compared in Figure 4.2.29a and 4.2.29b at gas velocity of 0.30 m/s. It can be seen from these figures that peak heights increase significantly as the slurry concentration is increased. The peaks are generally sharper and narrower at higher slurry concentrations. This indicates that effects due to increase in bubble size are taking over; narrower peaks, however, indicate a decrease in bubble wake size. The base lines are also lowered with increasing slurry concentrations. The influence of bubble-wake-induced turbulence is significantly reduced due to higher suspension viscosity. Lower base line values for higher slurry concentration can be attributed to lower bulk mixing due to increasing suspension viscosity.

Instantaneous heat transfer coefficients in the wall region are compared in Figures 4.2.30a to c for different systems. It is seen that generally, the peaks in slurry system are higher than in air-water system. This indicates that the addition of solid into water increases average size of small bubbles. This is also confirmed from bubble rise velocities measurements (sec. 4.1.3); the rise velocity of small bubbles increased with increasing slurry concentration.

4.2.2.3 Comparison between Bulk and Bottom Regions

Figure 4.2.31a and b compare instantaneous heat transfer coefficients in bulk and bottom regions. No significant peaks are observed in the distributor region, indicating absence of larger bubbles. Figure 4.2.32a and b compare heat transfer coefficients at halfway and at the wall in the bottom region. Only small fluctuations of heat transfer coefficient can be observed at both locations again, indicating absence of larger bubbles at the bottom of column.

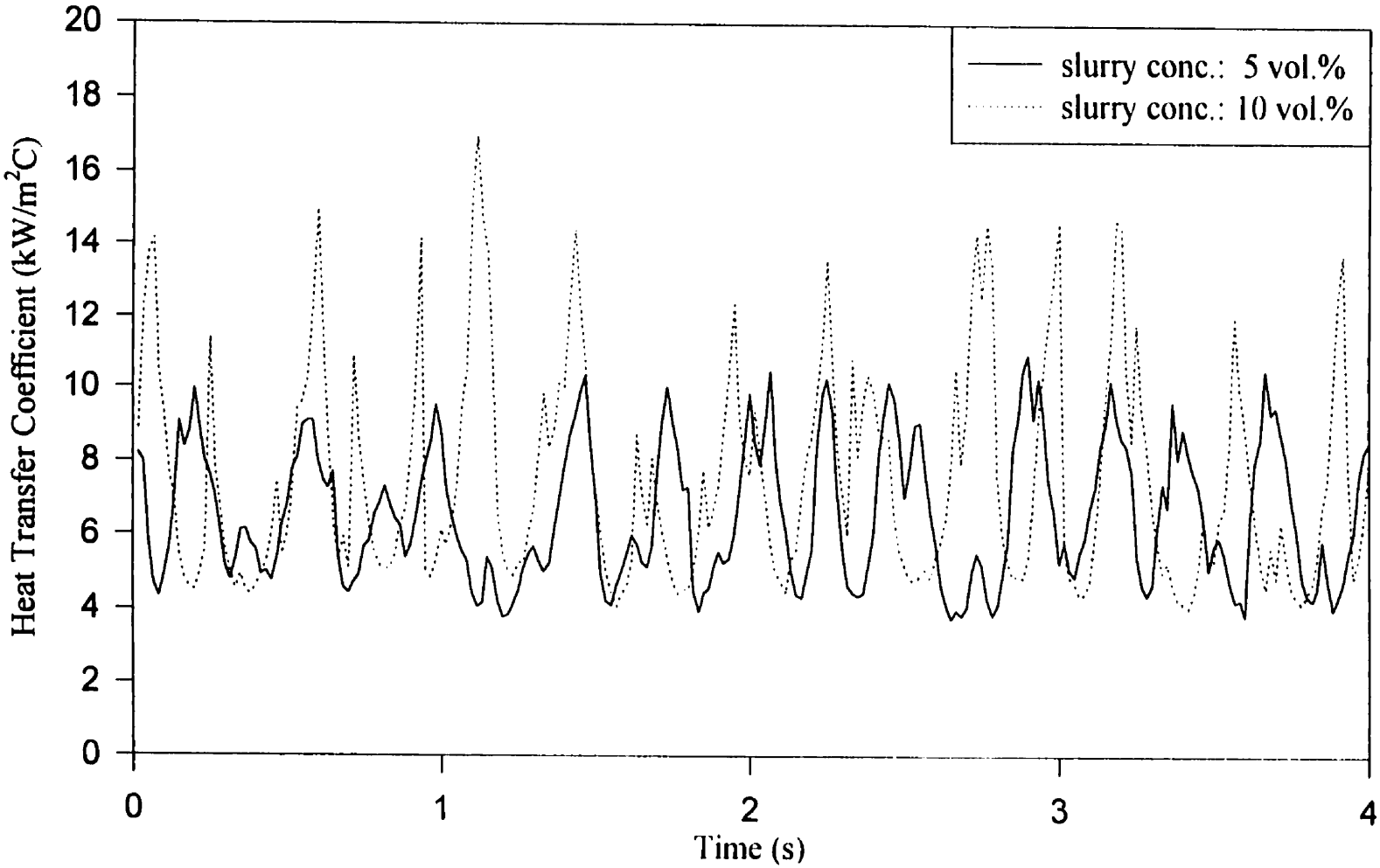

Figure 4.2.29a Comparison of instantaneous heat transfer coefficients between 5 and 10 vol.% slurry system (center; Vg=0.30 m/s; z=1.28 m)

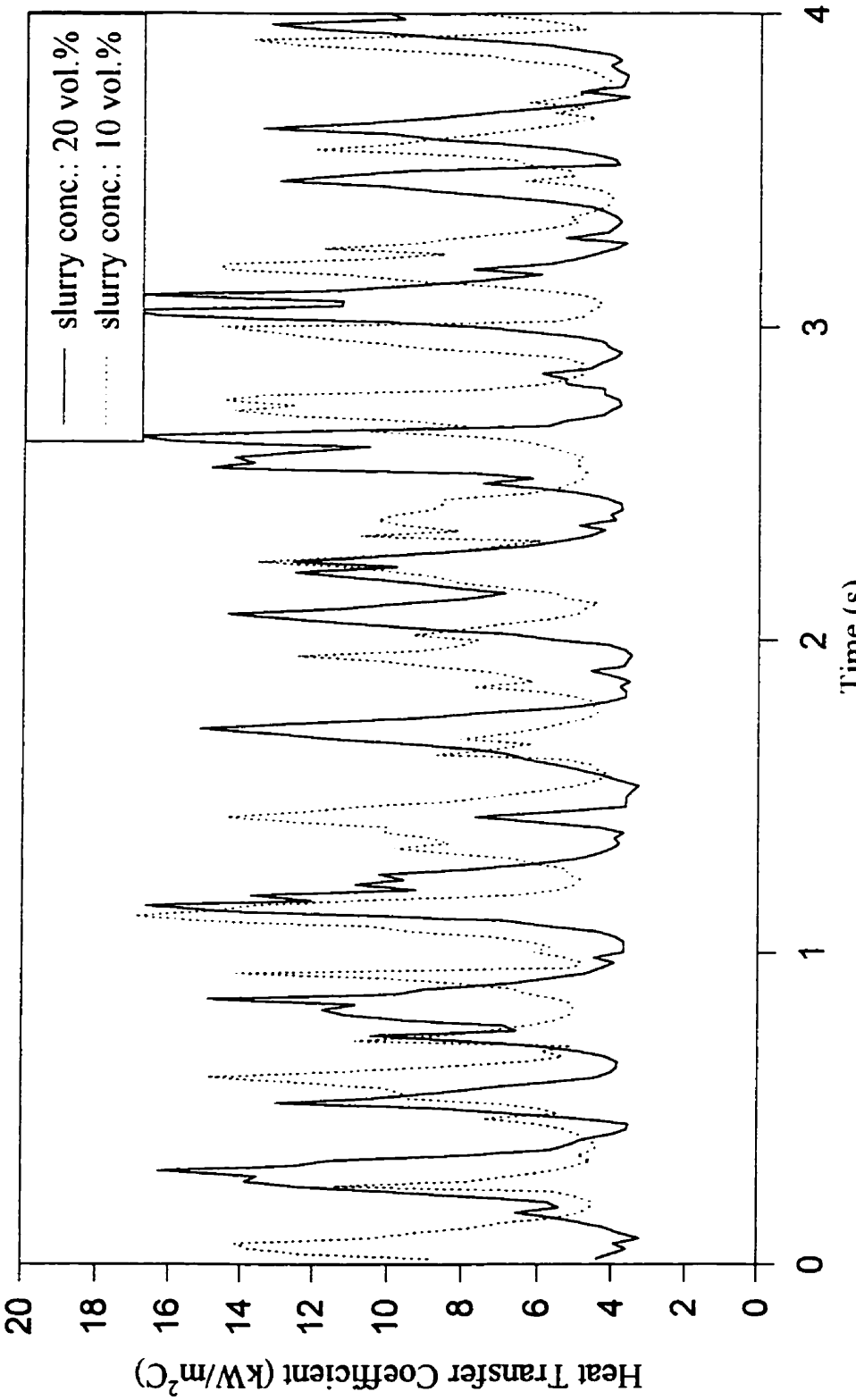

Figure 4.2.29b Comparison of instantaneous heat transfer coefficients between 10 and 20 vol.% slurry system (center; Vg=0.30 m/s; z=1.28 m)

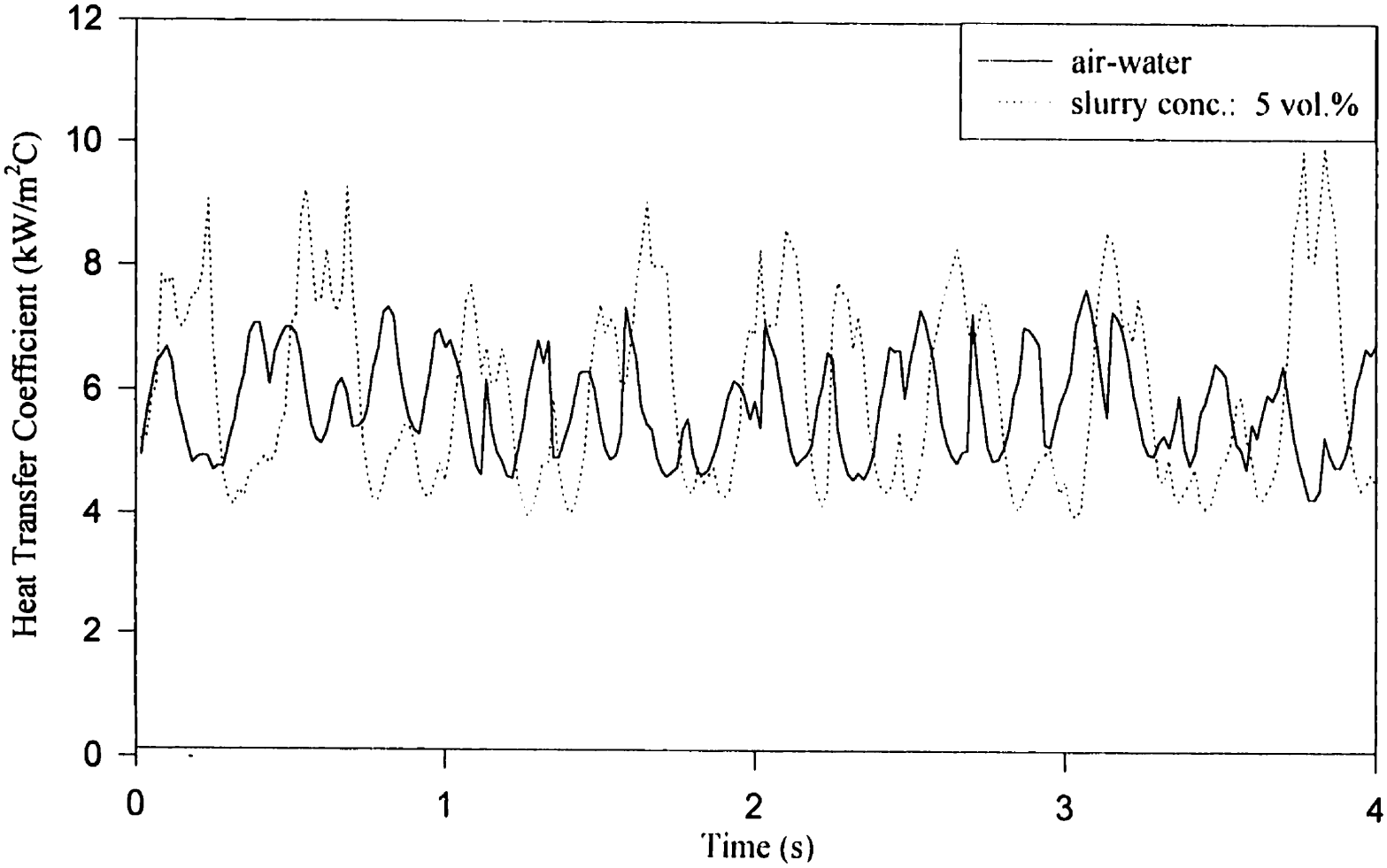

Figure 4.2.30a Instantaneous heat transfer coefficients in wall region (comparison between air-water and 5 vol.% slurry system; Vg=0.30 m/s; z=1.28 m)

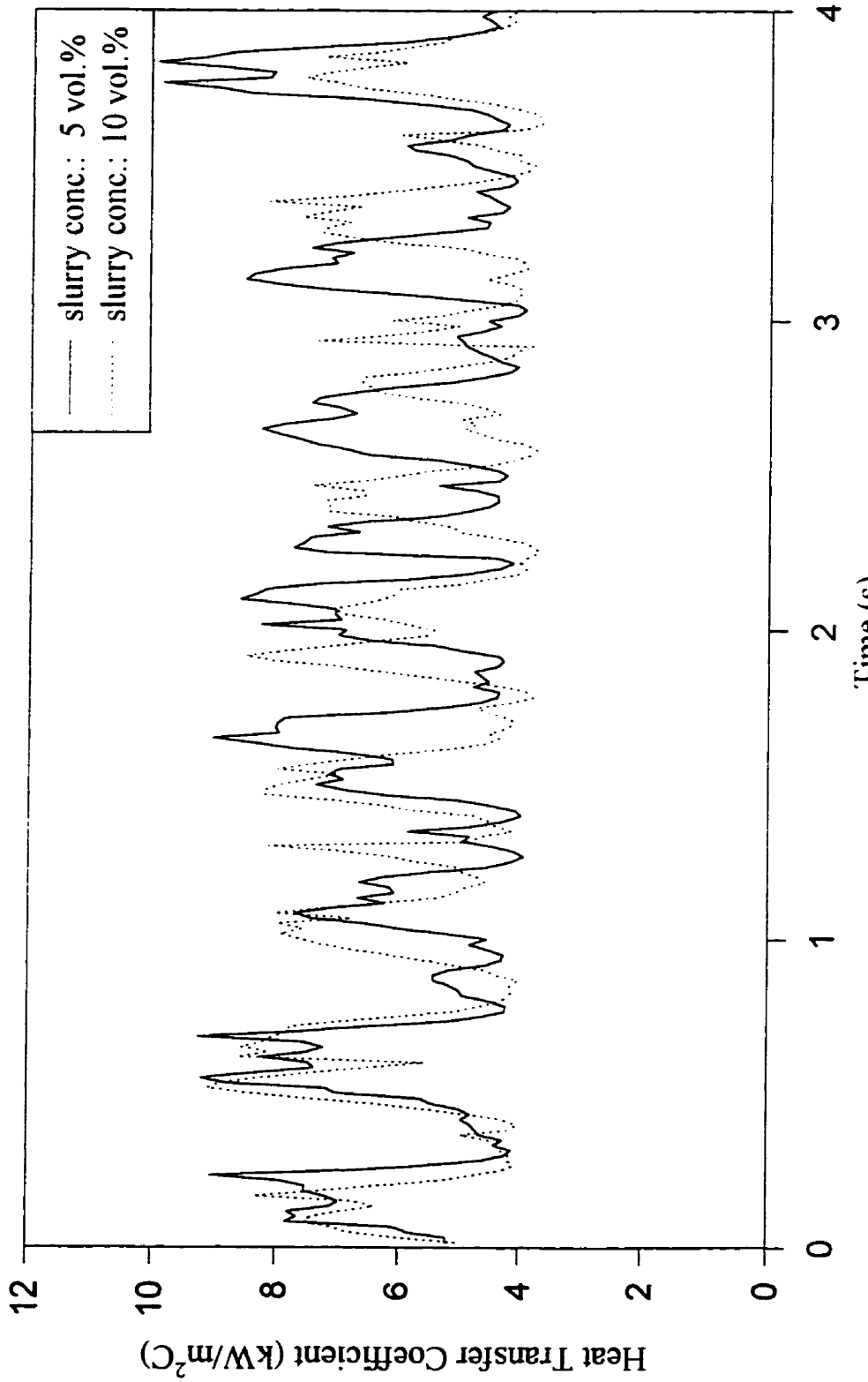

Figure 4.2.30b Instantaneous heat transfer coefficients in wall region (comparison between 5 and 10 vol.% slurry system; Vg = 0.30 m/s; z = 1.28 m)

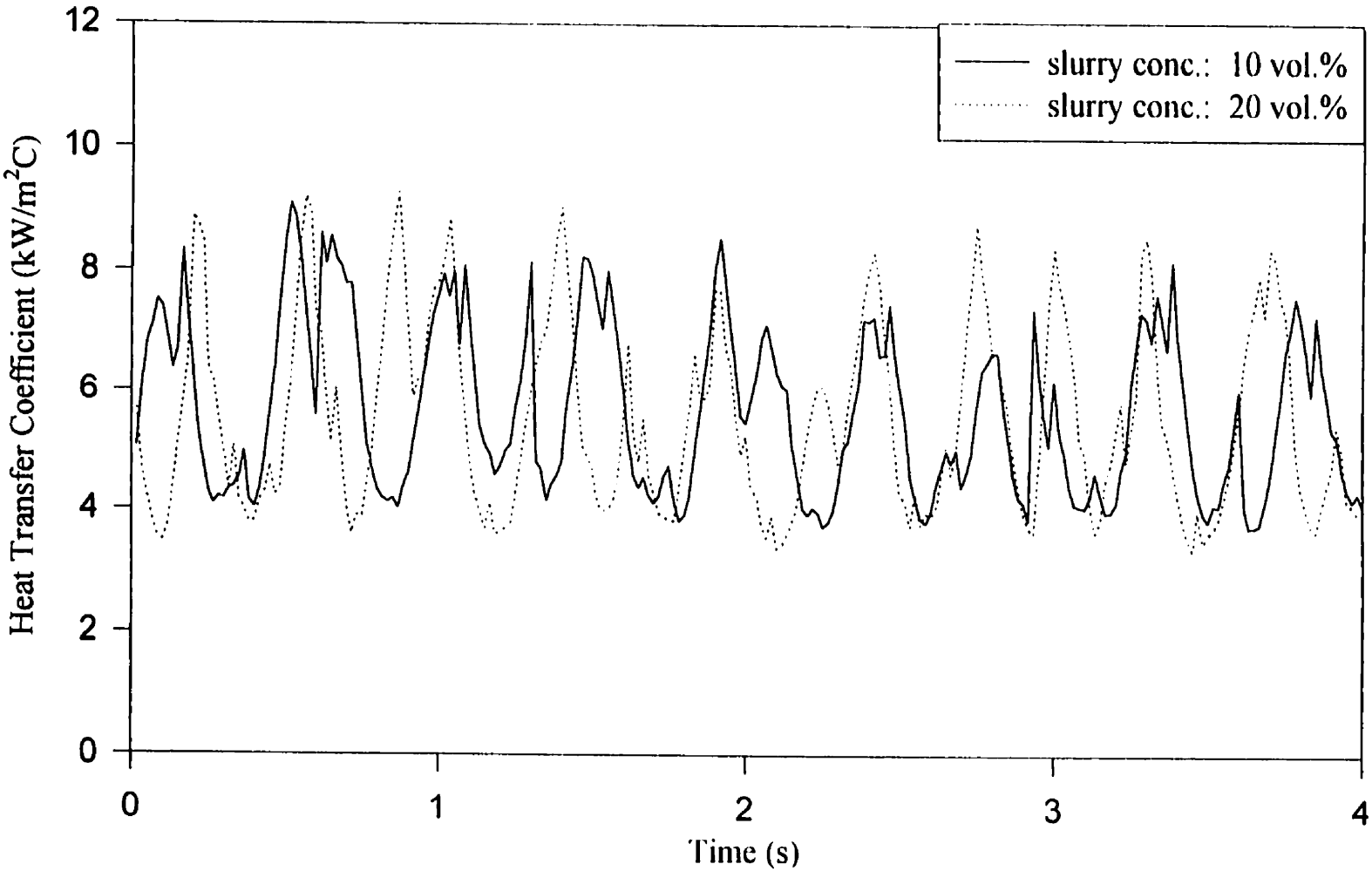

Figure 4.2.30c Instantaneous heat transfer coefficients in wall region (comparison between 10 and 20 vol.% slurry system; Vg = 0.30 m/s; z = 1.28 m)

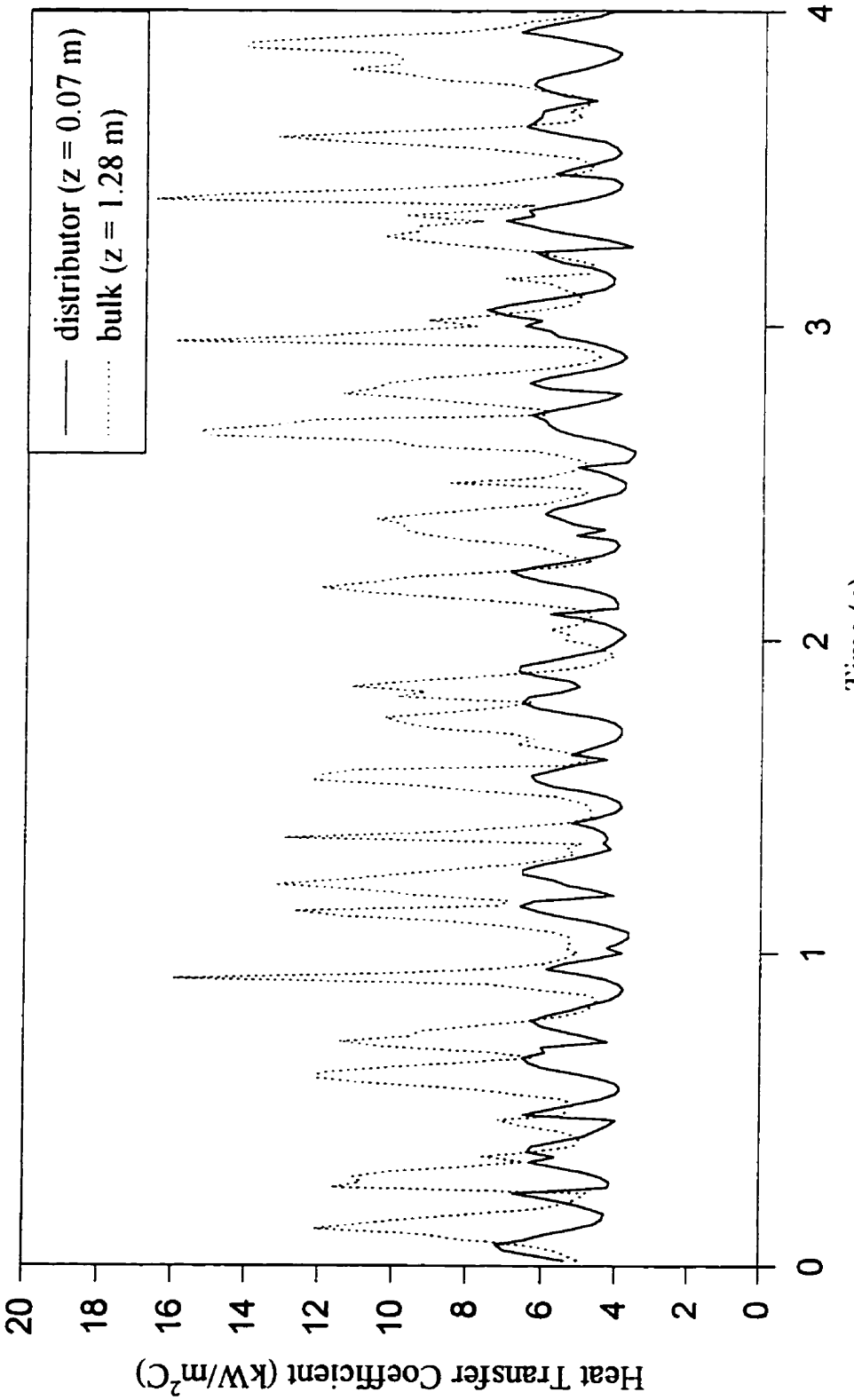

Figure 4.2.31a Comparison of instantaneous heat transfer coefficients between bulk and distributor region(air-water; Vg=0.30 m/s; r/R=0.5)

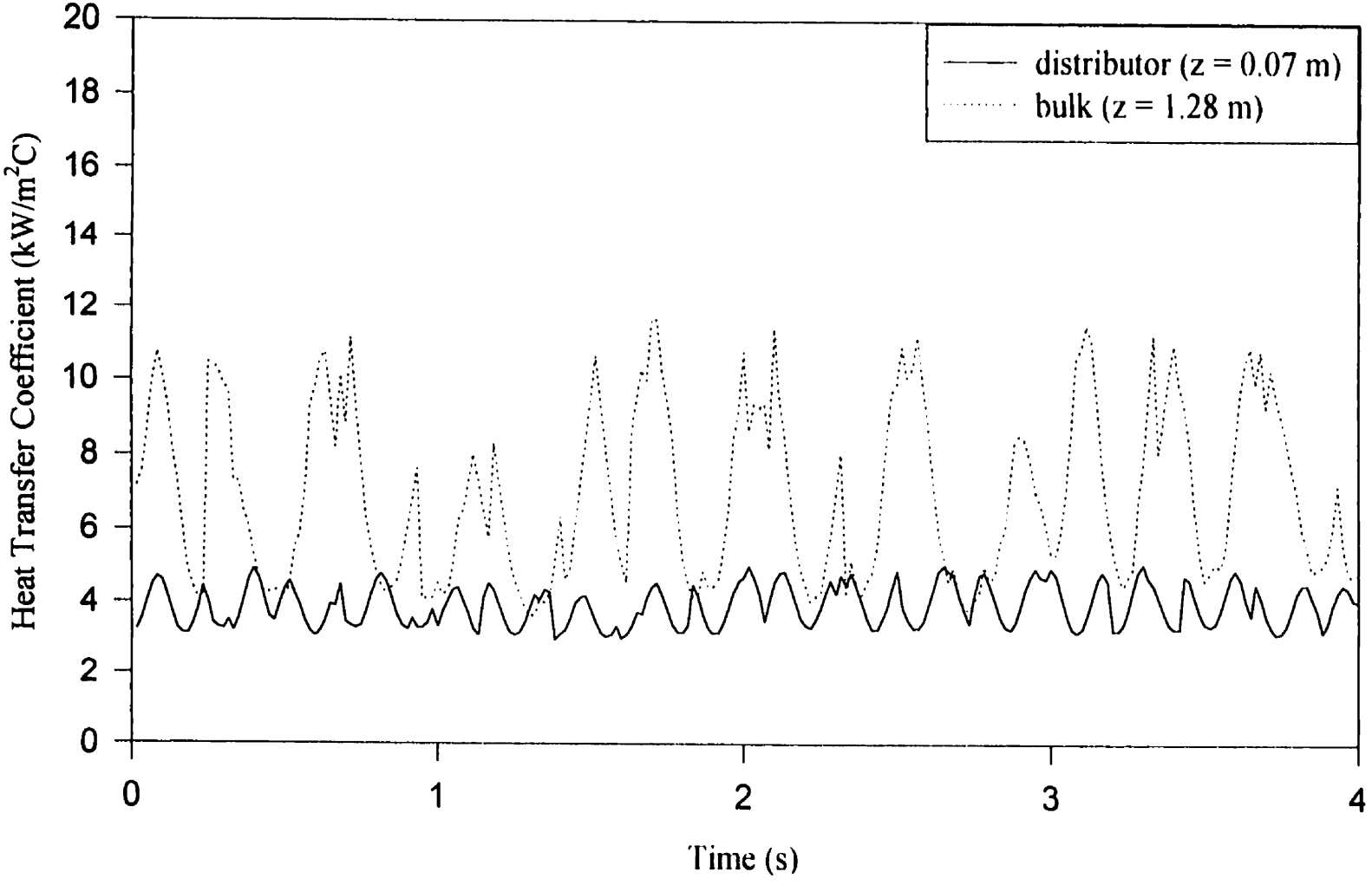

Figure 4.2.31b Comparison of instantaneous heat transfer coefficients between bulk and distributor region(slurry conc. = 10 vol.%; Vg=0.30 m/s; r/R=0.5)

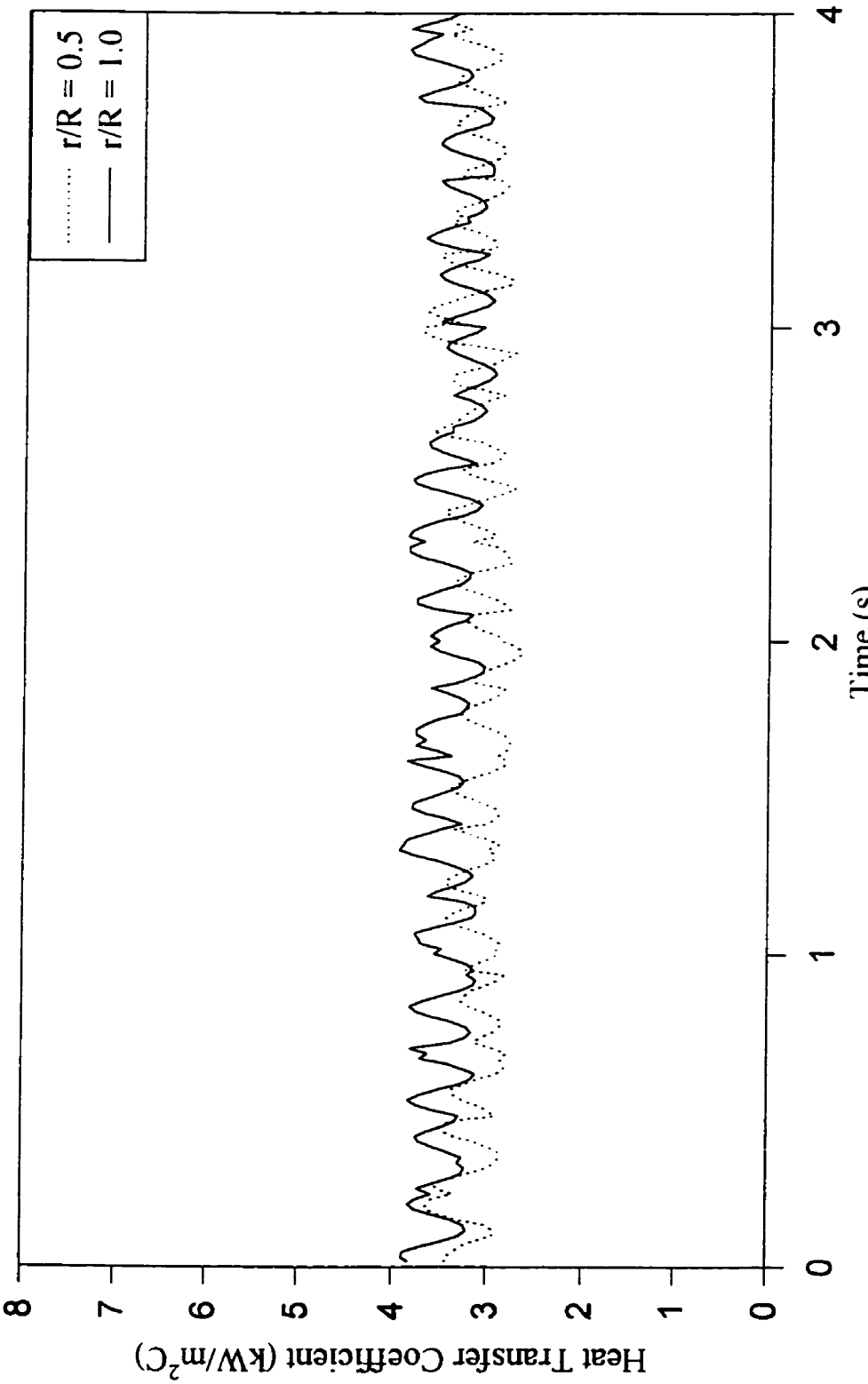

Figure 4.2.32a Instantaneous heat transfer coefficients in distributor region at different radial position(air-water; Vg=0.05 m/s; z=0.07 m)

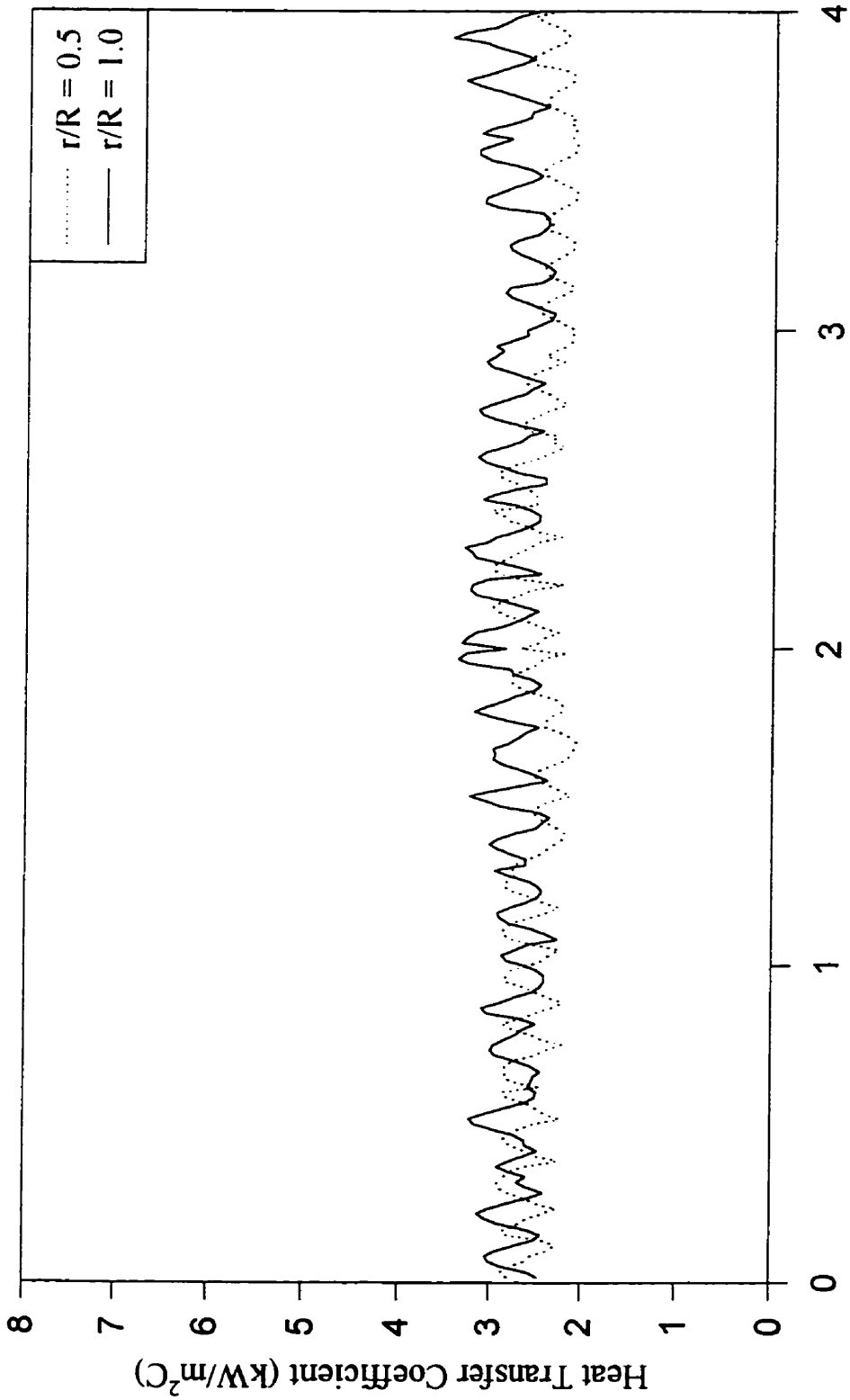

Figure 4.2.32b Instantaneous heat transfer coefficients in distributor region at different radial position (slurry conc. 10 vol.%; Vg=0.05 m/s; z=0.07 m)

The above measurement of instantaneous heat transfer coefficients were further analyzed based on effects of operating conditions on peak height distribution, peak area and peak frequency.

4.2.2.4 Procedure for Estimating Peak-Height Distribution

As discussed in previous sections, instantaneous heat transfer coefficients can be used to describe bubble wake behavior. As bubbles pass on the surface of the heat transfer probe, heat transfer is enhanced by the wakes associated with them. The higher peak should indicate higher intensity of turbulence induced by a larger bubble wake. Therefore, the information on peak heights should provide information on bubble wake behaviors in the region where the heat transfer probe is located. The measurement of instantaneous heat transfer coefficients (Figures 4.2.26 to 4.2.30) indicate that at the same operating condition(i.e. a time series heat transfer coefficient), the peak height is not uniformly distributed. Therefore, peak height fitting method described below was developed to obtain the distribution of peak heights. The distribution of peak heights can be related to bubbles dynamics for the system.

From peak-fitting method, other useful information, such as baseline, peak-frequency and unit area of peak are also obtained. As described below, baseline can be used to describe the behavior of bulk turbulence. Peak frequency can be related to larger-bubble frequency at different operating conditions. Unit area of peak provides average effect of bubble-wake turbulence on heat transfer at particular operating conditions, which can be related to the bubble wake size.

As discussed in previous section, no significant peaks are observed in the measurement of instantaneous heat transfer coefficient at the bottom. In this section, the peak-fitting method is not applied for analyzing instantaneous heat transfer coefficients in the distributor region. The discussion applies to heat transfer coefficients in bulk region.

To quantitatively describe the distribution of the peak heights at a given operating condition, peak heights can be divided into many equal spaced intervals. For example, all peak heights from 0 to 0.5 ($kW/m^2 C$) are counted as peak height of 0.25 ($kW/m^2 C$), which is an average value in the interval. Here, forty equal spaced interval (average peak height from 0.25 to 19.5 $kW/m^2 C$) are applied for determining peak height distributions.

To quantitatively describe the effect of bubble-wake, the area of individual peaks can be calculated. The area of each peak is obtained by multiplying sampling time with the measured heat transfer coefficient above base line. To calculate the area of individual peaks, the baseline should be determined. Here, the baseline is defined as the average value of the minimum heat transfer coefficients, which are lower than the average heat transfer coefficient. The minimum heat transfer coefficient is defined as:

$$\text{if } (h_i < h_{i-1} \text{ and } h_i < h_{i+1} \text{ and } h_i < h_{ave})$$

then h_i is a minimum heat transfer coefficient.

The average minimum heat transfer coefficients is an average value of h_i. Typical reconstructed time series heat transfer coefficients is shown in Figure 4.2.33. If instantaneous heat transfer coefficient is less than baseline value, it is replaced by the baseline value.

To calculate the area of each peak, two parameters are defined: time length and the height of peak. When a bubble passes on the surface of the probe, heat transfer coefficient increases, passes through a maximum, and then decreases. The height of each peak is defined as the maximum instantaneous heat transfer coefficient achieved for a passing bubble-wake minus baseline value. The time length of each peak is defined as the time between two minimum heat transfer coefficients in which one is before the peak and other after the peak. One should notice that the value of baseline is also a minimum heat transfer coefficient.

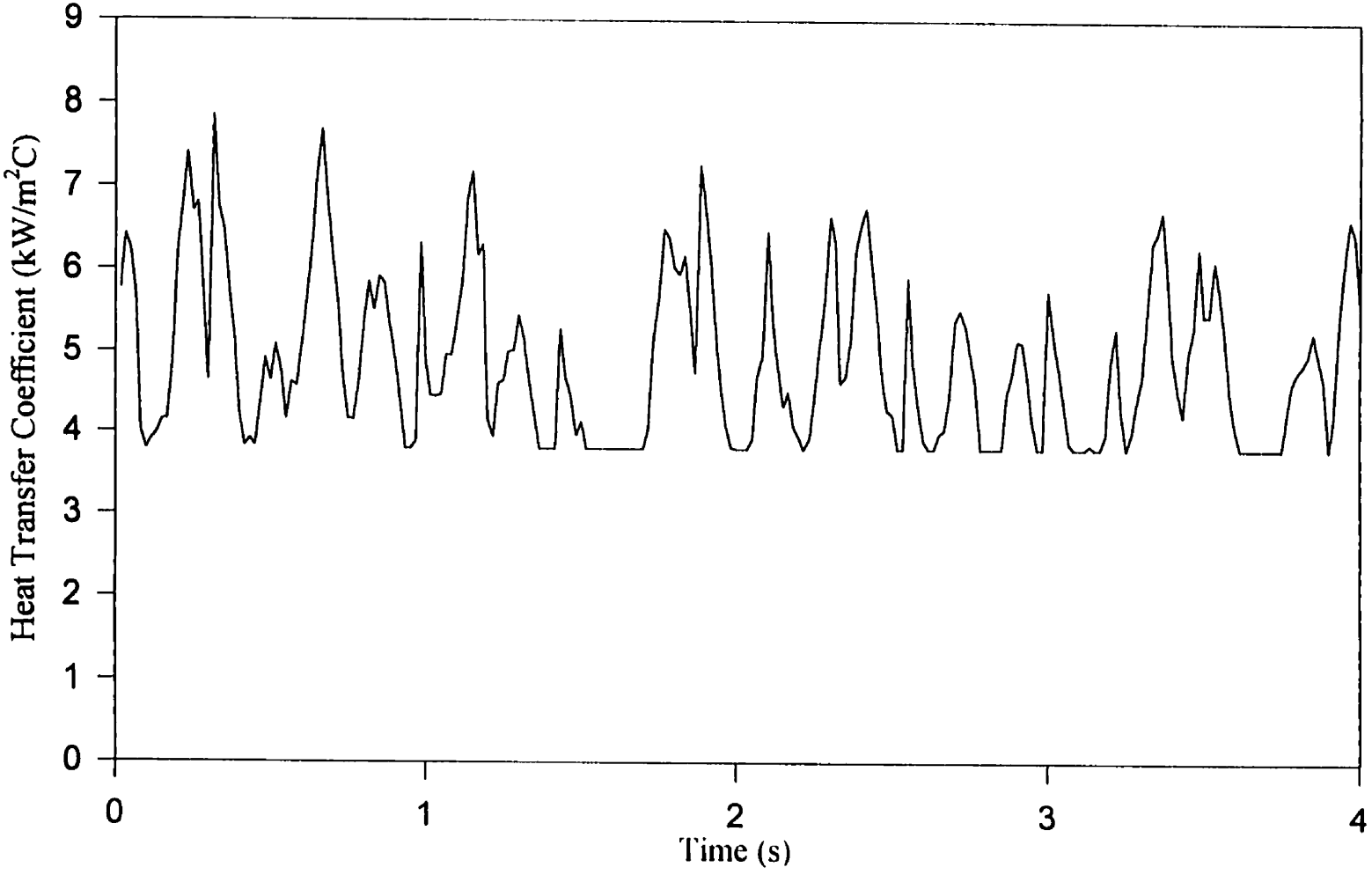

Figure 4.2.33 Reconstructed instantaneous heat transfer coefficients
(air-water; z=1.28 m; r/R=0; Vg=0.05 m/s)

The area of each peak can be calculated by using Simpson's integration method. For example, the area corresponding to the time length from 1 to N can be calculated as:

$$\text{Area} = \sum_{j=1}^{N-1} ((h_j + h_{j+1})/2 - h_{base}) \times \Delta t$$

here, h_j is heat transfer coefficient at time j; h_{base} is the value of baseline of heat transfer coefficient. If h_j or h_{j+1} is less than h_{base}, h_j or h_{j+1} is replaced by h_{base}. Δt is time interval between h_j and h_{j+1}.

Based on the above procedure, one can calculate the areas of individual peaks of instantaneous heat transfer coefficients. Then, the areas with same peak height are added up to obtain the summed area with peak-height (i). The cumulative area with peak height i represents total effect of bubble-wake-induced turbulence on heat transfer with peak height i. Then various cumulative areas with different peak-height i can be classified into an area distribution of various peak-heights of heat transfer coefficients.

By using the method described above, the area distribution of peak heights of heat transfer coefficients can be obtained. To normalize this distribution, which will be independent of the duration of collected data, the summed area for each peak height is divided by total area of all peaks:

$$\phi_i = \frac{\text{area of peak} - \text{height } i}{\text{total area}} \qquad (4.2.19)$$

The normalized distributions are shown in Figure 4.2.34a for the air-water system. This figure shows that the peak height distribution is close to the Gauss distribution for different gas velocities. The mean value and variance of Gauss distribution can therefore be applied to describe the distribution as below:

$$\bar{X} = \frac{\Sigma(\text{area of peak} - \text{height i}) \cdot (\text{peak} - \text{height i})}{\text{total area}} = \sum_{i=1}^{40} \phi_i (i/2 - 0.25) \tag{4.2.20}$$

$$\sigma = \frac{\Sigma(\text{area of peak} - \text{height i}) \cdot [(\text{peak} - \text{height i}) - \bar{X}]^2}{\text{total area}} = \sum_{i=1}^{40} \phi_i [(i/2 - 0.25) - \bar{X}]^2 \tag{4.2.21}$$

here, mean value represents an average value of peak-height (area average peak height) and variance represents the width of peak-height distribution of heat transfer coefficient. The another important statistical parameter is standard deviation, which is defined as:

$$S = \sqrt{\sigma} \tag{4.2.22}$$

Peak frequency and average peak area are other important parameters obtainable from measurements of instantaneous heat transfer coefficients. Here, the peak frequency relates to the frequency of larger bubble passing on the surface of the heat transfer probe. It was counted from sharp peak exhibited in time series measurements of heat transfer coefficients. As observed from Figures 4.2.26 to 4.2.30, a few of the peaks were close to base line which could be a result of local turbulent fluctuation. In order to avoid counting these low height peak-height, a minimum peak-height was defined. To define this minimum peak-height, average peak-height in air-water system at the wall in bulk region were chosen as the basis. For a given gas velocity, peak heights in the wall region were lowest for air-water system indicating absence of larger bubbles. It can be seen from table 4.2.3 that average peak height in the wall region for air-water systems increases with gas velocity.

Table 4.2.3 Average peak height in wall region for air-water system

gas velocity(m/s)	0.05	0.10	0.15	0.20	0.30
peak-height (kW/m^2C)	0.94	1.47	1.79	2.01	2.23

The maximum value of average peak height is in a range of 2.0-2.5. Thus, the minimum peak height to be counted was defined to be 2.25 i.e. whenever peak height is in the ranges of 0-0.5, 0.5-1.0, 1.0-1.5, 1.5-2.0 and 2.0-2.5, the peak is not counted.

By using this procedure, the peak frequency could be obtained by dividing the total peaks for a given time series experiment by data collection time. This peak frequency essentially provides the frequency of bubble-wake associated with larger bubbles.

The average peak area can be now obtained by dividing total area by peak-number. This result represent a combined effect of both intensity and residence time of bubble wake on heat transfer.

Three parameters namely peak-height, peak frequency, and average peak area were now used to analyze instantaneous heat transfer coefficient as a function of operating conditions in different locations of the column. Here, the physical meaning of three parameters can be summarized as follows:

1. peak-height indicates the intensity of a bubble wake turbulence
2. peak frequency indicates the frequency of bubble wake (peak-height > 2.25 kW/m^2C)
3. peak area indicates combined effect of intensity and bubble wake size.

4.2.2.5 Peak Height Distribution

Figure 4.2.34a to c present the distribution of peak heights in air-water system at various gas velocities at the center in the bulk region of the column. These figures show that the peak distribution is close to Gaussian distribution for different gas velocities and slurry concentrations. The mean value and variance of Gaussian distribution can therefore be applied to describe the distribution. It can be seen from Figures 4.2.34a to c that as gas velocity increases, mean value of peak height increases, indicating a stronger intensity of bubble-wake-induced turbulence with increasing gas velocity due to larger bubbles formation. It is also seen that as gas velocity increases, the width of peak-height distribution increases, indicating a wider distribution of bubble-wake-induced turbulence at a higher gas velocity.

As described above, distribution of peak height of instantaneous heat transfer coefficients follows Gauss distribution. Thus, the mean value and standard deviation of peak height distribution can represent the average peak height and the width of peak height distribution. Figures 4.2.35 and 4.2.36 show the variation of mean values of peak heights and their standard deviation with gas velocity for different slurry concentrations. It is seen that both mean and standard deviation of peak height distribution increase with increasing gas velocity and slurry concentration. It can also be observed from Figures 4.2.35 and 4.2.36 that the rate of increase of both average peak height and standard deviation are much faster in the central region compared to the wall region. A smaller variation of standard deviation in the wall region indicates more uniform bubble size distribution in the region.

The variations of peak heights with gas velocity can be compared with measurements of bubble size and bubble chord length distribution reported in literature (Rigby et al., 1970; Ham and Kim, 1990; Everson et al., 1993; Kwon et al., 1994). The size of larger bubbles increases with increasing gas velocity. The larger bubble size leads to higher bubble rise

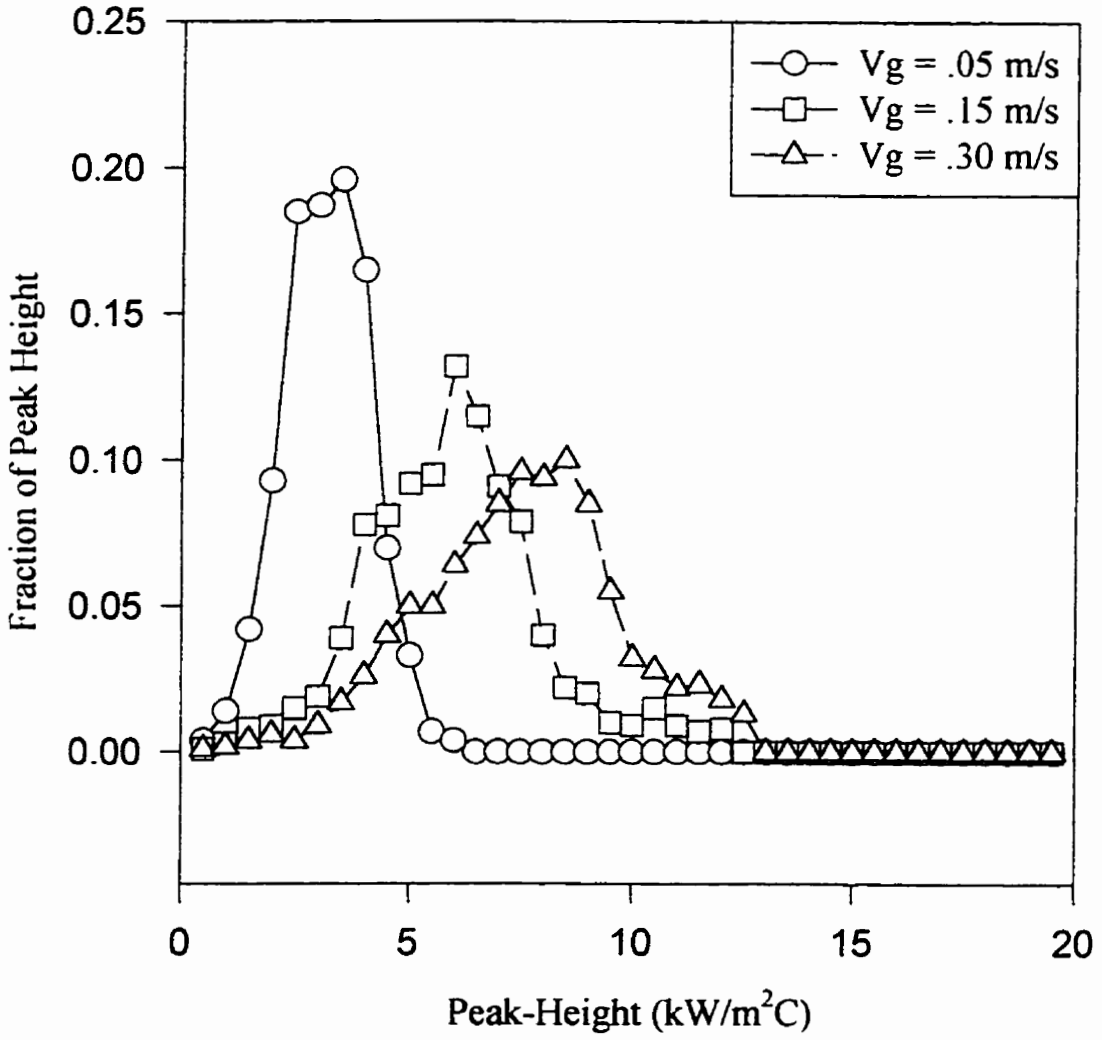

Figure 4.2.34a Peak-height distribution at different gas velocities in air-water system in central region (r/R = 0; z = 1.28 m)

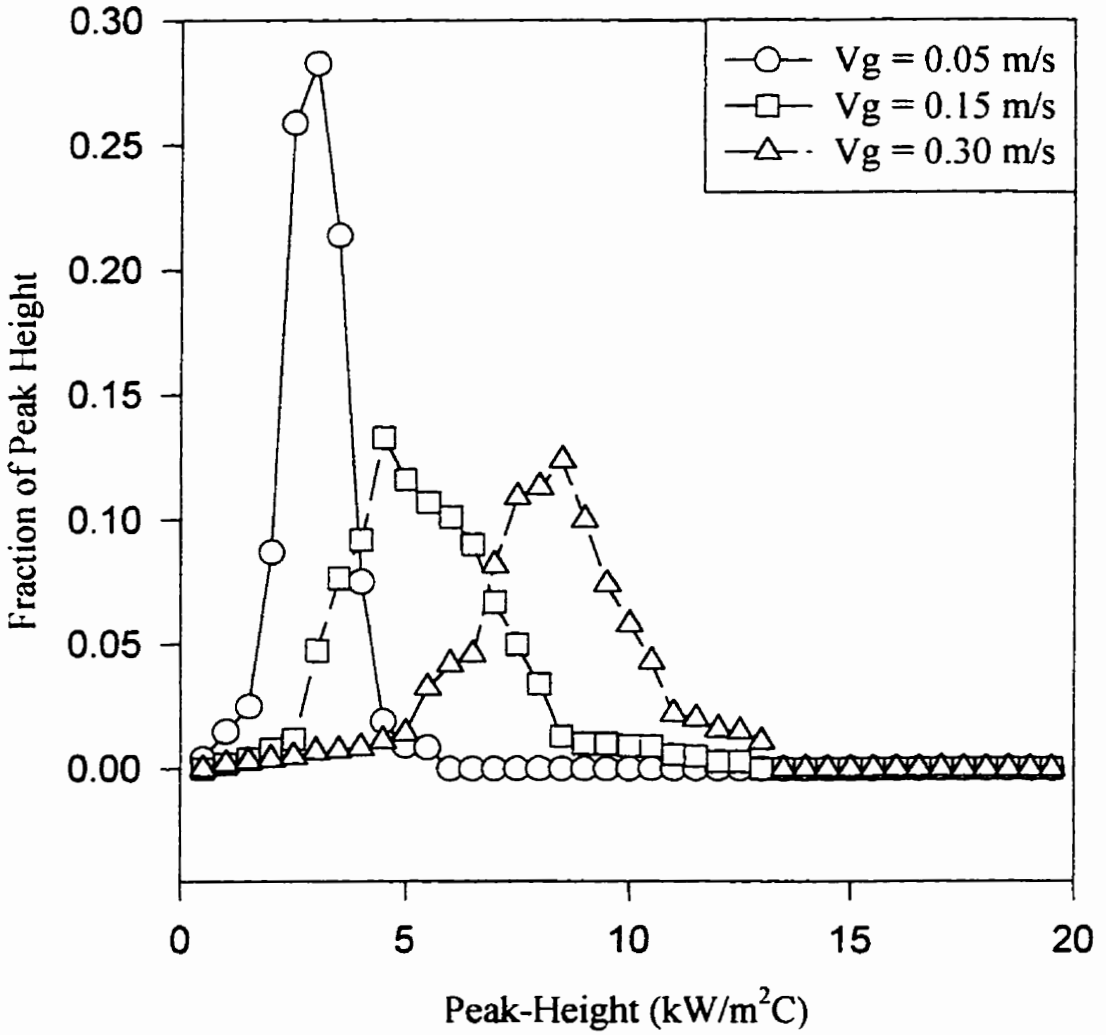

Figure 4.2.34b Peak-height distribution at different gas velocities in slurry concentration of 15 vol.% in central region (r/R = 0; z = 1.28 m)

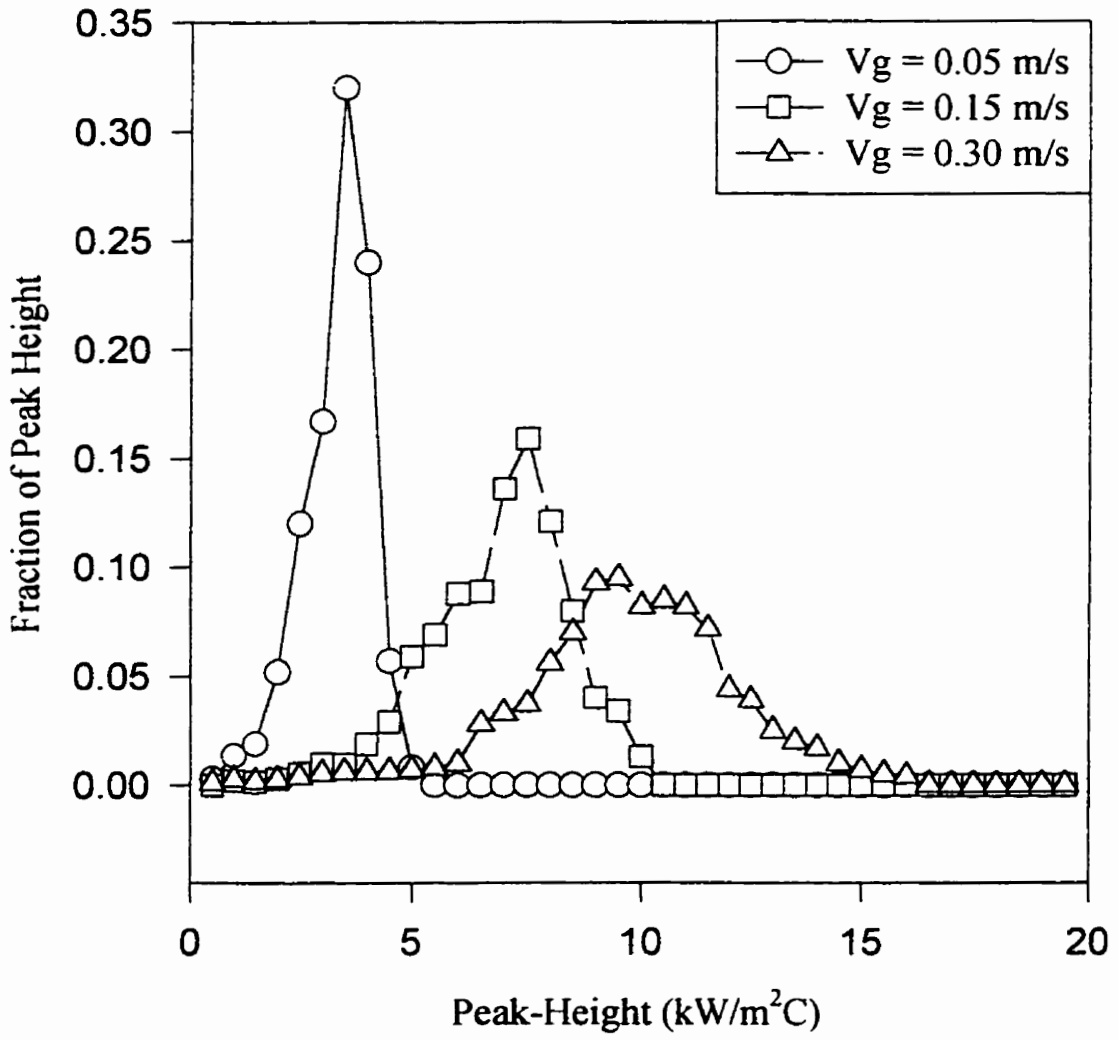

Figure 4.2.34c Peak-height distribution at different gas velocities in slurry concentration of 30 vol.% in central region (r/R = 0; z = 1.28 m)

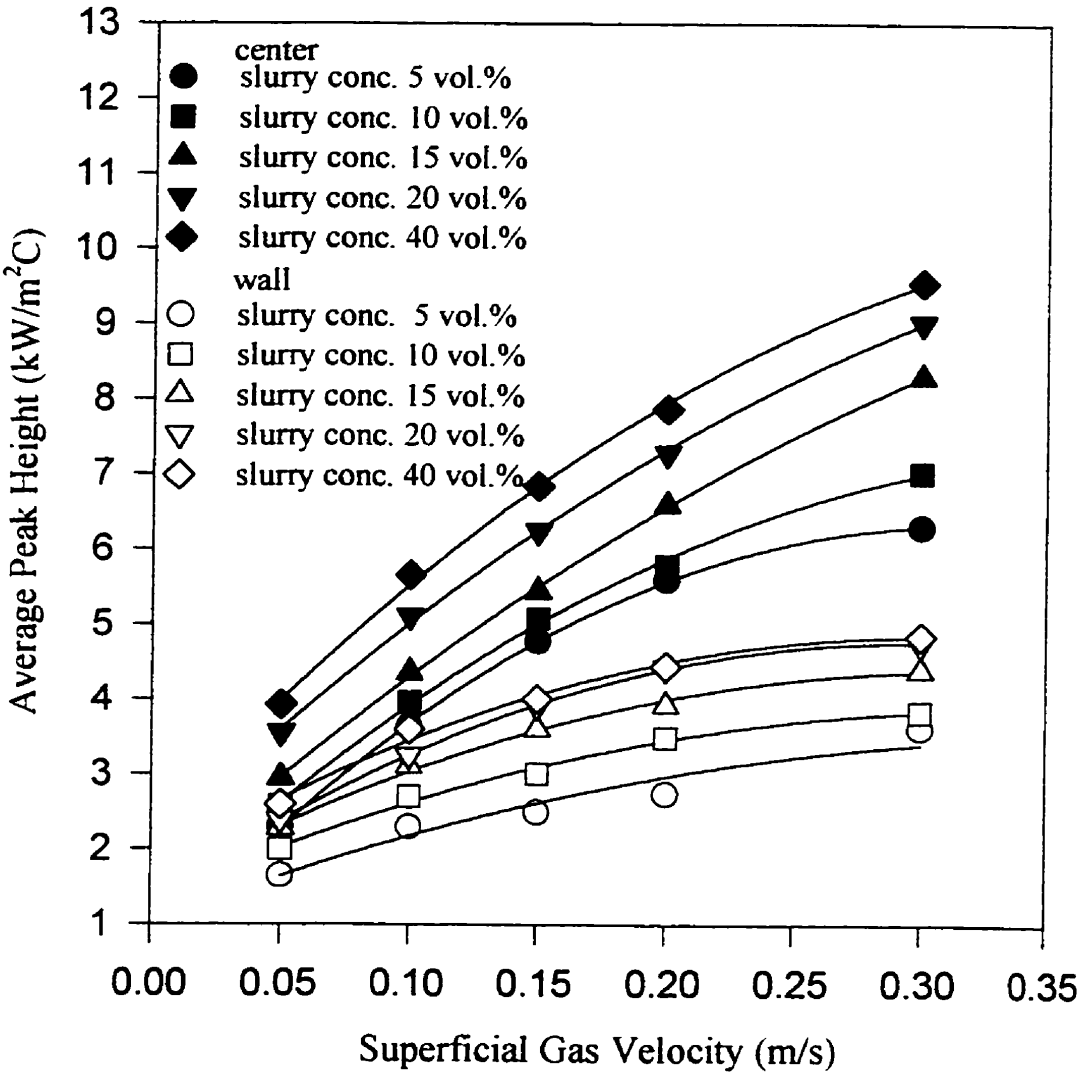

Figure 4.2.35 Variation of average peak-height with superficial gas velocity in central and wall region

(z = 1.28 m)

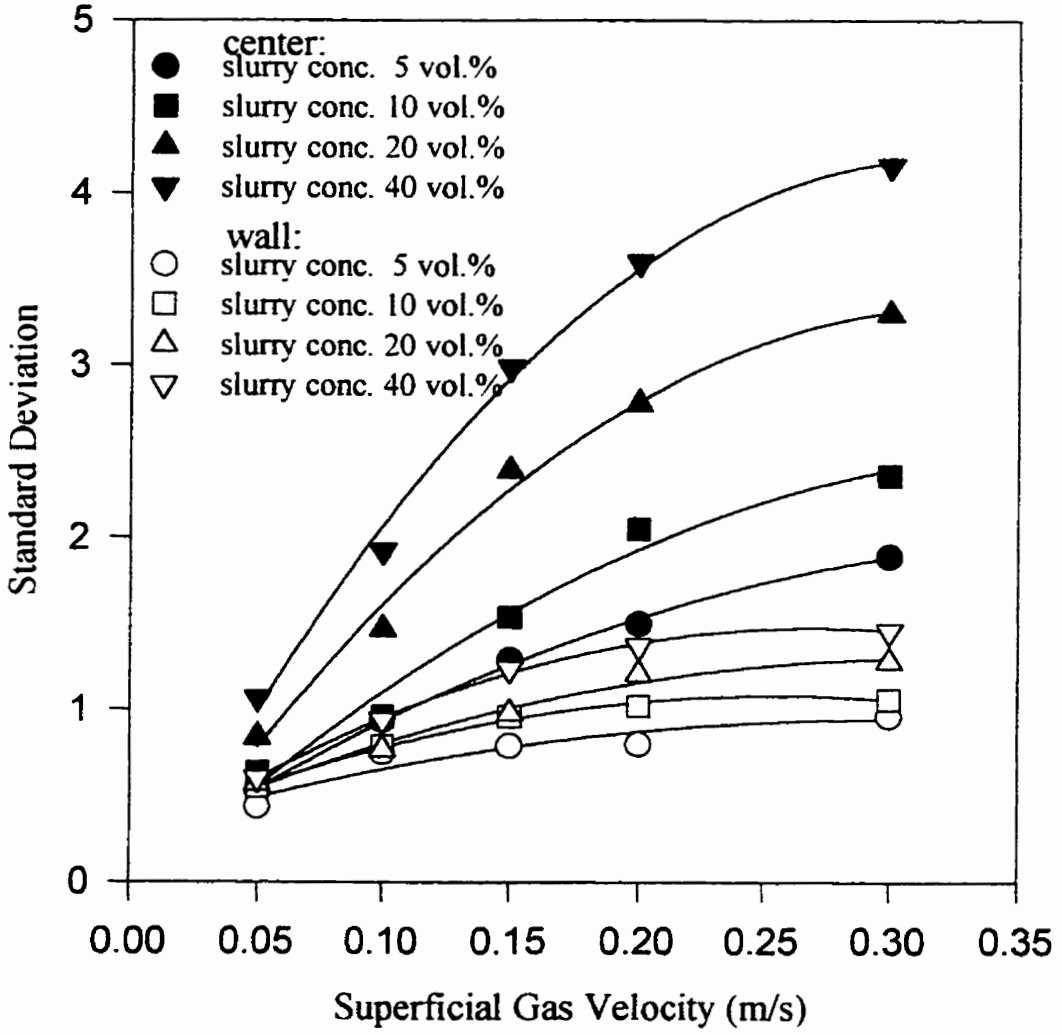

Figure 4.2.36 Variation of standard deviation of peak-height distribution with superficial gas velocity in central and wall region
(z = 1.28 m)

velocity (Rigby et al., 1970). The faster rising bubble would give rise to stronger bubble-wake-induced turbulence, resulting in higher peak height. However, the coalesced larger bubbles can also break up at high shear rate generated by higher gas velocities. Therefore, both bubble coalescence and break up determine the distribution of bubble size. Everson et al. (1993) measured bubble chord length distribution and concluded that the bubble coalescence occurred in a probabilistic manner, thereby giving rise to the broad distribution of bubble chord length in the bed. The standard deviation of the distribution of bubble chord length increased with increasing gas flow rate. Kwon et al. (1994) studied Bubble-Chord Length in a three phase fluidized bed. It was observed that the average bubble-chord length increases almost linearly when gas flow rate is increased from .02 m/s to .10 m/s. They also found that the standard deviation of distribution of bubble-chord length increases with gas velocity. By observing peak-height distribution of heat transfer coefficients, it is found that both mean value and variance of the peak-height increase as gas velocity increases.

In the measurement of instantaneous heat transfer coefficient, peak-height indicates the intensity of bubble-wake-induced turbulence. The increase of average peak-height and standard deviation of peak height distribution with increasing gas velocity can be attributed to the increase of both mean size and standard deviation of bubble size distribution with gas velocity. As gas velocity increases, coalesced larger bubble size increases and bubble rise velocity increases. A coalesced larger bubble would have a larger wake and stronger vortices associated with it. The intensity of bubble-wake-induced turbulence will increase, which results in higher peak-height of the heat transfer coefficient with an increase of gas velocity. A wider bubble size distribution will lead to a wider distribution of peak-height of the heat transfer coefficient.

Meanwhile, a more uniform peak-height distribution (small standard deviation) at low gas velocity (0.05 m/s) can be attributed to a more uniform distribution of bubble size due to low rate of bubbles coalescence or breakup.

The effects of solids addition and slurry concentrations on average peak height at the center are shown in Figure 4.2.37. The curves on Figure 4.2.37 can be divided into three main sections. At low slurry concentrations (< 20 vol.%), the average peak-height of heat transfer coefficient is generally lower than that in the air-water system at different gas velocities. In the range of slurry concentration from 5 vol.% to 20 vol.%, the average peak-height of heat transfer coefficient increases as slurry concentration increases. Average peak-height is unaffected by slurry concentration above 20 vol.%.

The standard deviation of peak height distribution are presented in Figure 4.2.38. It can be seen that the curves are generally similar to the average peak height curves (Figure 4.2.37), with a minimum at 5 vol.% slurry concentration. Standard deviation of peak height distribution, however, continue to increase up to 30 vol.% slurry concentration, especially for higher gas velocities (> 0.15 m/s). There is practically no change in standard deviation from 30 to 40 vol.% slurry for all gas velocities.

The lowering of average peak height in the first section can be attributed to the dampening effect of solid particles on bubble wake turbulence. The heterogeneous effects caused by the particles in the bubble-wake destroy ordered motion/circulation, resulting in reduced vortical strength inside the bubble-wake (Raghunathan et al., 1992). Moreover, the addition of fine particles also increases suspension viscosity, which would aid the reduction of the circulation rate inside the bubble-wake. Therefore, intensity of bubble-wake-induced turbulence is reduced due to solids addition into water.

The average peak-height increased as slurry concentration increased from 5 vol.% to 20 vol.%. As slurry concentration increases, larger bubble size increased, as observed from bubble population and bubble rise velocity study (sec. 4.1.3). However, the strength of the vortical flow would continue to decrease. Moreover, the ratio of wake volume to bubble volume also decreases as slurry concentration increases (sec. 4.2.2.7). Obviously, the increase in bubble size due to increasing slurry concentration is predominant in this range of slurry concentration.

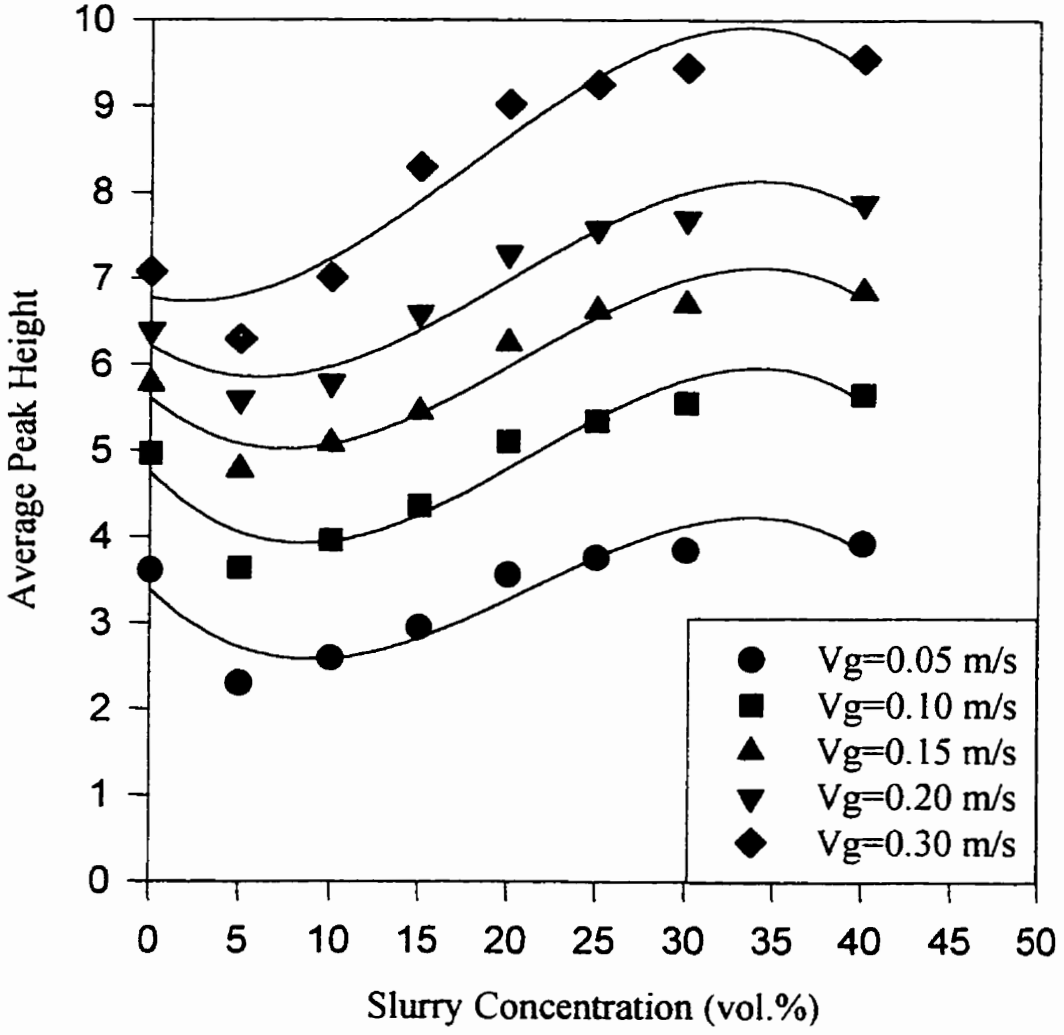

Figure 4.2.37 Variation of average peak height with slurry concentration in the central region

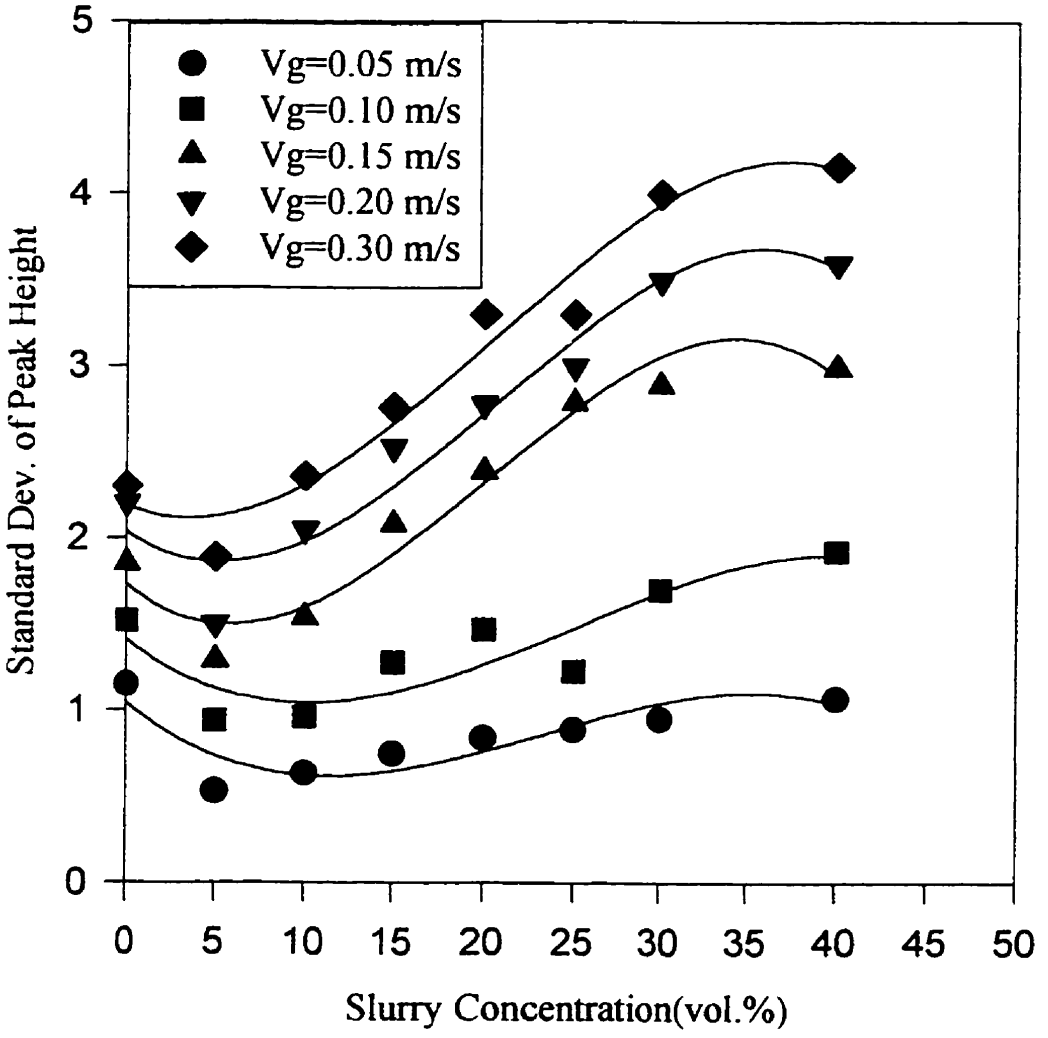

Figure 4.2.38 Standard deviation of peak height in center as a function of slurry concentration

As slurry concentration increases from 20 vol.% to 40 vol.%, the average peak height is not increased further. It may be pointed out that rise velocity of larger bubbles was also not found to increase significantly over the slurry concentration range of 20 to 40 vol.% (sec. 4.1.3). However, apparent slurry viscosity and particle-particle interactions would continue to increase with increasing slurry concentrations. There is, however, no apparent effect of these factors on average peak height.

The average heat transfer coefficient, however, was found to decrease with increasing slurry concentrations (sec. 4.2.1). The base line values of heat transfer coefficients were therefore compared. Figure 4.2.39 shows that baseline heat transfer coefficients continued to decrease with increasing slurry concentration, thus lowering the average heat transfer coefficients. The baseline values of instantaneous heat transfer coefficient measured at wall and central regions are compared in Figure 4.2.40. It is interesting to note that the baseline values for the two regions are close in air-water system and 40 vol.% slurry concentration. For intermediate slurry concentrations, baseline values at the center are higher than at wall.

The baseline values of heat transfer coefficient can be related to bulk turbulence in the region. The bulk turbulence can be attributed mainly to the micro eddies generated by dissipation of bubble wake formation and shedding process. This process seems to be nearly uniform in air- water system across column cross-section, when baseline values at wall and center are close. However, with addition of solids, a radial profile of solids concentration would begin to develop, with a higher solids concentration in the wall region. Radial concentration profiles in slurry bubble column have been reported in literature (Pandit and Joshi, 1984; Gandhi et al., 1998). Higher solids concentrations in the wall region will reduce eddies dissipation rate causing turbulence level to drop there. At highest slurry concentration of 40 vol.%, there is no difference in baseline values at wall and at center (Figure 4.2.40). This indicates that solids concentration gradients become nearly uniform across the column cross-section at this concentration. The radial

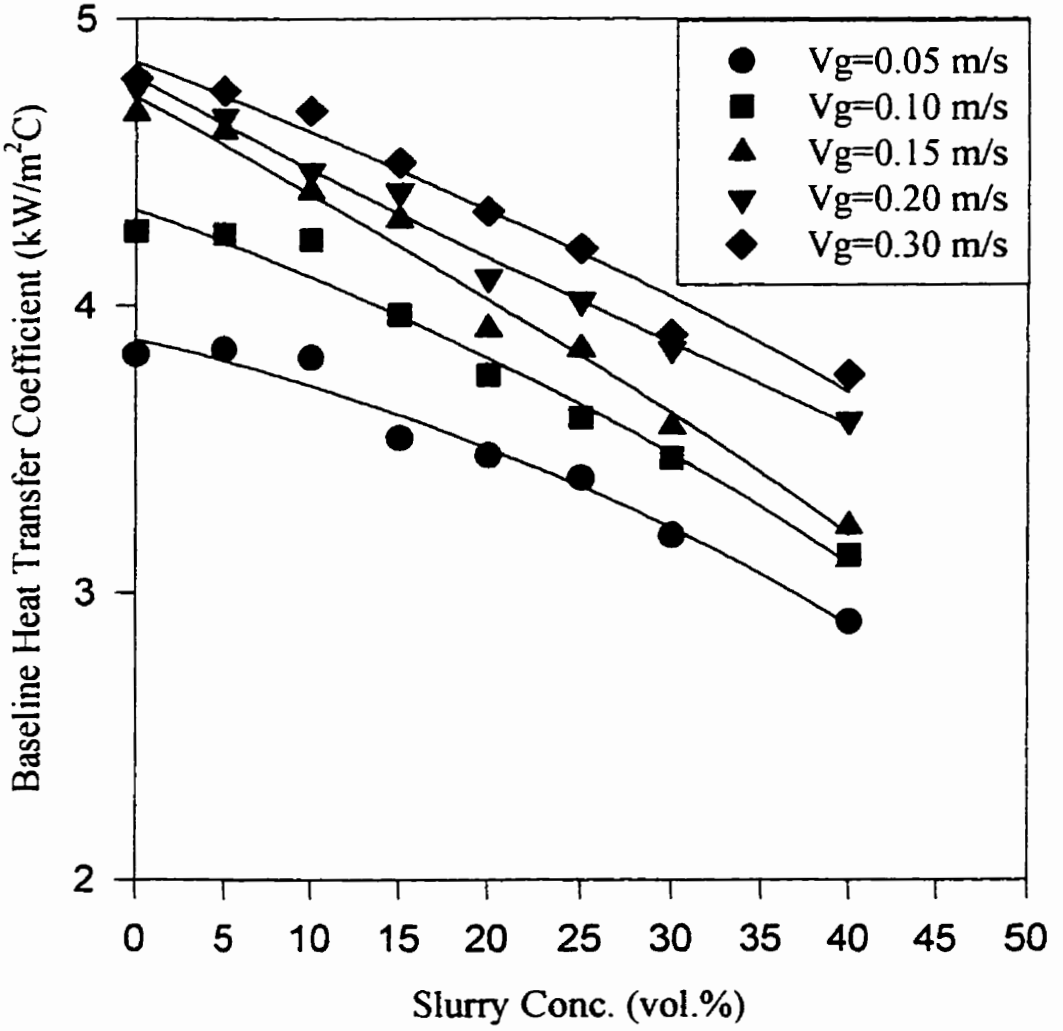

Figure 4.2.39 Baseline heat transfer coefficients as a function of slurry concentration at column center

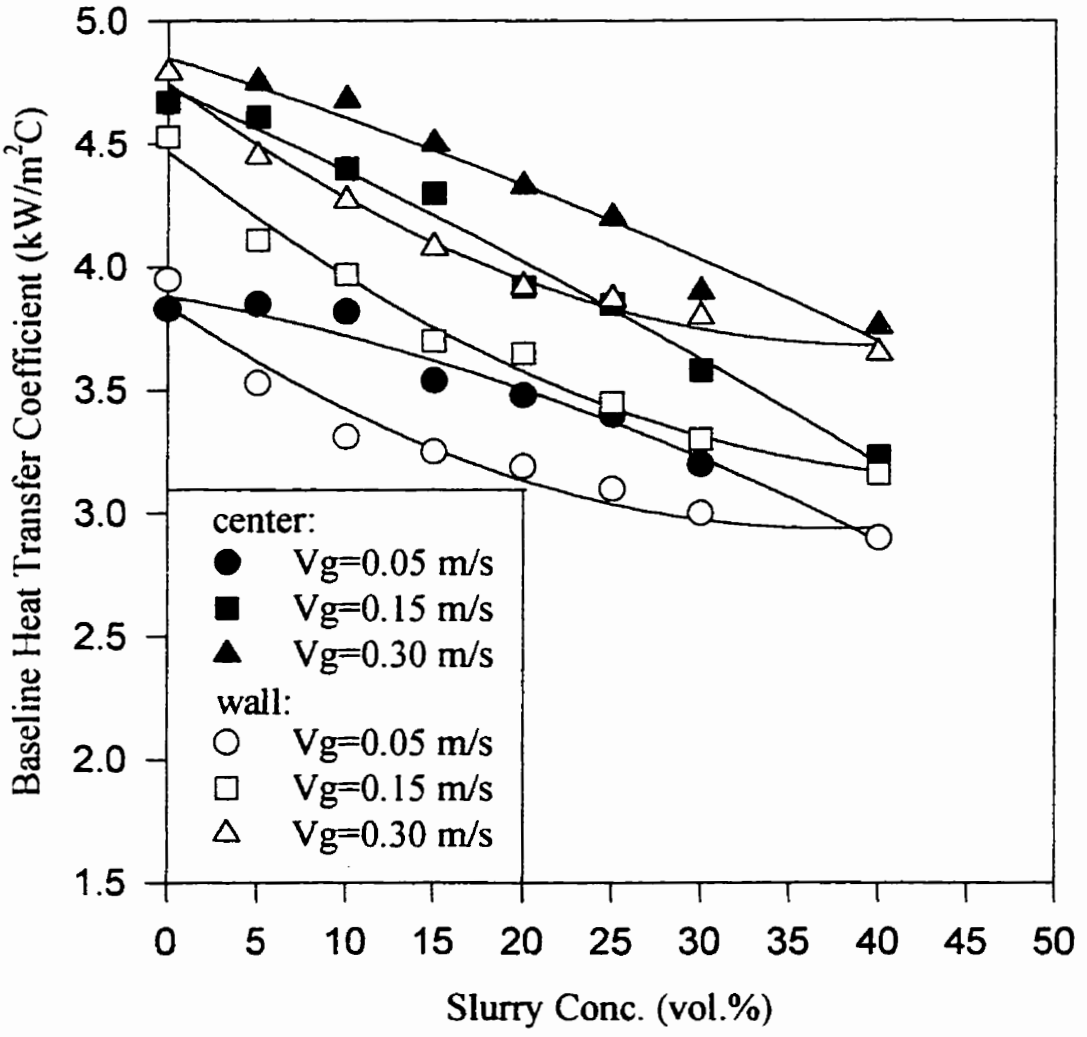

Figure 4.2.40 Comparison of baseline values of instantaneous heat transfer coefficients in center and in the wall

concentration profiles have been shown to become flatter with increasing slurry concentrations (Gandhi et al., 1998).

Average peak-height of heat transfer coefficients in the region near the column wall are shown in Figure 4.2.41 for various slurry concentrations. It can be seen that average peak height increases continuously with slurry concentration up to 20 vol.% with no minimum value was observed. Beyond slurry concentration of 20 vol.%, average peak-height remains essentially unchanged. The minimum is observed at center where bubbles are significantly larger and strength of vortical motion is higher. The addition of solids has a larger influence on dissipation of vortical motion in bubble wake.

Figure 4.2.42 shows that standard deviation of peak heights in the wall region follow the trends observed with average peak height variations. There is no minimum observed. Standard deviations don't vary significantly above slurry concentration of 20 vol.%. However, comparison of Figures 4.2.38 and 4.2.42 shows that standard deviation of peak heights in the wall region are low compared to central region, i.e. bubbles are more uniformly distributed in the wall region.

4.2.2.6 Peak Frequency

The peak frequency are presented in Figures 4.2.43 as a function of gas velocity in the center for bulk region of column. It can be seen that peak frequency becomes nearly constant above gas velocity of 0.15 m/s. Peak frequencies in the wall region are generally lower than at center. The difference is more significant at lower gas velocities ($\leq$ 0.15 m/s) and lower slurry concentration ($\leq$ 10 vol.%).

As described above, the peak frequency represents the number of bubble wakes detected by the heat transfer probe. The increase of bubble frequency with gas velocity have been reported by Rigby et al. (1970). These authors have reported lower frequency of bubbles in the wall region which supports the observations in this study.

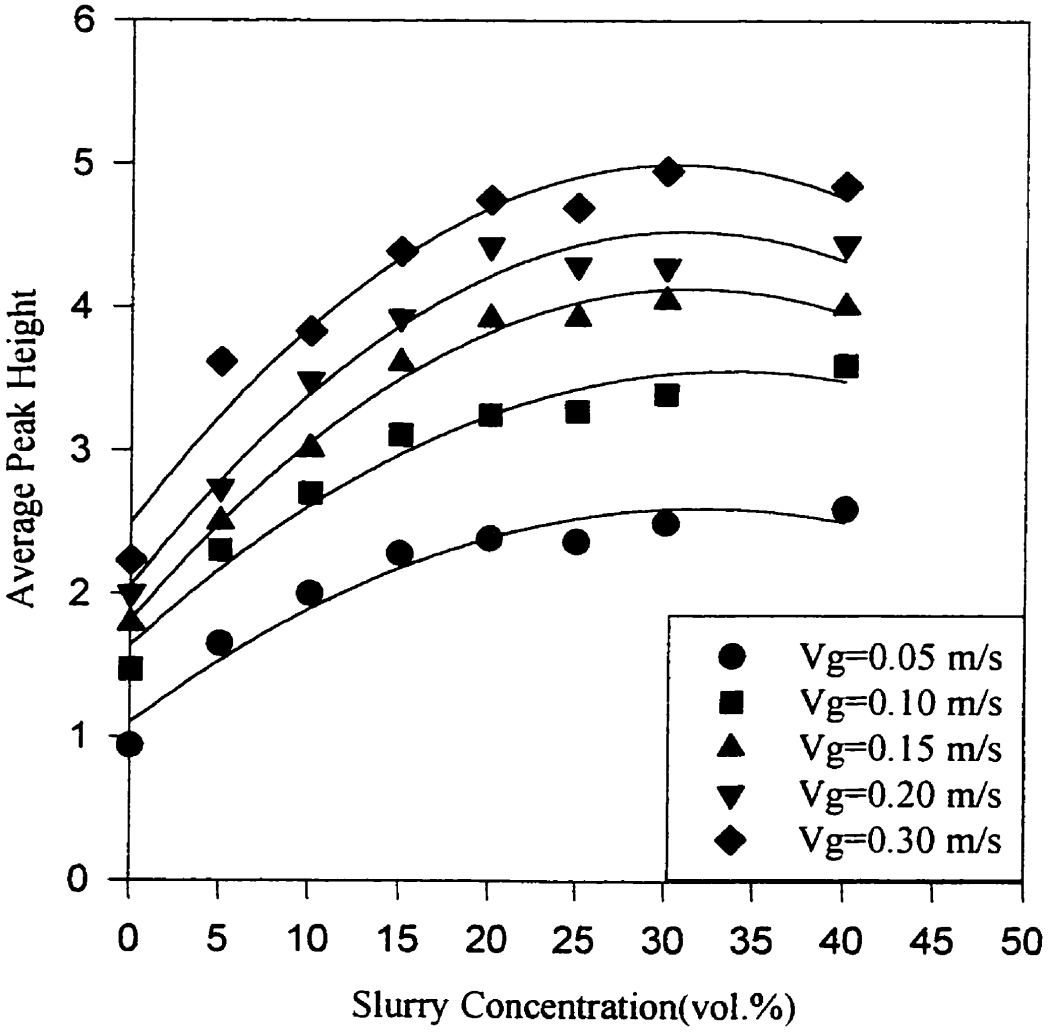

Figure 4.2.41 Variation of average peak height with slurry concentration in the wall region

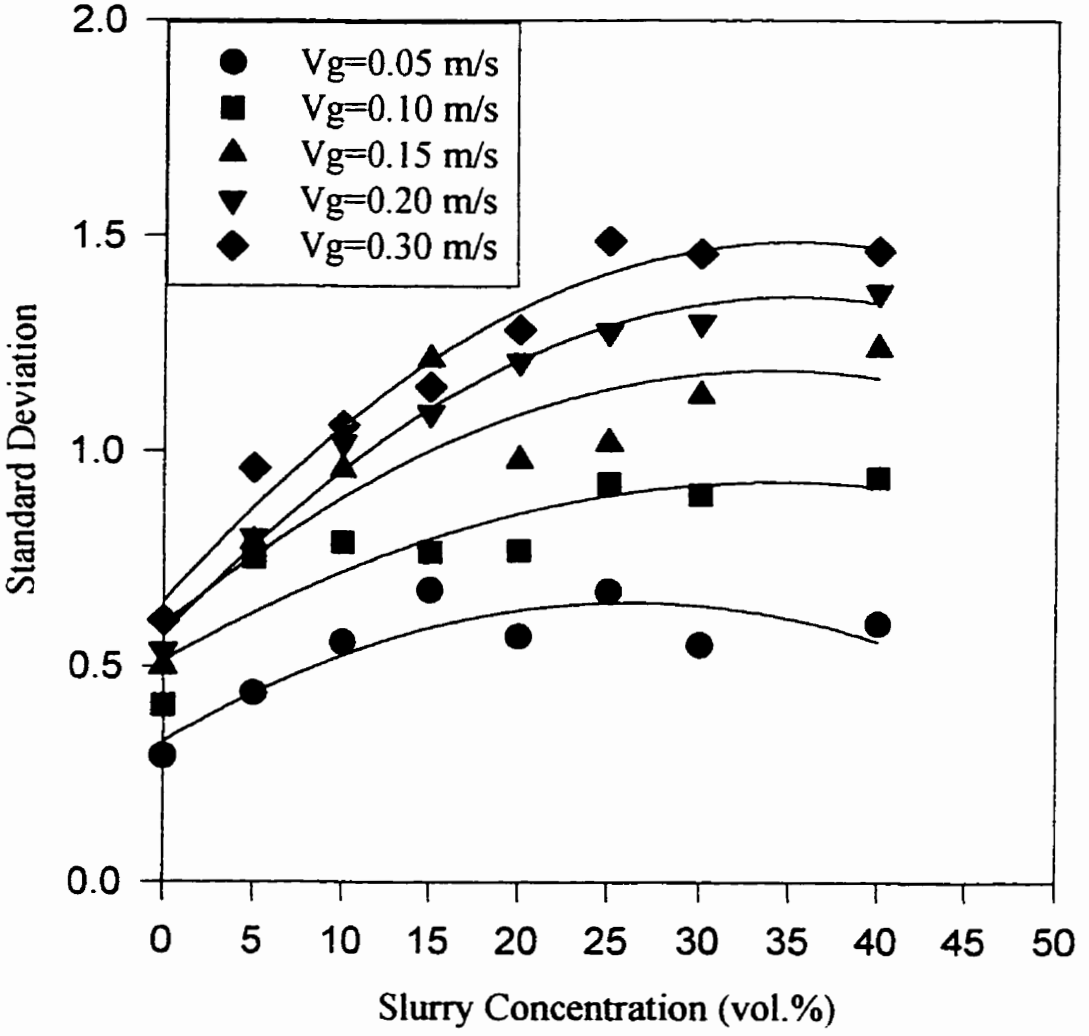

Figure 4.2.42 Standard deviation of peak height distribution in the wall

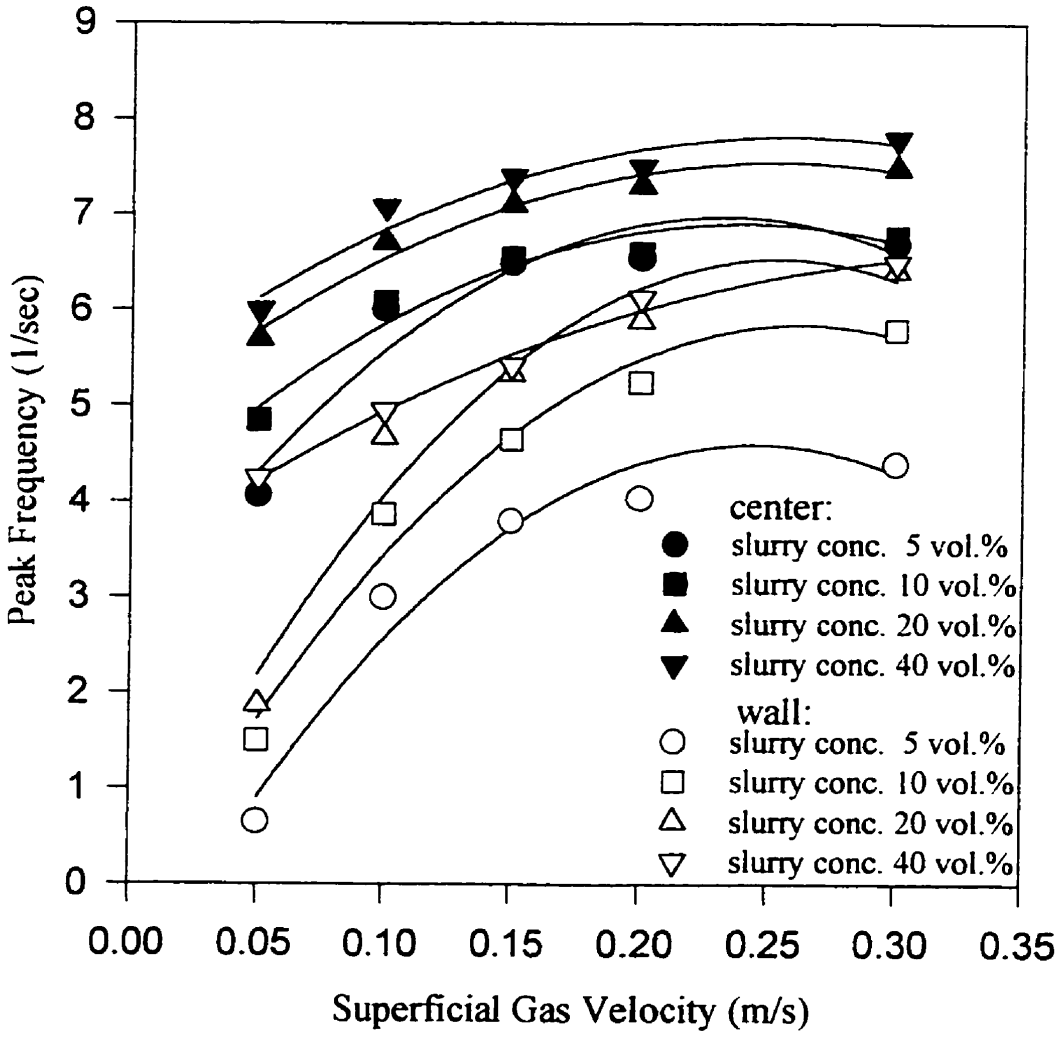

Figure 4.2.43 Variation of peak frequency with superficial gas velocity in central and wall region

Variations of peak frequencies with slurry concentration at central region of the column are presented in Figure 4.2.44. It is seen that the curves follow the trends observed with variation of average peak height with slurry concentration (Figure 4.2.37). First, there is a drop in peak frequency with the addition of solids. Peak frequency then increases as slurry concentrations increase from 5 to 20 vol.%. For higher slurry concentrations (> 20 vol.%) there is no significant change in peak frequency. It can also be observed from Figure 4.2.44 that there is a significant increase in peak frequency from gas velocity of 0.05 m/s to 0.10 m/s, transition from dispersed bubble flow regime to heterogeneous regime.

Figures 4.2.43 and Figure 4.2.44 also indicate that peak frequency reaches maximum value of about 7 s^{-1} asymptotically.

Comparison of peak frequencies in the central and wall regions (Figures 4.2.44 and 4.2.45) shows that there is no drop in frequency with the addition of solids at wall region. Instead peak frequency increases at a faster rate in the wall region with increasing slurry concentrations. For gas velocities higher than 0.05 m/s, the peak frequencies reach asymptotic values above slurry concentration of 20 vol.%, and generally get closer to values at the center. This indicates more uniform bubble distribution at higher slurry concentrations across column cross-section. For the low gas velocity of 0.05 m/s, the peak frequency continued to increase beyond slurry concentration of 20 vol.%, approaching the values in the central region. Again, the bubble distribution is becoming more uniform across the column.

4.2.2.7 Average Peak Area

Average peak-areas as a function of gas velocity are plotted in Figure 4.2.46 for slurry concentrations up to 40 vol.%. As gas velocity increases, the peak-area increases at a higher rate in the center and slowly in the wall region. As gas velocity increases,

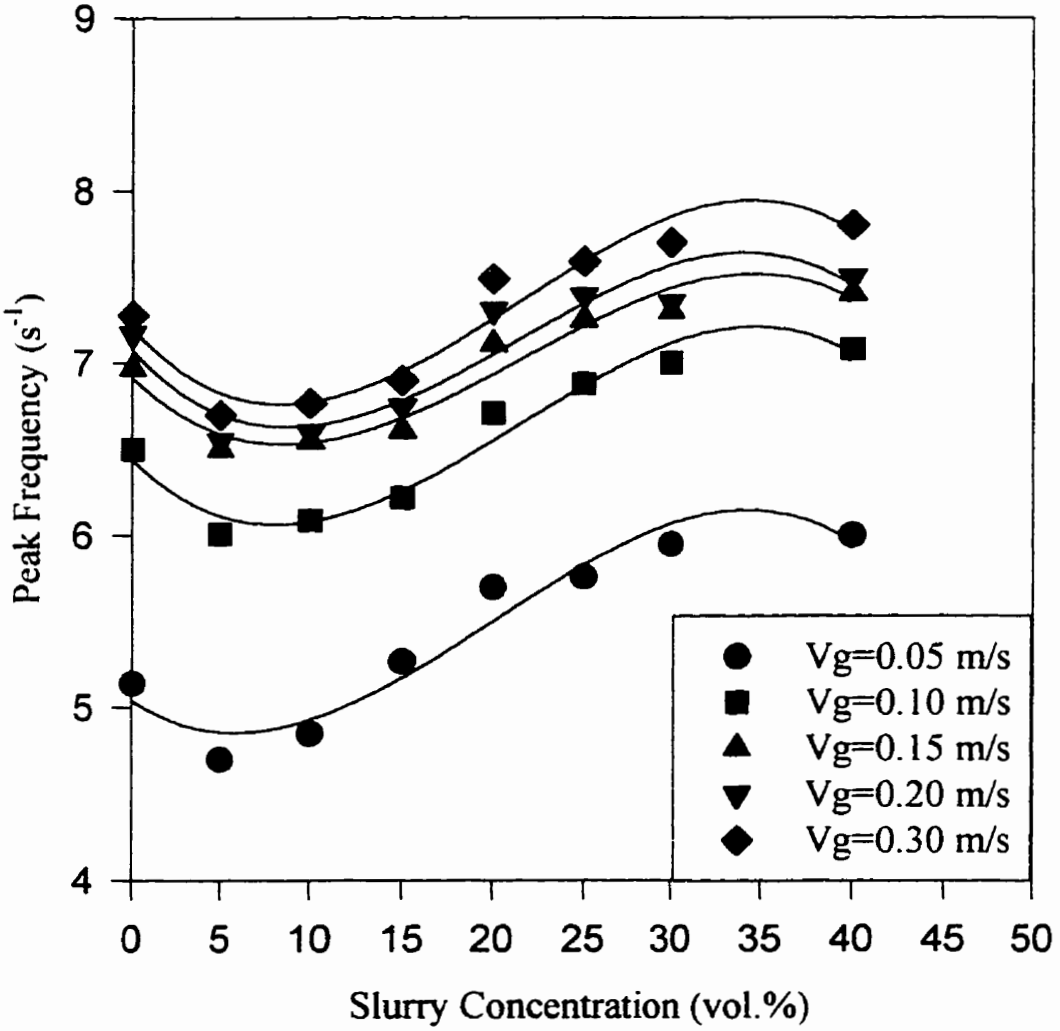

Figure 4.2.44 Variation fo peak frequency with slurry concentration in the central region

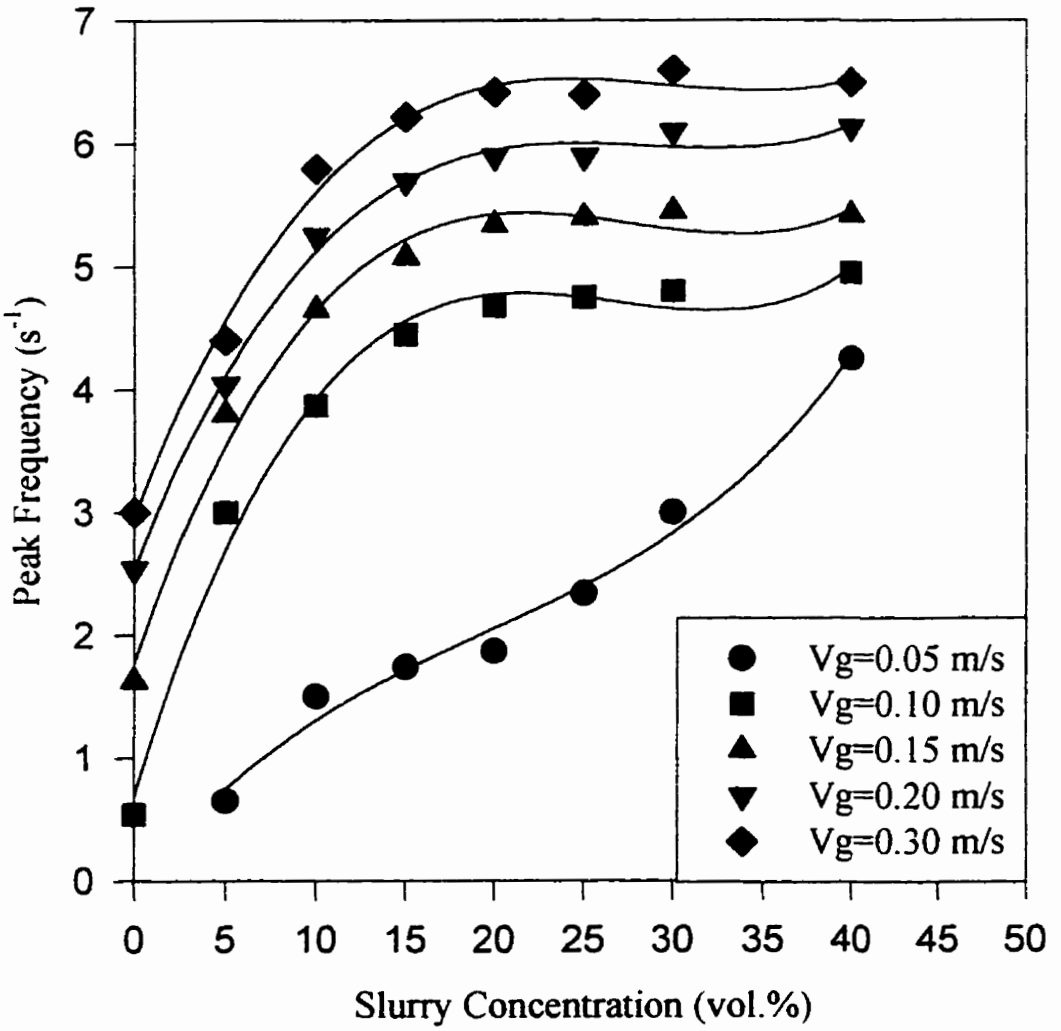

Figure 4.2.45 Variation of peak frequency with slurry concentration in the wall region

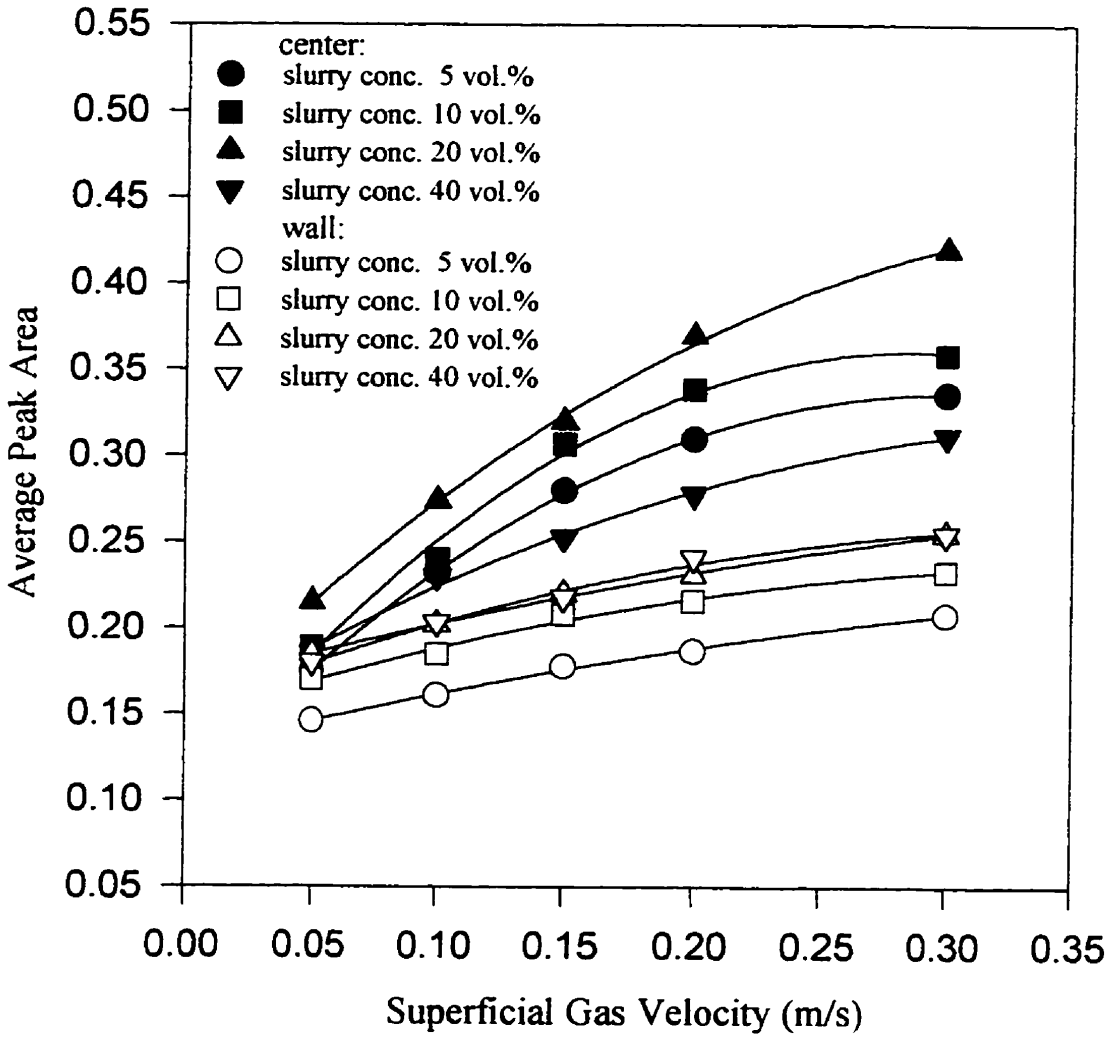

Figure 4.2.46 Variation of peak-area with superficial gas velocity in central and wall region

coalesced bubble size increases. As a result, the intensity of bubble-wake-induced turbulence will be increased. The wake-volume behind the larger bubble would also be increased, since bubble-wake volume is proportional to bubble volume.

The average peak-area in the central region is systematically higher than that in the wall region, due to larger bubbles passing in the central region. Figure 4.2.46 also shows that average peak areas in the central region are lower for a slurry concentration of 40 vol.% than for a 5 vol.% slurry, although there is an increase from 5 to 20 vol.% slurry concentration.

Figure 4.2.47 presents how the average peak area in the central region varied with slurry concentration for constant gas velocities. With the addition of solids, average peak areas passed through a minimum (at 5 vol.%) and through a maximum (at 20 vol.%) and generally drop to values below air-water system for high slurry concentration of 40 vol.%.

The average peak area is a combination of bubble wake turbulence intensity and its size. The initial drop in average peak area with the addition of solids can be attributed mainly to reduction in bubble-wake turbulence intensity compared to air-water system. The bubble rise velocity was found to increase with slurry concentration at a relatively fast rate up to slurry concentration of 20 vol.% (sec. 4.1.3). The faster rising bubbles and their associated wake would enhance heat transfer rates as they move past the probe. There is no significant increase in bubble rise velocity beyond slurry concentration of 20 vol.%. However, apparent slurry viscosity would continue to increase and fraction of wake volume would continue to decrease with increasing slurry concentration. The decrease in wake volume would reduce contact time or residence time of bubble wake at the probe. This is also supported by the observed decrease in peak width at higher slurry concentrations (Figure 4.2.48). It can be seen from Figure 4.2.48 that peak widths are generally lower in 30 vol.% slurry concentration compared to 5 vol.% slurry.

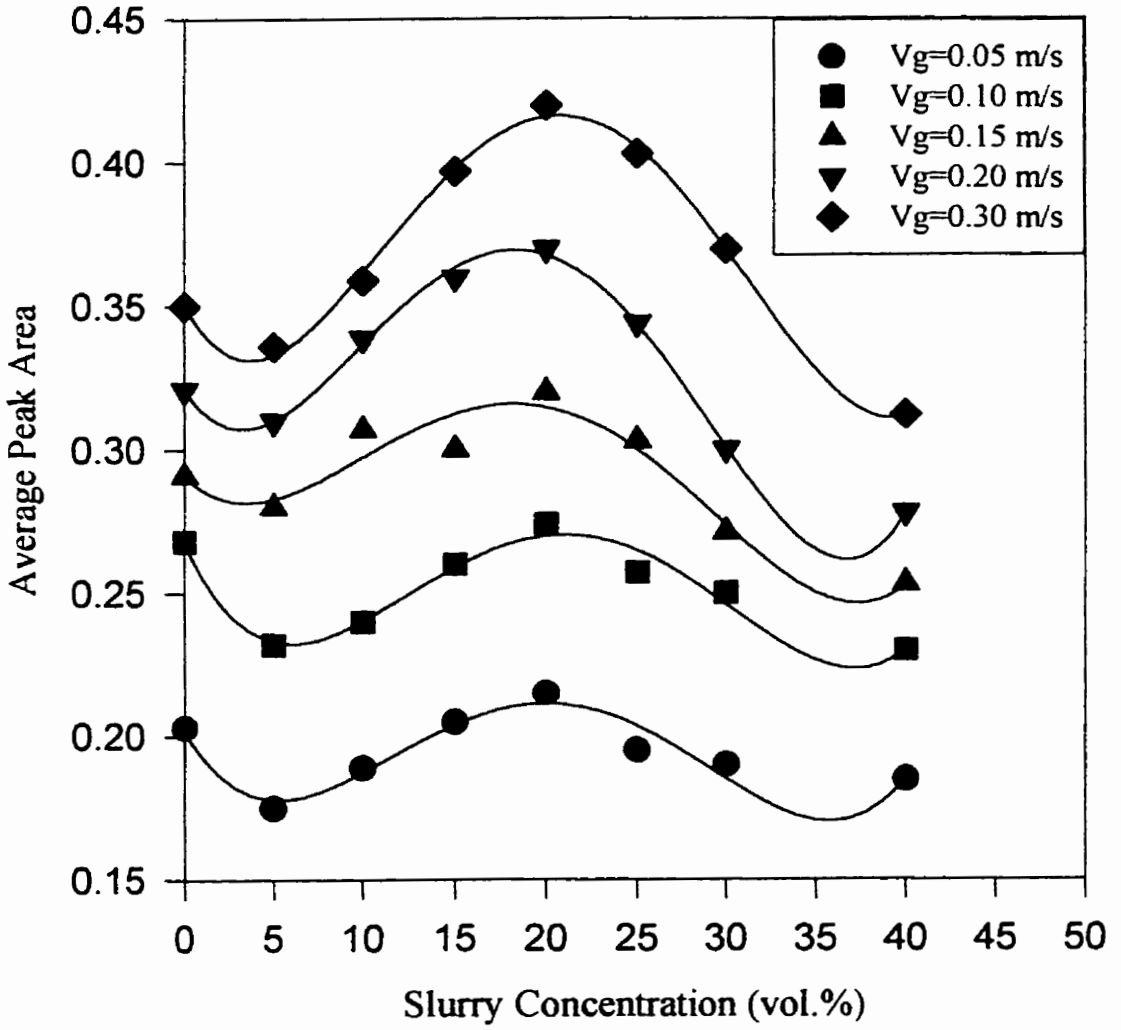

Figure 4.2.47 Variation of average peak area with slurry concentration in the central region

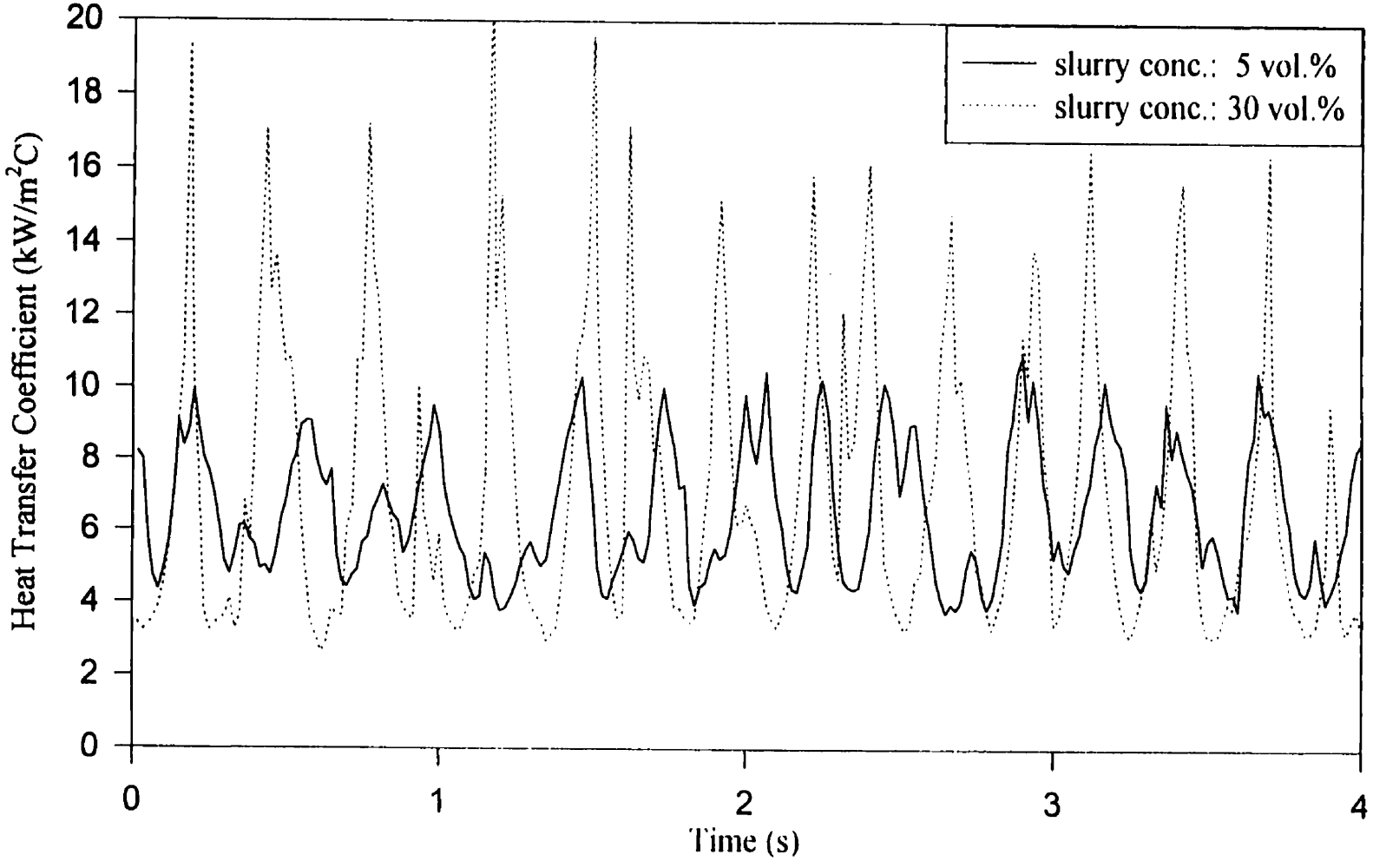

Figure 4.2.48 Comparison of instantaneous heat transfer coefficients in low and high slurry concentration systems (center; Vg=0.30 m/s)

Fan (1989) has summarized various correlations for predicting relative wake holdup k (the ratio of bubble-wake volume and bubble volume) in three phase system. For slurry bubble columns, the model proposed by Bhatia and Epstein (1974, in Fan, 1989) is generally recommended, which is expressed as:

$$k = k_o^{'}(1-\varepsilon_s)^3 \qquad (4.2.23)$$

here, $k_o^{'}$ is calculated by following equation (El-Temptamy and Epstein, 1978):

$$k_o^{'} = 0.61 + \frac{0.037}{\varepsilon_g + 0.013}$$

Figure 4.2.49 presents the results of calculations. It is can be seen that the ratio of bubble-wake volume to bubble volume decreases as slurry concentration increases, reaching between 0.2 to 0.3 at the highest slurry concentration.

In the wall region, the average peak areas, initially increased with increasing slurry concentration (up to 15 vol.%), reaching nearly a constant value (Figure 4.2.50). These observations can be compared with variations of average peak heights (Figure 4.2.41) and peak frequency (Figure 4.2.45) in the wall region. Both average peak height and peak frequency approach nearly constant values above slurry concentration of 15 vol.%. These values, however, increase with increasing gas velocity in the column.

4.2.2.8 Heat Transfer Mechanism due to Bubble Wake Dynamics

The above discussion can be summarized as presented below to elucidate the mechanism of the heat transfer process in the region:

1) Initially, when fine particles are added into water, the turbulence intensity of the wake drops due to the reduction of vortical strength. The solid particles can dampen the

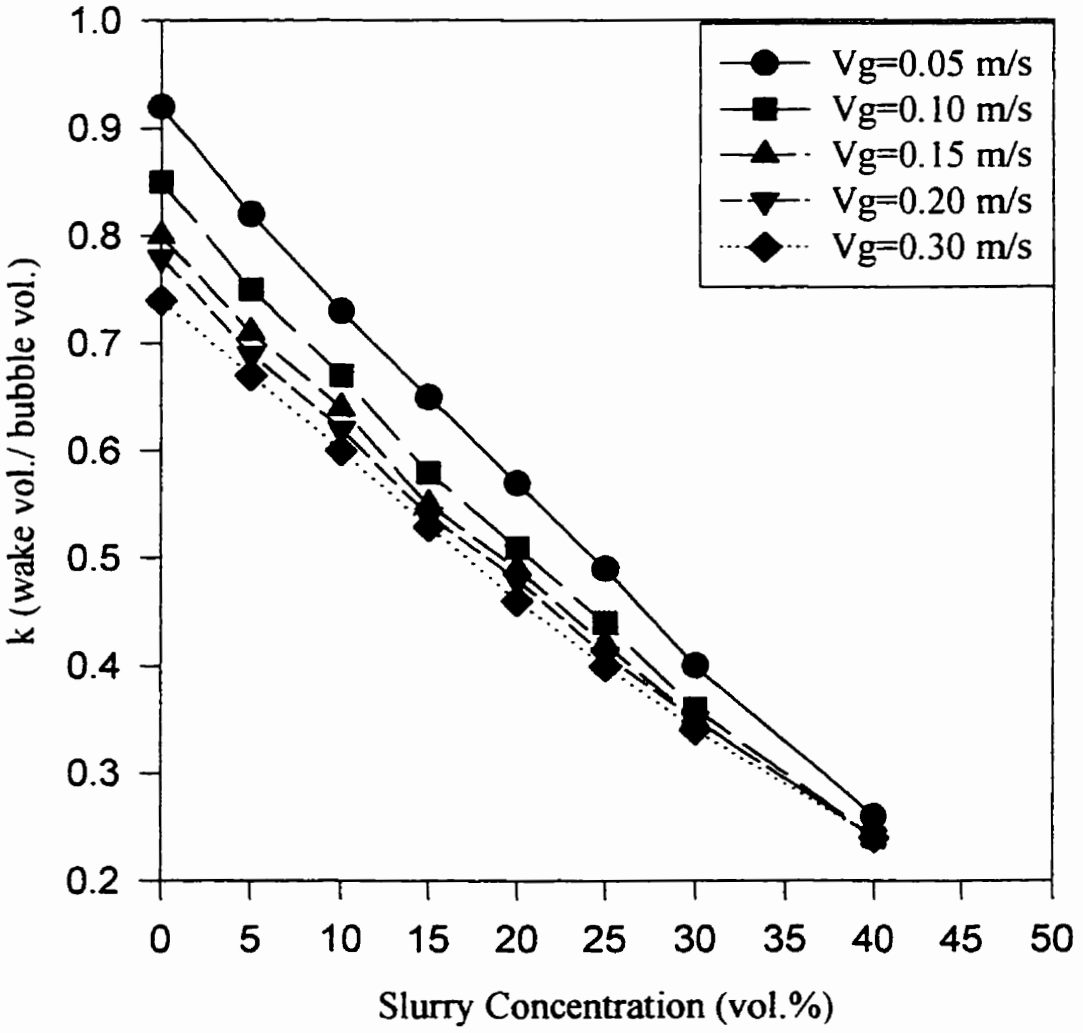

Figure 4.2.49 Ratio of wake volume to bubble volume as a function of slurry concentration

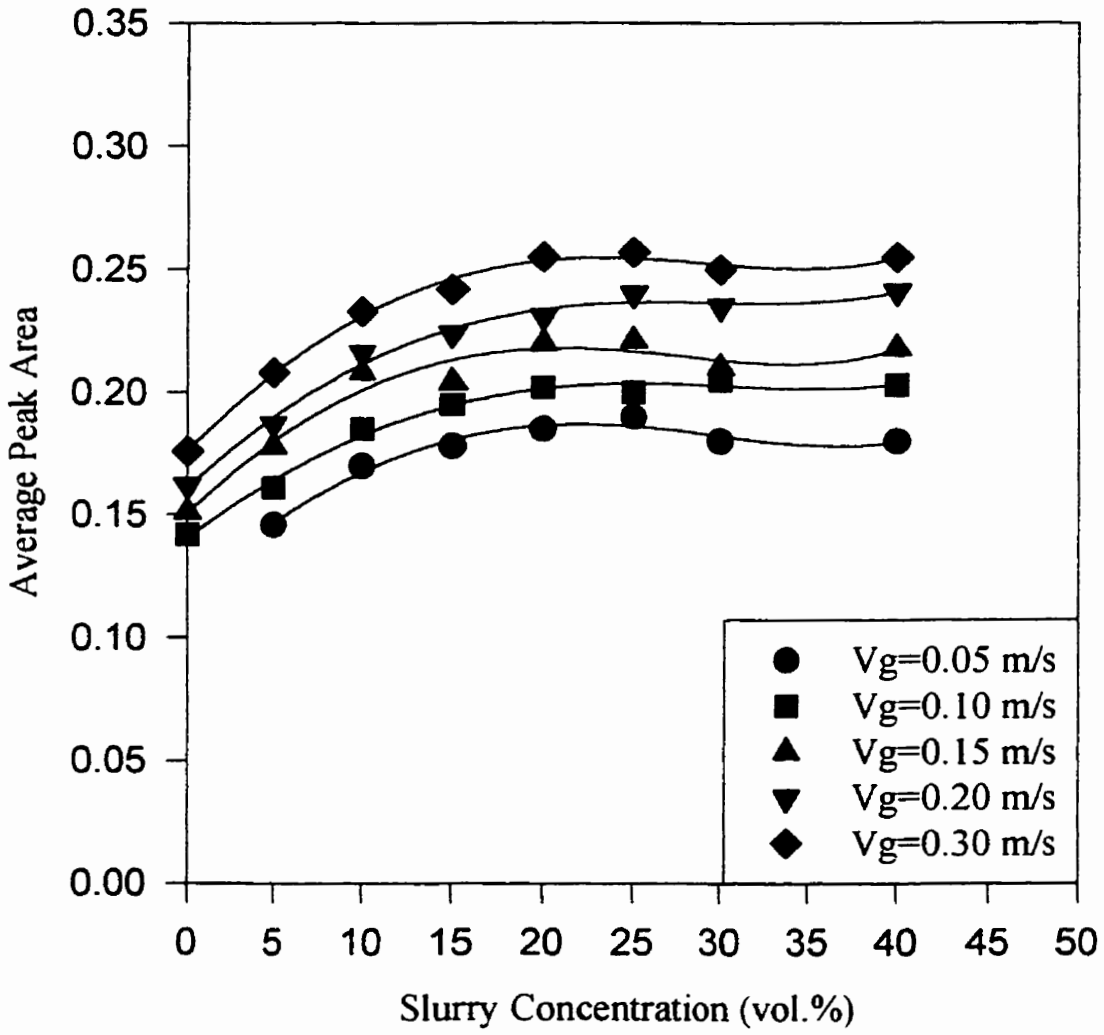

Figure 4.2.50 Effects of slurry concentration on average peak area in the wall region

strength of vortical motion and reduce the heat transfer coefficient. This leads to reduction of peak height and average peak area.

2) Secondly, in slurry concentration range from 5 vol.% to 20 vol.%, the larger bubble rise velocity increases with slurry concentration at a relatively fast rate (sec. 4.1.3). The faster rise velocity of larger bubbles would improve the turbulence intensity of the bubble-wake region although the increased slurry viscosity and reduced ratio of wake volume to bubble volume would tend to reduce the effect of turbulence induced by bubble-wake. The faster rising bubble rise velocity effects seem to predominate in this range. Both peak height and peak area increase with increasing slurry concentrations.

3) For slurry concentrations above 20 vol.%, the rise velocity of larger bubbles was not found to increase significantly (see sec. 4.1.3). Thus the bubble wake turbulence intensity is not significantly affected, resulting in relatively constant peak height values. However, the ratio of wake volume to bubble volume keep reducing and slurry viscosity is increasing with increasing slurry concentrations. These two effects, therefore, reduce the average peak area.

4.2.2.9 Radial Profile of Average Peak Height

Complete radial profiles of average peak heights of heat transfer coefficients are presented in Figure 4.2.51a to 4.2.51c. It can be seen that peak heights decrease with increasing radial distance from the center. This result can be compared to radial distribution of bubble size. Yu and Kim (1988) observed that the bubble chord length decreased with an increase of radial distance.

It can be seen from Figures 4.2.51a to 4.2.51c that the gradient is generally higher in the region from r/R = 0.5 to 1.0 and profiles are flatter in the region from r/R = 0 to 0.5. It can also be seen from these figures that profiles are steeper for air-water system and become flatter with addition of solids particles. This can again be attributed to formation

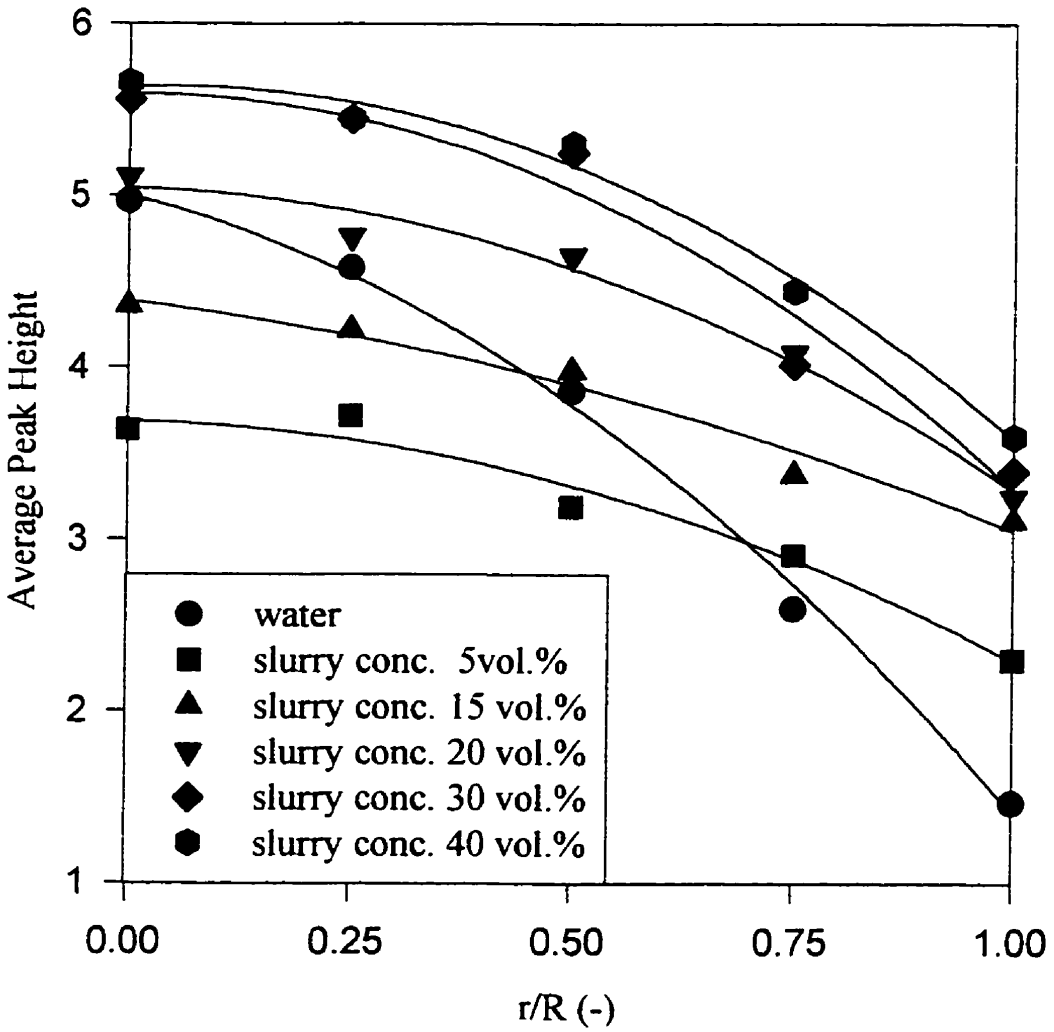

Figure 4.2.51a Radial profile of average peak heights for different slurry concentration (Vg= 0.10 m/s)

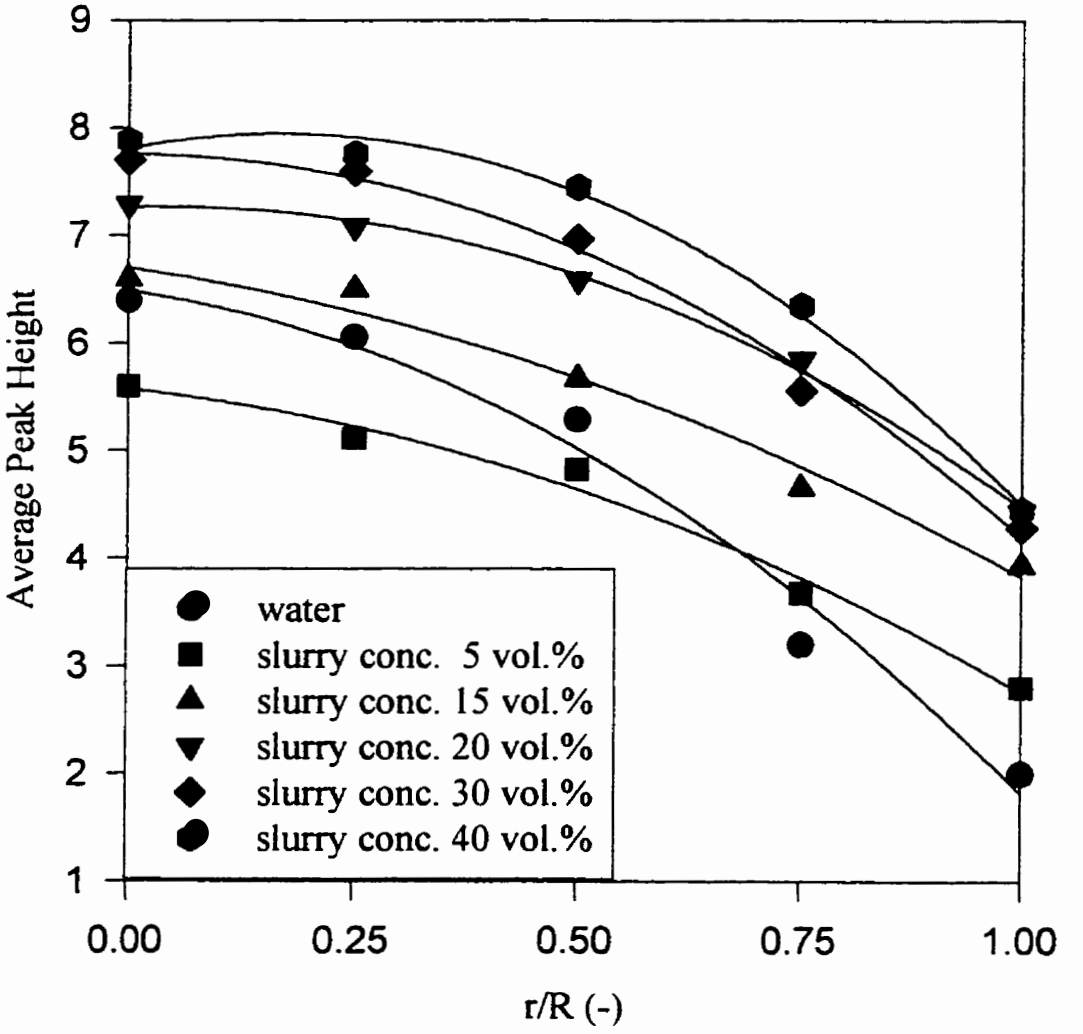

Figure 4.2.51b Radial profile of average peak heights for different slurry concentrations (Vg=0.20 m/s)

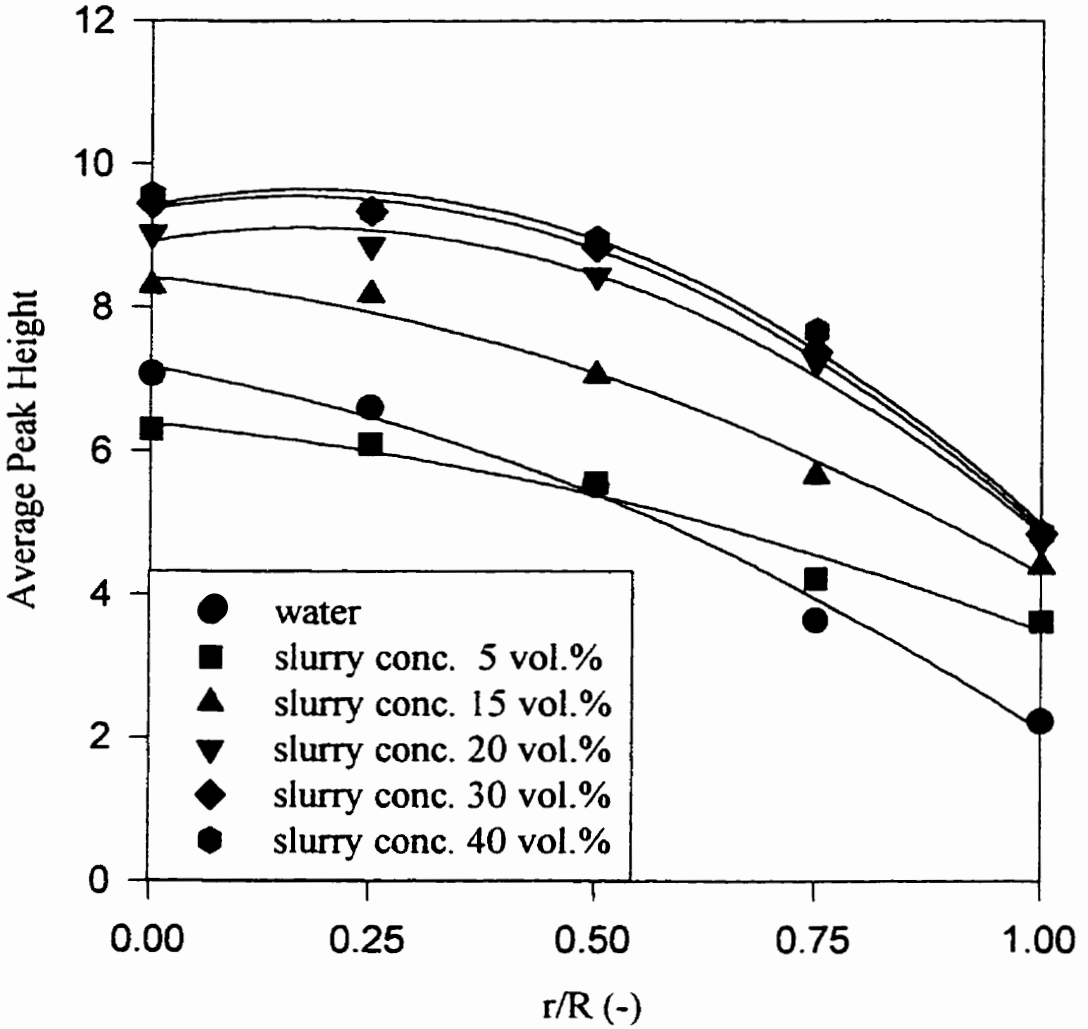

Figure 4.2.51c Radial profile of average peak heights for different slurry concentrations (Vg= 0.30 m/s)

of larger bubbles with increasing slurry concentration. Larger bubbles rise in the central region of the column (Chen et al., 1994). Thus cross sectional area of the column occupied by larger bubbles will be expanded as slurry concentration increases. The cross-sectional area for bubble-wake behind larger bubbles is expanded. The peak-height of heat transfer coefficients in the central region becomes more uniform and wider.

5 Conclusions and Recommendation

5.1 Conclusions

Two important hydrodynamic parameters, namely gas holdups and axial solids dispersion, have been analyzed for the first time over a wide range of slurry concentrations and gas velocities in a large diameter column. Gas holdups in slurry bubble columns were found to be an increasing function of gas velocity at all slurry concentrations. For a constant gas velocity, gas holdups decreased with increasing slurry concentrations up to slurry concentrations of about 25 vol.%. For higher slurry concentrations up to slurry concentrations (from 25 vol.% to 40 vol.%), gas holdups increased slightly. This has been attributed to decrease in rise velocity of small bubbles in dense suspensions.

Axial profiles of solid concentrations were measured and analyzed at different slurry concentrations and gas velocities. Particle hindered settling velocities and solid dispersion coefficients based on the sedimentation-dispersion model were estimated from measured axial profiles of solid concentrations. Hindered settling velocities increased with decreasing slurry concentrations and increasing gas velocities. The solid dispersion coefficient was an increasing function of gas velocity and column diameter. The literature correlations (Kato et al., 1972; Smith and Ruether, 1985; O'Dowd et al., 1987) were applicable for prediction of axial solids concentration in slurry bubble columns.

Bubble size population and bubble rise velocities were investigated by using dynamic gas disengagement technique. Gas holdups due to smaller bubbles were decreased as an increase of slurry concentration up to 25 vol.%, and slightly increased from 25 vol.% to 40 vol.% of slurry concentrations. Gas holdups due to larger bubbles slightly decreased as an increase of slurry concentration. Rise velocities of small bubbles slightly decreased as an increase of superficial gas velocities. Rise velocities of larger bubbles were

increased with increasing superficial gas velocities. Rise velocities of small bubbles increased with increase of slurry concentration up to 20 vol.%, and then slightly decreased. Rise velocities of larger bubbles increased with slurry concentrations up to 20 vol.%. Above slurry concentration of 20 vol.%, the larger bubble rise velocities slightly increase.

The new fast response heat transfer probe developed in this study provided quasi-instantaneous heat transfer coefficients at different axial and radial locations of the column. The probe also detected flow direction at a given radial or axial location in the column. The average heat transfer coefficients could be obtained by averaging a large number of instantaneous measurements at a given location.

Heat transfer coefficients increased with increasing gas velocities at all locations. Generally, average heat transfer coefficients decreased with increasing slurry concentrations at various axial and radial locations. In the bulk region, heat transfer coefficients in the center were systematically higher than near the wall. Heat transfer coefficients in the bulk region were significantly higher than in the distributor region. Heat transfer coefficients in the axial direction increased with increasing distance from the distributor region approaching constant values in the bulk region. The distributor region effect is shown to decrease with increasing gas velocity. The radial profile of heat transfer coefficients showed that as slurry concentration increased, the radial profile became flatter in the central region, indicating an enlarged central region attributed to enlarged bubble size.

In the bulk region of the column, the average heat transfer coefficients at column center were higher for downward facing probe than for the upward facing direction. These observations were reversed at the column wall i.e. the average heat transfer coefficients were higher for the upward facing direction. These observations were related to opposite flow directions in the center and wall regions based on boundary layer theory.

Available literature correlations for heat transfer coefficients were tested against the data of this study. The semiempirical model proposed by Deckwer et al. (1980) predicted well the heat transfer coefficients near the wall in the bulk region, but underestimated the heat transfer coefficients in the center. The modified model proposed by Saxena et al. (1992) was applicable for predictions of heat transfer coefficients in the center at low slurry concentrations. This study modified the model proposed by Deckwer et al. (1980) based on the observations that in the center, the larger bubble wakes play an important role in the heat transfer process. Therefore, for the central region, an enhancement factor is proposed to modified the original Deckwer et al. (1980) model. This enhancement factor (about 21%) indicates a contribution to surface renewal due to larger bubble wakes.

The instantaneous heat transfer measurements provided insights into bubble wake dynamics in different locations of column for different operating conditions. To quantitatively describe instantaneous heat transfer coefficients, a peak fitting method was developed to obtain peak height distribution. Then average peak height, average peak frequency and average peak area were obtained from peak height distributions. Generally, peak height is an increasing function of gas velocity at both center and wall in the bulk region of column. In the central region, three processes were identified with increasing slurry concentrations. Initially, when fine particles were added into water, peak height and peak area were reduced compared to those in water. As slurry concentration increased from 5 vol.% to 20 vol.%, peak height and peak area increased. Above a slurry concentration of 20 vol.%, peak height slightly increased and peak area decreased. In the wall region, average peak height and peak area increased as slurry concentration increased from 0 to 20 vol.% but the increase was not significant at higher slurry concentrations.

5.2 Recommendations

The increase in gas holdups observed at high slurry concentrations in this study need further investigations. This should include effects of particle size (up to 100 μm) and shape. These investigations should also include the effects of particle properties and slurry concentrations on suspension rheology. Further investigations are also recommended to quantify changes in bubble size distributions in different regions of the column. The gas-liquid mass transfer rates can be directly related to average bubble size. Since bubble size is observed to increase with increasing slurry concentrations, a drop in gas-liquid mass transfer rate is expected and may become limiting for a given application. It is therefore, recommended to investigate gas-liquid mass transfer at high slurry concentrations and identify ways to improve it as needed.

This study investigated heat transfer and hydrodynamics in a slurry bubble column with no internals. Future studies should investigate the effects of internals such as bundles of heat transfer tubes and their configurations on hydrodynamics and heat transfer rates. The fast response probe developed in this study can be used to analyze local effects due to the presence of internals.

The heat transfer coefficients in the distributor region were observed to be significantly lower than in the bulk region which also indicated that mixing in the region would also be low. The heat transfer probe developed in this study can be used to improve distributor designs. A new sparger with a multi-level sparging may be more effective and improve start-up operation at high slurry concentrations. The heat transfer probe developed in this study should also prove useful for other applications, i.e. measurement of local heat transfer in agitation tanks.

Further studies should also cover gas-liquid systems other than air-water and pressures higher than atmospheric. It is recommended to use helium and nitrogen gases with high

molecular weight hydrocarbons to cover wider range of thermophysical properties and gas densities.

Appendix A

Calibration of Gas Rotameter

Notation:

P: pressure (Pa);

Q: volume flowrate (m^3/s);

T: temperature (^oC);

subscript:

cali: calibrated;

act: actual;

ref: reference;

The gas flow rate measured by rotameter is corrected by reference pressure and temperature:

$$\frac{Q_{cali}}{Q_{read}} = \sqrt{\frac{T_{ref}}{T_{act}} \frac{P_{act}+P_{ref}}{P_{ref}}} \qquad (A.1)$$

where, P_{ref}=101.3 kPa; T_{ref}=296 K.

The flowrate reading out from rotameter were compared with flowrate measured by orifice plate. The setup for measurement by orifice plate is shown in Figure A1. The orifice plate diameter used for measurement was 7.7 mm. Figure A2 shows the comparison.

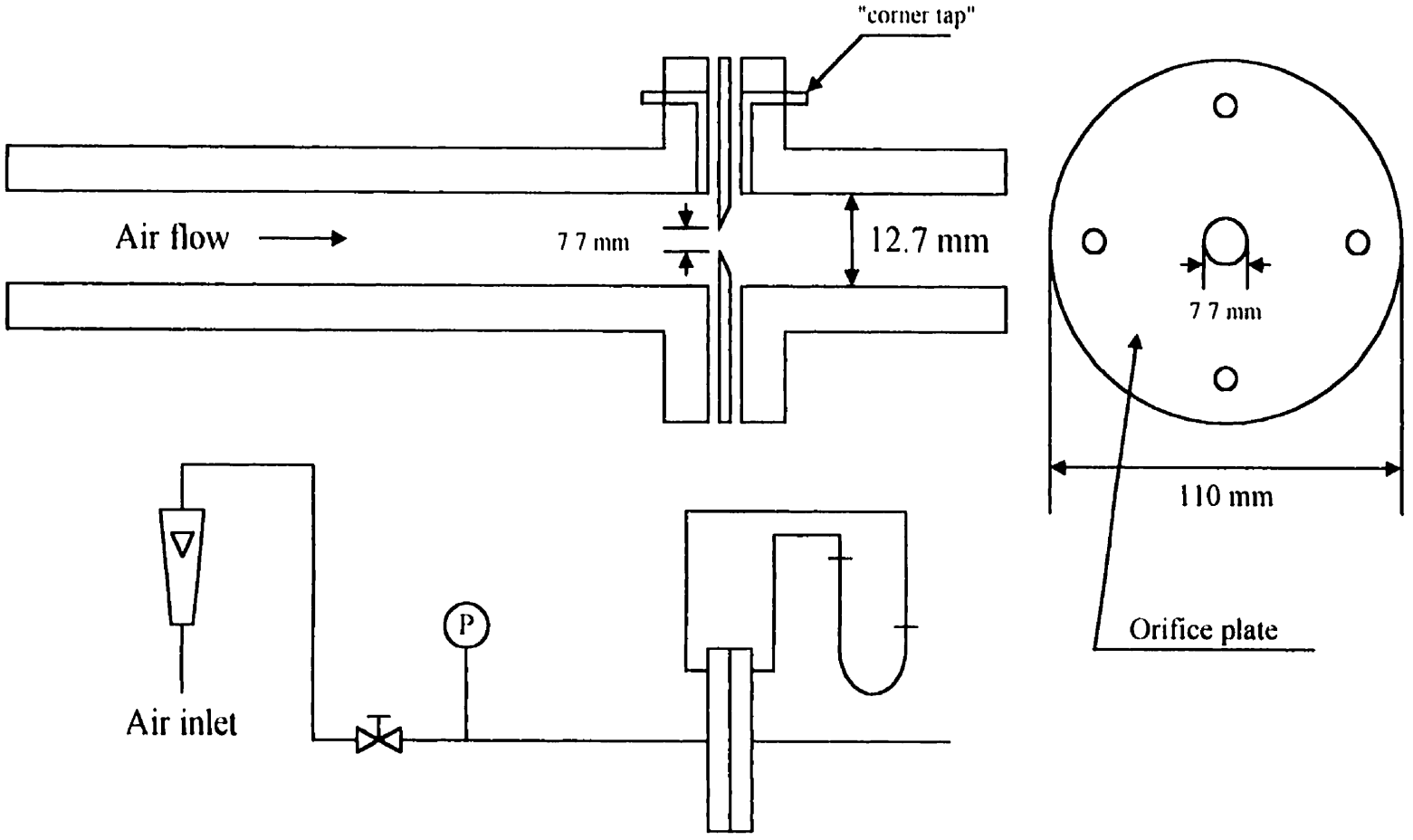

Figure A1 Orifice setup for calibration of rotameter

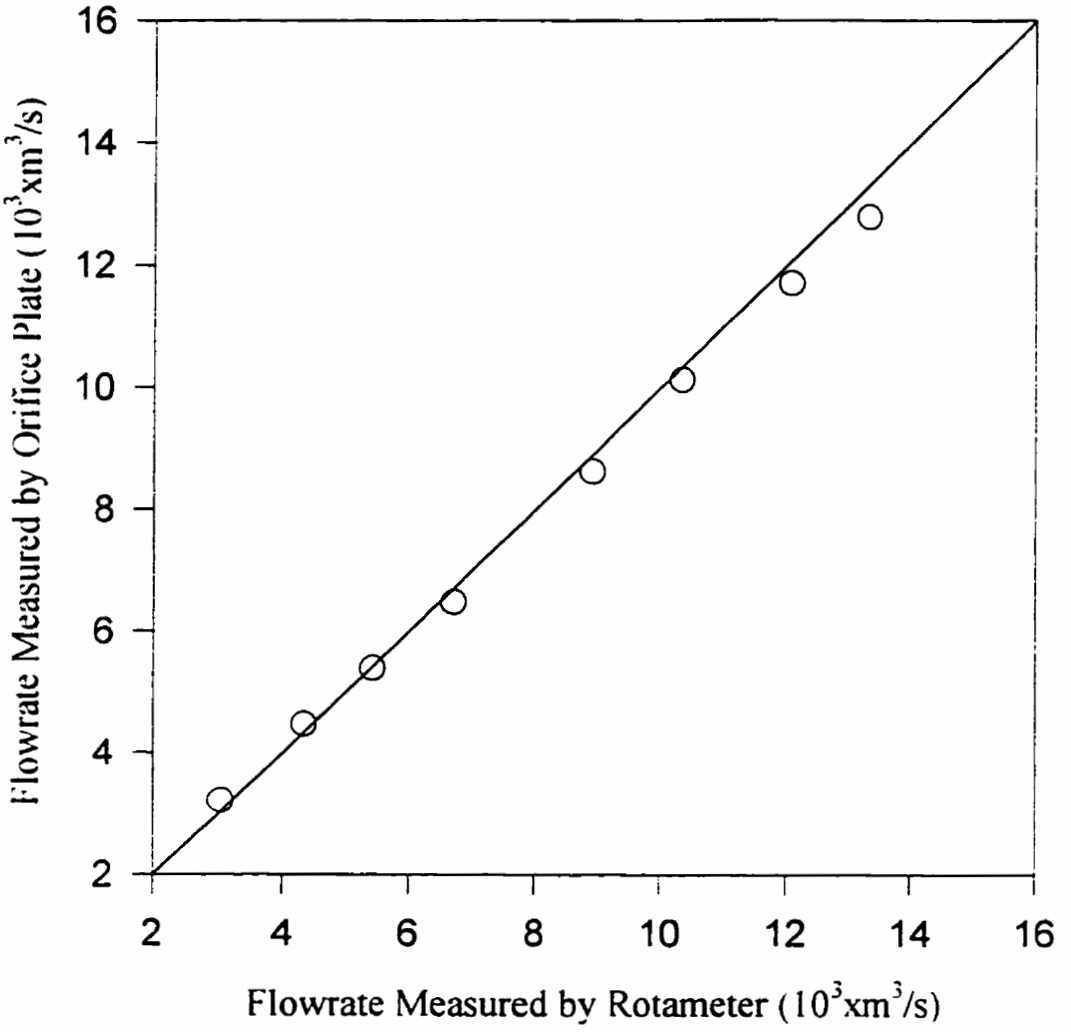

Figure A2 Comparison of flowrate measured by rotameter and orifice plate

Appendix B

Calibration of Heat Flux Sensor

Notation:

A_p: probe surface area (m^2);

I: electrical currenct (A);

L_p: length of the probe (m);

P_w: power (w);

R: electrical resistor (ohm);

r: radii of the probe(m)

V: electrical voltage (V);

The heat flux sensors were calibrated by RdF Co. at the temperature of 21 °C and their calibration factors were provided. The heat flux measured by the probes were also verified at different heat input rates. The experimental set up shown in Figure B1 was used for calibrations. The heat transfer probe was immersed in the water in a 2L container. The water entered at the bottom of the container and overflowed at the top to keep a constant water temperature in the bath. The power was supplied by a variable autotransformer. The heat flux sensors were tested at different power input rates, defined as:

$$P_w = I \cdot V = V^2 / R$$

where, I current, V voltage, R resistance of the heater installed in the probe. The heat transfer surface of the probe can be calculated as surface area of the probe outer diameter:

$$A_p = \pi \cdot r^2 \cdot L_p$$

where A_p surface area; r radii of probe (11 mm); L_p the length of brass tube (25.4 mm). The input heat flux can be defined as:

$$P_w / A_p$$

Figures B2 and B3 compare the input heat flux and measured heat flux from the heat transfer probes. During the experiment, the voltage for 1st probe was kept as 62 V and for 2nd was kept as 55 V.

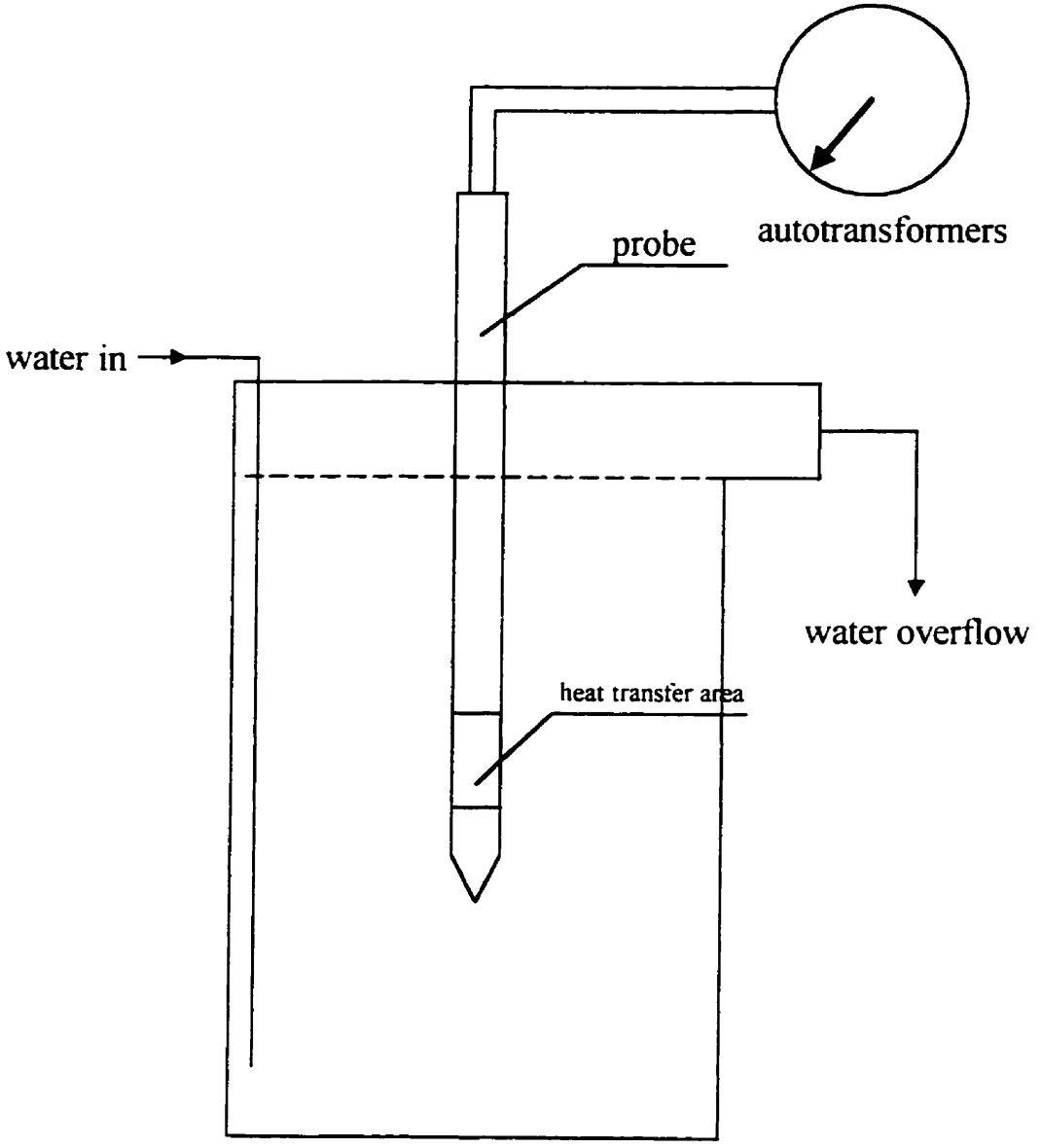

Figure B1 Experimental set up for testing and
and calibration of heat flux sensor

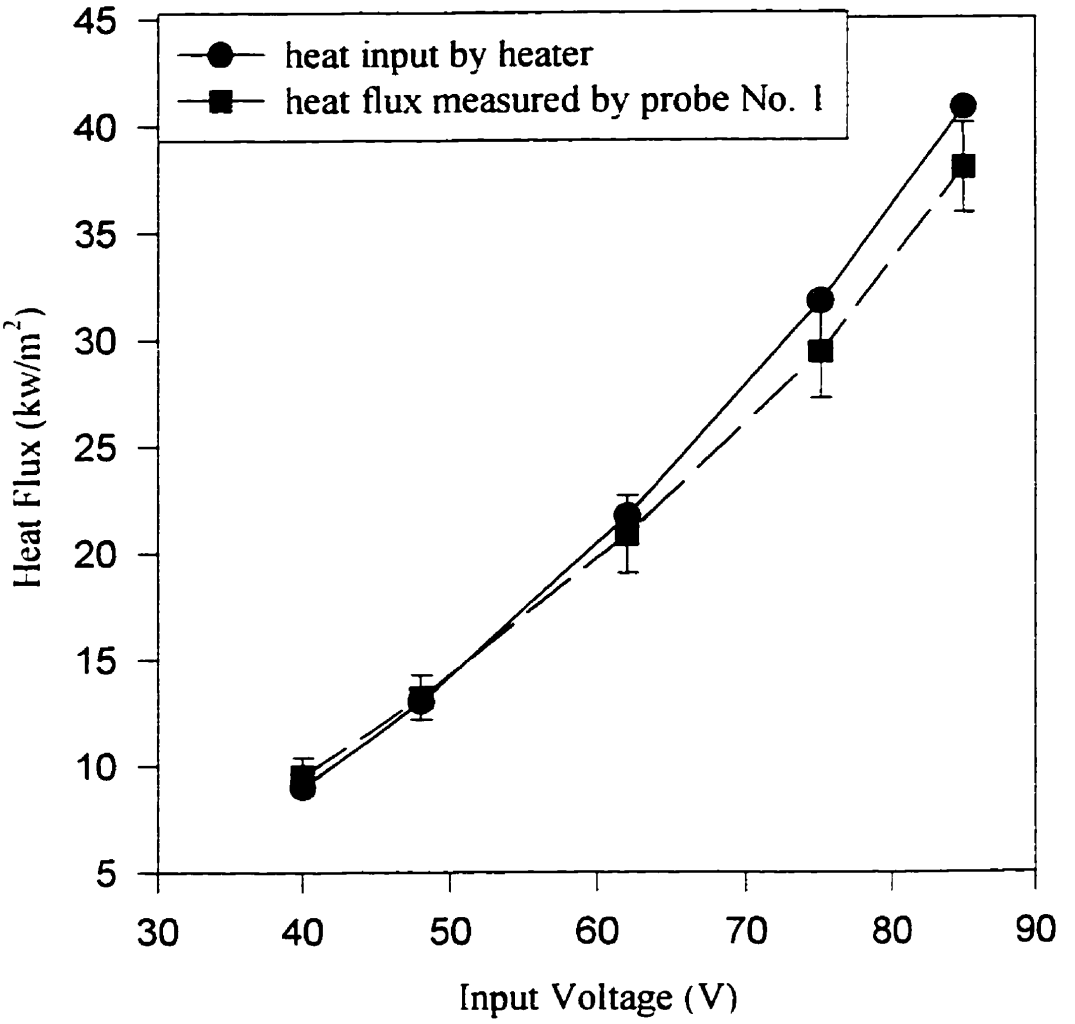

Figure B2 Comparison of heat input and measured heat flux by probe #1

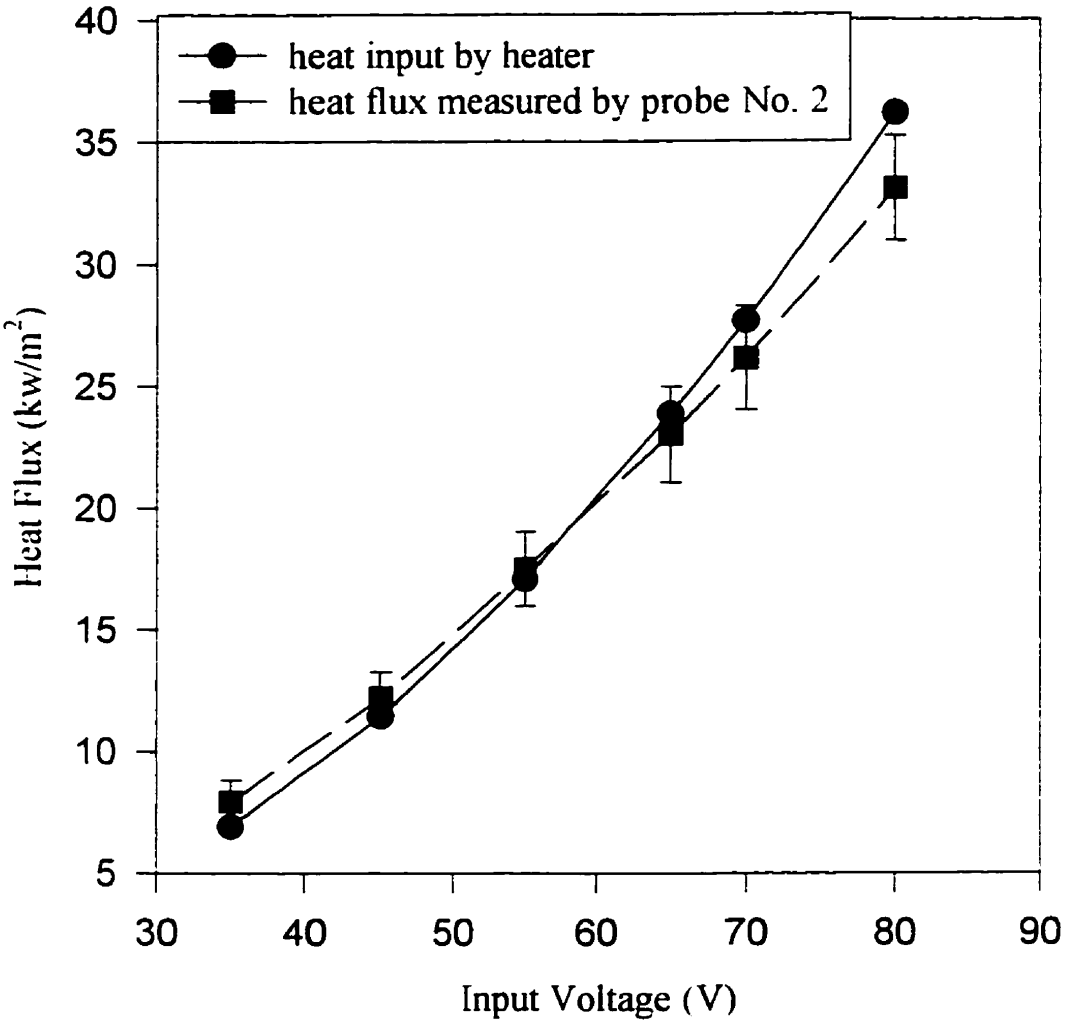

Figure B3 Comparison of heat input and measured heat flux by probe #2

Appendix C

Calibration of Surface Temperatures

The surface temperatures measured by two probes were calibrated with high accuracy thermometer. The calibration was conducted in the column filled with tap water. Initially, the bed temperature was brought up to a desired value. A small gas flow was introduced into the column for mixing water. Then gas flow was stopped and bed temperature was monitored by thermocouples. After about 30 minutes, the thermometer was inserted into the column at different locations. The measured temperature from the thermometer and surface temperature by probe were compared. Figures C1 and C2 show the calibration results for two probes.

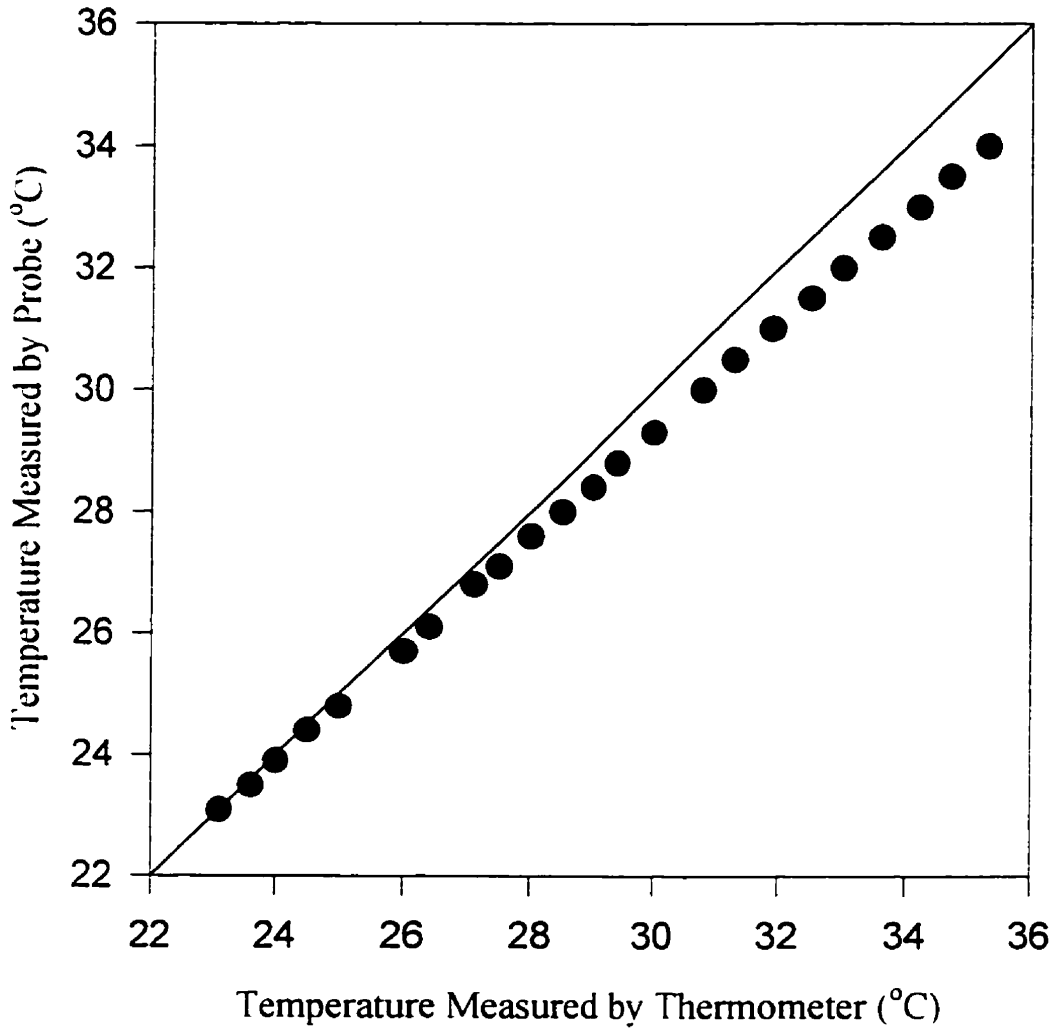

Figure C1 Calibration of surface temperature of heat transfer probe #1

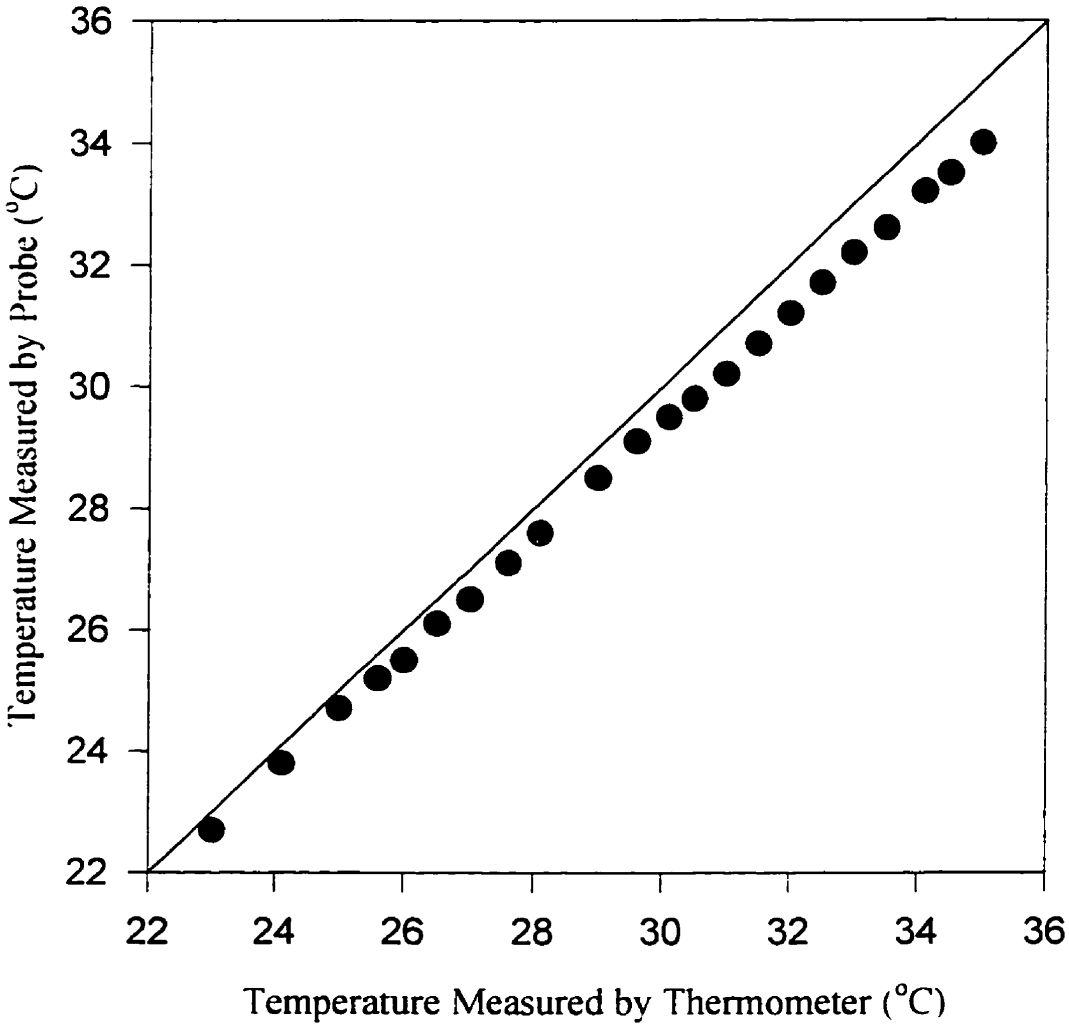

Figure C2 Calibration of surface temperature of heat transfer probe #2

Appendix D

Calibration of Pressure Transducers

The signals collected from pressure transducers are originally obtained in electrical voltage. The results are required to be transferred to pressure value. Therefore, the calibration was conducted in the column. The column initially was filled up to about 2.4 m high and then the water height was reduced at the desired water heights. The voltage collected from two transducers were recorded at each water height. Here, the water height was the height from the transducer to the top of water. Figures D1 and D2 show the calibration results.

It is found from Figures D1 and D2 that the voltages have a linear relationship with water height. Therefore, the linear equations can be used for transferring voltage signal to water height or pressure values.

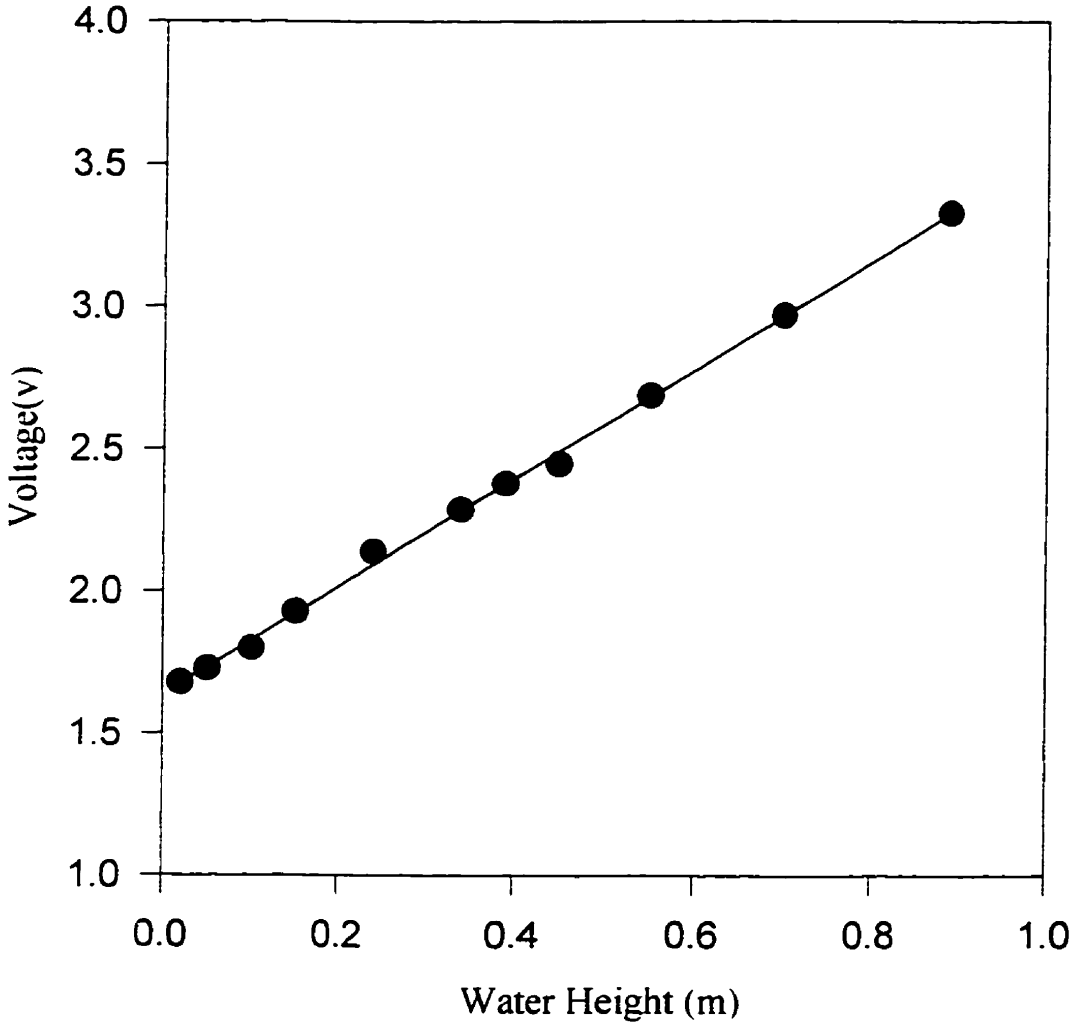

Figure D1 Calibration for pressure transducer used in the bulk region of the column

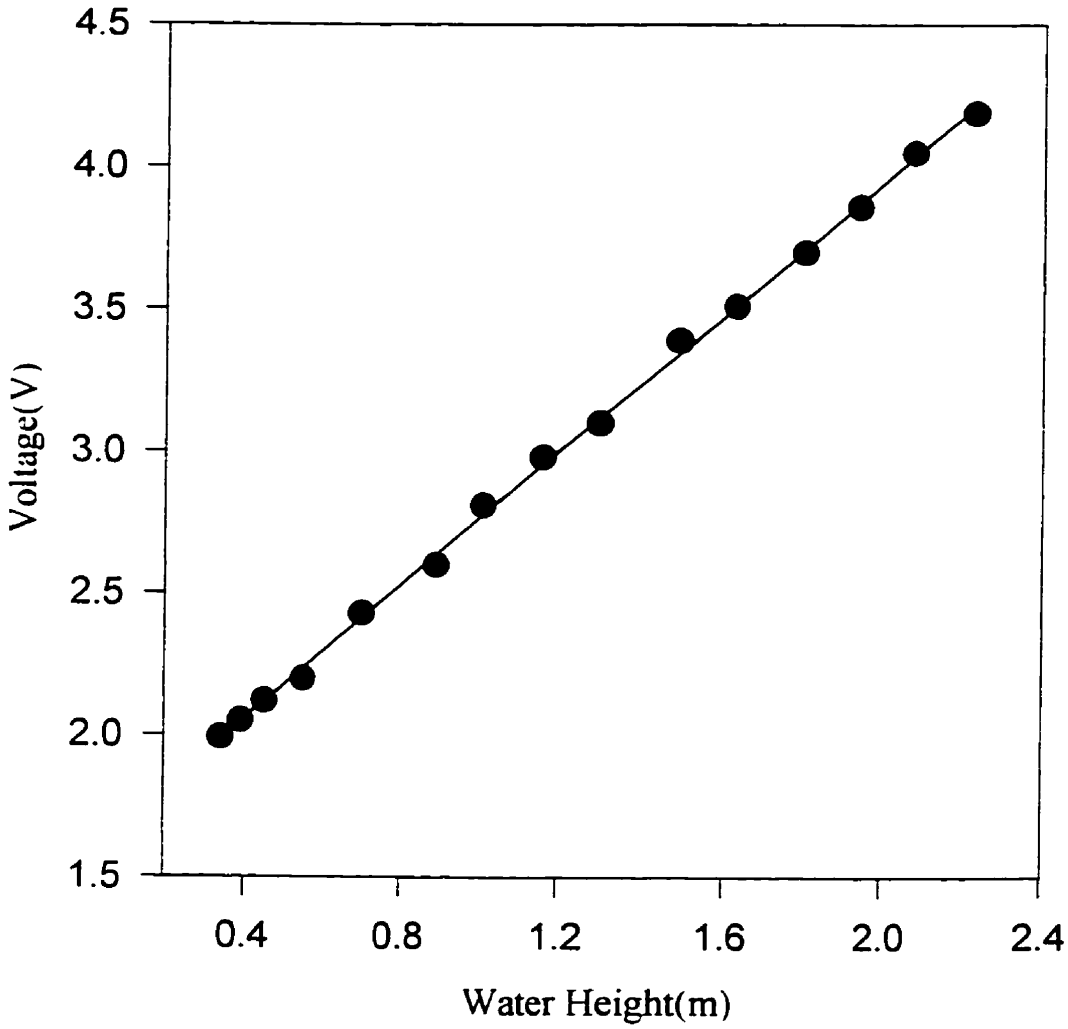

Figure D2 Calibration for the pressure transducer used at the bottom of the column

Appendix E Tabulated Raw Data

Appedix E1 Gas Holdups Presented in Figure 4.1.1-4.1.3

Gas: Air
Liquid: Tap Water
solids: Glass Bead (35 μ m)

	Vg=0.05 (m/s)	Vg=0.10 (m/s)	Vg=0.15 (m/s)	Vg=0.20 (m/s)	Vg=0.30 (m/s)
slurry conc. = 0	0.105	0.157	0.197	0.226	0.286
slurry conc.= 5	0.095	0.139	0.171	0.196	0.243
slurry conc.= 10	0.085	0.124	0.157	0.179	0.225
slurry conc.= 15	0.079	0.110	0.139	0.165	0.211
slurry conc.= 20	0.070	0.105	0.133	0.156	0.199
slurry conc.= 25	0.067	0.099	0.125	0.150	0.193
slurry conc.= 30	0.068	0.101	0.127	0.152	0.196
slurry conc.= 40	0.077	0.117	0.146	0.167	0.210

Appedix E2 Heat Transfer Coefficients (kw/m^{2}C) in Bulk Region (r/R 0) Presented in Figure 4.2.3, 4.2.5a-d

Gas: Air
Liquid: Tap Water
solids: Glass Bead (35 μ m)

	Vg=0.05 (m/s)	Vg=0.10 (m/s)	Vg=0.15 (m/s)	Vg=0.20 (m/s)	Vg=0.30 (m/s)
slurry conc. = 0	5.01	6.06	6.60	7.07	7.36
slurry conc.= 5	4.95	5.83	6.43	6.86	7.27
slurry conc.= 10	4.82	5.84	6.24	6.68	7.14
slurry conc.= 15	4.79	5.66	6.31	6.53	6.65
slurry conc.= 20	4.68	5.52	5.81	6.27	6.69
slurry conc.= 25	4.61	5.55	5.77	6.04	6.46
slurry conc.= 30	4.50	5.45	5.60	5.95	6.40
slurry conc.= 40	4.43	5.40	5.69	5.85	6.31

Appedix E3 Heat Transfer Coefficients (kw/m^{2}C) in Bulk Region (r/R=0.25) Presented in Figures 4.2.14a-c

Gas: Air
Liquid: Tap Water
solids: Glass Bead (35 μ m)

	Vg=0.05 (m/s)	Vg=0.10 (m/s)	Vg=0.15 (m/s)	Vg=0.20 (m/s)	Vg=0.30 (m/s)
slurry conc. = 0	4.85	5.76	6.40	6.91	7.14
slurry conc.= 5	4.80	5.75	6.29	6.75	7.01
slurry conc.= 10	4.67	5.67	6.10	6.64	6.94
slurry conc.= 15	4.80	5.53	6.09	6.44	6.50
slurry conc.= 20	4.60	5.40	5.68	6.15	6.59
slurry conc.= 25	4.46	5.54	5.70	5.98	6.47
slurry conc.= 30	4.44	5.37	5.59	5.90	6.35
slurry conc.= 40	4.44	5.37	5.59	5.80	6.30

Appedix E4 Heat Transfer Coefficients ($kw/m^2 C$) in Bulk Region (r/R=0.5) Presented in Figures 4.2.14a-c

Gas: Air
Liquid: Tap Water
solids: Glass Bead (35 μ m)

	Vg=0.05 (m/s)	Vg=0.10 (m/s)	Vg=0.15 (m/s)	Vg=0.20 (m/s)	Vg=0.30 (m/s)
slurry conc. = 0	4.65	5.34	5.73	6.33	6.35
slurry conc.= 5	4.53	5.34	5.73	6.29	6.50
slurry conc.= 10	4.48	5.17	5.40	5.96	6.48
slurry conc.= 15	4.54	5.17	5.46	6.03	6.23
slurry conc.= 20	4.40	5.27	5.40	5.76	6.12
slurry conc.= 25	4.27	5.29	5.42	5.76	6.02
slurry conc.= 30	4.25	5.25	5.39	5.66	6.16
slurry conc.= 40	4.25	5.25	5.45	5.66	6.16

Appedix E5 Heat Transfer Coefficients (kw/m^2C) in Bulk Region (r/R=0.75) Presented in Figure 4.2.14a-c

Gas: Air
Liquid: Tap Water
solids: Glass Bead (35 μ m)

	Vg=0.05 (m/s)	Vg=0.10 (m/s)	Vg=0.15 (m/s)	Vg=0.20 (m/s)	Vg=0.30 (m/s)
slurry conc. = 0	4.50	5.22	5.48	5.88	6.04
slurry conc.= 5	4.41	4.95	5.47	5.82	6.00
slurry conc.= 10	4.20	4.95	5.22	6.54	6.02
slurry conc.= 15	4.01	4.85	5.16	5.43	5.63
slurry conc.= 20	4.00	4.74	4.96	5.41	5.80
slurry conc.= 25	3.94	4.79	5.02	5.37	5.61
slurry conc.= 30	3.90	4.73	5.01	5.33	5.66
slurry conc.= 40	3.90	4.75	5.01	5.32	5.65

Appedix E6 Heat Transfer Coefficients (kw/m ^{2} C) in Bulk Region (r/R=1.0) Presented in Figures 4.2.4, 4.2.5a-e

Gas: Air
Liquid: Tap Water
solids: Glass Bead (35 μ m)

	Vg=0.05 (m/s)	Vg=0.10 (m/s)	Vg=0.15 (m/s)	Vg=0.20 (m/s)	Vg=0.30 (m/s)
slurry conc. = 0	4.43	5.08	5.38	5.70	5.83
slurry conc.= 5	4.25	4.86	5.12	5.65	5.82
slurry conc.= 10	4.09	4.77	5.10	5.37	5.80
slurry conc.= 15	3.83	4.64	5.03	5.23	5.37
slurry conc.= 20	3.86	4.70	5.09	5.30	5.46
slurry conc.= 25	3.72	4.51	4.75	5.19	5.44
slurry conc.= 30	3.73	4.60	4.75	5.10	5.43
slurry conc.= 40	3.74	4.60	4.74	5.06	5.42

Appedix E7 Heat Transfer Coefficients (kw/m ^{2} C) in distriButor Region (r/R=0.5) Presented in Figures 4.17 and 4.22

Gas: Air
Liquid: Tap Water
solids: Glass Bead (35 μ m)

	Vg=0.05 (m/s)	Vg=0.10 (m/s)	Vg=0.15 (m/s)	Vg=0.20 (m/s)	Vg=0.30 (m/s)
slurry conc. = 0	3.06	3.58	3.90	4.55	4.82
slurry conc.= 5	2.57	3.19	3.58	3.67	4.18
slurry conc.= 10	2.50	2.90	3.22	3.41	3.86
slurry conc.= 15	2.47	3.00	3.22	3.40	3.70
slurry conc.= 20	2.45	2.85	3.20	3.33	3.63
slurry conc.= 25	2.41	2.64	3.07	3.25	3.44
slurry conc.= 30	2.42	2.71	3.20	3.20	3.44
slurry conc.= 40	2.42	2.64	3.17	3.23	3.44

Appedix E8 Heat Transfer Coefficients ($kw/m^2 C$) in Distributor Region (r/R -1.0) Presented in Figures 4.17 and 4.22

Gas: Air
Liquid: Tap Water
solids: Glass Bead (35 μ m)

	Vg=0.05 (m/s)	Vg=0.10 (m/s)	Vg=0.15 (m/s)	Vg=0.20 (m/s)	Vg=0.30 (m/s)
slurry conc. = 0	3.50	3.95	4.45	4.89	5.01
slurry conc.= 5	3.01	3.53	3.91	4.00	4.39
slurry conc.= 10	2.88	3.32	3.61	3.80	4.00
slurry conc.= 15	2.71	3.47	3.54	3.88	3.86
slurry conc.= 20	2.67	3.13	3.33	3.52	3.78
slurry conc.= 25	2.56	3.05	3.23	3.30	3.66
slurry conc.= 30	2.50	2.96	3.23	3.26	3.63
slurry conc.= 40	2.45	2.81	3.22	3.26	3.60

Appedix E9 Heat Transfer Coefficients (kw/m^{2}C) in Different Axial Locations. Presented in Figures 4.2.20 and 4.2.21

Gas: Air; Liquid: Tap Water; solids: Glass Bead (35 μ m); slurry conc.: 10 vol.%

center:

	Vg=0.05 (m/s)	Vg=0.10 (m/s)	Vg=0.15 (m/s)	Vg=0.20 (m/s)	Vg=0.30 (m/s)
z= 0.52 (m)	4.35	4.74	5.52	5.85	6.39
z= 1.28 (m)	4.82	5.84	6.24	6.68	7.14
	Vg=0.06 (m/s)	Vg=0.11 (m/s)	Vg=0.17 (m/s)	Vg=0.24 (m/s)	Vg=0.35 (m/s)
z= 0.90 (m)	4.99	5.89	6.60	7.25	7.42

wall:

	Vg=0.05 (m/s)	Vg=0.10 (m/s)	Vg=0.15 (m/s)	Vg=0.20 (m/s)	Vg=0.30 (m/s)
z=0.07 (m)	2.88	3.32	3.61	3.80	4.00
z= 0.52 (m)	3.68	4.10	4.88	5.34	5.69
z= 1.28 (m)	4.09	4.77	5.10	5.37	5.70
	Vg=0.06 (m/s)	Vg=0.11 (m/s)	Vg=0.17 (m/s)	Vg=0.24 (m/s)	Vg=0.35 (m/s)
z= 0.90 (m)	4.15	4.65	5.15	5.60	5.60

Appedix E10 Heat Transfer Coefficients (kw/m^2C) in Different Orientations. Presented in Figures 4.2.25a and 4.2.25b

Gas: Air;
Liquid: Tap Water;
Solids: Glass Bead (35 μ m);

air-water (r/R=0)

	Vg=0.05 (m/s)	Vg=0.10 (m/s)	Vg=0.15 (m/s)	Vg=0.20 (m/s)	Vg=0.30 (m/s)
upside	4.51	5.54	6.24	6.42	6.73
laterat	5.05	6.06	6.60	7.07	7.36
downside	5.96	7.01	7.50	8.25	8.77

air-water (r/R=1)

	Vg=0.05 (m/s)	Vg=0.10 (m/s)	Vg=0.15 (m/s)	Vg=0.20 (m/s)	Vg=0.30 (m/s)
upside	4.64	5.30	5.65	6.21	6.30
laterat	4.43	5.08	5.38	5.70	5.83
downside	4.34	4.91	5.18	5.47	5.63

Appedix E10 Heat Transfer Coefficients (kw/m^{2}C) in Different Orientations.
Presented in Figures 4.2.25a and 4.2.25b (con't)

slurry conc. 10 vol.%) (r/R=0)

	Vg=0.05 (m/s)	Vg=0.10 (m/s)	Vg=0.15 (m/s)	Vg=0.20 (m/s)	Vg=0.30 (m/s)
upside	4.48	5.11	5.74	5.97	6.47
laterat	4.82	5.84	6.24	6.68	7.14
downside	5.94	6.85	7.40	7.95	8.56

slurry conc. 10 vol.%) (r/R=1)

	Vg=0.05 (m/s)	Vg=0.10 (m/s)	Vg=0.15 (m/s)	Vg=0.20 (m/s)	Vg=0.30 (m/s)
upside	4.25	5.02	5.43	5..59	6.02
laterat	4.09	4.77	5.10	5.37	5.80
downside	4.08	4.56	5.03	5.21	5.50

Appendix E11

Axial Slurry Concentrations

Average Slurry Conc.: 5 vol.%

Vg=0.06 m/s		Vg=0.11 m/s		Vg=0.17 m/s		Vg=0.24 m/s		Vg=0.35 m/s	
height (m)	conc. (vol.%)	height (m)	conc. (vol.%)	height (m)	conc. (vol.%)	height (m)	conc. (vol.%)	height (m)	conc. (vol.%)
0.07	5.20	0.07	5.08	0.07	5.28	0.07	5.17	0.07	5.27
0.47	4.98	0.47	5.01	0.47	5.13	0.47	5.18	0.47	5.12
0.87	4.88	0.87	4.75	0.87	5.12	0.87	4.97	0.87	5.00
1.27	4.68	1.27	4.69	1.27	4.83	1.27	4.77	1.27	4.86

Average Slurry Conc.: 10 vol.%

Vg=0.06 m/s		Vg=0.11 m/s		Vg=0.17 m/s		Vg=0.24 m/s		Vg=0.35 m/s	
height (m)	conc. (vol.%)	height (m)	conc. (vol.%)	height (m)	conc. (vol.%)	height (m)	conc. (vol.%)	height (m)	conc. (vol.%)
0.07	10.65	0.07	10.61	0.07	10.44	0.07	10.47	0.07	10.46
0.47	10.47	0.47	10.37	0.47	10.35	0.47	10.41	0.47	10.30
0.87	9.99	0.87	10.17	0.87	9.99	0.87	10.23	0.87	10.15
1.27	9.76	1.27	9.87	1.27	9.77	1.27	9.79	1.27	9.85

Average Slurry Conc.: 15 vol.%

Vg=0.06 m/s		Vg=0.11 m/s		Vg=0.17 m/s		Vg=0.24 m/s		Vg=0.35 m/s	
height (m)	conc. (vol.%)	height (m)	conc. (vol.%)	height (m)	conc. (vol.%)	height (m)	conc. (vol.%)	height (m)	conc. (vol.%)
0.07	15.69	0.07	15.69	0.07	15.67	0.07	15.52	0.07	15.54
0.47	15.35	0.47	15.67	0.47	15.57	0.47	15.28	0.47	15.42
0.87	14.98	0.87	15.07	0.87	15.03	0.87	14.91	0.87	15.00
1.27	14.51	1.27	14.81	1.27	14.86	1.27	14.79	1.27	14.85

Appendix E11

Axial Slurry Concentrations (con't)

Average Slurry Conc.: 20 vol.%

Vg=0.06 m/s		Vg=0.11 m/s		Vg=0.17 m/s		Vg=0.24 m/s		Vg=0.35 m/s	
height (m)	conc. (vol.%)	height (m)	conc. (vol.%)	height (m)	conc. (vol.%)	height (m)	conc. (vol.%)	height (m)	conc. (vol.%)
0.07	20.64	0.07	20.57	0.07	20.56	0.07	20.55	0.07	20.53
0.47	20.15	0.47	20.37	0.47	20.52	0.47	20.51	0.47	20.45
0.87	19.78	0.87	19.94	0.87	20.19	0.87	20.08	0.87	20.14
1.27	19.26	1.27	19.58	1.27	19.68	1.27	19.73	1.27	19.80

Average Slurry Conc.: 30 vol.%

Vg=0.06 m/s		Vg=0.11 m/s		Vg=0.17 m/s		Vg=0.24 m/s		Vg=0.35 m/s	
height (m)	conc. (vol.%)	height (m)	conc. (vol.%)	height (m)	conc. (vol.%)	height (m)	conc. (vol.%)	height (m)	conc. (vol.%)
0.07	30.66	0.07	30.58	0.07	30.55	0.07	30.50	0.07	30.46
0.47	30.16	0.47	30.20	0.47	30.43	0.47	30.30	0.47	30.19
0.87	29.79	0.87	30.23	0.87	29.93	0.87	30.03	0.87	30.04
1.27	29.17	1.27	29.35	1.27	29.51	1.27	29.59	1.27	29.60

Average Slurry Conc.: 40 vol.%

Vg=0.06 m/s		Vg=0.11 m/s		Vg=0.17 m/s		Vg=0.24 m/s	
height (m)	conc. (vol.%)	height (m)	conc. (vol.%)	height (m)	conc. (vol.%)	height (m)	conc. (vol.%)
0.07	40.53	0.07	40.65	0.07	40.60	0.07	40.47
0.47	40.24	0.47	40.30	0.47	40.29	0.47	40.14
0.87	39.68	0.87	40.08	0.87	40.01	0.87	39.97
1.27	39.06	1.27	39.65	1.27	39.76	1.27	39.66

References

Ahrendts, J., and H. Baehr, "The Use of Nonlinear Regression Processes in Establishing Thermodynamic Equations of State", *Int. Chem. Eng.*, **21**, 572-579 (1981)

Akita, K., and F. Yoshida, "Gas Holdup and Volumetric Mass Transfer Coefficient in Bubble Columns", *Ind. Eng. Chem. Process Des. Dev.*, **12**, 76-80 (1973)

Akita, K., and F. Yoshida, "Bubble Size, Interfacial Area, and Liquid-Phase Mass Transfer Coefficient in Bubble Columns", *Ind. Eng. Chem. Process Des. Dev.*, **13**, 84-91 (1974)

Arters, D.C., L.S. Fan, "Solid-Liquid Mass Transfer in Gas-Liquid-Solid Fluidized Beds", *Chem. Eng. Sci.*, **41**, 107-115 (1986)

Asai, S., and H. Yoshizawa, "Longitudinal Holdup Distribution of Gas and Dispersed Liquid in Bubble Columns with Two Immisible Liquids", *Ind. Eng. Chem. Res.*, **30**, 745-751 (1991)

Azbel, D., *Two-Phase Flows in Chemical Engineering*, Cambridge Univ. Press, Cambridge, London (1981)

Bach, H.F., and T. Pilhofer, "Variation of Gas Holdup in Bubble Columns with Physical Properties of Liquids and Operating Parameters of Columns", *Ger. Chem. Eng.*, **1**, 270-290 (1978)

Baker, C.G.J., S.D. Kim, and M.A. Bergougnou, "Wake Characteristics of Three Phase Fluidized Beds", *Powder Technology*, **18**, 201-207 (1977)

Baker, C.G.J., E.R. Armstrong, and M.A. Bergougnou, "Heat Transfer in Three Phase Fluidized Beds", *Powder Technology*, **21**, 195-204 (1978)

Ballesteros, R.L., J.P. Riba, and J.P. Couderic, "Dissolution of Non-spherical Particle in Solid-liquid Fluidization", *Chem. Eng. Sci.*, **37**, 1639 (1982)

Barnea, E., and J. Mizrahi, "A General Approach to the Fluid Dynamics of Particulate systems. Part 1. General Correlation for Fluidization and Sedimentation in Solid Multiparticle Systems", *Chem. Eng. J.*, **5**, 171-189 (1973)

Begovich, J.M., and J.S. Watson, "An Electroconductivity Technique for the Measurement of Axial Variation of Holdups in Three-Phase Fluidized Beds", *AIChE J.*, **24**, 351-354 (1978)

Bhaga, D. and M.E. Weber, "Bubbles in viscous liquids: Shapes, Wake and Velocities", *J. Fluid Mech.*, **105**, 61-85 (1981)

Bhatia, V.K., and N. Epstein, in *Fluidization and Its Applications* ed. by H. Angelino, J.P. Couderc, H. Gibert, and C. Laguerie, 380, Cepadues-Editions, Toulouse (1974)

Bhavaraju, S.M., T.W.F. Russel, and H.W. Blanch, "The Design of Gas Sparged Devices for Viscous Liquid System", *AIChE J.*, **24**, 454-466 (1978)

Bird, R.B., W.E. Stewart, and E.N. Lightfoot, *Transport Phenomena*, Wiley, New York (1960)

Brodkey, R.S., and H.C. Hershey, *Transport Phenomena - A Unified Approach* McGraw-Hill Inc. (1988)

Buchholz, R., W. Zakrzewski, and K. Schugerl, "Techniques for Determining the Properties of Bubbles in Bubble Columns", *Int. Chem. Eng.*, **21**, 180-187 (1981)

Bukur, D.B., and J.G. Daly, "Gas Holdup in bubble Columns for Fischer-Tropsch Synthesis", *Chem. Eng. Sci.*, **42**, 2967-2969 (1987)

Bukur, D.B., and S.A. Patel, "Hydrodynamic Studies with Foaming and Non-Newtonian Solutions in Bubble Columns", *Can. J. Chem. Eng.*, **67**, 741-751 (1989)

Bukur, D.B., S.A. Patel, and J.G. Daly, "Gas Holdup and Solids Dispersion in a Three-Phase Slurry Bubble Column", *AIChE J.*, **36**, 1731-1735 (1990)

Catros, A.B.P., *Hydrodynamics and Mass Transfer in Bubble and Three Phase Fluidized Column*, Ph.D. thesis, University of Western Ontario, London (1986)

Chen, R.C., and L.S. Fan, "Particle Image Velocimetry for Characterizing the Flow Structure in Three-Dimensional Gas-Liquid-Solid Fluidized Beds", *Chem. Eng. Sci.*, **47**, 3615-3622 (1992)

Chen, R.C., J. Reese, and L.S. Fan, "Flow Structure in a Three-Dimensional Bubble Column and Three Phase Fluidized Bed", *AIChE J.*, **40**, 1093-1104 (1994)

Chiu, T.M., and E.N. Ziegler, "Heat Transfer in Three Phase Fluidized Beds", *AIChE J.*, **29**, 677-685 (1983)

Chiu, T.M., and E.N. Ziegler, "Liquid Holdup and Heat Transfer Coefficient in Liquid-Solid and Three Phase Fluidized Beds", *AIChE J.*, **31**, 1504-1509 (1985)

Clark, K.N., "The Effect of High Pressure and Temperature on Phase Distributions in a Bubble Column", *Chem. Eng. Sci.*, **45**, 2301-2307 (1990)

Coppus, H.C., K. Rietema, and S.P.P. Ottengraf, "Wake Phenomena behind Spherical-Cap Bubbles and Solid Spherical-Bodies", *Trans. Instn. Chem. Eng.*, **55**, 122-129 (1977)

Crabtree, J.R. and J. Bridgwater, "The Wake behind Two-Dimensional Air Bubbles", *Chem. Eng. Sci.*, **22**, 1517-1518 (1967)

Daly, J.G., S.A. Patel, and D.B. Bukur, "Measurement of Gas Holdups and Sauter Mean Bubbles Diameters In Bubble Column Reactors by Dynamic Gas Disengagement Method", *Chem. Eng. Sci.*, **47**, 3647-3654 (1992)

Darton, R.C., and D. Harrison, "The Rise of Single Gas Bubble in Liquid Fluidized Beds", *Trans IChemE*, **52**, 301-306 (1974)

Darton, R.C., and D. Harrison, "Gas and Liquid Hold-up in Three Phase Fluidisation", *Chem. Eng. Sci.*, **30**, 581-586 (1975)

Darton, R.C., R.D. LaNauze, J.F. Davidson, and D. Harrison, "Bubble Growth due to Coalescence in Fluidized Beds", *Trans IChemE*, **55**, 274-280 (1977)

Deckwer, W.D., R. Burckhart, and G. Zoll, "Mixing and Mass Transfer in Tall Bubble Columns", *Chem. Eng. Sci.*, **29**, 2177 (1974)

Deckwer, W.D., "On the mechanism of Heat Transfer in Bubble Column Reactor", *Chem. Eng. Sci.*, **35**, 1341-1346 (1980)

Deckwer, W.D., Y. Luoisi, A. Zaidi, and M. Ralek, "Hydrodynamic Properties of the Fischer-Tropsch Slurry Process", *Ind. Eng.Chem. Process Des. and Dev.*, **19**, 699-708 (1980)

Deckwer, W.D. and A. Schumpe, "Improved Tools for Bubble Column Reactor Design and Scale-Up", *Chem. Eng. Sci.*, **48**, 889-911 (1993)

De Lasa, H., S.L.P. Lee, and M.A. Bergougnou, "Bubble Measurement in Three Phase Fluidized Beds Using a U-shaped Fiber", *Can. J. Chem. Eng.*, **62**, 165-169 (1984)

De Swart, J.W.A., and R. Krishna, "Influence of Particles Concentration on the Hydrodynamics of Bubble Column Slurry Reactors", *Trans IChemE*, **73**, Part A, 308-313 (1995)

Del Pozo, M., C.L. Briens, and G. Wild, "Effect of Column Inclination on the Performance of Three-Phase Fluidized Beds", *AIChE J.*, **38**, 1206-1212 (1992)

Ellenberger, J., and R. Krishna, "A Unified Approach to the Scale-Up of Gas-Solid Fluidized Bed and Gas-Liquid Bubble Column Reactors", *Chem. Eng. Sci.*, **49**, 5391-5411 (1995)

El-Temtamy, S.A., Y.O. El-Sharnoubi, and M.M. El-Halwagi, "Liquid Dispersion in Gas-Liquid Fluidized Beds Part I: Axial Dispersion. The Axial Dispersed Plug-Flow Model", *Chem. Eng. J.*, **18**, 151-159 (1979)

Efremov, G.I., and I.A. Vakhrushev, "A Study of the Hydrodynamics of Three-Phase Fluidized beds", *Int. Chem. Eng.*, **10**, 37-41 (1970)

Everson, R.C., D. Eyre, C.T. O'Connor, and J.P. Tucker, "Measurement and Analysis of Small Bubble Size Distribution", *Chem. Eng. Sci.*,**48**, 3399-3403 (1993)

Fair, J.R., A.J. Lambright, and J.W. Andersen, "Heat Transfer and Gas Holdup in a Sparger Contactor", *Ind. Eng.Chem. Process Des. and Dev.*, **1**, 33-36 (1962)

Fan, L.S., A. Matsuura, and S.S. Chern, "Hydrodynamic Characteristics of a Gas-Liquid-Solid Fluidized Bed Containing a Binary Mixture of Particles", *AIChE J.*, **31**, 1801-1810 (1985)

Fan, L.S., R.H. Jean, and K. Kitano, "On the Operating Regimes of Cocurrent Upward Gas-Liquid-Solid Systems with Liquid as the Continuous Phase", *Chem. Eng. Sci.*, **42**, 1853-1855 (1987a)

Fan, L.S., K. Kitano, and B.E. Kreischer, "Hydrodynamics of Gas-Liquid-Solid Annular Fluidization", *AIChE J.*, **33**, 225-231 (1987b)

Fan, L.S., *Gas-Liquid-Solid Fluidization Engineering*, Butterworth, Boston (1989)

Fan, L.S., and K. Tsuchiya, *Bubble Wake Dynamics in Liquid and Liquid-Solid Suspension*, Butterworth-Heinemann, Stoneham, MA (1990)

Fan, L.S., "Bubble Dynamics in Liquid-Solid Suspension", Developments in Fluidization and Fluid-Particle Systems, *AIChE Symp. Ser.* 91(308) (1995)

Fukuma, M., K. Muroyama, and S. Morooka, "Properties of Bubble Swarm in a Slurry Bubble Column", *J. Chem. Eng. Japan*, **20**, 28-33 (1987)

Fukuma, M, M. Sato, K. Muroyama and A. Yasunishi, "Particle-to-Liquid Mass Transfer in Gas-Liquid-Solid Fluidization", *J. Chem. Eng. Japan*, **21**, 231-237 (1988)

Gandhi, B., *Hydrodynamic Studies in a Slurry Bubble Column*, M.S. thesis, University of Western Ontario (1997)

Gandhi, B., A. Prakash and M.A. Bergougnou, "Hydrodynamic Behavior of Slurry Bubble Columns at High Solids Concentration", *Powder Tech.* (submitted)

Godbole, S.P., S. Joseph, and Y.T. Shah, "Hydrodynamics and Mass Transfer in a Bubble Column with an Organic Liquid", *Can. J. Chem. Eng.*, **62**, 440-445 (1984)

Grober, H., S. Erk, and U. Grigull, *Fundamentals of Heat Transfer*, McGraw Book Company, New York (1961)

Grover, G.S., C.V. Rode, and R.V. Chaudhari, "Effect of Temperature on Flow Regimes and Gas Holdup in a Bubble Column", *Can. J. Chem. Eng.*, **64**, 501-504 (1986)

Han, J.H., and S.D. Kim, "Radial Dispersion and Bubble Characteristics in Three-Phase Fluidized Beds", *Chem. Eng. Comm.*, **94**, 9-26 (1990)

Han, J.H., G. Wild, and S.D. Kim, "Phase Holdup Characteristics in Three Phase Fluidized Beds", *Chem. Eng. J.*, **43**, 67-73 (1990)

Haque, M.W., K.D.P. Nigam, and J.B. Joshi, "Optimum Gas Sparger Design for Bubble Columns with Low Height-to-Diameter Ratio", *Chem Eng. J.*, **33**, 63-69 (1986)

Hassanien, S., H. Delmas, and J.P. Riba, "Transfert de matere Liquid-Particules en Fluidisation a trois phases", *Entropie*, **119**, 17-26 (1984)

Hatate, Y., H. Nomura, T. Fujita, S. Tajiri, and A. Ikari, "Gas Holdup and Pressure Drop in Three Phase Horizontal Flows of Gas-Liquid-Fine Solid Particles System", *J. Chem. Eng. Japan*, **19**, 330-335 (1986)

Heriksen, H.K., and K. Ostergaard, "Characteristics of Large Two-Dimensional Air Bubbles in Liquids and in Three-Phase Fluidized Beds", *Chem. Eng. J.*, **7**, 141-146 (1974)

Hikita, H., S. Asal, K.Tanigawa, K. Segawa, and M. Kitao, "Gas Holdup in Bubble Column", *Chem. Eng. J.*, **20**, 59-67 (1980)

Hikita, H., S. Asal, K.Tanigawa, K. Segawa, and M. Kitao, "The volumetric Liquid-Phase Mass Transfer Coefficient in Bubble Columns", *Chem. Eng. J.*, **22**, 61-69 (1981a)

Hikita, H., S. Asal, H. Kikukawa, T. Zalke, and M. Ohue, "Heat Transfer Coefficient in Bubble Column", *Ind. Eng.Chem. Process Des. and Dev.*, **20**, 540-545 (1981b)

Hills, J.H., "Radial Non-Uniformity of Velocity and Voidage in a Bubble Column", *Trans. Instn. Chem. Engrs.*, **52**, 1-9 (1974)

Hills, J.H., "The Operation of a Bubble Column at High Throughputs. I Gas holdup Measurement", *Chem. Eng. J.*, **12**, 89-99 (1976)

Hinze, J.O., *Turbulence*, McGraw-Hill, New Uork (1958)

Holman, J.P., *Heat Transfer*, McGraw-Hill Book Company, New York (1986)

Hudson, C.L., *Effect of Inclination on Hydrodynamics in Bubble Columns and Fluidized Beds* , Ph.D. thesis, University of Western Ontario (1996)

Hughmark, G.A., "Holdup and Mass Transfer in Bubble Columns", *I&EC Process Design and Development*, **6**, 218-220 (1967)

Hyndman, C.L., F. Larachi, and C. Guy, "Understanding gas-phase hydrodynamics in bubble columns: a convective model based on kinetic theory", *Chem. Eng. Sci.*, **52**, 63-77 (1977)

Idogawa, K., K. Ikeda, T. Fukuda, and S. Morooka, "Behavior of Bubbles of the Air-Water System in a Column under High Pressure", *Int. Chem. Eng.*, **26**, 468-474 (1986)

Idogawa, K., K. Ikeda, T. Fukuda, and S. Morooka, "Effect of Gas and Liquid Properties on the Behavior of Bubbles in a Column under High Pressure", *Int. Chem. Eng.*, **27**, 93-99 (1987)

Ishida, M., and Tanaka, H., "An Optical Probe to Detect Both Bubbles and Suspended Particles in a three-Phase Fluidized Bed", *J. Chem. Eng. Japan*, **15**, 389-391 (1982)

Jamialahmadi, M., C. Branch, and H. Muller-Steinhagen, "Effect of Solid Particles on Gas Hold-up in Bubble Columns", *Can. J. Chem. Eng.*, **69**, 390-393 (1991)

Jamialahmadi, M., C. Branch, and H. Muller-Steinhagen, "Terminal Bubble Rise Velocity in Liquids", *Trans IChemE*, **72**, Part A, 119-122 (1994)

Joshi, J.B., and M.M. Sharma, "Mass Transfer Characteristics of Horizontal Sparged Contactors", *Tran. Instn. Chem. Engrs.*, **54**, 42-53 (1976)

Joshi, J.B., and M.M. Sharma, "Liquid Phase Backmixing in Sparged Contactors", *Can. J. Chem. Eng.*, **56**, 116-119 (1978)

Joshi, J.B., and M.M. Sharma, "A Circulation Cell Model for Bubble Columns", *Tran. Instn. Chem. Engrs.*, **57**, 244-251 (1979)

Joshi, J.B., M.M. Sharma, Y.T. Shah, C.P.P. Singh, M. Ally, and G.E. Klingzing, "Heat Transfer in Multiphase Contactors", *Chem. Eng. Commun.*, **6**, 257-271 (1980)

Kang, Y, I.S. Suh, and S.D. Kim, "Heat Transfer Characteristics of Three Phase Fluidized Beds", *Chem. Eng. Commun.*, **34**, 1-13 (1985)

Kang, Y, and S.D. Kim, "Radial Dispersion Characteristics of Two and Three Phase Fluidized Beds", *Ind. Eng. Chem. Process Des. Dev.*, **25**, 717-722 (1986)

Kang, Y., B.T. Min, J.B. Nah, and S.D. Kim, "Mass Transfer in Continuous Bubble Columns with Floating Bubble Breakers", *AIChE J.*, **36**, 1255-1258 (1990)

Kang, Y., M.H. Ko, S.D. Kim, M. Yashima and L. Fan, "Pressure Fluctuations and Particle Dispersion in Liquid Fluidized Deds", *AIChE J.*, **42**, 1164-1169 (1996)

Kang, Y., K.J. Woo, M.H. Ko, and S.D. Kim, "Particle Dispersion and Pressure Fluctuations in Three-Phase Fluidized Beds", *Chem. Eng. Sci.*, **52**, 3723-3732 (1997)

Kara, S., B.G. Kelkar, Y.T. Shah, and N.L. Carr, "Hydrodynamics and Axial Mixing in a Three-Phase Bubble Column", *Ind. Eng.Chem. Process Des. and Dev.*, **21**, 584-594 (1982)

Kato, Y., A. Nishiwaki, T. Fukuda, and S. Tanaka, "The Behavior of Suspended Solid Particles and Liquid in Bubble Columns", *J. Chem. Eng. Japan*, **5**, 112-118 (1972)

Kato, Y., A. Nishiwaki, T. Kago,T. Fukuda, and S. Tanaka, "Gas Holdup and Overall Volumetric Absorption coefficient in Bubble Columns with Suspended Solid Particles. Absorption Rate of Oxygen by an Aqueous Solution of Sodium Sulfite", *Int. Chem. Eng.* , **13**, 562-567 (1973)

Kato, Y., K. Uchida, T. Kago, and S. Morooka, "Liquid Holdup and Heat Transfer Coefficient between Bed and Wall in Liquid-Solid and Gas-Liquid-Solid Fluidized Beds", *Powder Technology*, **28**, 173-179 (1981)

Kato, Y., S. Morooka, T. Kago, T. Saruwatari, and S.Z. Yang, "Axial Holdup Distributions of Gas and Solid Particles in Three-Phase Fluidized Bed For Gas-Liquid(Slurry)-Solid Systems", *J. Chem. Eng. Japan*, **4**, 308-313 (1985)

Kawagoe, K., T. Inoue, K. Nakao, and T. Otake, "Flow-Pattern and Gas Holdup Conditions in Gas-Sparged Contactors", *Int. Chem. Eng.*, **16**, 176-183 (1976)

Kelkar, B.G., S.P. Godbole, M.F. Honath, Y.T. Shah, N.L. Carr, and W.D. Deckwer, "Effect of Addition of Alcohols on Gas Holdup and Backmixing in Bubble Columns", *AIChE J.*, **29**, 361-369 (1983)

Kelkar, B.G., Y.T. Shah, and N.L. Carr, "Hydrodynamics and Axial Mixing in a Three-Phase Bubble Column. Effects of Slurry Properties", *Ind. Eng. Chem. Process Des. Dev.*, **23**, 308-313 (1984)

Khare, A.S., and J.B. Joshi, "Effect of Fine Particles on Gas Holdup in Three-Phase Sparged Reactors", *Chem. Eng. J.*, **44**, 11-25 (1990)

Kitano, K, and L.S. Fan, "Near Wake Structure of a Single Gas Bubble in a Two-Dimensional Liquid-Solid Fluidized Bed: Solids Holdup", *Chem. Eng. Sci.*, **43**, 1355-1361 (1988)

Kim, C.H., H. Delmas, and J.P. Riba, "Liquid-Solid Mass Transfer and Axial Dispersion in Three-Phase Fluidization", *Int. Chem. Eng.*, **31**, 303-314 (1991)

Kim, S.D., C.G.J. Baker, and M.A. Bergougnou, "Holdup and Axial Mixing Characteristics of Two and Three Phase Fluidized Beds", *Can. J. of Chem. Eng.*, **50**, 695-701 (1972)

Kim, S.D., C.G.J. Baker, and M.A. Bergougnou, "Bubble Characteristics in Three Phase Fluidized Beds", *Chem. Eng. Sci.*, **32**, 1299-1306 (1977)

Kim, S.D., and C.H., Kim, "Axial Dispersion Characteristics of Three Phase Fluidized Beds", *J. Chem. Eng. Japan*, **16**, 172-178 (1983)

Kim, S.D., Y. Kang, and H.K. Kwon, "Heat Transfer Characteristics in Two- and Three-Phase Slurry-Fluidized Beds", *AIChE J.*, **32**, 1397-1400 (1986)

Kim, S.D., and A. Laurent, "The State of Knowledge on Heat Transfer in Three-Phase Fluidized Beds", *Int. Chem. Eng.*, **31**, 284-302 (1991)

Kim, S.D., and Y. Kang, "Heat and Mass Transfer in Three-Phase Fluidized-Bed Reactors-an Overview", *Chem. Eng. Sci.*, **52**, 3639-3660 (1997)

Kleiintjens, R.H., van der Lans, R.G. J.M. Luyben, "Particle Suspension Hydrodynamics in a Tapered Gas Agitated Reactor" *Can. J. Chem. Eng.*, **72**, 392-404 (1994)

Knudsen, J.G., and D.L. Katz, *Fluid Dynamics and Heat Transfer*, McGraw Hill Book Co., New York (1958)

Koide, K., S. Morooka, K. Ueyama, A. Matsuura, F. Yamashita, S. Iwamoto, Y. Kato, H. Inoue, M. Shigeta, S. Suzuki, and T. Akehata, "Behavior of Bubbles in Large Scale Bubble Column", *J. Chem. Eng. Japan*, **12**, 98-104 (1979)

Koide, K., A. Takazawa, M. Komura and H. Matsunga, "Gas Holdup and Volumetric Liquid Phase Mass Transfer Coefficient in Solid-Suspended Bubble Column", *J. Chem. Eng. Japan*, **17**, 459-466 (1984)

Koide, K., "Design Parameters of Bubble Column Reactors with and without Solid Suspensions", *J. Chem. Eng. Japan*, **29**, 745-759 (1996)

Kojima, H., and K. Asano, "Hydrodynamic Characteristics of a Suspension-Bubble Column", *Int. Chem. Eng.*, **21**, 473-481 (1981)

Kolbel, H., E. Borchers and K. Muller, "Warmeubergang in Blasensaulen; II. Messungen an viskosen Suspensionen", *Chem. Ing. Tech.*, **30**, 729-734 (1958)

Kolbel, H.E., E. Borchers and J. Martins, "Warmeubergang in Blasensaulen; III. Messungen an Gasdurchstromten Suspensionen", *Chem. Ing. Tech.*, **32**, 84-88 (1960)

Krishna, R., P.M. Wilkinson, and L.L. Van Dierendonck, "A Model for Gas Holdup in Bubble Columns Incorporating the Influence of Gas Density on Flow Regime Transitions", *Chem. Eng. Sci.*, **46**, 2491-2496 (1991)

Krishna, R., J.W.A. de Swart, D.E. Hennephof, J. Ellenberger, and H.C.J. Hoefsloot, "Influence of Increased Gas Density on Hydrodynamics of Bubble-Column Reactors", *AIChE J.*, **40**, 112-119 (1994)

Krishna, R., and J. Ellenberger, "Gas Holdup in Bubble Column Reactors Operating in the Churn-Turbulent Flow Regime", *AIChE J.*, **42**, 2627-2634 (1996)

Krishna, R., J.W.A. de Swart, J. Ellenberger, G.B. Martina, and C. Maretto, "Gas Holdup in Slurry Bubble Columns: Effect of Column Diameter and Slurry Concentrations", *AIChE J.*, **43**, 311-316 (1997)

Kubie, J., "Bubble Induced Heat Transfer in a Two Phase Gas-Liquid Flow", *Int. J. Heat Transfer*, **18**, 537-551 (1975)

Kumar, S., K. Kusakabe, K. Raghuathan, and L.S. Fan, "Mechanism of Heat Transfer in Bubbly Liquid and Liquid-Solid Systems: Single Bubble Injection", *AIChE J.*, **38**, 733-741 (1992)

Kumar, S., K. Kusakabe, and L.S. Fan, "Heat Transfer in Three Phase Fluidization and Bubble-Columns with High Gas Holdups", *AIChE J.*, **39**, 1399-1405 (1993a)

Kumar, S., K. Kusakabe, and L.S. Fan, "Heat Transfer in Three Phase Fluidized Beds Containing Low-Density Particles", *Chem. Eng. Sci.*, **48**, 2407-2418 (1993b)

Kumar, S., and L.S. Fan, "Heat Transfer Characteristics in Viscous Gas-Liquid and Gas-Liquid-Solid Systems", *AIChE J.*, **40**, 745-755 (1994)

Kwon, H.W., Y. Kang, S.D. Kim, M. Yashima, and L. Fan, "Bubble-Chord Length and Pressure Fluctuations in Three-Phase Fluidized Beds", *Ind. Eng. Chem. Res.*, **33**, 1852-1857 (1994)

Lamont, A.G.W., "Air Agitation and Pachuca Tanks", *Can. J. Chem. Eng.*, **36**, 153-160 (1958)

Lee, D.H., J.O. Kim, and S.D. Kim, "Mass Transfer and Phase Holdup Characteristics in Three-Phase Fluidized Beds", *Chem. Eng. Comm.*, **119**, 179-196 (1993)

Lee, S.L.P., H.I. de Lasa, and M.A. Bergougnou, "Bubble Phenomena in Three Phase Fluidized Beds as viewed by a U-shaped fiber Optic Probe", *AIChE Symp. Ser.*, 80(241), 110-116 (1984)

Lee, S.L.P., and H.I. de Lasa, "Phase Holdups in Three-Phase Fluidized Beds", *AIChE J.*, **33**, 1359-1370 (1987)

Lee, J.C., A.J. Sherrard, and P.S. Buckley, in *Fluidization and Its Applications* ed. by H. Angelino, J.P. Couderc, H. Gibert, and C. Laguerie, 407, Cepadues-Editions, Toulouse (1974)

Lee, Y.H., Y.J. Kim, B.G. Kelkar, and C.B. Weinberger, "A Simple Digital Sensor for Dynamic Gas Holdup Measurements in Bubble Columns", *Ind. Eng. Chem. Fundam.*, **24**, 105-107 (1985)

Li, H. and A. Prakash, "Local and Instantaneous Heat Transfer Measurement in a Three Phase Slurry Bubble Column", Heat-Transfer-Baltimore, *AIChE Symp. Ser.* 93 (314), 295-298 (1997)

Li, H. and A. Prakash, "Heat Transfer and Hydrodynamics in a Three Phase Slurry Bubble Column", *Ind. & Eng. Chem. Res.*, **36**, 4688-4694 (1997)

Lin, T.J., J. Reese, T. Hong, and L.S. Fan, "Quantitative Analysis and Computation of Two-Dimensional Bubble Columns", *AIChE J.*, **42**, 301-318 (1996)

Lockett, M.J., and R.D. Kirkpatrick, "Ideal Bubbly Flow and Actual Flow in Bubble Columns", *Trans. Instn Chem. Eng.*, **53**, 267-273 (1975)

Luo, X.K., P.J. Jiang, and L.S. Fan, "High pressure Three-phase Fluidization: Hydrodynamics and heat transfer", *AIChE J.*, **43**, 2432-2445 (1997)

MacTaggart, R.S., H.A. Nasr-El-Din, and J.H. Masliyah, "Sample Withdrawal from a Slurry Mixing Tank", *Chem. Eng. Sci.*, **48**, 921-931 (1993)

Magiliotou, M., Y.M. Chen, L.S. Fan, "Bed-Immersed Object Heat Transfer in a Three Phase Fluidized Bed", *AIChE J.*, **34**, 1043-1047 (1988)

Marchese, M.M., A. Uribe-Salas, J.A. Finch, "Measurement of Gas Holdup in A Three-Phase Concurrent Downflow Column", *Chem. Eng. Sci.*, **47**, 3475-3482 (1992)

Maroyama, K., and L.S. Fan, "Fundamentals of Gas-Liquid-Solid Fluidization", *AIChE J.*, **31**, 1-34 (1985)

Matsuura, A, and L.S. Fan, "Distribution of Bubble Properties in a Gas-Liquid-Solid Fluidized Bed", *AIChE J.*, **30**, 894-903 (1984)

Matsumoto, T., N. Hidaka, Y Takebayasi, and S. Morooka, "Axial Mixing and Segregation in a Gas-Liquid-Solid Three-Phase Fluidized Bed of Solid Particles of Different Sizes and Densities", *Chem. Eng. Sci.*, **52**, 3961-3970 (1997)

Maxworthy, T., "A note on the Existence of Wake behind Large, rising Bubbles", *J. Fluid Mech.*, **27**, 367-368 (1967)

Maezawa, A., S. Muramatsu, S. Uchida, and S. Okamura, "Measurement of Gas Hold-up in three-Phase Systems by Ultrasonic Technique", *Chem. Eng. Technol.*, **16**, 260-262 (1993)

Mersman, A., H. Noth, D. Ringer, and R. Wunder, "Maximum Heat Transfer in Equipment with Dispersed Two-Phase Systems", *Int. Chem. Eng.*, **22**, 16-29 (1982)

Miller, D.N., "Gas Holdup and Pressure Drop in Bubble Column Reactors", *Ind. Eng. Chem. Precess Des. Dev.*, **19**, 371-377 (1980)

Miyahara, T., K. Tsuchiya, and L.S. Fan, "Wake Properties of a Single Gas Bubble in a Three-Dimensional Liquid-Solid Fluidized Bed", *Int. J. Multiphase Flow*, **14**, 749-763 (1988)

Morooka, S., T. Mizoguchi, T. Kago, and Y. Kato, "Effect of Fine Bubbles on Flow Properties in Bubble Column with Suspended Solid Particles", *J. Chem. Eng. Japan*, **19**, 507-512 (1986)

Muroyama, K., M. Fukuma, and A. Yasunishi, "Wall-to-Bed Heat Transfer Coefficient in Gas-Liquid-Solid Fluidized Beds", *Can. J. of Chem. Eng.*, **62**, 199-208 (1984)

Muroyama, K., M. Fukuma, and A. Yasunishi, "Wall-to-Bed Heat Transfer in Liquid-Solid and Gas-Liquid-Solid Fluidized Beds. Part II: Gas-Liquid-Solid Fluidized Beds", *Can. J. of Chem. Eng.*, **64**, 409-418 (1986)

Nicklin, D.J., "Two-Phase Bubble Flow", *Chem. Eng. Sci.*, **17**, 693-702(1962)

Nigam, K.D.P., and A. Schumpe, *Three-Phase Sparged Reactors*, Gordon and Breach Publishers, The Netherlands (1996)

Nikov, I., and H. Delmas, "Solid-Liquid Mass Transfer in Three-Phase Fixed and Fluidized Beds", *Chem. Eng. Sci.*, **42**, 1089-1093 (1987)

Nore, O., G. Wild, C.L. Briens, and A. Margaritis, "Wall-to-Bed Heat Transfer in Three-Phase Fluidized Beds of Low Density Particles", *Can. J. of Chem. Eng.*, **72**, 546-550 (1994)

Nottenkamper, R., A. Steiff and P.M. Weinpach, "Experimental Investigation of Hydrodynamics of Bubble Columns", *Ger. Chem. Eng.*, **6**, 143-155 (1983)

O'Dowd, W, D.N. Smith, J.A. Ruether, and S.C. Saxena, "Gas and Solids Behavior in a Baffled and Unbaffled Slurry Bubble Column", *AIChE J.*, **33**, 1959-1970 (1987)

Oels, U., J. Lucke, R. Buchholz, and K. Schugerl, "Influence of Gas Distributor Type and Composition of Liquid on the Behavior of a Bubble Column Bioreactor", *Ger. Chem. Eng.*, **1**, 115-129 (1978)

Orell, A., "On the liquid Flow Reversal in Bubble Columns", *Chem. Eng. Commun.*, **115**, 149-159 (1992)

Ostergaard, K., and M.L. Michelsen, "On the use of Imperfect Tracer Pulse Method for Determining Holdup and Axial Mixing", *Can. J. Chem. Eng.*, **47**, 107 (1969)

Ozturk, S.S., A. Schumpe and W.D. Deckwer, "Organic Liquids in a Bubble Column: Holdups and Mass Transfer Coefficients", *AIChE J.*, **33**, 1473-1480 (1987)

Pandit, A.B., and J.B. Joshi, "Three Phase Sparged Reactors Some Design Aspects", *Rev. Chem. Eng.*, 1-84 (1984)

Patel, R.D., and J.M. Simpson, "Heat Transfer in Aggregative and Particulate Liquid-Fluidized Beds", *Chem. Eng. Sci.*, **32**, 67-74 (1977)

Patel, S.A., J.G. Daly, and D.B. Bukur, "Holdup and Interfacial Area Measurements Using Dynamic Gas Disengagement", *AIChE J.*, **35**, 931-942 (1989)

Peeles, F.N., and H.J. Garber, "Studies on the motion of Gas Bubbles in Liquids", *Chem. Eng. Prog.*, **49**,88-97 (1953)

Peterson, D.A., R.S. Tankin, and S.G. Bankoff, "Holographic Measurement of Bubble Size and Velocity in a Three Phase System", IUTAM Symposium, Measuring Techniques in Gas-Liquid Two Phase Flows, Springer Verlag Berlin, 1-21 (1984)

Pino, L.R.Z., M.M. Yepez and A.E. Saez, "Hydrodynamics of a Semibatch Slurry Bubble Column with a Foaming Liquid", *AIChE J.*, **36**, 1758-1762 (1990a)

Pino, L.R.Z., M.M. Yepez and A.E. Saez, "An Experimental Study of Gas Holdup in Two-Phase Bubble Column with a Foaming Liquid", *Chem. Eng. Comm.*, **89**, 155-175 (1990b)

Prakash, A., C.L. Briens and M.A. Bergougnou, "Mass Transfer Between Solid Particles and Liquid in a Three-Phase Fluidized Bed", Proceedings of the 34th Canadian Society of Chemical Engineering Conference, Quebec city, Quebec, Sept. 30-Oct. 4 (1984)

Prakash, A., C.L. Briens and M.A. Bergougnou, "Mass Transfer Between Solid Particles and Liquid in a Three-Phase Fluidized Bed", *Can. J. Chem. Eng.*, **65**, 228-235 (1987)

Prakash, A., *Enhancement of Mass Transfer in Multiphase Contactors*, Ph.D. thesis, University of Western Ontario (1991)

Prince, M.J., and H.W. Blanch, "Bubble Coalescence and Break-up in Air-Sparged Bubble Columns", *AIChE J.*, **36**, 1485-1499 (1990)

Raghunathan, K., S. Kumar, and L.S. Fan, "Pressure Distribution and Vortical Structure in the Wake Behind Gas Bubbles in Liquid and Liquid-Solid Systems", *Int. J. Multiphase Flow*, **18**, 41-50 (1992)

Ramachandran, P.A., and R.V. Chaudhari, *Three-Phase Catalytic Reactors*, Gordon and Breach Science Publishers, New York (1983)

Reese, J., and L.S. Fan, "Transient Flow Structure in the Entrance Region of A Bubble Column Using Particle Image Velocimetry", *Chem. Eng. Sci.*, **49**, 5623-5636 (1994)

Reilly, I.G., D.S. Scott, T. de Bruijn, A. Jain, and J. Piskorz, "A Correlation for Gas Holdup in Turbulent Coalescing Bubble Columns", *Can. J. of Chem. Eng.*, **64**, 705-717 (1986)

Richardson, J.F., M.N. Romani, and K.J. Shakiri, "Heat Transfer from Immersed Surfaces in Liquid Fluidized Beds", *Chem. Eng. Sci.*, **31**, 619-624 (1976)

Rigby, G.R, and C.E. Capes, "Bed Expansion and Bubble Wakes in Three-Phase Fluidization", *Can. J. Chem. Eng.*, **48**, 343-348 (1970)

Rigby, G.R, G.P. Van Blockland, W.H. Park, and C.E. Capes, "Properties of Bubbles in Three-Phase Fluidized Beds as Measured by Electroresistivity Probe", *Chem. Eng. Sci.*, **25**, 1729-1741 (1970)

Saberian-Broudjenni, M., G. Wild, N. Midoux, and J.C. Charpentier, "Contribution to the study of Wall Heat Transfer in Reactors with a Gas-Liquid-Solid Fluidized Bed at Low Liquid Velocities", *Can. J. Chem. Eng.*, **63**, 553-564 (1985)

Sada, E., H. Kumazawa, and C. Lee, "Influence of Suspended Fine Particles on Gas Holdup and Mass Transfer Characteristics in a Slurry Bubble Column", *AIChE J.*, **32**, 853-856 (1986a)

Sada, E., H. Kumazawa, C. Lee and T. Iguchi, "Gas Holdup and Mass-Transfer Characteristics in a Three-Phase Bubble column", *Ind. Eng. Chem. Process Des. Dev.*, **25**, 472-476 (1986b)

Sauer, T. and D.C. Hempel, "Fluid Dynamics and Mass Transfer in a Bubble Column with Suspended Particles", *Chem. Eng. Technol.*, **10**, 180-189 (1987)

Saxena, S.C., R. Vadivel, and A.C. Saxena, "Gas Holdup and Heat Transfer from Immersed Surfaces in Two- and Three-Phase Systems in Bubble Columns", *Chem. Eng. Commun.*, **85**, 63-83 (1989)

Saxena, S.C., N.S. Rao, and A.C. Saxena, "Heat Transfer and Gas Holdup Studies in a Bubble Column: Air-Water-Glass Bead System", *Chem. Eng. Commun.*, **96**, 31-35 (1990a)

Saxena, S.C., N.S. Rao, and A.C. Saxena, "Heat Transfer from a Cylindrical Probe Immersed in a Three-Phase Slurry Bubble Column", *Chem. Eng. J.*, **44**, 141-156 (1990b)

Saxena, S.C., N.S. Rao, and A.C. Saxena, "Estimation of Heat Transfer Coefficient for Immersed surfaces in Bubble Columns involving Fine Powders", *Powder Technology*, **63**, 197-202 (1990c)

Saxena, S.C., N.S. Rao, and M. Yousef, "Hydrodynamic and Heat Transfer Investigations conducted in a Bubble Column with Fine Powders and a Viscous Liquid", *Powder Technology*, **44**, 265-275 (1991)

Saxena, S.C., N.S. Rao, and A.C. Saxena, "Heat Transfer and Gas Holdup Studies in a Bubble Column: Air-Water-Sand System", *Can. J. Chem. Eng.*,**70**, 33-41 (1992a)

Saxena, S.C., N.S. Rao, and P.R. Thimmapuram, "Gas Phase Holdup in Slurry Bubble Columns for Two- and Three-Phase Systems", *Chem. Eng. J.*, **49**, 151-159 (1992b)

Saxena, S.C., and Z.D. Chen, "Hydrodynamics and Heat Transfer of Baffled and Unbaffled Slurry Bubble Columns", *Rev. Chem. Eng.*, 193-400 (1994)

Schluter, S., A. Steiff, and P.-M. Weinspach, "Heat Transfer in Two- and Three-Phase Bubble Column Reactors with Internals", *Chemical Engineering and Processing*, **34**, 157-172 (1995)

Schlichting, H., *Boundary Layer Theory*, MaGraw Hill, 1960.

Schumpe, A., and G. Grund, "The Gas Disengagement Technique for Studying Gas Holdup Structure in Bubble Column", *Can. J. Chem. Eng.*, **64**, 891-896 (1986)

Shah, Y.T., S.P. Godbole, and W.D. Deckwer, "Design Parameters Estimations for Bubble Column Reactors", *AIChE J.*, **28**, 353-379 (1982)

Shetty, S.A., M.V. Kantak, and B.G. Kelkar, "Gas-Phase Backmixing in Bubble-Column Reactors", *AIChE J.*, **38**, 1013-1026 (1992)

Sigrist, L., O. Dossenbach and N. Ibl, "Mass Transport in Electrolytic Cells with Gas Sparging", *Int. J. Heat Mass Transfer*, **22**, 1393-1399 (1979)

Siquier, S., M.M. Yepez, and A.E. Saez, "Solid Distribution in a Slurry Bubble Column with Two Immeiscible Liquid Phases", *AIChE J.*, **37**, 466-469 (1991)

Slaughter, I. and A.E. Wraith, "The Wake of a Large Gas Bubble", *Chem. Eng. Sci.*, **23**, 932-932 (1968)

Smith, D.N., W. Fuchs, R.J. Lynn, D.H. Smith, and M. Hess, "Bubble Behavior in a Slurry Bubble Column Reactor Model" Chem. and Catalytic Reactor Modeling, *ACS Symp. Ser.* **237**, 125 (1984)

Smith, D.N., and J.A. Ruether, "Dispersed Solid Dynamics in a Slurry bubble Column", *Chem. Eng. Sci.*, **40**, 741-754 (1985)

Soong, Y., I.K. Gamwo, A.G. Blackwell, R.R. Schehl, and M.F. Zarochak, "Measurement of Solids Concentration in a Three-Phase Reactor by an Ultrasonic Technique", *Chem. Eng. J.*, **60**, 161-167 (1995)

Sriram, K. and R. Mann, "Dynamic Gas Disengagement: A New Technique for Assessing the Behavior of Bubble Columns", *Chem. Eng. Sci.*, **32**, 571-580 (1977)

Stewart, P.S.B., and J.F. Davidson, "Three-Phase Fluidization: Water, Particles and Air", *Chem. Eng. Sci.*, **19**, 319-322 (1964)

Stolojanu, V., and A. Prakash, "Hydrodynamic Measurements in a slurry Bubble Column using Ultrasonic Technique", *Chem. Eng. Sci.*, **52**, 4255-4230 (1997)

Suh, I.S., G.T. Jin, and S.D. Kim, "Heat Transfer Coefficients in Three Phase Fluidized Beds", *Int. J. Multiphase Flow*, **11**, 255-259 (1985)

Suh, I.S., and W.D. Deckwer, "Unified Correlation of Heat Transfer Coefficients in Three-Phase Fluidized Beds", *Chem. Eng. Sci.*, **44**, 1455-1458 (1989)

Tang, W.T., and L.S. Fan, "Hydrodynamics of a Three-Phase Fluidized Bed Containing Low-Density Particles", *AIChE J.*, **35**, 355-364 (1989)

Thimmapuram, P.R., N.S. Rao, and S.C Saxena, "Characterization of Hydrodynamic Regimes in a Bubble Column", *Chem. Eng. Sci.*, **47**, 3355-3362 (1992)

Thomas, D.G., "Transport Characteristics of Suspensions: VIII. A Note on the Viscosity of Newtonian Suspensions of Uniform Spherical Particles", *J. Colloid Sci.*, **20**, 267-277 (1965)

Tsuchiya, K. and L.S. Fan, "Near-Wake Structure of a Single Gas Bubble in a Two-Dimensional Liquid-Solid Fluidized Bed: Vortex Shedding and Wake Size Variation", *Chem. Eng. Sci.*, **43**, 1167-1181 (1988)

Tsuchiya, K., G.H. Song, and L.S. Fan, "Effects of Particle Properties on Bubble Rise and Wake in a Two-Dimensional Liquid-Solid Fluidized Bed", *Chem. Eng. Sci.*, **45**, 1429-1434 (1990)

Tsuchiya, K., G.H. Song, W.T. Tang, and L.S. Fan, "Particle Drift Induced by a Bubble in a Liquid-Solid Fluidized Bed with Low-Density Particles", *AIChE J.*, **38**, 1847-1851 (1992)

Turner, J.C.R., "Two Phase Conductivity: The Electrical Conductance of Liquid-Fluidized Beds of Spheres", *Chem. Eng. Sci.*, **31**, 487-492 (1976)

Tzeng, J.W., R.C. Chen, and L.S. Fan, "Visualization of Flow Characteristics in a 2-D Bubble Column and Three-Phase Fluidized Bed", *AIChE J.*, **39**, 733-744 (1993)

Ueyama, K., and T. Miyauchi, "Properties of Recirculating Turbulent Two Phase Flow in Gas Bubble Columns", *AIChE J.*, **25**, 258-266 (1979)

Ueyama, K., S. Morooka, K. Koid, H. Kaji, T. Miyauchi, "Behavior of Gas Bubbles in Bubble Columns", *Ind. Eng. Chem. Process Des. Dev.*, **19**, 592-599 (1980)

Vand, V., "Viscosity of solutions and suspensions", *J. Phys. Chem.*, **52**, 277-321 (1948)

Vasalos, I.A., D.N. Rundell, K.E. Megiris and G.J. Tjatjopoulos, "Holdup Correlations in slurry-Solid Fluidized Beds", *AIChE J.*, **28**, 346-348 (1982)

Vermeer, D.J., and R. Krishna, "Hydrodynamics and Mass Transfer in Bubble Columns Operating in the Churn-Turbulent Regime", *Ind. Eng. Chem. Process Des. Dev.*, **20**, 475-482 (1981)

Wachi, S., and H. Morikawa, "Gas Holdup and Axial Dispersion in Gas-Liquid Concurrent Bubble Column", *J. Chem. Eng. Japan*, **20**, 309-316 (1987)

Wallis, G.B. "The terminal Speed of Single Drops or Bubbles in an Infinite Medium", *Int. J. Multiphase Flow*, **1**, 491 (1974)

Warsito, A. Maezawa, S. Uchida, and S. Okamura, "A Model for Simultaneous Measurement of Gas and Solid Holdups in a Bubble Column Using Ultrasonic Method", *Can. J. Chem. Eng.*, **73**, 734-742 (1995)

Wasan, D.T., and M.S. Ahluwalia, "Consecutive Film and Surface renewal Mechanism for Heat or Mass Transfer from the Wall", *Chem. Eng. Sci.*, **24**, 1535-1542 (1969)

Wilkinson, P.M., and L.L. van Dierendonck, "Pressure and Gas Density Effects on Bubble Break-up and Gas Holdup in Bubble Columns", *Chem. Eng. Sci.*, **45**, 2309-2315 (1990)

Wilkinson, P.M., A.P. Spek, and L.L. van Dierendonck, "Design Parameters Estimation for Scale-Up of High-Pressure Bubble Columns", *AIChE J.*, **38**, 544-554 (1992)

Wolff, C., F.U. Briegleb, J. Bader, K. Hektor, and Hans Hammer, "Measurement with Multi-point Microprobes", *Chem. Eng. Technol.*, **13**, 172-184 (1990)

Yamashita, F., "Effect of Foam Layer on Gas Holdup in a Bubble column", *J. Chem. Eng. Japan*, **28**, 837-840 (1995)

Yamashita, F, and H. Inoue, "Gas Holdup in Bubble Columns", *J. Chem. Eng. Japan*, **8**, 334-336 (1975)

Yamashita, F., "Effect of Liquid Depth, Column Inclination and Baffle Plates on Gas Holdup in Bubble Columns", *J. of Chem. Eng. Japan*, **18**, 349-63 (1985).

Yasunishi, A., M. Fukuma and K. Muroyama, "Measurement of Behavior of Gas Bubbles and Gas holdup in a slurry Bubble Column by a Dual Electroresistivity Probe Method", *J. Chem. Eng. Japan*, **19**, 444-449 (1986)

Yasunishi, A., M. Fukuma and K. Muroyama, "Wall-to-Liquid Mass Transfer in Packed and Fluidized beds with Gas-Liquid Concurrent Upflow", *J. Chem. Eng. Japan*, **21**, 522-528 (1988)

Ying, D.H., E.N. Givens, and R.F. Weimer, "Gas Holdup in Gas-Liquid and Gas-Liquid-Solid Flow Reactors", *Ind. Eng.Chem. Process Des. and Dev.*, **19**, 635-638 (1980)

Yu, Y.H., S.D. Kim, "Bubble Characteristics in the Radial Direction of Three-Phase Fluidized Beds", *AIChE J.*, **34**, 2069-2072 (1988)

Zehner, P., "Momentum, Mass and Heat Transfer in Bubble Columns. Part 1. Flow Model of the Bubble Column and Liquid Velocity", *Int. Chem. Eng.*, **26**, 22-28 (1986a)

Zehner, P., "Momentum, Mass and Heat Transfer in Bubble Columns. Part 2. Axial Blending and Heat Transfer", *Int. Chem. Eng.*, **26**, 29-34 (1986b)

Zou, R., X. Jiang, B. Li, Y. Zu, and L. Zhang, "Studies on Gas Holdup in a bubble Column Operated at Elevated Temperatures", *Ind. Eng. Chem. Res.*, **27**, 1910-1916 (1988)

IMAGE EVALUATION
TEST TARGET (QA-3)

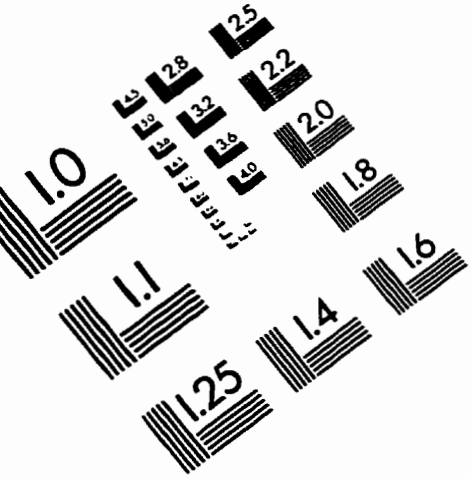

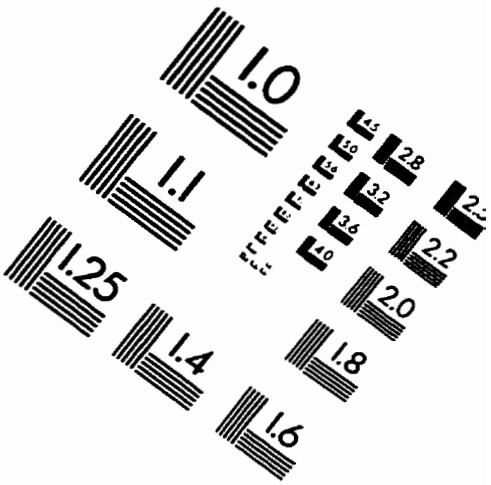

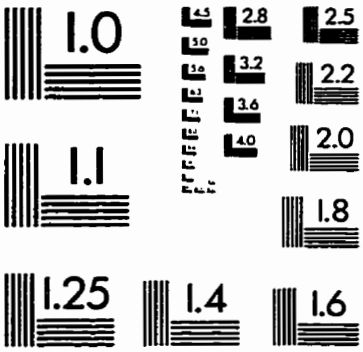

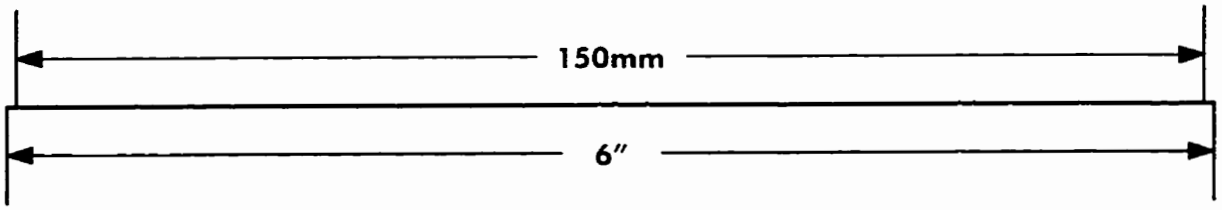

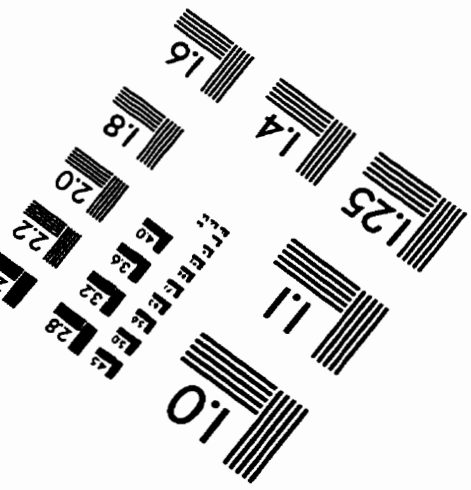

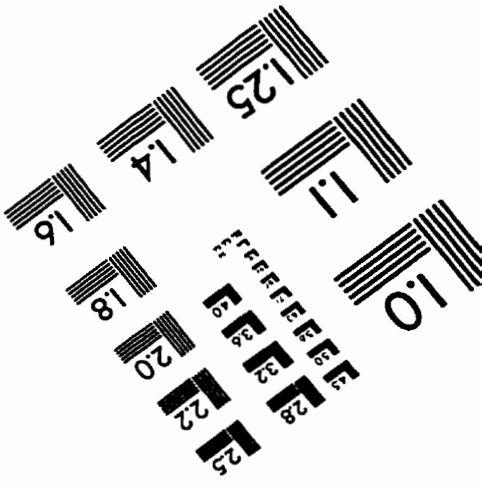

APPLIED IMAGE, Inc
1653 East Main Street
Rochester, NY 14609 USA
Phone: 716/482-0300
Fax: 716/288-5989

© 1993, Applied Image, Inc., All Rights Reserved